Targeting the Translational Machinery in Aggressive Cancers

Ella Kim Lineham

Submitted for degree of Doctor of Philosophy

University of Sussex

January 2019

Abstract

Eukaryotic initiation factor 4E (eIF4E) is a key focus in cancer research due to its central role in controlling the translation of tumour-associated proteins that drive an aggressive migratory phenotype. eIF4E activity, modulated *via* its availability and phosphorylation are regulated by the PI3K/AKT/mTOR and mitogen-activated protein kinase interacting protein kinases (MNK1/2). The latter phosphorylates eIF4E on Ser209 whereas mTORC1 phosphorylates and de-activates the eIF4E inhibitor, 4E-BP1, to release translational repression. The work presented here describes the synthesis and characterisation of 4-((4-fluoro-2-isopropoxyphenyl)amino)-5-methyl thieno[2,3-d] pyrimidine-6- carboylic acid, known as compound **1**, a MNK1/2 inhibitor.

Further analysis of compound **1** in combination with mTORC1/2 inhibitors show that inhibiting these pathways simultaneously effectively slows the rate of cell migration in MDA-MB-231 triple negative breast cancer (TNBC) cells. As an alternative approach, novel, cleavable dual MNK1/2 and PI3K/mTOR inhibiting hybrids were synthesised and characterised in MDA-MB-231 cells. These were found to be less effective at slowing cell migration than the combination of individual inhibitors. Molecular modelling of compound **1** revealed a large hydrophobic pocket which was exploited with a bulkier ferrocene group. Two novel ferrocene-containing compounds based upon compound **1** were synthesised and screened for MNK1/2 inhibition.

To target migration more specifically, work was also carried out with an alternative translational protein, DDX3X. Both genetic knockdown and pharmacological inhibition alone and in combination with compound **1** reveal its potential as an anti-cancer target.

Contents

List of Figures

List of Tables

Acknowledgements

I would like to begin by saying thank you to Prof. Simon Morley for his continued support and generosity. Simon is always there for a chat and has a great way of putting things into perspective. It has been a fantastic four years and I hope we will keep in touch and enjoy a regular Small Batch coffee! A special thanks to my secondary supervisor, Prof. John Spencer, for all of his support and help in the chemistry lab. John has been a brilliant teacher and his enthusiasm and encouragement have been invaluable.

I would like to express my gratitude to Prof. Sarah Newbury, Prof. Mark O'Driscoll, Dr. Mark Paget, Prof. Timothy Chevassut and Prof. Chris Pepper for their advice and helpful discussions. A special thanks to all of the support staff in the Life Sciences, who often go unnoticed but are essential to the smooth running of the lab.

I would also like to thank Prof. Spiros Linardopoulos for the opportunity to work with his group at the ICR. Spiros has been very supportive throughout my PhD and I will always be grateful for the chance to work alongside Dr. Grace Mak, Dr. Katrin Gutsche and Dr. Amir Faisal.

Over my years at Sussex I have formed many friendships, I would like to thank all members of the Morley and Spencer Labs, past and present. Many thanks to Dr. Helen Stewart, Dr. Raysa Kahn and Dr. Melvyn Ansell for their help and support throughout my time at Sussex. Special thanks to Dr. Luke Young, Dr. Teresa Gagliano and Hilda Veenstra for their friendship, football matches and coffee breaks!

Lastly, I would like to thank my family for supporting me throughout my university career. They have always been there for me and have helped me to negotiate a few detours! I will be forever grateful for their encouragement, love and support.

Abbreviations

4E-BP1	eIF4E-binding protein 1
4E-SE	eIF4E-sensitivity element
5'TOP	5’ terminal oligopyrimidine tract
5'UTR	5’ untranslated region
A site	Amino acid site
ADME	Absorption, distribution, metabolism, excretion
ALK4	Activin receptor-like kinase 4
AML	Acute myeloid leukaemia
ARE	AU-rich elements
ARE-BP	AU-rich element binding protein
ATCC	American type culture collection
ATG13	Autophagy-related protein 13
ATP	Adenosine triphosphate
BDNF	Brain-derived neutrophic factor
BLAST	Basic local alignment search tool
CCDC	Cambridge crystallographic data centre
CML	Chronic myelogenous leukaemia
cPLA2	Cytoplasmic phospholipase A2
CRISPR	Clustered regularly interspaced short palindromic repeats
C-terminal	Carboxyl-terminal
CYFIP1	Cytoplasmic FMRP interacting protein 1
DCM	Dichloromethane
DDR	DNA damage response
DMAP	4-Dimethylaminopyridine
DMF	Dimethylformamide
DMSO	Dimethyl sulfoxide
DSB	Double strand break
DSMZ	German collection of microorganisms and cell cultures
DTT	Dithiothreitol

E site	Exit site
ECACC	European collection of cell cultures
EDC	1-ethyl-3-(3-dimethylaminopropyl)carbodiimide
EDTA	Ethylenediaminetetraacetic acid
EGFR	Epidermal growth factor receptor
eIF	Eukaryotic initiation factor
EMT	Epithelial-mesenchymal transition
FBS	Foetal bovine serum
FDA	Food and drug administration
FGF	Fibroblast growth factor
FMRP	Fragile X mental retardation protein
GBM	Glioblastoma
GDI	Guanine nucleotide exchange inhibitor
GTP	Guanosine triphosphate
GEF	Guanine nucleotide exchange factors
GM-CSF	Granulocyte-macrophage colony stimulating factor
GSH	Glutathione
GSK3	Glycogen synthase kinase 3β
HCC	Hepatocellular carcinoma
HDAC	Histone deacetylase
HIF-1	Hypoxia-inducible factor-1
hnRNP A1	Heterogeneous nuclear ribonucleoprotein A1
HNSCC	Head and neck squamous cell carcinoma
HOBT	1-hydroxybenzotriazole hydrate
IGF1	Insulin-like growth factor 1
IRES	Internal ribosome entry site
IRS1	Insulin receptor substrate 1
ITAF	IRES *trans*-acting factor
Jak3	Janus kinase 3
KO	Knockout

LC3B	Microtubule-associated protein 1 light chain 3 beta
m^6A	N^6-methyladenosine
m^7GTP	7-Methylguanosine 5′-triphosphate
MCL-1	Induced myeloid leukaemia cell differentiation protein
MDM2	Mouse double minute 2 homolog
MDR	Multi-drug resistance
MEM	Minimal essential medium
MFC	Multifactorial complex
mGluR	Metabotropic glutamate receptor
MMP	Matrix metalloproteinase
MNK	Mitogen-activated protein kinase interacting protein kinase
mRNP	Messenger ribonucleoprotein
MRP1	Multidrug resistance associated protein 1
MSA	Multiple sequence alignment
MSS	Microsatellite stable
MTA1	Metastasis associated 1
mTOR	Mechanistic (formerly mammalian) target of rapamycin
NES	Nuclear export signal
NHEJ	Non-homologous end joining
NLS	Nuclear localisation signal
NMR	Nuclear magnetic resonance
N-terminal	Amino terminus
P site	Polypeptide site
PABP	Poly(A)-binding protein
PAM	Protospacer adjacent motif
PARP	Poly (ADP-ribose) polymerase
PBS	Phosphate Buffered Saline
PD-1	Programmed death-1
PDB	Protein data bank
PEG	Polyethylene glycol

P-gp	P-glycoprotein
PIC	Pre-initiation complex
PIP3	Phosphatidylinositol (3,4,5)-trisphosphate
PKA	Protein kinase A
PKC	Protein kinase B
PR	Progesterone receptor
PSF	Protein-associated splicing factor
PTB	Polypyrimidine-tract-binding protein
P-TEFb	Positive transcription elongation factor b
PTEN	Phosphatase and tensin homolog
PTM	Post-translational modification
qRT-PCR	Quantitative reverse transcription polymerase chain reaction
REN	Ring expanded nucleotide
RMSD	Root-mean-square deviation
ROS	Reactive oxygen species
RT	Room temperature
RTCA DP	Real-time cell analyser dual-plate
RTK	Receptor tyrosine kinases
SDS-PAGE	Sodium dodecyl sulphate polyacrylamide gel electrophoresis
SF1	Superfamily 1
SF2	Superfamily 2
SGC	Structural genomics consortium
SGK	Serum- and glucocorticoid-regulated kinase
sgRNA	Small guide RNA
SH2	Src homology 2
SH3	Src homology 3
SIN1	Stress-activated map kinase-interacting protein 1
SLP	Stem loop pairs
SNP	Sodium nitroprusside
SOS	Son of sevenless

Spry2	Sprouty2
SREBP	Sterol regulatory element-binding proteins
SV40	Simian virus 40
TC	Ternary complex
TNBC	Triple negative breast cancer
TNF	Tumour necrosis factor
TPSA	Total polar surface area
tracrRNA	Transacting RNA
TRAIL	Tumour necrosis factor-related apoptosis-inducing ligand
tRNAi	Initiator transfer RNA
TSC2	Tuberous sclerosis complex 2
UCSF	University College San Francisco
ULK1	Unc-51 like autophagy activated kinase
VEGF	Vascular endothelial growth factor
WT	Wildtype
YB1	Y-box binding protein
zDOPE	Normalised discrete optimized protein energy

1 Introduction

1.1 Introduction to Translational Control

1.1.1 Cap-dependent Translation Initiation

Translation can be divided into three phases: initiation, elongation and termination. Translation initiation begins with the formation of a complex on the mRNA, the large ribosomal subunit binds to the complex causing the release of initiation factors. The large subunit of the ribosome has three sites to which mRNA and tRNA molecules can bind to, these are the A site, P site and E site (Figure 1-1) (Clancy & Brown, 2008).

Gene expression is regulated at both the transcriptional and post-translational levels. Translational control is critical for maintaining protein levels within the cell and achieving homeostasis. The majority of mRNA is translated by the cap-dependent mechanism. This is primarily regulated at the level of the initiation phase and involves eukaryotic initiation factors (eIFs) and accessory proteins (summarised in Figure 1-2, Table 1-1 and reviewed in Sonenberg & Hinnebusch, 2009). Initiation factors coordinate vital checkpoints during this process and determine both whether a specific mRNA is translated, therefore, contributing to the total abundance of specific protein within the cell (Ruggero, 2013).

Prior to translation initiation, eIF3 binds to the 40S ribosomal subunit and contributes to the rate of association of the 40S and 60S subunits (Sonenberg & Hinnebusch, 2009). This allows the 40S ribosomal subunit to bind to eIF1A and the ternary complex, eukaryotic initiation factor 2 (eIF2)-GTP-methionyl tRNAi (eIF2-GTP-Met tRNAi). Additional factors such as eIF5 and eIF1 join to form a multifactorial complex (MFC) and lead to the construction of the 43S pre-initiation complex (43S PIC). The 43S PIC then binds to the mRNA, together with the cap-binding complex eIF4F (eIF4E, eIF4G and eIF4A) at the 5’end of the mRNA (Ruggero, 2013).

Circularisation of the mRNA occurs when eIF4G binds to poly(A)-binding protein PABP, bringing together the 5’ and 3’ ends of the mRNA (Wells et al., 1998). eIF4B also binds to PABP (Bushell et al., 2001). eIF4G contains a binding site for eIF3, specifically interacting with the eIF3c, eIF3d, and eIF3e subunits, which also circularises the mRNA (Villa et al., 2013). Upon recognition of the correct start codon by ribosomal scanning, eIF5, a GTPase activating protein, induces the hydrolysis of eIF2-GTP. This triggers its release from the 48S complex along with other eIFs (Das & Maitra, 2001).

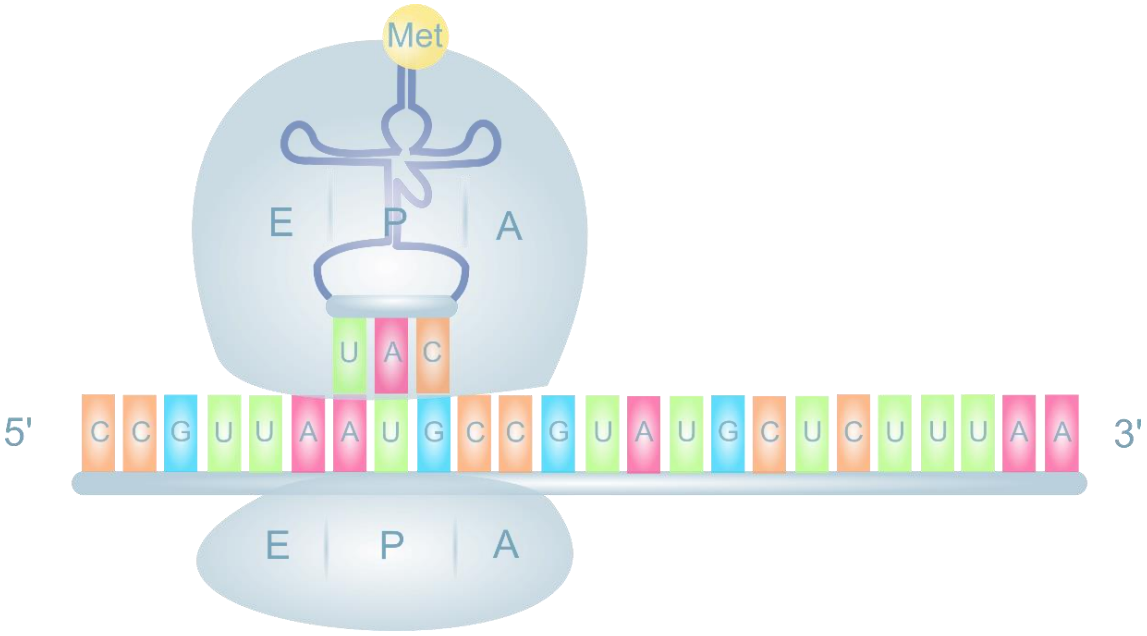

Figure 1-1. The large ribosomal subunit binds to the complex causing the release of initiation factors. The A (amino acid) site is where the aminoacyl-tRNA anticodon base pairs with the mRNA codon. The P (polypeptide) site holds the amino acid which is transferred from the tRNA to the growing polypeptide chain. The E (exit) site holds the tRNA without the amino acid, before it is subsequently released back into the cytoplasm. The elongation phase describes the process of the ribosome translocating from one codon to the next along the mRNA molecule in a 5' to 3' direction. The charged tRNA molecule that occupies the A site is shifted to the P site, where it is added to the growing polypeptide chain. The "empty" A site receives the next charged tRNA molecule and the process repeats itself until all of the codons in the mRNA have been read by the tRNA molecules. Termination occurs when a termination codon (UAA, UAG or UGA) is found in the protein-coding sequence. Adapted from Clancy & Brown, 2008.

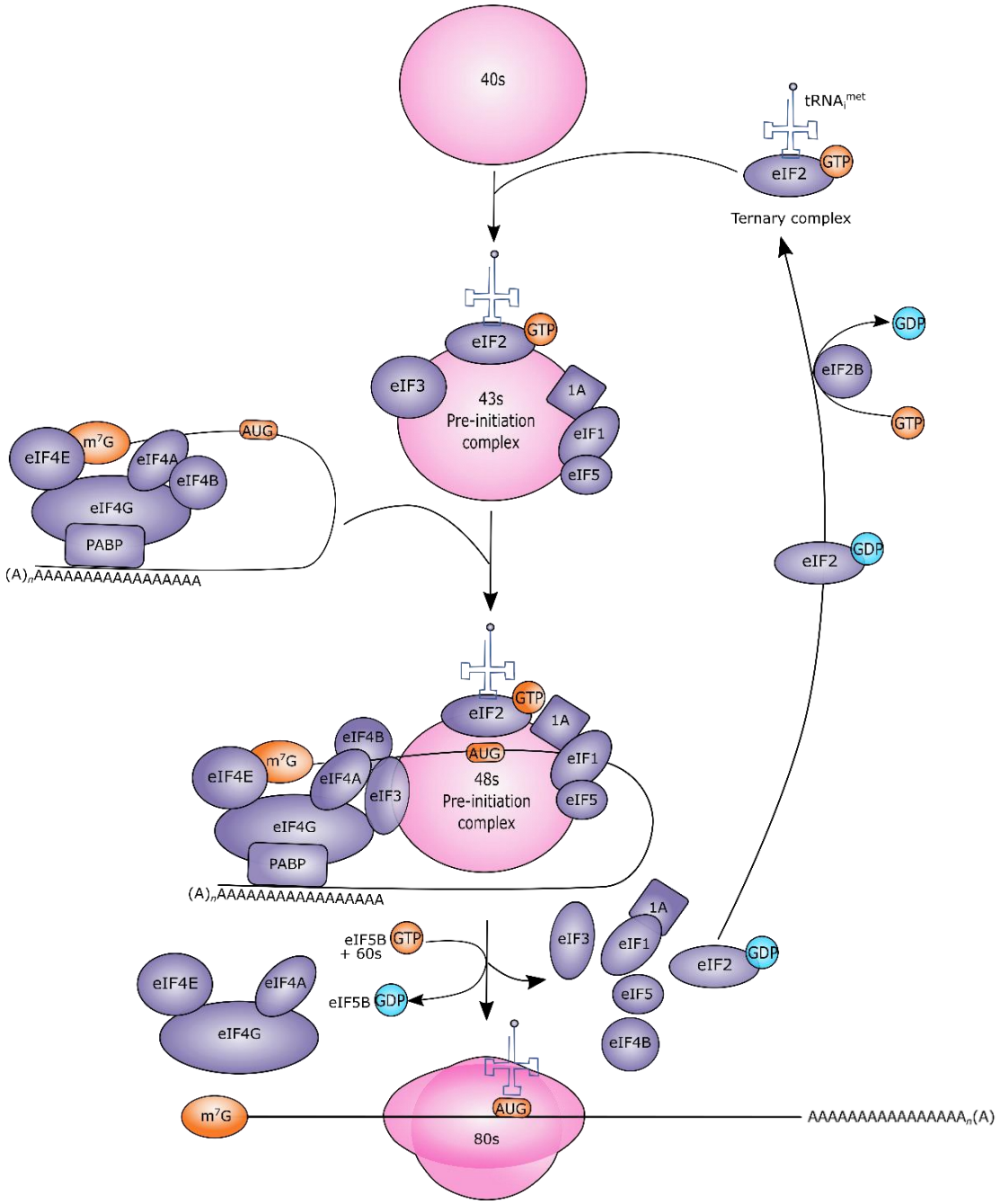

Figure 1-2. Eukaryotic cap-dependent translation initiation. Eukaryotic initiation factors (eIFs) such as eIF1, eIF1A and eIF3 form a 43S pre-initiation complex (PIC), together with the ternary complex (eIF2-GTP-Met tRNAi), and the 40S subunit. After binding of the ternary complex to the 40S subunit, eIF5 interacts with eIF2. The mRNA is activated by the binding of the eIF4F complex (eIF4A, eIF4E and eIF4G) to the cap and PABP to the poly(A) tail, circularising the mRNA. The interaction of eIF3/eIF5 with eIF4G facilitates the binding of the 43S PIC near the cap, forming the 48S initiation complex. This 48S initiation complex scans the 5'leader for the AUG codon in an ATP-dependent reaction, partial hydrolysis of eIF2-GTP to eIF2-GDP also occurs. Upon start codon recognition, eIF1/eIF1A dissociates, allowing the release of eIF2-GDP +Pi. The joining of the 60S ribosomal subunit is promoted by eIF5B, along

with the release of other eIFs to yield the final 80S initiation complex and translation can then begin. eIF2B, a guanine nucleotide exchange factor, converts the inactive eIF2-GDP to the active eIF2-GTP allowing the ternary complex to be reformed.

Initiation Factor	Subunits	Function
eIF1	Monomer	Necessary for scanning and involved in initiation site selection. Promotes the assembly of 48S ribosomal complexes at the initiation codon.
eIF1A	Monomer	Required for maximal rate of protein biosynthesis. Enhances ribosome dissociation into subunits and stabilises the binding of the initiator Met-tRNA to 40S ribosomal subunits.
eIF2	α, β, γ	Functions in the early steps of protein synthesis by forming a ternary complex with GTP and initiator tRNA.
eIF2B	α, β, γ, δ, ε	Catalyses the exchange of eIF2-bound GDP for GTP.
eIF3	Multimeric	RNA-binding component of the eIF3 complex, which is required for several steps in translation initiation. The eIF3 complex associates with the 40S ribosome and facilitates the recruitment of eIF1, eIF1A, eIF2-GTP-methionyl-tRNAi and eIF5 to form the 43S pre-initiation complex (43S PIC).
eIF4A	Trimer	ATP-dependent RNA helicase, which is a subunit of the eIF4F complex. Involved in cap recognition and required for mRNA binding to the ribosome. eIF4A unwinds RNA secondary structures in the 5'-UTR of mRNAs which is necessary to allow efficient binding of the small ribosomal subunit, and subsequent scanning.
eIF4B	Monomer	Required for the binding of mRNA to ribosomes. A subunit of the eIF4F complex and functions in close association with eIF4A. Binds near the 5'-terminal cap of mRNA and promotes the ATPase activity and the ATP-dependent RNA unwinding activity of eIF4A.
eIF4E	Monomer	Recognises and binds the 7-methylguanosine mRNA cap during translation initiation and facilitates ribosome binding by inducing the unwinding of the mRNAs secondary structures. Component of the CYFIP1-eIF4E-FMRP1 complex which binds to the mRNA cap and mediates translational repression.
eIF4E2	Monomer	Recognises and binds the 7-methylguanosine-containing mRNA cap during an early step in the initiation. Acts as a repressor of translation initiation. In contrast to eIF4E, it is unable to bind eIF4G (eIF4G1, eIF4G2 or eIF4G3), suggesting that it acts by competing with eIF4E and block assembly of eIF4F at the cap.
eIF4G1	Monomer	Component of eIF4F complex. It is a multi-domain phosphoprotein that contains binding sites for eIF4E, eIF4A, MNK1/2 and poly(A)-binding protein (PABP).
eIF4G2	Monomer	Appears to play a role in the switch from cap-dependent to IRES-mediated translation during mitosis, apoptosis and viral infection.
eIF4G3	Monomer	Probable component of the eIF4F complex and thought to be a functional homolog of eIF4G1.
eIF4H	Monomer	Stimulates the RNA helicase activity of eIF4A in the translation initiation complex.
eIF5	Monomer	Catalyses the hydrolysis of GTP bound to the 40S ribosomal initiation complex, with the subsequent joining of a 60S ribosomal subunit.
eIF5B	Monomer	GTPase that catalyses the joining of the 40S and 60S subunits to form the 80S initiation complex, with the initiator methionine-tRNA in the P-site.
eIF6	Monomer	Binds to the 60S ribosomal subunit and prevents its association with the 40S ribosomal subunit to form the 80S initiation complex in the cytoplasm. Associates with pre-60S subunits in the nucleus and is involved in its nuclear export. Involved in miRNA-mediated gene silencing by the RNA-induced silencing complex (RISC).

Table 1-1. Initiation factors and their role in translation. Data compiled using the UniProt database (www.uniprot.org/).

eIF2B, a guanine nucleotide exchange factor, recycles eIF2-GDP back to its active form, eIF2-GTP (Webb & Proud, 1997). The formation of the 80S ribosomal complex is promoted by the dissociation of these factors and eIF5B, which regulates the association of the 40S and 60S ribosomal subunits (Pestova et al., 2000). The process of peptide bond synthesis can then begin (Klann & Dever, 2004, Sonenberg & Hinnebusch, 2009).

1.1.1.1 The Roles of Specific eIFs

eIF1 is a highly conserved protein that plays several roles in the regulation of translation initiation (Nanda et al., 2009). eIF1 cooperates with eIF1A in the MFC to promote ribosome scanning by stabilising the open conformation of the PIC, allowing the mRNA to pass through the complex (Passmore et al., 2007). Upon AUG codon recognition, eIF1 dissociates from the complex triggering a conformational change from an open form to a closed formation (Maag et al., 2005). The dissociation of eIF1 is necessary to elicit downstream events in translation initiation, including the release of phosphate from eIF2 (Nanda et al., 2009). Mutations in eIF1 weaken the binding of eIF1 to the PIC, leading to the release of eIF1 at non-cognate AUG codons, and alternative initiation codon selection (Nanda et al., 2009).

eIF3 is the largest of the translation initiation factors and is composed of 13 subunits (eIF3a-eIF3m) (Cate, 2017). Cryo-EM reconstructions have shown that eIF3 has a five-lobed structure, with highly flexible regions outside of its core (Querol-Audi et al., 2013, Siridechadilok et al., 2005) (Figure 1-3A). Genetic evidence has revealed multiple roles for eIF3. eIF3 wraps around the 40S subunit, preventing its association with the 60S subunit and also forms a scaffold for the assembly of other translation initiation factors (Figure 1-3B). In addition to its role in canonical cap-dependent translation, eIF3 also drives specialised translation (Lee et al., 2015). Recent work has discovered a novel translation pathway driven by the interaction of eIF3 with an internal RNA stem loop structure in a subset of mRNAs (Lee et al., 2016). eIF3 was found to both activate and repress translation in a transcript-specific manner, through the direct binding of a RNA stem loop in the 5’UTR (Lee et al., 2015).

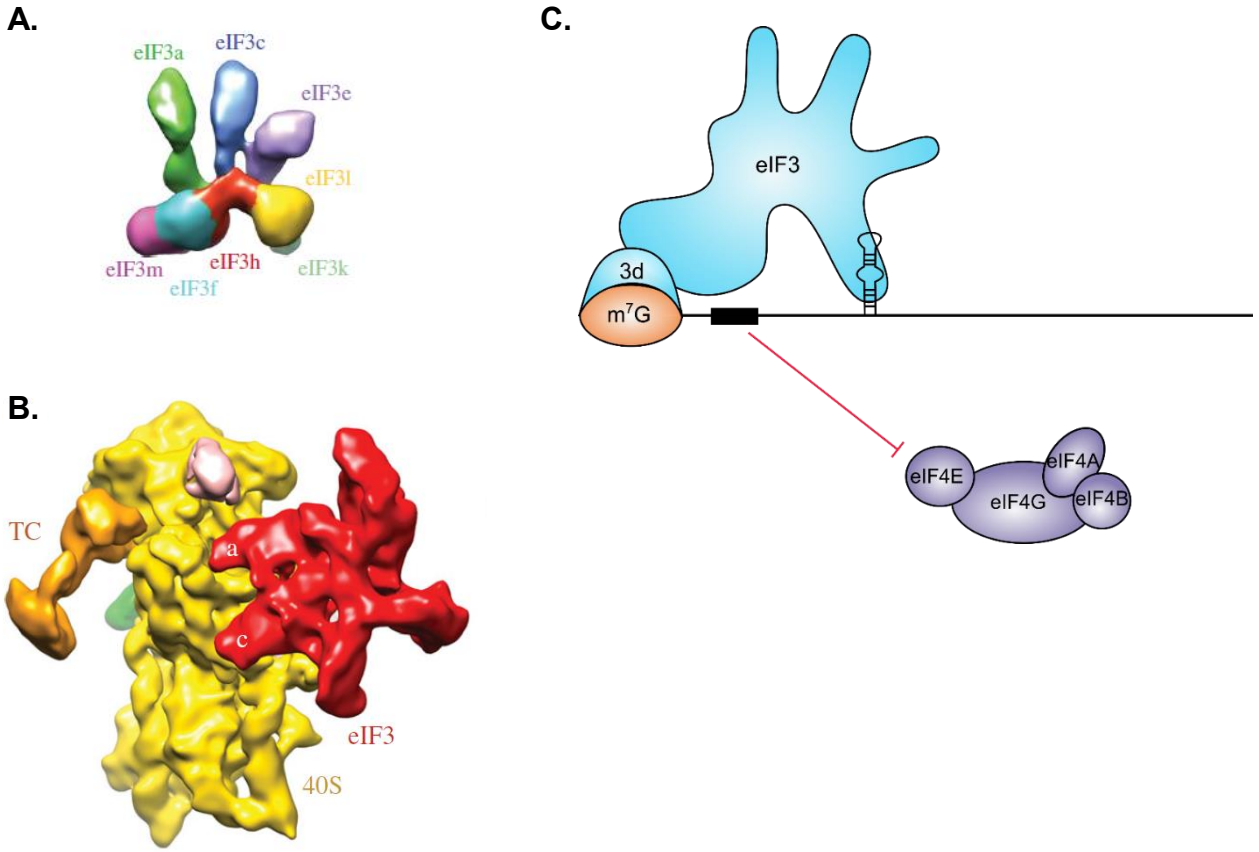

Figure 1-3. The structure and roles of eIF3. A. Cryo-EM reconstruction of the core subunits of human eIF3 taken from Querol-Audi et al., 2013. **B.** eIF3 (red) binds to the 40S ribosomal subunit (yellow). The ternary complex (TC) is also bound to the 40S subunit, forming the 43S pre-initiation complex. Taken from Cate, 2017. **C.** Mechanism of eIF3 binding to the m^7GTP cap of c-jun mRNA. Adapted from Lee et al., 2016. The eIF3d subunit of eIF3 binds to the m^7GTP cap to promote translation, following the recruitment of eIF3 to the stem loop in the 5'UTR of c-jun mRNA. An RNA element in the 5'UTR also prevents eIF4F recruitment to the m^7GTP cap of c-jun mRNA.

For example, the translation of c-jun mRNA is activated by the recruitment of eIF3 to the 5'UTR. The eIF3d subunit recognises and binds to the cap (m^7GTP) on the mRNA (Figure 1-3C). This mechanism allows specific mRNAs to be translated in conditions where eIF4F complex components are sparse. Interestingly, c-jun mRNA translation initiation complexes are depleted of the eIF4F complex and it has been hypothesised that c-jun mRNA contains an RNA element which blocks the recruitment of eIF4F (Lee et al., 2016). Additionally, eIF3 has been shown to directly bind to mRNAs containing N^6-methyladenosine (m^6A) in their 5'UTR. This post-translational modification is abundant under conditions of cell stress. The binding of eIF3 to m^6A recruits the 43S pre-initiation complex, promoting translation of the mRNA in the absence of eIF4E (Meyer et al., 2015).

eIF4E recognises the 5'cap necessary for the start of cap-dependent translation initiation. Structural studies of eIF4E in complex with m^7GTP/m^7GpppA have elucidated a well conserved core structure of eIF4E, with highly flexible N- and C-terminal regions (Tomoo et al., 2002). Model studies by Ishida et al (1998) showed that the m^7G moiety of the cap structure is sandwiched between the two aromatic side chains of Trp56 and Trp102 (Figure 1-4) (Ishida et al., 1988, Ishida et al., 1991). Two hydrogen bonds between the cap m^7G amines and the oxygen in the carboxy group of Glu103 stabilise the stacking interaction. The first and second phosphate groups of the m^7GpppA complex form direct or water-mediated hydrogen bonds with basic amino acids situated in the cap-binding pocket (Arg112, Arg157 and Lys162). The third phosphate group of the m^7GpppA complex forms a water-mediated hydrogen bond with the side chain of Arg112. The adenosine nucleoside of the m^7GpppA complex is located in the C-terminal loop region of eIF4E, and forms water-mediated hydrogen bonds with Thr205 and Thr211. Van der Waals forces between the adenosine and Ser207 (and neighbouring residues) stabilise the interaction (Tomoo et al., 2002). The adenosine is thought to be important for regulating the flexibility and orientation of the C-terminal loop region.

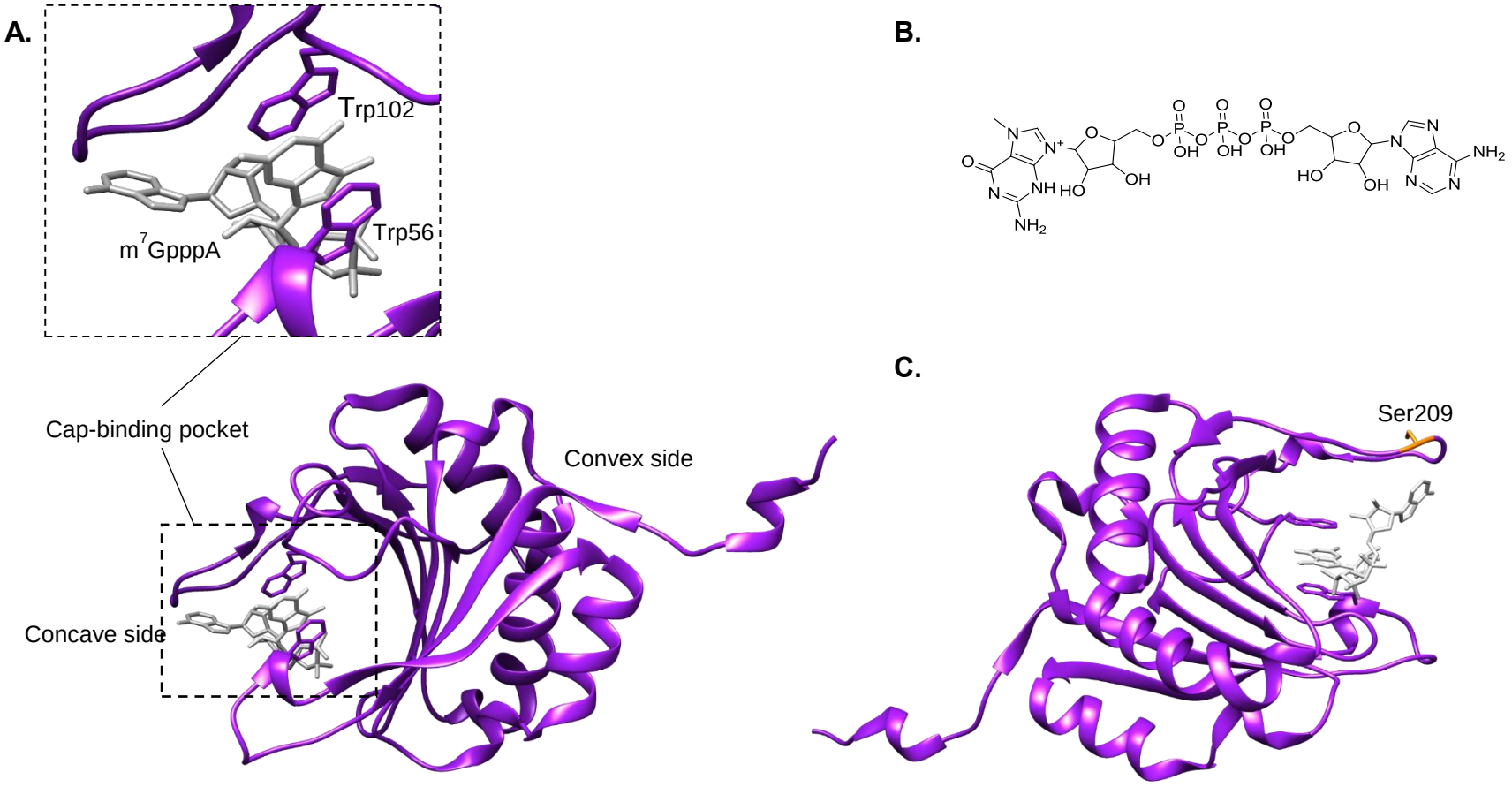

Figure 1-4. eIF4E in complex with m^{7}GpppA (PDB code: 1IPB). A. The m^{7}G moiety of the cap structure (grey) is sandwiched between the two aromatic side chains of Trp56 and Trp102 (purple). **B.** Structure of the m^{7}GpppA. The 5′ guanosine is methylated at the N7 position and is linked to the first nucleoside of the mRNA chain, adenosine, *via* an inverted 5′-5′ triphosphate bridge. **C.** eIF4E in complex with m^{7}GpppA showing Ser209 orientated away from the cap-binding region. Molecular graphics and analyses were performed with the UCSF Chimera package (Pettersen et al., 2004).

Biophysical studies on eIF4E-m^{7}GTP complex suggest a probable two-step mechanism for binding. The negatively charged phosphate groups in the cap are thought to act as a molecular anchor, interacting with the basic residues of the cap-binding pocket, enabling the further formation of intermolecular interactions (Niedzwiecka et al., 2002). It has been reported previously, that the formation of a competent interaction between the cap and the protein results from the recruitment of water molecules in the binding interface (Niedzwiecka et al., 2002). These water molecules are thought to be critical in the selectivity of the mRNA cap analogues (Lama et al., 2017).

The structure of eIF4E resembles a cupped hand; the concave surface of eIF4E binds to the cap and the convex surface interacts with eIF4G (Morley et al., 2005, Tomoo et al., 2002). Crystal structures of eIF4E in complex with eIF4G revealed an extensive, conserved eIF4E-eIF4G interface (Gruner et al., 2016). eIF4G was observed binding to the lateral surface of eIF4E in addition to the known dorsal aspect. The availability of eIF4E is regulated by eIF4E binding proteins (4E-BPs); these are discussed in detail below (Section 1.1.5.1) (Sonenberg & Dever, 2003, Sonenberg & Hinnebusch, 2009, Van Der Kelen et al., 2009). Both eIF4G and 4E-BPs compete for eIF4E binding, and the lateral surface of eIF4E is no longer exclusive to 4E-BPs (Gruner et al., 2016). This recent observation of an extended eIF4E-eIF4G interaction offers the opportunity to develop translational inhibitors with increased potency.

The presence of the cap structure on eukaryotic mRNA facilitates the recruitment of eukaryotic initiation factors to allow ribosome binding and initiation at the correct start site (Morley et al., 2005). eIF4G functions as a scaffold protein, necessary for the coordinated attachment of translation initiation machinery and the ribosome to the 5’end of the mRNA (Sonenberg & Hinnebusch, 2009). It is a multi-domain phosphoprotein that contains binding sites for eIF4E, eIF4A, MNK1/2 and poly(A)-binding protein (PABP) (Mamane et al., 2006).

1.1.1.2 DEAD-box Helicases

DEAD-box RNA helicases are ATP-dependent RNA-binding proteins, associated with the remodelling of RNA structures and RNA-protein complexes (Linder & Jankowsky, 2011). RNA helicases are characterised by two linked RecA-like domains (domains 1 and 2) that contain seven to eight conserved motifs (Figure 7.1), classified into superfamily 1 (SF1) or superfamily 2 (SF2) depending on their primary sequence (Soto-Rifo & Ohlmann, 2013). The DEAD-box family of helicases belong to the SF2 superfamily and typically have the sequence Asp-Glu-Ala-Asp (DEAD) in motif II (Fairman-Williams et al., 2010).

eIF4A, a member of the DEAD box RNA helicase family (Parsyan et al., 2011), is an abundant eIF and is present as part of the eIF4F complex. eIF4A is negatively regulated by pdcd4. The phosphorylation of pdcd4 by p70S6K results in its ubiquitination and subsequent degradation, permitting eIF4A to participate in the eIF4F complex (Yang et al., 2003). There are three isoforms of eIF4A; eIF4AI, eIF4AII and eIF4AIII. eIF4AI and eIF4AII have roles in protein synthesis, whereas eIF4AIII has been identified as a component of the exon junction complex (EJC) (Table 1-1) (Chan et al., 2004).

eIF4A is brought to the 5'end of the mRNA where it directly interacts with eIF4E. eIF4A possesses weak bidirectional RNA-dependent ATPase helicase activity, stimulated by eIF4B, eIF4F and eIF4H (Grifo et al., 1984, Richter-Cook et al., 1998, Rogers et al., 2001). Experiments showed ATP-dependent structural changes induced by the unwinding activity of eIF4A (Ray et al., 1985, Rozen et al., 1990). eIF4A resolves complex secondary structure in the 5' untranslated regions (UTR) and facilitates scanning of the 43 initiation complex. eIF4A has the ability resolve most 5'UTR regions. Although, it has been observed that additional helicases are required to support cap-dependent translation in the case of 5'UTRs with multiple stem loops and a highly complex structure (Heerma van Voss et al., 2017). DDX3, another DEAD box helicase has been found to have potent unwinding activity and is involved in facilitating translation initiation by resolving complex structures in the 5'UTR (Marsden et al., 2006). Secondary structures, such as G-quadruplexes were found to be significantly

higher among (proto) oncogenes than tumour suppressor genes. Cancer cells rely heavily on RNA helicases to meet increased protein demand. These oncogenes have a greater dependency on RNA helicase activity in order to be expressed (Eddy & Maizels, 2006, Pickering & Willis, 2005). DDX3 was found to be required for the translation of several oncogenes with complex 5'UTRs, including cyclin E1 (Lai et al., 2010) and RAC1 (Chen et al., 2015). There is evidence for several roles of DDX3 in translation, although the exact mechanisms are yet to be fully investigated (see Figure 1-5).

DDX3X is universally expressed in all tissues. Similar enzyme activity is observed with the *Saccharomyces cerevisiae* orthologue, Ded1p (Sharma & Jankowsky, 2014). DDX3X shares 92% sequence similarity with its human homologue, DDX3Y, which is specifically expressed in spermatocytes and associated with spermatogenesis (Ditton et al., 2004). Crystallographic studies of DDX3X have revealed a two-domain structure, with an N-terminal DEAD-box domain linked to a C-terminal helicase domain (Figure 1-6B and 1-7) (Hogbom et al., 2007). Sequence alignments have identified nine conserved motifs in the helicase core of DEAD-box proteins. Motifs Q, I (Walker A), II (Walker B) III, V and VI are involved in ATP binding and hydrolysis, whereas Motifs Ia, Ib, IV are involved in RNA binding (Figures 1-6B and 1-7) (Chang et al., 2006). A specific DDX3 insertion between motifs I and Ia was recently found to be important for RNA interaction (Figures 1-6B and 1-7) (Garbelli et al., 2011).

DDX3X demonstrates both nuclear and cytoplasmic function and recent work has identified DDX3X as a candidate for anti-viral therapy, due to its role in promoting viral replication (Garbelli et al., 2011). DDX3X is essential for the translation of HIV mRNA and was found to directly bind to the 5'UTR of HIV mRNA and interact with eIF4G and PABP. It was also observed that cytoplasmic DDX3X could be retained on an m^7GTP affinity matrix independently of eIF4E.

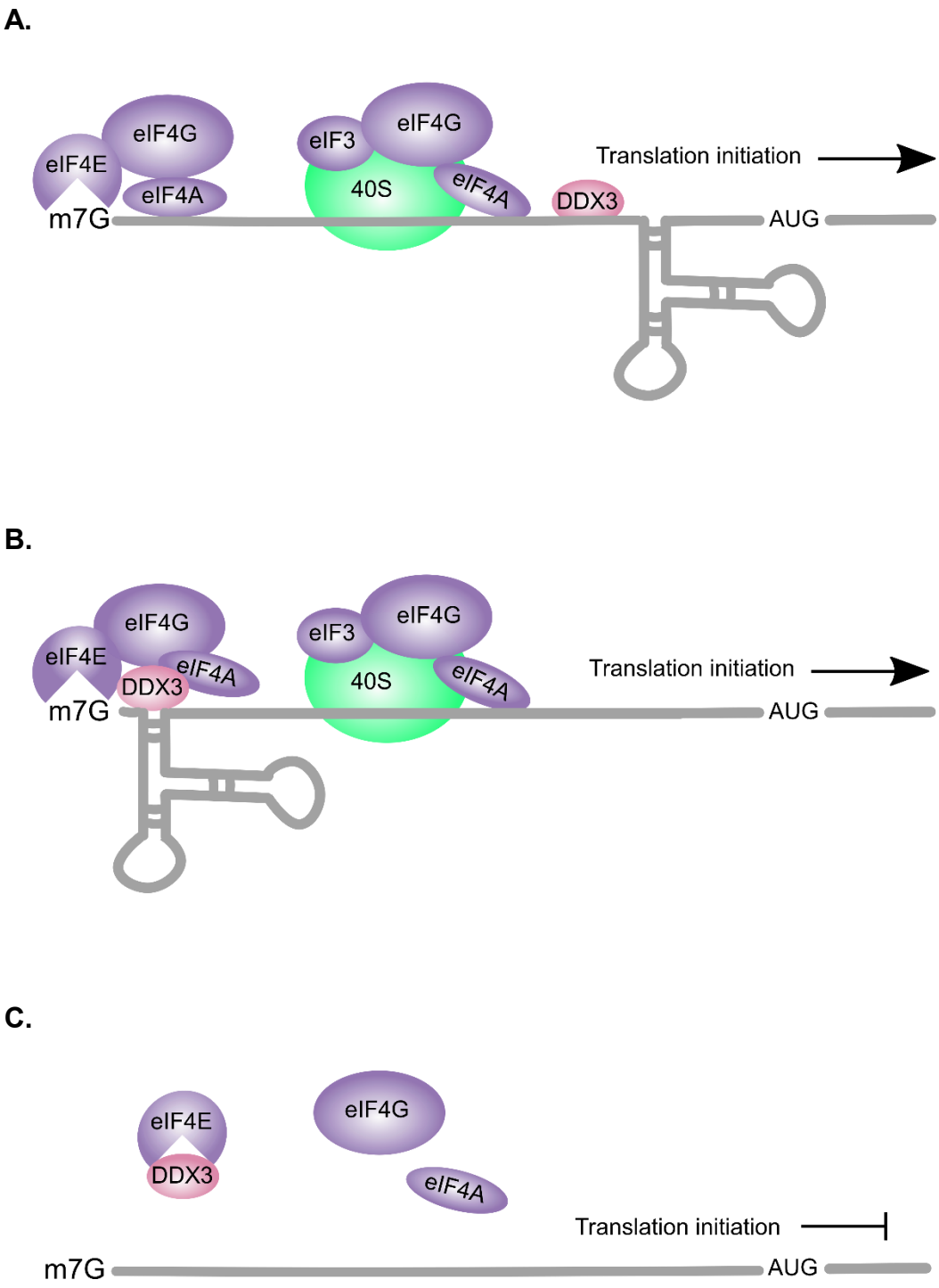

Figure 1-5. DDX3 mediates cap-dependent translation. A. DDX3 facilitates the translation of complex secondary structure in mRNAs such as cyclin E1 and RAC1. **B.** DDX3 resolves complex structures in mRNAs within the vicinity of the m^7GTP cap. **C.** DDX3 has an alternative role as a translational repressor through sequestration of eIF4E.

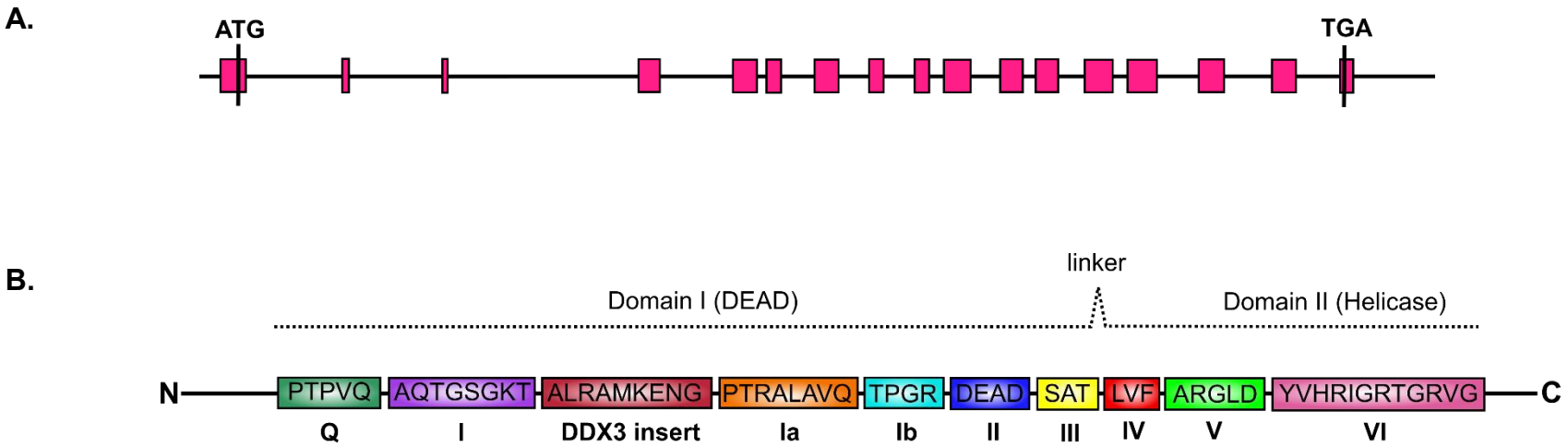

Figure 1-6. DDX3X gene and protein structure. A. Schematic representation of the DDX3X gene, with the 17 exons coloured in pink (not to scale). **B.** Schematic representation of the DDX3X protein showing the domain structure and conserved motifs.

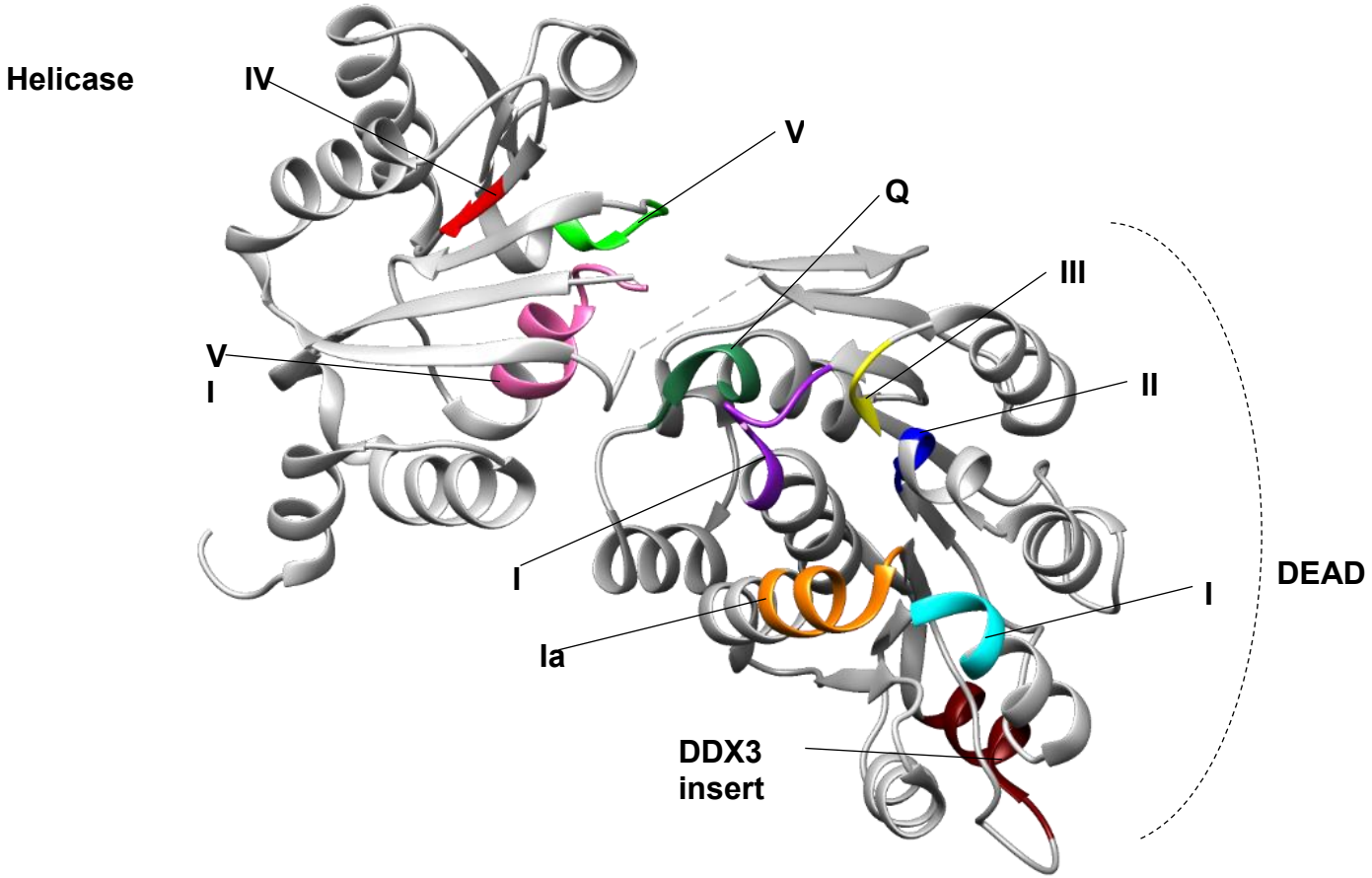

Figure 1-7. Overall structure of DDX3X showing the two domains and the consensus motifs (PDB: 2I4I). The disordered linker region is depicted by dashed lines connecting the helicase domain and DEAD domain.

This indicated that cytoplasmic DDX3X could assemble a pre-initiation complex on the HIV mRNA in the absence of eIF4E (Soto-Rifo et al., 2012, Soto-Rifo et al., 2013). The helicase activity of DDX3X has been proposed to enable the threading of HIV mRNA through the nuclear pore and into the cytoplasm, instigating a surge in the development of small molecule inhibitors which inhibit this interaction (Brai et al., 2016).

DDX3X has been reported to be involved in many cellular processes, including miRNA biogenesis, transcriptional control, mRNA splicing and export of mRNA from the nucleus (Botlagunta et al., 2008; Zhao et al., 2016; Garbelli et al., 2011; Soto-Rifo et al., 2013). However, one of the most extensively studied functions of DDX3X is in translational control. Direct interactions have been observed between DDX3X and eIF4E, and DDX3X and eIF4G (Shih et al., 2008, Soto-Rifo et al., 2012). As with 4E-BP1, DDX3X physically interacts with eIF4E and contains a consensus eIF4E-binding motif (YIPPHLR). DDX3X traps eIF4E in a translationally inactive complex by blocking interaction with eIF4G; in this context, DDX3X appears to have a tumour suppressor role (Shih et al., 2008). The role of DDX3X in translation appears to be heavily context dependent, reflecting its properties as both an oncogene and a tumour suppressor under different cellular conditions. DDX3X has been found to promote the translation of specific mRNAs containing highly structured sequences in their 5'UTRs, including cyclin E1, which facilitates G1/S transition and cell proliferation (Lai et al., 2008, Soto-Rifo et al., 2012). DDX3X also modulates efficient expression of RAC1, thereby regulating actin dynamics (Lai et al., 2010) and contributing to cell adhesion and motility (Gungabissoon et al., 2003). The oncogenic properties of DDX3X are further supported by its role in the inhibition of apoptosis. DDX3X blocks tumour necrosis factor-related apoptosis-inducing ligand (TRAIL) mediated apoptosis by associating with the TRAIL receptor 2 and prevents apoptotic signalling (Li et al., 2006, Sun et al., 2008). Overexpression of DDX3X in MCF10A cells also induces an epithelial-mesenchymal transition (EMT) and promotes an aggressive cellular phenotype (Botlagunta et al., 2008).

DDX3X is known to contribute to the formation of cytoplasmic stress granules (Chen et al., 2015), which sequester mRNAs in response to exogenous or endogenous stress and, with the exception of some stress-related mRNAs, halts their translation (Anderson et al., 2009; Shih et al., 2012) . It can also inhibit influenza viral mRNA translation by binding to eIF4E-viral mRNP complexes, trapping them in a translationally inactive state and thereby sequestering the eIF4E–viral mRNPs into stress granules (Buchan et al., 2009).

The role of DDX3X in cancer is controversial; DDX3X is a “double-edged sword” gene that can play a tumour suppressive or oncogenic role depending on the type of cancer (Zhao et al., 2016). DDX3X is frequently mutated in cancers such as chronic lymphocytic leukaemia (Ojha et al., 2015), lymphoma (Jiang et al., 2015), head and neck squamous cell carcinoma (Stransky et al., 2011), breast (Botlagunta et al., 2008) and lung cancer (Bol et al., 2015). It is also one of the most frequently amplified genes in prostate cancer (Xie et al., 2016). Whole exome sequence analysis identified DDX3X amplification in 22% of 114 cases of prostrate cancer (Beltran et al., 2016), where it has the ability to promote cell migration and metastasis

With so many potential regulatory roles in RNA metabolism, it is unsurprising that DDX3X has been a focus for the development of small molecule inhibitors. A ring-expanded nucleoside analogue (REN), NZ51, was originally trialled as an anti-viral agent for the treatment of HIV (Figure 1-8A). NZ51 was reported to inhibit DDX3X helicase activity and molecular modelling supported the hypothesis that NZ51 bound to the ATP-binding site of DDX3X (Xie et al., 2015). NZ51 was investigated as an anti-cancer compound *in vitro* and showed promising activity. However, when NZ51 was trialled in the mouse model it showed no reduction in tumour size in comparison to untreated mice (Xie et al., 2015). It is possible that structural features of NZ51 may be responsible for poor solubility and hence reduced distribution *in vivo*. More recently, a derivative of NZ51, with a third ring added to the 7-membered ring was synthesised. This tricyclic diimidazodiazepine analogue, termed RK-33 (Figure 1-8B), was reported to induce apoptosis, cause G1 cell cycle arrest, and also promote radiation sensitisation in DDX3X over-expressing cells. In addition, tumour

regression was demonstrated in pre-clinical mouse models when RK-33 was given in combination with radiation therapy (Bol et al., 2015).

A. **B.**

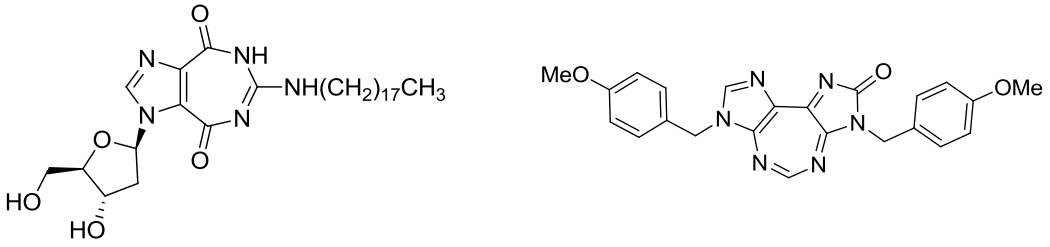

NZ51 **RK-33**

Figure 1-8. Chemical structures of DDX3X inhibitors. A. NZ51, **B.** RK-33.

1.1.1.3 Alternative Mechanisms for Cap-dependent Translation Initiation

In most eukaryotic mRNA's, translation is initiated at the first AUG codon nearest the 5'end. However, there are several alternative mechanisms for cap-dependent translation initiation. These include processes such as leaky scanning, termination re-initiation and ribosomal shunting.

Leaky scanning may occur if the first AUG codon is found in a suboptimal context. For example, the canonical scanning model states that the 40S ribosomal subunit recognises and binds to the first AUG codon that occurs in the Kozak sequence (Kozak, 1995). The Kozak sequence has the consensus sequence gccGCCACCAUGG, and forms a favourable context for the 40S ribosomal subunit to initiate at the AUG site (Kozak, 1987). However, mutations to critical positions in the consensus sequence provide a suboptimal context for initiation. This often leads to the 40S ribosome bypassing the first AUG codon and initiating at a downstream site (Kozak, 1989).

Termination re-initiation describes the process of ribosomal re-initiation at an internal downstream AUG codon, following termination of translation of an upstream reading frame. Ribosomes remain associated with the mRNA and are able to re-initiate downstream (Peabody & Berg, 1986).

Ribosomal shunting is an alternative mechanism of cap-dependent translation often employed by viruses. Ribosomes bind to the 5'cap and physically bypass parts of the 5'UTR to reach the initiator codon. This allows the translation of downstream open reading frames in polycistronic mRNAs (Pooggin & Ryabova, 2018). Ribosomal shunting supports the translation of specific mRNAs under conditions of stress, as it is less dependent on the scanning-mediated process mediated by eIF4F (Ryabova et al., 2002).

1.1.2 Cap-independent Translation Initiation

An alternate mode of translation initiation in eukaryotic cells bypasses the requirement for cap-dependent scanning. This allows the 40S ribosomal subunit to directly bind to sites on the mRNA, known as internal ribosome entry sites (IRES). The vast majority of IRES elements are located within the 5' UTR immediately upstream of the initiation codon (Komar & Hatzoglou, 2011).

Under normal cellular conditions the majority of mRNA translation initiation occurs by the cap-dependent mechanism, although cellular IRES support low levels of translation initiation of mRNAs containing cellular IRES with highly structured 5' UTR that are incompatible with efficient scanning (Komar & Hatzoglou, 2011). However, under a variety of physiological and stress conditions, cap-dependent translation is compromised and translation initiation occurs largely *via* an IRES element. Cellular IRES sequences offer a cell the flexibility to switch to cap-independent translation initiation. For example, hypoxia inhibits cap-dependent protein synthesis but leads to translation of growth factors that promote blood vessel formation, including IRES-driven proteins such as the alpha subunit of hypoxia-inducible factor-1 (HIF-1) and fibroblast growth factor 2 (Jackson, 2013, Niepmann, 2009).

In silico analyses estimates that up to 10% of cellular mRNAs may contain an IRES element. This allows their translation to be maintained under conditions in which cap-dependent translation is inhibited, such as mitosis or physiological stress (Spriggs et al., 2008). Cap-independent translation generally has a reduced requirement for canonical translation initiation factors, such as eIF4E and eIF4G. In contrast, IRES *trans*-acting factors (ITAFs) have been identified for their role in modulating internal initiation (Komar & Hatzoglou, 2011). Although their mechanism of action remains unclear, ITAFs have several roles in modulating the translation of IRES-containing mRNAs. They may act as RNA chaperones, by stabilising the secondary structure of the IRES or by recruiting other proteins to the IRES element (Stoneley & Willis, 2004). IRES elements have differing requirements for specific initiation factors and ITAFs. The activity of a given IRES is cell-line dependent, due to the difference in the availability of ITAFs. For example, the c-myc IRES was found to be 20-fold more active in HeLa cells than in MCF7 cells (Stoneley et al., 2000). One of the most studied ITAFs, polypyrimidine-tract-binding protein (PTB), is an RNA binding protein that is required for most IRESs to function. ITAFs such as PTB may be positive or negative regulators of IRES activity (Cho et al., 2005, Kim et al., 2000). ITAFs have also been implicated in cancer; mutated IRES elements can alter the binding affinity of ITAFs, which in turn can lead to the dysregulation of cellular processes (Cobbold et al., 2008, Cobbold et al., 2010).

1.1.3 eIF4E and its Role in Cancer

eIF4E is a critical component of the eIF4F complex (eIF4E, eIF4A and eIF4G) and the level of eIF4E expression is an important determinant in the translation of mRNAs (Truitt et al., 2015). Although translation initiation is considered to be the rate-limiting step of protein synthesis and the primary level of modulation, recent work has found that substantial regulation also occurs at the elongation stage (Faller et al., 2015, Truitt & Ruggero, 2017). Cellular mRNAs differ in the amount of eIF4E required for their translation, and protein homeostasis is achieved by maintaining the translation of essential mRNAs and limiting the translation of proto-oncogenes. eIF4E is a general translation factor but has the potential to selectively enhance the translation of mRNAs that lead to the

production of malignancy-associated proteins (Hou et al., 2012). In addition to its cap-binding ability, eIF4E possesses a second function in translation initiation by strongly stimulating eIF4A helicase function (Feoktistova et al., 2013). The generation of an eIF4E-haplo-insufficient mouse has challenged the dogma that eIF4E dose is limiting for normal development. Truitt et al (2015) found that a 50% reduction in eIF4E expression was compatible with regular development and global protein synthesis, revealing that eIF4E is present at levels exceeding those required for normal translational control. Interestingly, these mice were physiologically normal but resistant to neoplastic transformation. eIF4E appears to be limiting for the expression of oncogenic proteins and further enforces the importance of eIF4E in cancer development (Truitt et al., 2015, Truitt & Ruggero, 2017, Yanagiya et al., 2012).

The overexpression of eIF4E leads to an increase in the translation of a subset of mRNAs that favour oncogenesis, in particular those with highly structured 5’ UTRs (Graff et al., 2008). Housekeeping mRNAs, for example, those encoding cytoskeleton proteins, require a low level of eIF4E, whereas proto-oncogenic and pro-survival proteins such as c-myc, cyclin D1, PIM1, survivin, BCL-2, VEGF, fibroblast growth factor 2 (FGF-2) and matrix metalloprotease -9 (MMP-9) have a much higher dependency on eIF4E for translation (Grzmil et al., 2014, Lu et al., 2016). These mRNAs are termed “weak mRNAs” and are greatly influenced by an increase in eIF4E levels, observed in 30% of human cancers (Asimomytis et al., 2016, Feoktistova et al., 2013, Liu et al., 2016).

A study proposed the mechanism by which eIF4E promotes the translation of specific mRNAs is by increasing their cytoplasmic levels and therefore the capacity of these mRNAs to associate and form the eIF4F complex. eIF4E stimulates the nuclear transport of mRNAs housing an eIF4E-sensitivity element (4E-SE), a ~50 nucleotide structurally conserved element in the 3’ UTR. This structural motif was found to consist of two adjacent stem loop pairs (SLP) (Culjkovic et al., 2006). Notably, mRNAs containing this motif encode proteins associated with growth and malignancy (Thumma et al., 2015). For example, eIF4E promotes the nuclear export of cyclin D1 mRNAs *via* an element in the 3' UTR of the target mRNA (Culjkovic et al., 2005). It has been proposed that

either eIF4E by itself binds both the mRNA cap and 4E-SE or that some other factors mediate 4E-SE sensitivity in the nucleus. eIF4E also regulates the expression of E3 ubiquitin-protein ligase (MDM2), an important negative regulator of p53 by promoting the export of the mRNA encoding MDM2 into the cytoplasm in a MNK1-dependent manner (Garcia-Recio et al., 2016, Phillips & Blaydes, 2008).

The oncogenic potential of eIF4E has been recapitulated both *in vitro* and *in vivo.* A number of studies have found that high levels of eIF4E phosphorylation coincided with poor clinical outcome in human cancers (Bhat et al., 2015, Li et al., 2017, Mamane et al., 2007). One possible explanation for this is that the phosphorylation of eIF4E promotes expression of mesenchymal markers such as N-cadherin, fibronectin and vimentin, along with the acquisition of invasive properties (Robichaud et al., 2015). Additional studies found that eIF4E phosphorylation enhanced the nuclear export of cyclin D1 and Hdm2 mRNAs, subsequently increasing their concentration in the cytoplasm (Phillips & Blaydes, 2008, Topisirovic et al., 2004). It has been known for many years that overexpression of eIF4E leads to the transformation of immortalised murine fibroblasts and human epithelial cells in culture (Avdulov et al., 2004, Lazaris-Karatzas et al., 1990, Ruggero, 2013). In one study, eIF4E overexpression was associated with an increase in cyclin D1 expression and a subsequent rise in cell proliferation (Rosenwald et al., 1993). Multiple studies have shown a link between increased eIF4E availability and tumourigenesis (Graff et al., 2007, Ruggero et al., 2004, Wendel et al., 2004, Wendel et al., 2007). High levels of eIF4E expression were also shown to promote the aberrant expression of tumour related proteins by positively regulating the expression of VEGF in a head and neck squamous cell carcinoma (HNSCC) cell line. Low levels of eIF4E were found to downregulate VEGF and MMP-2 and MMP-9 simultaneously in colon cancer. MMP-2 promotes tumour invasiveness by degrading type IV collagen, a vital component of the basement membrane. The increase in expression frequency of eIF4E, VEGF-C, N-cadherin and MMP-2 was associated with the depth of tumour invasion, lymph node metastasis and clinical stage in colorectal cancer (Gao et al., 2016).

1.1.4 Mechanisms for Regulating Translation

Translational control of mRNA is critical for maintaining cellular homeostasis and for modulating rapid changes in the cellular concentrations of proteins. The majority of regulation occurs at the initiation stage of translation, summarised in Figure 1-9. Key mechanisms governing translation regulation include translational control *via* the cap-recognition process and a more selective process of translational control by microRNAs (miRNAs) (Sonenberg & Hinnebusch, 2009); reviewed in Eulalio (Eulalio et al., 2008).

1.1.4.1 eIF4E-4E-BP1

An extensively used mechanism to control the rate of translation initiation involves the mRNA 5′-cap recognition process by eIF4F. eIF4E-binding proteins (4E-BPs) inhibit the interaction between eIF4G and eIF4E in the eIF4F complex. 4E-BP1 competes with eIF4G for a shared binding site on eIF4E (Figure 1-10) (Peter et al., 2015). The interaction strength of 4E-BP1 binding to eIF4E depends on the phosphorylation status of 4E-BP1 (Merrick, 2015). Hypo-phosphorylated 4E-BP1 binds strongly to eIF4E whereas hyper-phosphorylated 4E-BP1 weakens its interaction with eIF4E (Gingras et al., 2001, Hsieh & Ruggero, 2010, Sonenberg & Hinnebusch, 2009, Van Der Kelen et al., 2009).

4E-BP1 contains at least seven sites of phosphorylation, of which four (T37, T46, S65, T70) are known to be regulated by mTORC1 and associated signalling pathways (Beugnet et al., 2003, Hsieh & Ruggero, 2010) (Figure 1-11). Activated mTORC1 remains at the mRNA 5’ cap where it can promote cap-dependent mRNA translation by phosphorylating and inactivating 4E-BP1, activating p70S6K and increasing overall protein synthesis by stimulating rRNA transcription and ribosome biogenesis (Laplante & Sabatini, 2012, Qin et al., 2016).

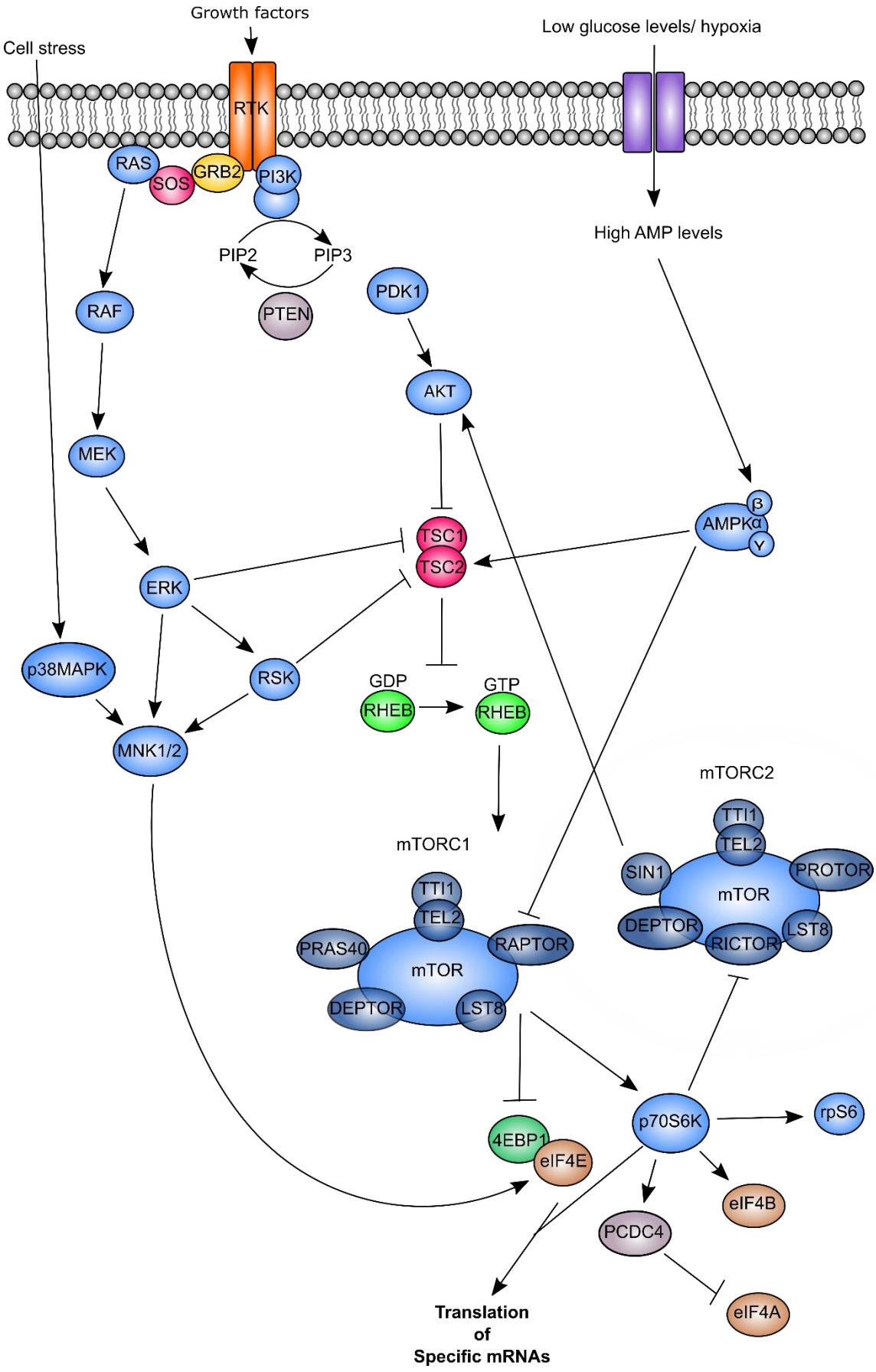
Growth factors
Cell stress
Low glucose levels/ hypoxia
RTK
RAS
SOS
GRB2
PI3K
PIP2
PIP3
PTEN
High AMP levels
PDK1
RAF
AKT
MEK
AMPKα
β
γ
TSC1
TSC2
ERK
p38MAPK
RSK
GDP
GTP
RHEB
RHEB
MNK1/2
mTORC2
mTORC1
TTI1
TEL2
SIN1
PROTOR
mTOR
DEPTOR
LST8
RICTOR
TTI1
TEL2
PRAS40
RAPTOR
mTOR
DEPTOR
LST8
4EBP1
eIF4E
p70S6K
rpS6
eIF4B
PCDC4
eIF4A
Translation
of
Specific mRNAs

Figure 1-9. Key components of major signalling pathways affecting protein translation. Growth factors bind to receptors including Receptor Tyrosine Kinases (RTKs) in the cell membrane, stimulating a cascade of signals. The activated RTK is phosphorylated on its tyrosine residues, GRB2 docks the phosphotyrosine residues via its SH2 domain and subsequently binds the guanine nucleotide exchange factor, SOS, by its SH3 domains. Activated SOS promotes the release of GDP from RAS, enabling the binding of GTP to form RAS-GTP. Activated RAS recruits RAF to the plasma membrane, where it phosphorylates and activates MEK1/2, which in turn activates ERK. ERK phosphorylates and activates many proteins including MNK1/2 and p90RSK. In addition, ERK phosphorylates and inactivates TSC2. MNK1/2 lie at the convergence point of both the p38MAPK pathway and ERK pathways and upon activation, phosphorylate eIF4E. Class I PI3 kinases are activated by RTKs resulting in the conversion of PIP2 to PIP3, a secondary messenger that is essential for AKT translocation to the plasma membrane. The level of PIP3 is negatively regulated by the tumour suppressor, PTEN. AKT is partially activated by PDK1 and becomes fully activated upon phosphorylation at Ser473, a process that can be catalysed by multiple proteins. mTOR forms two distinct multiprotein complexes, mTORC1 and mTORC2. mTORC1 comprises mTOR, regulatory-associated protein of mTOR (RAPTOR), mammalian lethal with SEC13 protein 8 (mLST8), DEP domain containing mTOR-interacting protein (DEPTOR), proline-rich AKT substrate 40kDa (PRAS40) and the TTI1/TEL2 complex. mTORC2 comprises mTOR, mammalian lethal with SEC13 protein 8 (mLST8), DEP domain containing mTOR-interacting protein (DEPTOR), the TTI1/TEL2 complex, rapamycin-insensitive companion of mTOR (RICTOR), mammalian stress-activated map kinase-interacting protein 1 (SIN1) and protein observed with RICTOR (PROTOR). In response to stimulation, activated AKT phosphorylates and inactivates the TSC1-TSC2 complex, which allows RHEB-GTP to activate mTORC1 on the lysosome. Activated mTORC1 complex stimulates protein translation by phosphorylating 4E-BP1 on several residues, releasing eIF4E allowing it to participate in translation initiation. In addition to phosphorylating other translational targets, mTORC1 also phosphorylates p70S6 kinase (p70S6K), which becomes fully activated following PDK1-mediated phosphorylation. p70S6K targets a number of proteins that control protein translation, including ribosomal protein S6, eIF4B and pdcd4. Low glucose levels and hypoxic conditions result in high AMP levels and lead to AMPK activation and subsequent mTORC1 inhibition. mTORC2 promotes cell survival through the phosphorylation of AKT on Ser473 and modulates the cytoskeleton following stimulation of cell growth.

A.

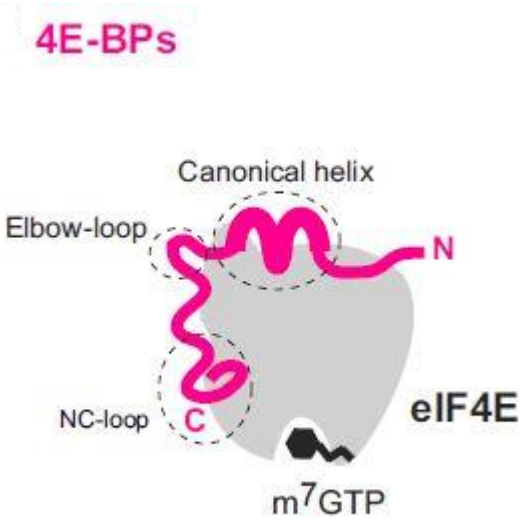

B.

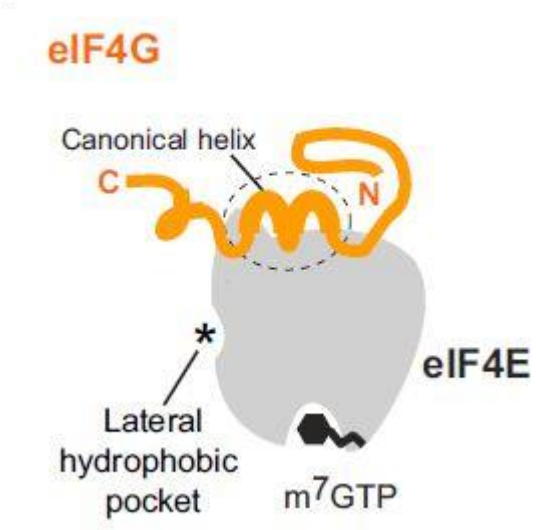

Figure 1-10. Schematic of eIF4E bound to 4E-BP1 and eIF4G. A. 4E-BP1 interacts with eIF4E through a conserved motif, termed the canonical 4E-binding motif. 4E-BP1 also contains non-canonical 4E-binding motifs that bind to the lateral surface of eIF4E (PDB: 4UED). **B.** eIF4G contains the canonical 4E-binding motif and competes with 4E-BP1 for binding to the same site on the dorsal surface of eIF4E (PDB: 4UEC). Taken from Peter et al., 2015.

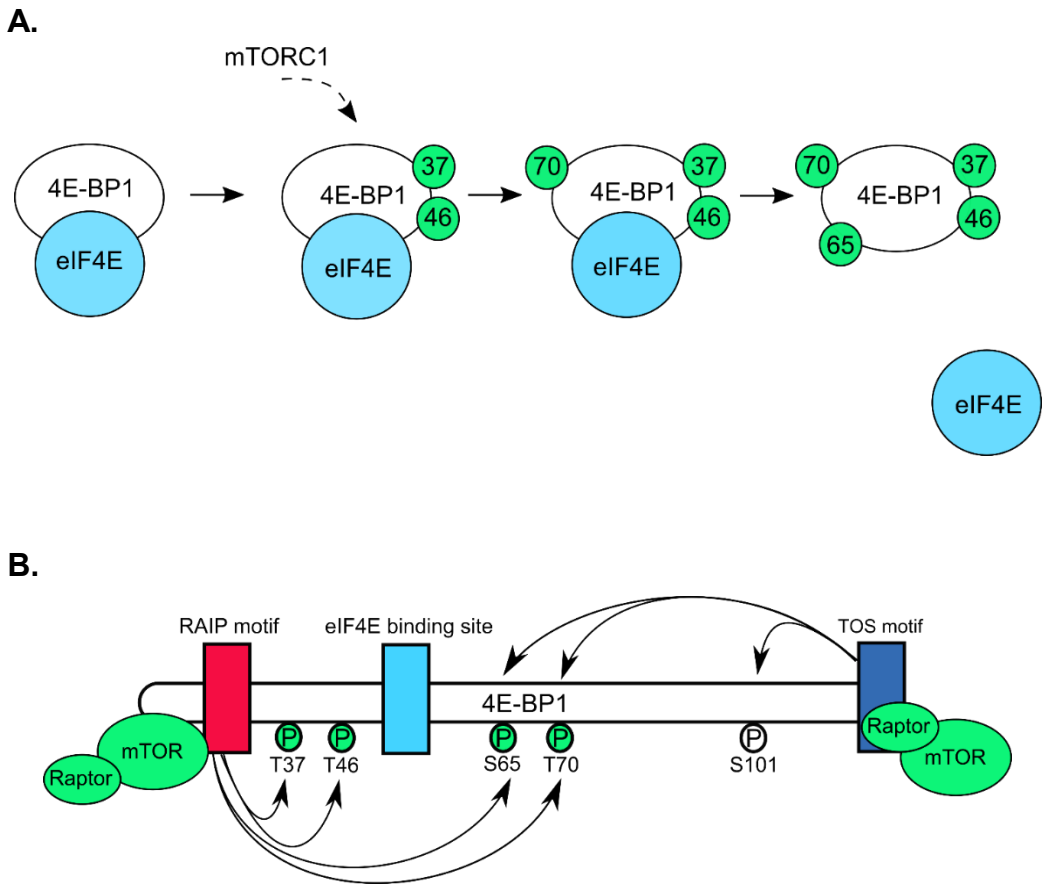

Figure 1-11. Schematic representation of the control of 4E-BP1 phosphorylation by growth factor-activated kinases. A. mTORC1 promotes the hierarchical phosphorylation of 4E-BP1. Hyper-phosphorylated 4E-BP1 is released from eIF4E, thereby allowing eIF4E to bind to eIF4G. **B.** The RAIP and TOS motifs present in 4E-BP1 are important for the phosphorylation of the protein. The N-terminal RAIP motif is required for the phosphorylation of T37, T46, S65 and T70, whereas the TOS motif binds to RAPTOR and regulates the phosphorylation of S65, T70 and the rapamycin in-sensitive S101 site (see text for details).

1.1.4.2 CYFIP1-FMRP

In addition to its role in cancer, translational control has also been implicated in neuropsychiatric disorders such as fragile X mental retardation (FMR) syndrome (Sonenberg & Hinnebusch, 2009) and autism (Bramham et al., 2016). This is caused by mutated or reduced expression of fragile X mental retardation protein (FMRP), an RNA-binding protein that normally inhibits the translation of specific mRNAs. The loss of FMRP results in excessive synaptic plasticity and has been linked to intellectual defects, anxiety and repetitive behaviours. FMR syndrome is the most frequent monogenic cause of autism (Bramham et al., 2016).

It has been reported that FMRP binds to eIF4E *via* CYFIP1 (cytoplasmic FMRP interacting protein 1), repressing the translation of specific mRNAs by displacing eIF4G (Figure 1-12) (Abekhoukh & Bardoni, 2014, Bramham et al., 2016, Napoli et al., 2008). CYFIP1 is best known for being a component of the Wiskott-Aldrich syndrome family Verprolin homologous proteins (WAVE) regulatory complex (WRC), which is involved in actin remodelling (Bramham et al., 2016). However, in the context of eIF4E, CYFIP1 acts as a translational repressor with binding surfaces overlapping that found in common with eIF4G and 4E-BP1 (Figure 1-10).

In recent work, the MNK proteins, which phosphorylate eIF4E, have been implicated in the regulation of the CYFIP1-FMRP translational repressor complex in neuronal cells (Genheden et al., 2015, Panja et al., 2014). MNK1 was found to be required for the activation of protein synthesis in response to brain-derived neutrophic factor (BDNF) and metabotropic glutamate receptor (mGluR) signalling in mouse cortical neurons (Genheden et al., 2015). MNK1 activation promoted the release of CYFIP1/ FMRP from eIF4E, allowing the formation of the eIF4F complex and the subsequent translation of mRNA (Genheden et al., 2015, Panja et al., 2014). However, it is not known whether this reflected a conformational change in eIF4E following phosphorylation on Ser209 or direct phosphorylation of CYFIP1/FMRP by MNK proteins.

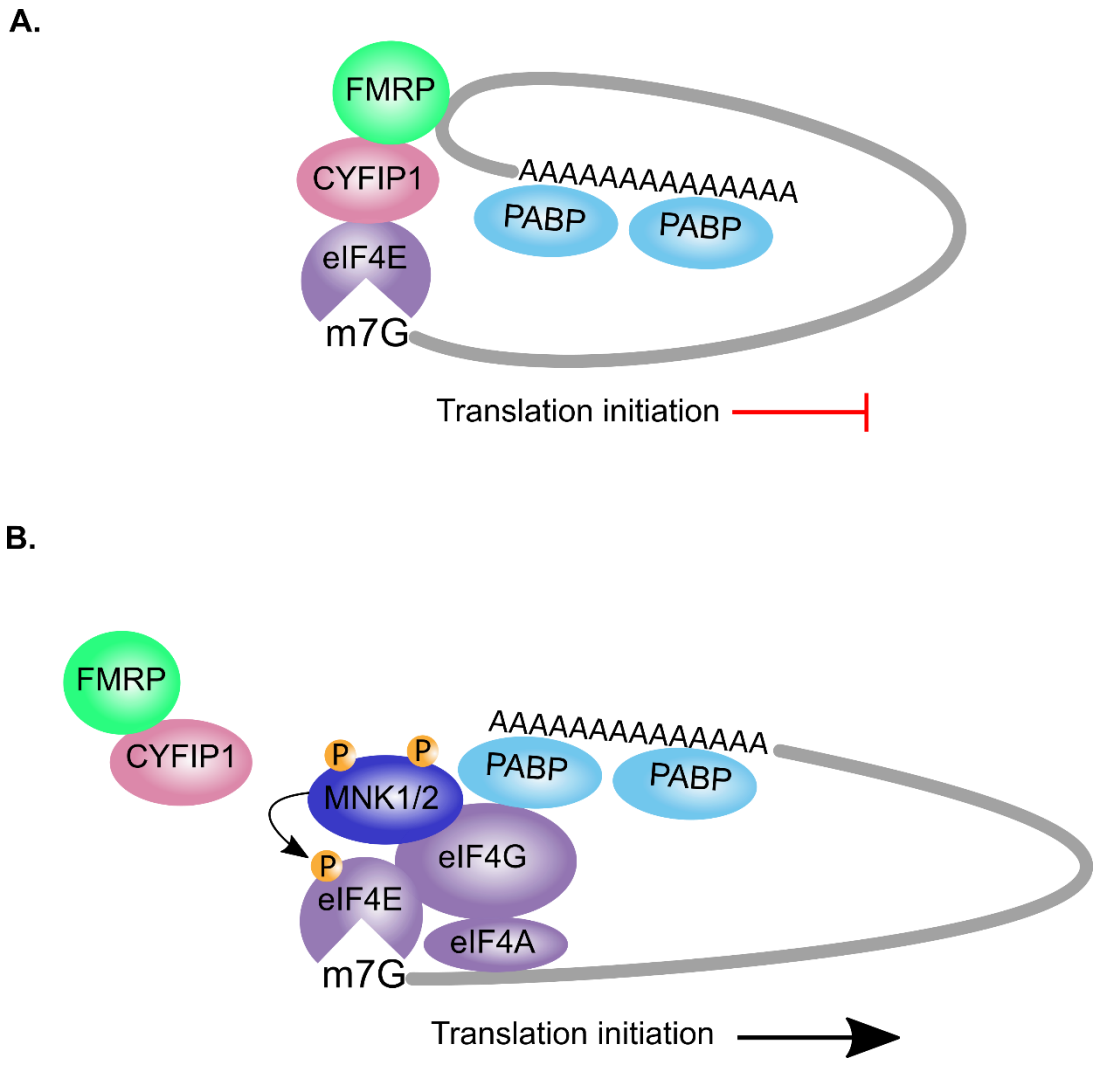

Figure 1-12. CYFIP1-FMRP translational repression. A. CYFIP1 in complex with FMRP binds to and inhibits the formation of the eIF4F complex and halts translation. **B.** MNK1/2 signalling phosphorylates eIF4E, stimulating the release of CYFIP1. eIF4E is free to participate in the eIF4F complex and translation begins (Adapted from Bramham et al., 2016).

1.1.4.3 eIF2

eIF2 is a multimeric protein complex consisting of three subunits termed α, β and γ. The smallest subunit, eIF2α, contains a phosphorylation site on Ser51; four different protein kinases can phosphorylate this specific site leading to the blockage of guanine nucleotide exchange (Pavitt & Ron, 2012). The four protein kinases; HRI, PKR, GCN2 and PERK all phosphorylate this residue and elicit the same response involving the down regulation of general translation and the translational induction of specific transcription factor mRNAs (Jackson et al., 2010, Wek, 2018). eIF2β contains phosphorylation sites for CK-II, PKC and PKA. The C-terminal portion contains a binding domain for the guanine nucleotide exchange factor, eIF2B. Both eIF5 and eIF2B compete for binding to eIF2β. eIF2B promotes eIF2 activity by exchanging GTP for GDP where as eIF5 functions as both a GAP (GTPase activating protein) and a GDI (guanine nucleotide exchange inhibitor) by preventing nucleotide exchange. eIF2γ binds GTP which is essential for binding Met-tRNAi to form the ternary complex (Hinnebusch & Lorsch, 2012, Pavitt & Ron, 2012).

eIF2/GTP localises Met-tRNAi to the multifactor complex associated with the 40S ribosomal subunit. As eIF2 is released from the ribosome as an eIF2/GDP complex, and eIF2 has a higher affinity for GDP than GTP, GDP bound to eIF2 must be exchanged for GTP (Hinnebusch, 2005). This reaction is catalysed by eIF2B which is present in cells in limiting amounts relative to eIF2 levels. Phosphorylation of Ser51 of eIF2α increases the binding affinity of eIF2B to eIF2 and eIF2-GDP acts as a competitive inhibitor of the guanine nucleotide exchange reaction. This leads to the formation of an inactive eIF2-eIF2B complex; as eIF2B is present in limited amounts compared to eIF2, no ternary complex is formed and translation initiation is inhibited (Hinnebusch & Lorsch, 2012, Pestova et al., 2001). Hence, a small increase in phosphorylation of eIF2α can have a large impact on protein synthesis initiation. For example, in amino acid starvation, free tRNAs accumulate, activating the kinase GCN2. GCN2 phosphorylates eIF2α, which inhibits the eIF2B-dependent GDP exchange and subsequent translation initiation (Harding et al., 2000, Hinnebusch, 2005).

1.2 The MAP Kinase-Interacting Kinases (MNKs)

1.2.1 Overview

The MAPK-interacting kinases 1 and 2 (MNKs) were first discovered in mice in 1997 (Waskiewicz et al., 1997). The MNKs are serine/threonine protein kinases that lie downstream of both p38MAPK and ERK pathways (Figure 1-6), which are often subject to upregulation in tumour cells (Hou et al., 2012). These upstream kinases activate mouse MNK1 *via* phosphorylation on Thr197/202 (Joshi & Platanias, 2014). The MNKs associate with the C-terminus of eIF4G, a vital interaction that brings the kinase into close enough proximity to phosphorylate eIF4E on Ser209 (Figure 1-4C) (Buxade et al., 2008, Mamane et al., 2006, Pyronnet et al., 1999). Serine/threonine-protein kinase PAK 2 (PAK2) can interfere with the MNK1/2-eIF4G interaction by phosphorylating the MNKs on specific threonine and serine residues resulting in decreased affinity for eIF4G (Orton et al., 2004). The phosphorylation of eIF4E enhances translation of specific mRNAs involved in cell survival (Beggs et al., 2015). A number of studies using a mouse lymphoma model have demonstrated that the phosphorylated form of eIF4E is required for the translation of a subset of mRNAs that oppose apoptosis and favour tumourigenesis (Bianchini et al., 2008, Feoktistova et al., 2013, Furic et al., 2010, Grzmil et al., 2011, Joshi & Platanias, 2014, Wendel et al., 2007). The role of the MNKs has now been linked to the pathogenesis of many cancers (Diab et al., 2016, Kosciuczuk et al., 2016).

1.2.2 Isoforms and Subcellular Distribution

There are four human MNK isoforms; each MNK gene produces both a long isoform and a short isoform through variation in splicing (Figure 1-13) (O'Loghlen et al., 2004, Slentz-Kesler et al., 2000). The N-termini of all four isoforms are similar; each one containing a nuclear localization signal (NLS) and an eIF4G-binding site. The central region houses a kinase domain (Hou et al., 2012). The C-terminal region of the isoforms differs; the longer isoforms

(MNK1a and MNK2a) contain a MAPK binding site, which is lacking in the shorter isoforms

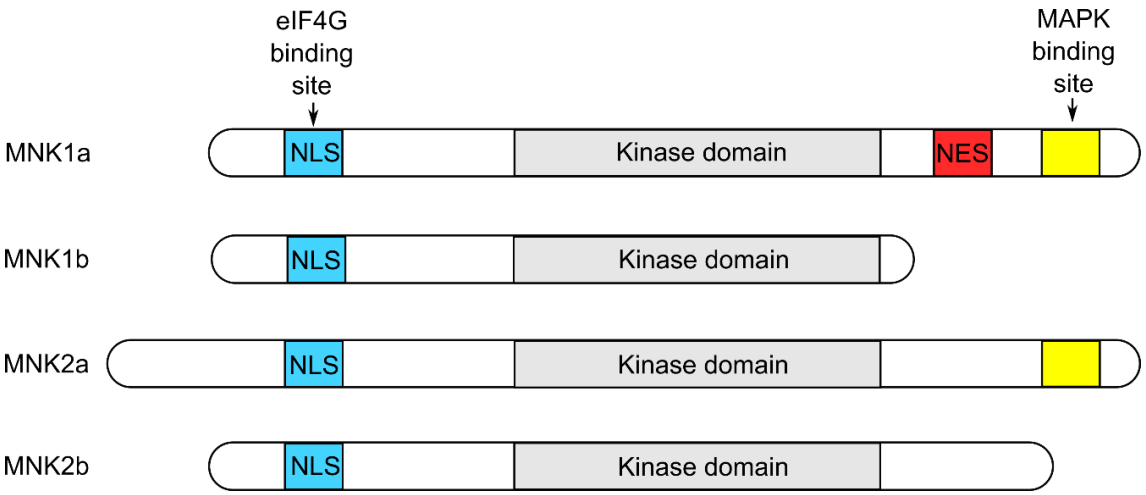

Figure 1-13. Schematic of the four human MNK isoforms. (NLS: nuclear localisation signal, NES: nuclear export signal).

(MNK1b and MNK2b) (O'Loghlen et al., 2004, Slentz-Kesler et al., 2000). The MNK1a MAPK binding domain interacts with both p38MAPK and ERK1/2, whereas the MNK2a MAPK-binding domain only binds to ERK1/2. This variation is reflected in a single amino acid change in the MAPK binding site and determines the difference observed in their regulation (Scheper et al., 2001). MNK1a has low basal activity, and is activated and tightly regulated by ERK and p38 kinases in response to mitogens and stress (Beggs et al., 2015, Ueda et al., 2004). MNK2 displays high basal activity and is predominantly regulated by ERK1/2, although MNK2a is regulated by mTORC1 through at least one site in its C-terminal region (Diab et al., 2014, Stead & Proud, 2013).

There is speculation as to why mammalian cells possess two kinases that perform the same function but show a variation in basal activity. Knockout mouse studies have revealed that MNK2 maintains a basal level of eIF4E phosphorylation under conditions of starvation, where MNK1 is inactive, and ensures the synthesis of housekeeping proteins. Data show that changes in the phosphorylation status of eIF4E in response to growth factors and stress are MNK1-dependent (Cargnello & Roux, 2011, Scheper et al., 2001, Ueda et al., 2004). MNK1a is primarily responsible for inducible activity as MNK1b lacks a MAPK binding site (O'Loghlen et al., 2004). The subcellular location of MNK isoforms likewise differs; MNK1 is predominantly localised in the cytoplasm. MNK1a contains a CRM1-dependent nuclear export signal (NES) in its C-terminus, allowing its transport to the cytoplasm (Parra-Palau et al., 2003). MNK1b lacks a nuclear export signal, and is localised both in the nucleus and cytoplasm. MNK2a and MNK2b are predominantly nuclear (Bramham et al., 2016, Garcia-Recio et al., 2016). MNK2b has been associated with eIF4E and nuclear bodies, implying that MNK2b is responsible for eIF4E phosphorylation in the nucleus (Scheper et al., 2003). Both MNK1 and MNK2 mRNAs have been found ubiquitously expressed in a variety of tissues by Northern blot analysis. Fan et al. (2016) recently observed a considerably higher percentage of active phospho-MNK in astrocytomas, further endorsing the role of active MNK in cancer (Fan et al., 2016, Scheper et al., 2001). High levels of phosphorylated MNK1 are also observed in HER-2 positive breast cancer and in glioblastoma multiforme primary tumours. Silencing of MNK1 through the transfection of a

U87MG glioma cell line with a small hairpin RNA attenuated eIF4E phosphorylation and reduced proliferation (Astanehe et al., 2012, Diab et al., 2014).

1.2.3 MNK Structure

The crystal structures of MNK1 and MNK2 are available in the DFD-out (Asp-Phe-Asp) conformation (Figure 1-14). Their catalytic domains share 78% sequence identity and the active sites are highly conserved (Beggs et al., 2015, Oyarzabal et al., 2010). MNK1 and MNK2 display the canonical bilobal arrangement of the ATP-binding cleft sandwiched in between the C-terminal and N-terminal lobes. The C-terminal lobe is predominantly α-helical and is composed of the activation segment, the P-loop and the catalytic loop; elements required for substrate binding and phosphate transfer. Kinase activation occurs when the activation loop is phosphorylated, resulting in a conformational change. The P-loop enables the optimal alignment of the phosphoryl groups of ATP, while the catalytic loop encompasses highly conserved residues vital for phosphotransfer. The N-terminal lobe comprises five β-strands and the regulatory αC-helix. The αC-helix is misaligned in inactive kinases and its correct alignment is required for ATP binding, and hence kinase activity (Kannan et al., 2015, Sebolt-Leopold & English, 2006). The conserved DFD motif marks the beginning of the activation loop (Hou, Teo et al., 2013, Kannan et al., 2015). The DFD motif (Asp191-Phe192-Asp193 in MNK1 and Asp226-Phe227-Asp228 in MNK2) has less affinity for ATP than the equivalent DFG motif present in other kinases. This is due to a 180° rotation relative to the DFG motif, which locks the kinase in the DFD-out conformation. This unique structure coupled with specific regions of the catalytic domain (insertions 1-3) distinguishes the MNKs from other kinases and provide an opportunity to design specific MNK inhibitors (Figure 1-15) (Di Tommaso et al., 2011, Hou et al., 2012, Jauch et al., 2005).

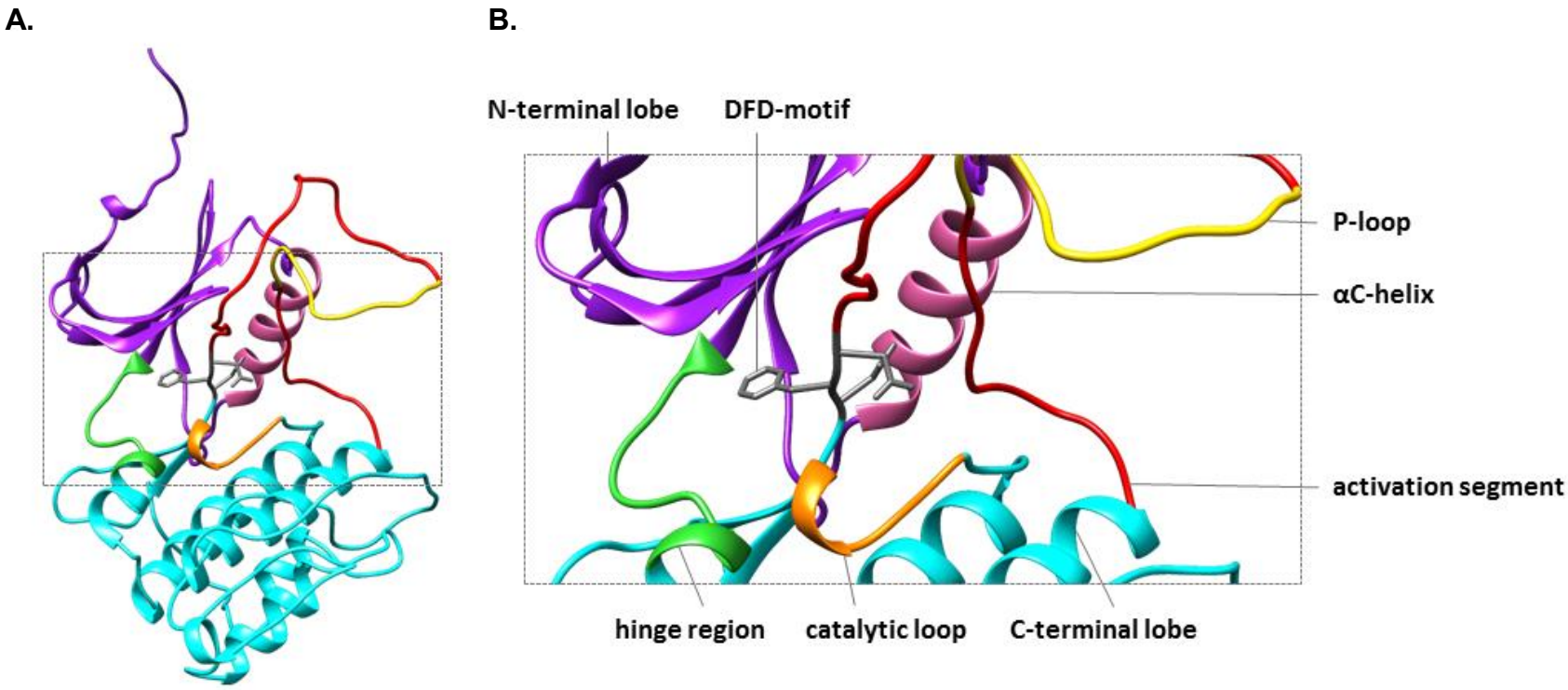

Figure 1-14. Apo-form of MNK1 in inactive conformation DFD-Out conformation (PDB ID: 2HW6). Structural elements coloured accordingly: N-terminal lobe (purple), C-terminal lobe (cyan), αC-helix (pink), hinge region (green), catalytic loop (orange), DFD-motif (grey), activation segment (red) and p-loop (gold). Auto-inhibition due to Phe230 in the activation segment pushing out Phe192 away from DFD towards the ATP binding site, obstructing the ATP binding pocket. Molecular graphics and analyses were performed with the UCSF (University of California) Chimera package (Pettersen et al., 2004).

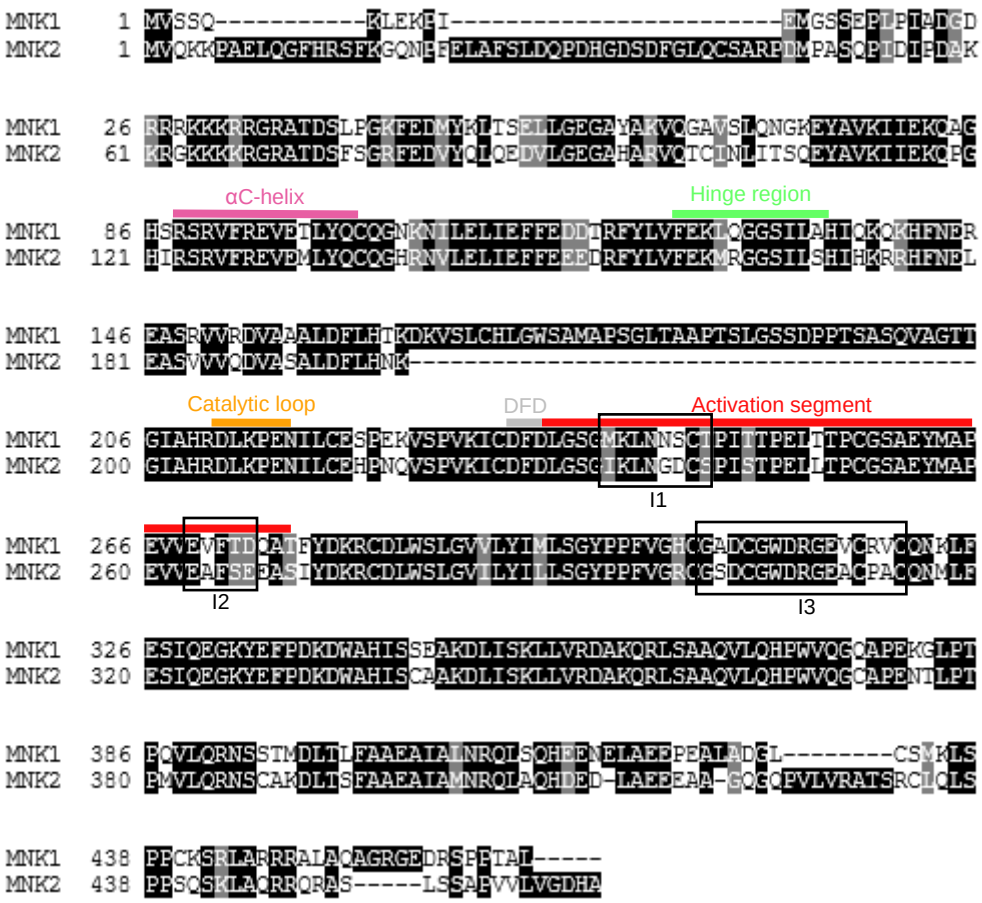

Figure 1-15. Multiple sequence alignment of MNK1 and MNK2. The alignment was made with T-Coffee (Tommaso et al., 2011) and edited manually. A darker background indicates a higher conservation. Functional elements are colour-coded and labelled: αC-helix- pink; hinge region- green; catalytic loop- orange; DFD motif- grey; activation segment- red. Insertions that are specific for MNKs (I1–I3) are outlined.

1.2.4 Regulation of MNK Activity

1.2.4.1 Upstream Signalling Pathways

The MNKs bind to eIF4G, which brings them into close enough proximity to phosphorylate eIF4E (Shveygert et al., 2010). The MNKs lie at the convergence point of major intracellular signalling pathways (Figure 1-9). Depending on the isoform, MNKs can be activated by either ERK1/2 or ERK1/2 and p38MAPK (Cargnello & Roux, 2011). In mammalian cells p38MAPK isoforms are activated by environmental stresses or inflammatory cytokines (Cuadrado & Nebreda, 2010). In addition activation can occur by the Rho family GTPases, RAC1 and CDC42, linked into cell architecture (Bagrodia et al., 1995).

1.2.4.1.1 RAS-RAF-MEK1/2-ERK1/2 Pathway

The RAS-RAF-MEK1/2-ERK1/2 pathway is a key intracellular pathway that regulates a breadth of cellular functions, including cell proliferation, cell survival and cell migration (Friday & Adjei, 2008). The importance of this pathway in numerous cellular processes and its implication in oncogenesis has made it a focus for therapeutic targeting. Multiple receptors are capable of activating the pathway, hence, a wide range of stimuli can initiate a cellular response. The canonical activation pathway is initiated by growth factors binding receptor tyrosine kinases at the cell surface and culminates in gene transcription in the nucleus (Yarden & Sliwkowski, 2001). Although the pathway is described as linear, considerable cross-talk occurs between numerous signalling cascades. The epidermal growth factor receptor (EGFR) pathway serves as a model for studying the RAS-RAF-MEK1/2-ERK1/2 signalling cascade, and is described below (Figure 1-16).

Epidermal growth factor binds to the extracellular domain of EGFR. A conformational change leads to the dimerisation of the receptor and subsequent autophosphorylation of specific tyrosine residues leads to activation of the intracellular tyrosine kinase (Zhang et al., 2006). Adaptor proteins such as GRB2 connect RAS to the tyrosine kinase receptor.

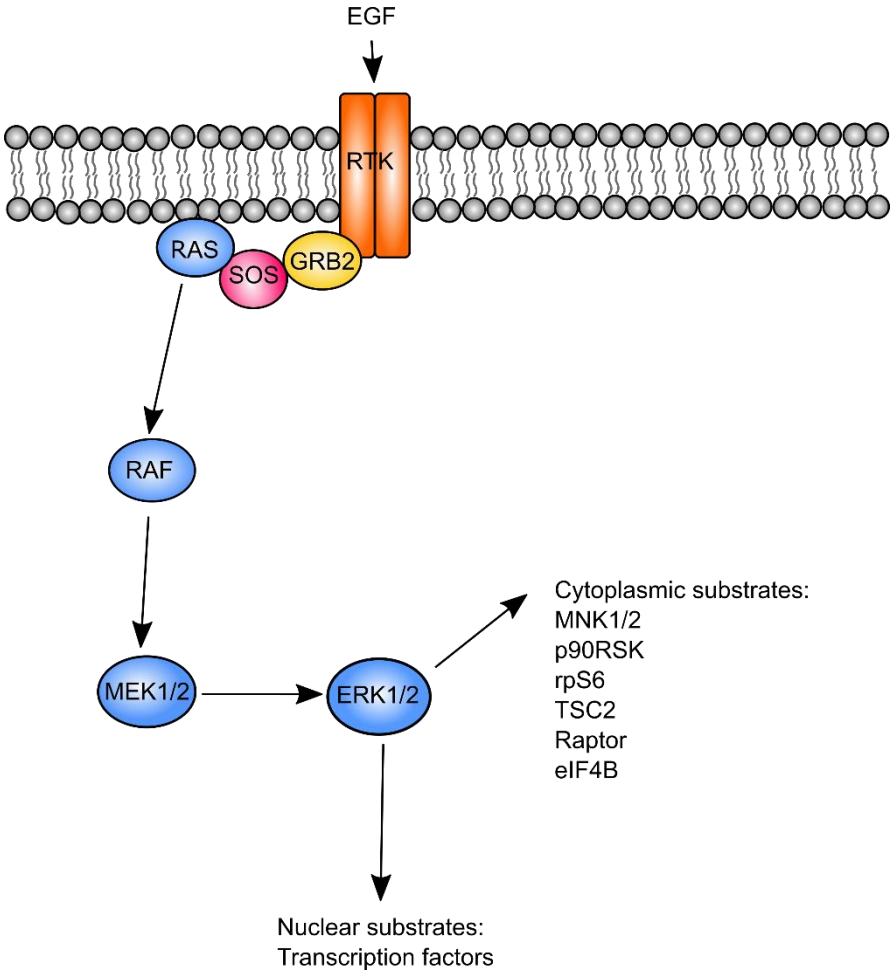

Figure 1-16. The RAS-RAF-MEK1/2-ERK1/2 pathway. Epidermal growth factor (EGF) binds to receptor tyrosine kinase (RTK) at the cell membrane and activates the downstream signalling cascade. GRB2 docks the phosphotyrosine residues on the activated RTK *via* its SH2 domain and subsequently binds the guanine nucleotide exchange factor, SOS, by its SH3 domains. Activated SOS promotes the release of GDP from RAS, enabling the binding of GTP to form RAS-GTP. Activated RAS recruits RAF to the plasma membrane, where it phosphorylates and activates MEK1/2, which in turn activates ERK1/2.

GRB2 contains a SH-2 domain, which binds to the phosphotyrosine residue on the activated tyrosine kinase receptor. GRB2 interacts with RAS *via* guanine nucleotide exchange factors, such as SOS1 using two SH3 domains in the latter (Yamazaki et al., 2002). The RAS family of proteins are small G proteins with discrete domains for localisation of RAS to the membrane and regions for GDP/GTP binding. RAS has intrinsic GTPase activity, which switches the protein off, reverting it back to its inactive state. This activity is stimulated by a family of proteins, RAS-GAPs (GTPase activating protein). RAS is activated by guanine nucleotide exchange factors (GEF) which promote the exchange of GDP for GTP (Hallberg et al., 1994).

RAS-GTP binds to and activates the serine/ threonine kinase, RAF, by recruiting it to the membrane where it is phosphorylated by an array of protein kinases. RAF activation also involves the release of an auto-inhibitory mechanism (Song et al., 2001, Tzivion et al., 2001). The binding of RAS-GTP to Arg89 of RAF is necessary for its activation by RAS-GTP (Fabian et al., 1994); activated RAF, functioning as a dimeric signal transducer propagates the signal away from the membrane by phosphorylating MEK1/2, dual tyrosine and serine/ threonine kinases. MEK1/2 go on to phosphorylate and activate their only known substrates, ERK1 and ERK2 (Cox et al., 2014).

ERK1/2 are serine/threonine kinases that link the cytoplasmic signal to the regulation of gene expression. The signal to the nucleus occurs by a variety of mechanisms, including the direct translocation of ERK1/2. ERK1/2 is able to phosphorylate and activate transcription factors that regulate specific genes required for cell growth (Berti & Seger, 2017). The AP-1 transcription factor is one such target of ERK1/2. AP-1 is composed of jun and fos gene products, the expression of which are regulated by ERK1/2 (Glauser & Schlegel, 2007). Increased expression of both jun and fos genes result in an increase of AP-1 activity, leading to an increase in activation of AP-1 target, cyclin D1, a crucial regulator of the cell cycle (Vartanian et al., 2011).

ERK1/2 cytoplasmic targets include MNK1/2, (as discussed in Section 1.2.2) and p90RSK. Activated ERK docks with p90RSK at the C-terminus, where it

phosphorylates p90RSK on Thr365, Ser369 and Thr577 to activate the C-terminal kinase domain. This phosphorylates Ser386 and generates a binding site for PDK1. PDK1 phosphorylates Ser277 in the N-terminal kinase domain resulting in activation (Cargnello & Roux, 2011). Upon activation, p90RSK phosphorylates multiple substrates and regulates many biological responses. The four isoforms of p90RSK have roles in nuclear signalling, cell cycle, cell proliferation, cell growth, cell survival and protein synthesis (Cargnello & Roux, 2011). p90RSK isoforms have been found to phosphorylate rpS6 on Ser235 and Ser236 *in vivo,* in response to RAS-RAF-MEK1/2-ERK1/2 stimulation. This facilitated the assembly of the pre-initiation complex and increased cap-dependent translation (Roux et al., 2007). In addition, other substrates of p90RSK include TSC2 (Ma, Chen et al., 2005), RAPTOR (Carriere et al., 2008), eEF2 kinase (Wang et al., 2001) and eIF4B (Shahbazian et al., 2006), implicating the importance of p90RSK in mRNA translation. Recent work also shows that MNK1 can also be phosphorylated by p90RSK in a mechanism that confers trastuzumab resistance in HER-2 positive breast cancers (Astanehe et al., 2012).

1.2.4.2 MNK substrates

Whilst the MNK kinases phosphorylate multiple downstream targets, the only fully validated substrate is the cap-binding protein, eIF4E, discussed in Section 1.1.1.1 MNK1 was also found to phosphorylate eIF4GI and eIF4GII *in vitro* (Pyronnet et al., 1999) but the functional consequences of this, if any, are not known. The following sections describe proteins that have also been identified as MNK substrates.

1.2.4.2.1 Sprouty 2

Sprouty2 (Spry2) acts as a negative feedback modulator of tyrosine kinase pathways. MNK1 was reported to phosphorylate Spry2 on conserved serine residues, Ser112 and Ser121, leading to an accumulation of Spry2 and its stabilisation (DaSilva et al., 2006). Spry2 activity can be rapidly modified through ERK signalling, since MNK1 activity is regulated by ERK1/2. A more

recent publication contradicts this finding, showing that MNK2 dependent phosphorylation of Sprouty2 promotes its degradation by the binding of Nedd4, a HECT domain family E3 ubiquitin ligase (Edwin et al., 2010).

1.2.4.2.2 hnRNP A1

The MNK kinases regulate tumour necrosis factor (TNF) α production, through the phosphorylation of AU-rich element binding proteins (ARE-BPs), such as heterogeneous nuclear ribonucleoprotein A1 (hnRNP A1) that bind to the 3'UTR of the TNFα mRNA and repress translation (Guil et al., 2006). hnRNP A1 is phosphorylated at two sites *in vitro* and *in vivo* by the MNKs in response to T cell activation, decreasing its binding to the TNFα mRNA (Buxade et al., 2005). hnRNP A1 is an abundant nuclear protein, involved in alternative splicing. hnRNP A1 shuttles continuously between the nucleus and the cytoplasm, and in addition to its role in splicing, is involved in mRNA export and regulation of mRNA stability.

hnRNP A1 was also found to be present in stress granules. Stress granules are cytoplasmic aggregations that contain translationally stalled mRNAs, which accumulate in cells exposed to stress (Guil et al., 2006). Stress-induced phosphorylation of hnRNP A1 prevented its interaction with the import transporter, transportin, leading to its cytoplasmic accumulation (Allemand et al., 2005). In the cytoplasm, mRNA-bound hnRNP A1 is phosphorylated by the MNK kinases in response to stress stimuli, resulting in the recruitment of the mRNA-bound hnRNP A1 to the stress granule and its translational repression (Guil et al., 2006).

1.2.4.2.3 cPLA2

Cytoplasmic phospholipase A2 (cPLA2) catalyses the hydrolysis of arachidonic acid from membrane phospholipids. Arachidonic acid is involved in signalling processes, such as inflammation, and also provides a precursor for eicosanoids (Six & Dennis, 2000). There is evidence that MNK1 is responsible

for Ser727 phosphorylation of cPLA2 in thrombin- and collagen-stimulated platelets, enhancing its activity (Hefner et al., 2000).

1.2.4.2.4 PSF

In addition to the MNK kinases phosphorylating the ARE-binding protein, hnRNP A1, one study found that MNK2 phosphorylated another ARE-binding protein, polypyrimidine tract-binding protein-associated splicing factor (PSF) on Ser8 and Ser283 *in vitro.* MNK2-mediated phosphorylation of PSF was found to enhance its binding to the AREs in the 3' UTR TNFα mRNA, inhibiting translation and providing further evidence for a regulatory role of the MNKs in inflammation (Buxade et al., 2008).

1.2.5 MNKs in Cancer

MNK1/2 present an attractive potential therapeutic target as they act at the convergence point of two critical signalling pathways, (the p38MAPK and ERK pathways). The MNK1/2 substrate, eIF4E, is also regulated by the mTORC1 pathway, which is activated in about 70% of cancers (Hou et al., 2012, Joshi & Platanias, 2014, Ueda et al., 2010, Wendel et al., 2007). Mice with a targeted deletion of MNK1 and MNK2 exhibit a total lack of eIF4E phosphorylation and do not display developmental or reproductive defects (Grzmil et al., 2011, Joshi & Platanias, 2014, Ueda et al., 2004). Additionally, knock-in mice expressing a mutant form of eIF4E (S209A), which is unable to be phosphorylated by MNK1/2, show resistance to neoplastic transformation by c-myc, constitutively active RAS and PTEN loss-induced prostate cancer. These mice also exhibit a reduction in VEGF and MMP3 associated with tumour invasiveness (Furic et al., 2010). Clinical development of MNK inhibitors may provide a means to selectively target cancer cells, as MNKs are dispensable for normal development. The treatment of acute myeloid leukaemia (AML) cell lines with MNK inhibitor, cercosporamide (Figure 1-17B) resulted in suppression of MNK kinase activity and leukemic progenitor cell growth. In addition, anti-leukemic effects were amplified when cercosporamide was used in conjunction with mTORC1/2 inhibitor, rapamycin (Figure 1-20A) (Altman et al., 2013).

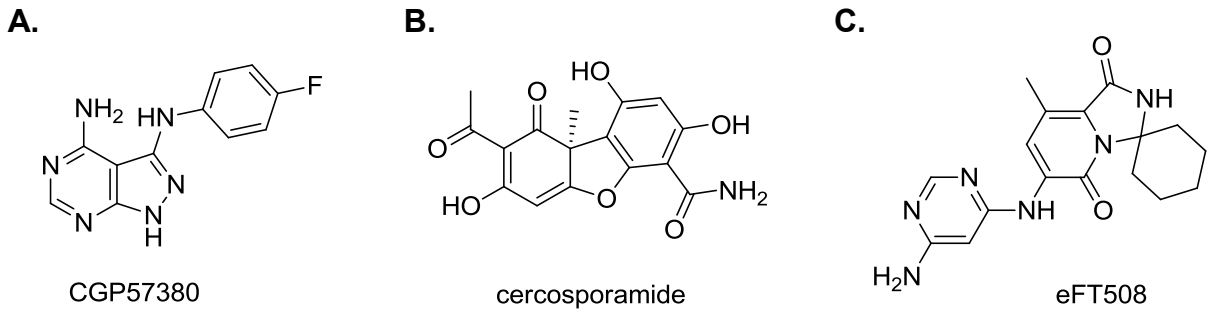

Figure 1-17. Chemical structure of MNK inhibitors.

Recent findings indicate that MNK kinases act as negative feedback regulators in response to chemotherapy and hence, contribute to chemoresistance. The level of eIF4E phosphorylation significantly increased in cancer patients during treatment with doxorubicin and cyclophosphamide, the standard treatment for advanced stage breast cancer. The siRNA knockdown or pharmacological inhibition of MNK1/2 was found to enhance the chemotherapeutic response in both AML and advanced stage breast cancer cell lines (Altman et al., 2013, Li et al., 2017).

1.2.6 MNK Inhibitors

Until recently, there has been little progress made since the discovery of CGP57380 (Figure 1-17A), which exhibits low micromolar MNK inhibition (Teo et al., 2015a). CGP57380 inhibits both MNK1 and MNK2 and has subsequently been used in a number of studies (Bianchini et al., 2008, Chrestensen et al., 2007, Grzmil et al., 2011, Knauf et al., 2001). Cercosporamide (Figure 1-17B), a natural anti-fungal agent, was found to be a potent inhibitor of MNK1/2, in the nanomolar range. However, its off-target effects limit its uses as an effective treatment as it also inhibits a number of other kinases, including Jak3 (Janus kinase 3), GSK3β (Glycogen synthase kinase 3β), ALK4 (Activin receptor-like kinase 4) and PIM1 (Serine/threonine-protein kinase pim-1) at low micromolar potency (Hou et al., 2012, Konicek et al., 2011, Liu et al., 2016). Both compounds have mainly served as pharmacological tools for MNK target validation due to the low potency of CGP57380 and the lack of specificity of cercosporamide.

It is important to note that at this time there are no FDA approved drugs which specifically act on MNK kinases. However, recently two compounds have entered clinical trials. A small molecule MNK1 inhibitor, BAY 1143269 (structure unavailable), showed potent and selective activity against its target MNK1 (IC_{50}: 40 nM) and against cancer models both *in vitro* and *in vivo* (Santag et al., 2017). A phase I dose escalation and expansion of oral BAY 1143269 in combination with intravenous docetaxel (a microtubule stabilising agent) trial

was undertaken; however, it was terminated early. eFT508 (Figure 1-17C), an orally bioavailable MNK1/2 inhibitor with an IC_{50} of 1-2 nM against both MNK isoforms in cell-free assays, is currently being investigated in several clinical trials (Reich et al., 2018). Following full characterisation in non-clinical safety pharmacology and toxicology studies, eFT508 is being evaluated in subjects with advanced triple negative breast cancer (TNBC), hepatocellular carcinoma (HCC) (Clinical trial ID: NCT03318562) and haematological malignancies (Clinical trial ID: NCT02937675). In addition, an on-going clinical trial is investigating eFT508 alone and in combination with Avelumab (a monoclonal antibody targeting the programmed death-1 (PD-1) receptor) in patients with microsatellite stable (MSS) colorectal cancer (Clinical trial ID: NCT03258398). eFT508 holds much promise for targeting dysregulated translation in the clinical setting.

1.3 mTOR

1.3.1 mTOR Overview

The mechanistic (formerly mammalian) target of rapamycin (mTOR) was identified in 1994 as the direct target of the rapamycin-FKBP12 complex in mammals (Sabatini et al., 1994). The mTOR pathway is highly conserved as a major growth regulator in eukaryotes. mTOR is a Ser/Thr protein kinase that lies downstream in the PI3K/AKT signalling pathway and coordinates cellular growth in response to nutrients and extracellular signals (Figures 1-9 and 1-18) (Saxton & Sabatini, 2017). mTOR belongs to the phosphatidylinositol 3-kinase (PI3K) family, and forms the catalytic subunit of two multiprotein complexes; mTORC1 and mTORC2. mTORC1 is defined by the regulatory-associated protein of mTOR (RAPTOR) whereas mTORC2 is defined by the rapamycin-insensitive companion of mTOR (RICTOR) (see Figure 1-9) (Wang et al., 2013).

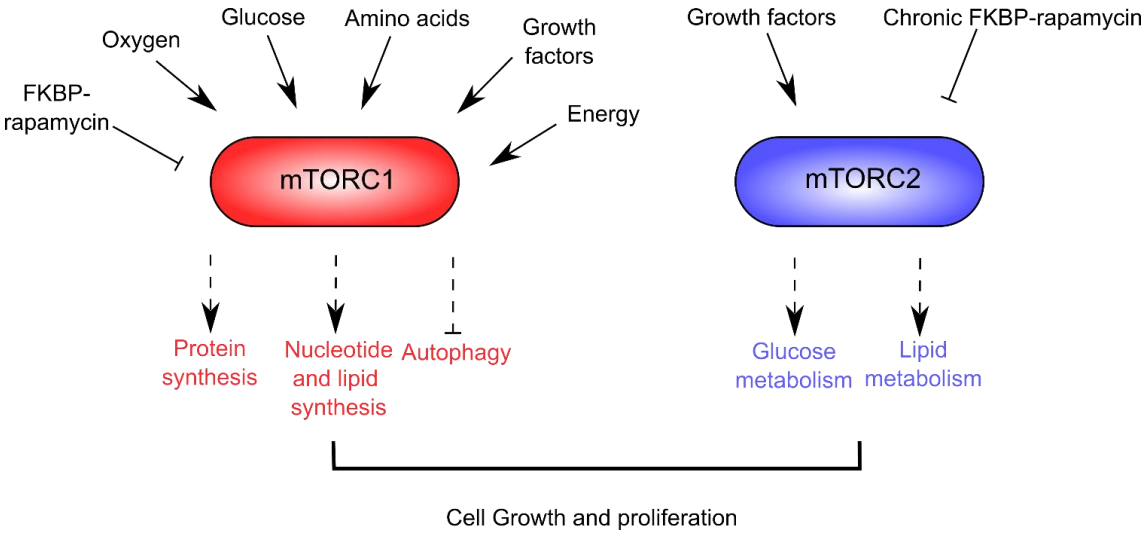

Figure 1-18. Schematic showing the signalling inputs sensed by mTORC1 and mTORC2 and the processes they regulate to control growth and proliferation.

1.3.2 mTORC1

1.3.2.1 Upstream of mTORC1

mTORC1 is activated in nutrient rich conditions to stimulate cell growth and energy storage (Sabatini, 2017). mTORC1 is regulated by multiple upstream pathways, most of which signal through the tuberous sclerosis (TSC) proteins 1 and 2, a tumour suppressor complex that inhibits RAS homolog enriched in brain (RHEB) by stimulating its GTPase activity. RHEB, in its GTP-bound form, binds directly to mTORC1 and is required for its activation (Figure 1-9) (Hay & Sonenberg, 2004). Proteins in these upstream pathways are commonly mutated in cancer and allow oncogenic signalling through mTORC1 (Saxton & Sabatini, 2017). The activity of mTORC1 is coupled with amino acid concentration and the availability of growth factors (reviewed in Sabatini, 2017). In simple terms, mTORC1 regulation by amino acids involves Rag GTPases, heterodimeric proteins that are tethered to the lysosomal membrane. A high concentration of amino acids converts Rag GTPases into their active GTP-bound form, which enables them to bind to the regulatory protein, RAPTOR. mTORC1 is then recruited to the lysosomal membrane by RAPTOR where it localises with RHEB/GTP. mTORC1 signalling requires both Rag and RHEB GTPases for activation, ensuring mTORC1 is only active when nutrients and growth factors are available (Sancak et al., 2008, Saxton & Sabatini, 2017). Growth factor signalling through mTORC1 is primarily mediated by the PI3K/AKT pathway. Tyrosine kinase receptors at the cell membrane transduce the signal initiated by the binding of growth factors and hormones, such as insulin, leading to PI3K activation. PI3K stimulates AKT, which phosphorylates and inhibits TSC2, dissociating it from the lysosomal membrane and preventing its interaction with RHEB and its tumour suppressor function (Manning et al., 2002, Menon et al., 2014).

mTORC1 is also activated through RAS signalling, *via* ERK1/2 and p90RSK, both of which phosphorylate and inhibit TSC2, preserving RHEB/GTP levels (Ma et al., 2005, Roux et al., 2004). Additionally, the Wnt pathway and inflammatory cytokine, TNFα, both activate mTORC1 by inhibition of the

TSC1/2 complex (Inoki et al., 2006, Lee et al., 2007). Intracellular and extracellular stresses such as low levels of ATP, hypoxia or DNA damage elicits an inhibitory response from mTORC1, through the activation of AMPK (Figure 1-6) (Saxton & Sabatini, 2017). mTORC1 is both directly inhibited by AMPK through the phosphorylation of adaptor protein, RAPTOR, and indirectly by the phosphorylation of TSC2; the latter activates TCS2 and reduces levels of RHEB/GTP (Gwinn et al., 2008, Inoki et al., 2003). Hypoxic conditions also induce the expression of protein regulated in development and DNA damage response 1 (REDD1), a protein that modulates TSC2 activity, leading to inhibition of mTORC1 (Morita et al., 2015). In response to DNA damage, DNA damage response (DDR) pathways induce the expression of P53 target genes, such as TSC2, AMPKβ and PTEN, all of which increase TSC1/2 complex activity and inhibit mTORC1 through regulation of RHEB/GTP levels (Feng et al., 2007).

Signalling pathways involving mTORC1 are complex, and there are many negative loops which add a further level of regulation (summarised in Figure 1-19). One such loop involves the phosphorylation of insulin receptor substrate 1 (IRS1), either directly by activated mTORC1 or via mTORC1-activated p70S6K. This leads to its degradation and results in a decrease in PI3K/AKT signalling and subsequently a downregulation of mTORC1 activity (Cope et al., 2014, Rozengurt et al., 2014).

1.3.2.2 Downstream of mTORC1

In order to regulate cell growth, mTORC1 controls the balance between anabolic and catabolic processes. Cancer cells often hijack the PI3K/AKT/mTOR pathway in order to meet the demands of increased growth rate, as observed in patients with AML (Jhanwar-Uniyal et al., 2017, Showkat et al., 2014, Zhang et al., 2015). This involves an increase in protein, lipid and nucleotide synthesis and the suppression of autophagy. mTORC1 has a central role in stimulating protein synthesis through the phosphorylation of two key substrates, 4E-BP1 and p70S6K (Figure 1-9) (Hsieh et al., 2012, Morita et al.,

2015). The interaction between eIF4G and eIF4E in the eIF4F complex is inhibited by 4E-BPs.

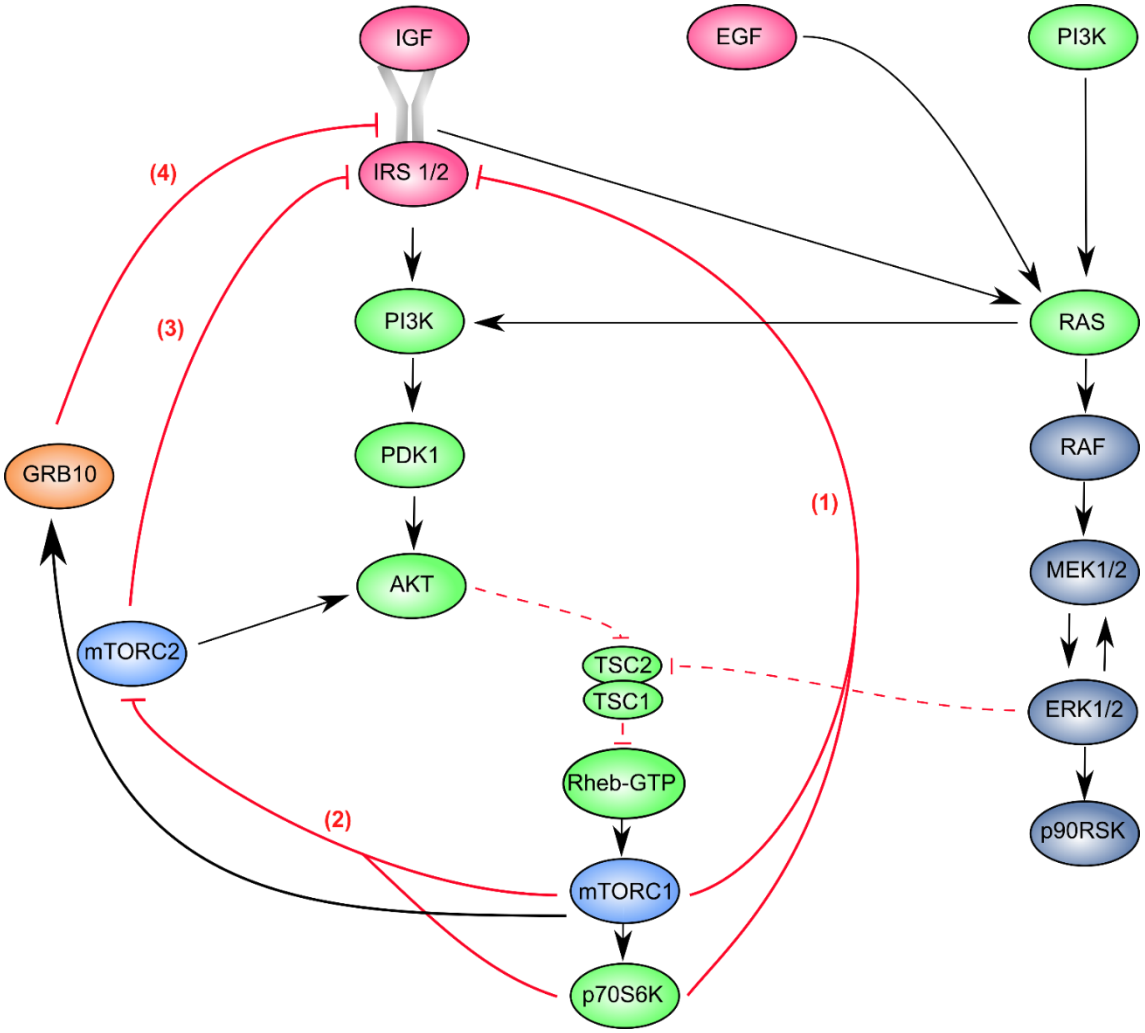

Figure 1-19. Negative feedback loops in the PI3K-mTOR and RAS-RAF-MEK1/2-ERK1/2 pathways. Intrinsic negative loops stem from distal components of the same pathway, whereas extrinsic feedback loops originate from components of alternate pathways. Both intrinsic and extrinsic feedback loops inhibit upstream signalling nodes (coloured and numbered in red). Feedback loop **(1)**: activated mTORC1 and p70S6K inhibits IRS1. Feedback loop **(2)**: activated mTORC1/p70S6K disrupts mTORC2 via phosphorylation of SIN1, and subsequent dissociation from mTORC2 complex. Feedback loop **(3)**: mTORC2 negatively feeds back to inhibit IRS1. Feedback loop **(4)**: GRB10, is phosphorylated and activated by sustained mTORC1 activity, which potentiates its inhibitory effect on IGF receptor signalling. Adapted from Liu et al., 2015 and Rozengurt et al., 2014).

4E-BP1 competes with eIF4G for a shared binding site on eIF4E, preventing the assembly of the eIF4F complex (Figure 1-11). The interaction strength of 4E-BP1 binding to eIF4E depends on the phosphorylation status of 4E-BP1 (Merrick, 2015). Hypo-phosphorylated 4E-BP1 binds strongly to eIF4E whereas hyper-phosphorylated 4E-BP1 weakens its interaction with eIF4E (Hsieh & Ruggero, 2010, Sonenberg & Hinnebusch, 2009, Van Der Kelen et al., 2009). 4E-BP1 contains at least seven sites of phosphorylation, of which four (T37, T46, S65, T70) are known to be regulated by mTORC1 and associated signalling pathways (Figure 1-11A) (Hsieh & Ruggero, 2010). mTORC1 phosphorylates p70S6K; a subsequent phosphorylation by PDK1 leads to its full activation and its release from eIF3 (Holz et al., 2005, Showkat et al., 2014). Active p70S6K subsequently phosphorylates several positive regulators of translation; ribosome protein S6 (rpS6), eIF4G and eIF4B. Additionally, p70S6k phosphorylates and promotes degradation of pdcd4, an inhibitor of eIF4A and fragile X mental retardation protein (FMRP), an mRNA binding protein (Guertin & Sabatini, 2007, Wang et al., 2012).

In order to meet the demands of an increased growth rate, mTORC1 promotes nucleotide synthesis, required for DNA replication and increases overall protein synthesis by stimulating rRNA transcription and ribosome biogenesis (Laplante & Sabatini, 2012, Qin et al., 2016). mTORC1 also has a prominent role in lipid synthesis by promoting sterol responsive binding protein (SREBP) transcription factors, responsible for the expression of genes involved in fatty acid and cholesterol synthesis (Saxton & Sabatini, 2017). *De novo* lipid synthesis is required for the generation of cellular membrane during proliferation (Laplante & Sabatini, 2012).

mTORC1 is a negative regulator of autophagy, an important cellular process in which damaged organelles and intracellular pathogens are degraded inside lysosomes (Showkat et al., 2014). mTORC1 on lysosomes phosphorylates unc-51 like autophagy activated kinase (ULK1) and its positive regulator, autophagy-related protein 13 (ATG13), inhibiting autophagosome formation (Chiarini et al., 2015, Cope et al., 2014, Laplante & Sabatini, 2012). The phosphorylation of

ULK1 prevents its activation by AMPK, an important activator of autophagy (Saxton & Sabatini, 2017).

1.3.3 mTORC2

1.3.3.1 Upstream of mTORC2

mTORC2 is an effector of the insulin/PI3K pathway, it responds to growth factors such as EGF (Figure 1-18). mTORC2 activity is stimulated by a mutation in EGFR in glioblastoma (GBM), leading to uncontrolled growth *via* the activation of NF-κB (Tanaka et al., 2011). Recent cryo-electron microscopy of mTORC2 has revealed distinct similarities and differences in comparison to mTORC1. The common regulatory proteins interact with mTOR in the same way for both complexes (mTORC1 and mTORC2). However, there are differences in the way that the other accessory proteins are arranged, which accounts for the variation in the roles of the mTOR complexes (Stuttfeld et al., 2018). One such mTORC2 protein, mSin1, contains a phosphoinositide-binding PH domain that inhibits mTORC2 in the absence of insulin. This auto-inhibition is released by the binding of PIP3, the product of PI3K signalling, at the plasma membrane. This allows mTORC2 to partially activate AKT in a PI3K-dependent manner, discussed in the following section (Liu et al., 2015).

mTORC2 signalling is also regulated by negative feedback loops involving mTORC1, which leads to an inhibition of the PI3K/AKT/mTORC1 pathway (Liu & Liu, 2014). An endogenous negative regulator of the insulin/insulin-like growth factor pathway, GRB10, is phosphorylated and activated by sustained mTORC1 activity (Figure 1-19). GRB10 phosphorylation leads to its interaction with RAPTOR, an activator of mTORC1. GRB10 prevents RAPTOR binding to mTORC1 and suppresses mTORC1 signalling (Hsu et al., 2011). The downstream target of mTORC1, p70S6K, phosphorylates insulin receptor substrate 1 (IRS1), promoting its degradation and the suppression of mTORC2 signalling (Shah et al., 2004). These negative feedback loops involving mTORC1 have repercussions for the therapeutic targeting of mTOR (Figure 1-19).

1.3.3.2 Downstream of mTORC2

mTORC2 is involved in cell survival and cell cycle progression through the phosphorylation of Ser473 on AKT, and through activation of serum- and glucocorticoid-regulated kinase (SGK) and protein kinase C (PKC) (Cope et al., 2014, Hou et al., 2012, Laplante & Sabatini, 2012, Liu et al., 2013, Wang et al., 2013). The full activation of AKT requires phosphorylation on Ser473 by mTORC2, alongside phosphorylation on Thr308 by PDK1. AKT phosphorylates FoxO1 and FoxO3, transcription factors involved in pro-apoptotic signalling in the absence of growth factors. AKT activation results in their exclusion from the nucleus and subsequent degradation, promoting cell survival (Guertin et al., 2006, Tothova et al., 2007).

1.3.4 mTOR and its role in Cancer

mTORC1 lies downstream of commonly mutated PI3K/AKT and RAS/RAF/MEK/ ERK pathways and oncogenic signalling results in mTORC1 hyperactivation in many cancers (Figure 1-9) (Saxton & Sabatini, 2017). Inactivating mutations in the tumour suppressor gene, PTEN, a phosphatase that antagonises PI3K function are a common feature in cancer cells (Jhanwar-Uniyal et al., 2017). This causes an up-regulation of PI3K activity in the cell and constitutive stimulation of the PI3K/AKT/mTOR pathway (Bianchini et al., 2008, Hay, 2010). Activated mTORC1 has a multitude of consequences in cancer development, one of the most important being the mTORC1-dependent phosphorylation of 4E-BP1. This causes its release from eIF4E, driving eIF4F complex formation (Truitt et al., 2015, Truitt & Ruggero, 2017). Ribosome profiling studies using nano-cap analysis of gene expression (nanoCAGE) technology reveal that some mTOR translationally regulated mRNAs possess a 5’ terminal oligopyrimidine tract, also termed 5’TOP (Gandin et al., 2016a, Gandin et al., 2016b). These mRNAs include those encoding YB1 (Y-box binding protein), vimentin, metastasis associated 1 (MTA1) and CD44, all of which have a significant role in the process of metastasis. Hyperactive mTOR signalling has a profound effect on the translational landscape of cancer cells by

positively regulating this four-gene invasion signature alongside metabolic effects (Alain et al., 2012, Hsieh et al., 2012). A hallmark of cancer cell reprogramming is the switch to aerobic glycolysis metabolism. Activated mTORC1 also increases the transcription and translation of HIF1α, which in turn regulates glycolytic genes, enabling the tumour cell to meet the high demands required for survival and progression (Slotkin et al., 2015, Zhang et al., 2015).

mTORC2 activity has also been implicated in cancer, mainly due its role in the AKT-driven uptake of glucose and the inhibition of apoptosis (Hietakangas & Cohen, 2008). In mouse models of prostate cancer driven by PTEN loss, tumours were reliant on mTORC2 activity and the mTORC2 specific regulator protein, RICTOR, was found to be essential (Guertin et al., 2009). There is also evidence that both mTORC1 and mTORC2 are implicated in the epithelial-mesenchymal transition (EMT) (Gulhati et al., 2011). EMT in relation to cancer can be defined as the conversion of differentiated epithelial cells into migratory mesenchymal cells through the loss of epithelial markers and the gain of mesenchymal markers (Tiwari et al., 2012). This is thought to occur in part, through the modulation of genes that code for proteins associated with cytoskeleton rearrangement, such as RhoA, RAC1 and CDC42 GTPases. mTORC1 mediated signalling also plays a role in the phosphorylation of focal adhesion proteins and the promotion of cell motility (Zaytseva et al., 2012).

1.3.5 mTORC1/2 Inhibitors

Rapamycin (Sirolimus), the first known inhibitor of mTOR was isolated from the bacteria, *Streptomyces hygroscopicus*, inhabiting the soil in Easter Island (Sehgal et al., 1975, Vezina et al., 1975). Its antifungal properties were eclipsed by its potent immunosuppressant ability, which led to its licensing under the brand name Rapamune (Pfizer), for use in renal transplantation (Johnson, 2002). The discovery of rapamycin has since led to the development of synthetic analogues, known as “rapalogs”. These compounds have been developed by modifying the C40 hydroxyl group to improve the pharmokinetics of rapamycin. These include everolimus (Norvartis) and temsirolimus (Pfizer) (Figure 1-20), which have superior aqueous solubility without the loss of

immunosuppressant properties. Everolimus is modified at the C40 position by the introduction of a 2-hydroxyethyl group and temsirolimus is the ester derivative of rapamycin (Gu et al., 2005, Sedrani et al., 1998).

Rapamycin and rapalogs are allosteric inhibitors of mTORC1, and work by recruiting FKBP-12, an accessory protein, to the FRB domain of mTOR. The formation of this drug–protein complex causes a conformational change in mTORC1, distal from the kinase domain, leading to its inhibition (Liu et al., 2012, Showkat et al., 2014). Recent structural studies have further elucidated the mechanism by which rapamycin inhibits mTORC1 (Aylett et al., 2016). In contrast, the rapamycin-FKBP complex does not target mTORC2 directly, although prolonged treatment (24 hours) leads to inhibition through the disruption of mTORC2 signalling (Jacinto et al., 2004). Rapamycin-FKBP binds to free mTOR and prevents its incorporation into mTORC2 (Sarbassov et al., 2006).

Deregulation of the mTOR pathway is correlated with poor clinical outcome and drug resistance (Slotkin et al., 2015). There are currently only two FDA approved mTOR inhibitors available for cancer treatment (temsirolimus and everolimus). However, both have had limited success in the clinic due several factors. Rapamycin and rapalogs fail to block the phosphorylation of all mTORC1 substrates, in particular 4E-BPs (Thoreen et al., 2009). In fact the 4E-BP/eIF4E ratio can be used to predict the sensitivity of cancer cell lines to mTOR inhibitors (Alain et al., 2012). In one study, rapamycin treated myeloma cells led to the phosphorylation and activation of MNK1 along with its target, eIF4E (Bianchini et al., 2008, Joshi & Platanias, 2014). Furthermore, the inhibition of mTORC1 can lead to the activation of AKT, promoting cell survival and preventing apoptosis (Figure 1-19) (Sarbassov et al., 2005). Rapalogs have had some success in cancers with mutations in the components of mTOR pathway itself (Iyer et al., 2012, Wagle et al., 2014).

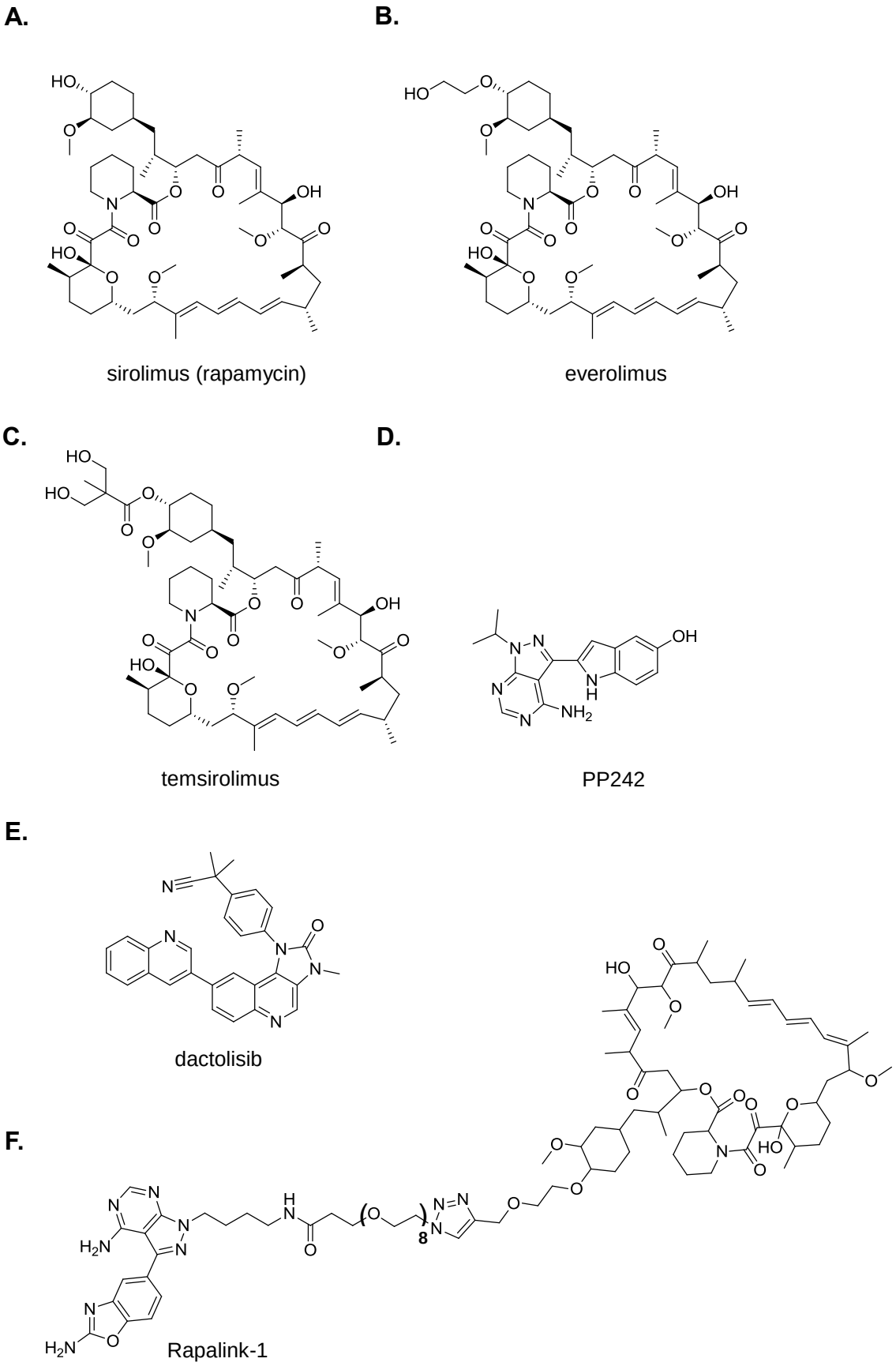

Figure 1-20. Chemical structures of mTOR inhibitors.

However, after an initial response to treatment, the cancer gained acquired resistance (Wagle et al., 2014).

“Second generation” mTOR catalytic site inhibitors hold much promise due to their potent inhibition of both mTORC1 and mTORC2, thus attenuating the feedback mechanism involving AKT phosphorylation (Efeyan & Sabatini, 2010, Liu, Wang et al., 2011, Powles et al., 2016). These inhibitors are ATP analogues that contain a heterocyclic structure to exploit the adenine-binding pocket and can form hydrogen bonds with the hinge region of the kinase (Basnet et al., 2015). Type II inhibitors (discussed in more detail below) introduce additional specificity by binding not only the ATP pocket but also an adjacent allosteric pocket (Wu et al., 2016, Zhao et al., 2014). The recently solved crystal structure of the mTOR kinase domain in complex with ATP-competitive inhibitor, PP242 (Figure 1-20D), will no doubt facilitate the design and synthesis of further active-site (catalytic) mTOR inhibitors (Rodrik-Outmezguine et al., 2016, Yang et al., 2013). However, long-term treatment of catalytic inhibitors eventually leads to the release of negative feedback on the insulin/PI3K signalling pathway and AKT is reactivated *via* phosphorylation on Thr308. The initial suppression due to mTORC2 inhibition is overcome (Rodrik-Outmezguine et al., 2011). This has led to the concept of dual PI3K/mTOR inhibitors as a possible solution to block negative feedback stimulation of AKT. The similarity in the C-terminal kinase domain of both mTOR and PI3K allows the development of single compounds with dual inhibitory properties (Zheng & Jiang, 2015). Dactolisib (Novartis) (Figure 1-20E) is an imidazoquinoline derivative capable of binding to the ATP binding sites of both mTORC1/2 and PI3K (p110α, γ, δ, β) (Maira et al., 2008). Studies using Dactolisib found that dual inhibition of PI3K/ mTOR had a stronger anti-proliferative activity than inhibiting mTOR alone (Serra et al., 2008).

A new class of mTOR inhibitor has recently been developed that chemically links a catalytic site inhibitor with an allosteric inhibitor. This novel inhibitor, known as “Rapalink” allows simultaneous inhibition of both the ATP- and FRB-binding sites of mTOR. The bivalent interaction overcomes resistance to

existing inhibitors and was found to potently inhibit cancer cell growth *in vitro* (Figure 1-20F) (Renna, 2016).

The effects of mTOR inhibition are multifaceted, owing to the diverse functions of both complexes. For example, although acute mTORC1 inhibition suppresses global protein translation, it primarily affects mRNAs containing a 5' TOP. These mRNAs are typically involved in protein synthesis (Hsieh et al., 2012). mTORC1 inhibition is also correlated with an increase in proteasome-dependent proteolysis and the induction of autophagy, which enables cancer cell survival in nutrient poor microenvironments (Palm et al., 2015, Zhao et al., 2015). It is therefore worth considering the repercussions of mTOR inhibition when implementing a therapeutic approach to target cancer.

1.3.5.1.1 Protein kinase inhibitors

Protein kinases are a large family of enzymes that transfer a γ-phosphate from ATP to a tyrosine, serine or threonine residue on the protein substrate (Bhullar et al., 2018). Protein kinases are classified into two main categories: serine/ threonine kinases and tyrosine kinases. A group of dual-specificity kinases that phosphorylate both tyrosine and serine/ threonine residues have also been identified (Garcia-Aranda & Redondo, 2017). Aberrant protein kinase activity or kinase over-expression often promotes cell survival and drives cellular pathways that are implicated in oncogenesis (Kittler & Tschandl, 2018, Maurer et al., 2011, Paul & Mukhopadhyay, 2004).

The majority of protein kinase inhibitors target the ATP-binding site, which is sandwiched between the N-terminal and C-terminal lobes of the enzyme. The "hinge region" connects the two lobes of the enzyme and residues in this region often make hydrogen bonds with kinase inhibitors (Bhullar et al., 2018). The activation loop of the kinase determines the activity of the enzyme and occurs in the open (active ATP-bound) or closed (inactive) conformation. Phosphorylation of specific residues by upstream kinases on the activation loop alters the position of the N-terminal DFG (Asp Phe Gly) motif. This allows the Asp in the DFG motif to coordinate the magnesium ion, which positions the phosphates

belonging to ATP for phosphotransfer. In addition, the Phe residue is also orientated towards the binding pocket (DFG-in) and is important for the correct positioning of the activation loop for catalysis (Cowan-Jacob, 2006, Fabbro et al., 2015). Once the phosphoryl group is transferred from ATP to the substrate protein, the kinase reverts back to its inactive (DFG-out) conformation (Cowan-Jacob, 2006). In the inactive form, an additional hydrophobic pocket is exposed. This provides an opportunity to design kinase inhibitors that bind to and stabilise the inactive form (Garuti et al., 2010).

Protein kinase inhibitors are classified according to their binding mechanism. Type I inhibitors are ATP-competitors that mimic the adenine moiety of ATP and bind to the kinase in the active conformation. Type I inhibitors display low selectivity due to the conservation of the ATP-binding site throughout the kinome, resulting in a significant number of off-targets effects (Bhullar et al., 2018). Lapatinib is a type I kinase inhibitor FDA-approved for the treatment of metastatic $HER2^+$ breast cancer. Lapatinib is a dual tyrosine kinase inhibitor that targets the HER2 and EGF receptors (Higa & Abraham, 2007, Segovia-Mendoza et al., 2015). It is also used in combination with anastrazole for post-menopausal breast cancer that co-expresses HER2 and hormone receptors (Johnston et al., 2009). Palbociclib is also a type I inhibitor; binding to the ATP-binding pocket of the kinase in its active (DFG-in) conformation (Roskoski, 2016). Palbociclib inhibits the cell cycle and is a selective cyclin-dependent kinase 4/cyclin-dependent kinase 6 (CDK4/6) inhibitor (Finn et al., 2009, Fry et al., 2004). It is currently administered to individuals with ER^+ breast cancer in combination with fulvestrant or an aromatase inhibitor (Masuda et al., 2018, Walker et al., 2016).

Type II kinase inhibitors bind to the inactive (DFG-out) conformation of the protein kinase and exploit the additional hydrophobic pocket that is exposed adjacent to the ATP-binding site (Kufareva & Abagyan, 2008). These compounds occupy part of the adenine binding pocket and form hydrogen bonds with the hinge region of the enzyme. The interactions made in these regions provide increased selectivity in comparison with type I inhibitors that only recognise the highly conserved ATP-binding site (Davis et al., 2011). An

example of a type II kinase inhibitor is imatinib (Gleevec), used for the treatment of chronic myelogenous leukaemia (CML) and gastrointestinal stromal tumours (GIST) (Iqbal & Iqbal, 2014).

The third class of kinase inhibitor (type III) are non-ATP competitive or allosteric inhibitors, and exert their action by binding to sites adjacent to the ATP-binding pocket, without making any interactions with the hinge region. These inhibitors achieve high selectivity by exploiting specific interactions exclusive to the particular kinase (Roskoski, 2016). Trametinib (Mekinist) is a type III kinase inhibitor, approved by the FDA in 2013 for the treatment of BRAF V600E mutated metastatic melanoma. Trametinib is a highly selective allosteric inhibitor of MEK1 and MEK2 (Lugowska et al., 2015).

Substrate-directed inhibitors, also known as type IV inhibitors, bind reversibly to the substrate-binding site outside of the ATP pocket. These inhibitors are non-ATP competitive and currently no type IV inhibitors have been approved (Gavrin & Saiah, 2013, Wu et al., 2016). Recent work describes the development of substrate-directed inhibitors of BCR-ABL that overcome the resistance of imatinib (Gumireddy et al., 2005, Maekawa et al., 2007).

Type V or covalent inhibitors represent the final class of kinase inhibitors. These inhibitors incorporate an electrophilic moiety that targets an exposed nucleophilic cysteine residue in the ATP-binding pocket of the active site, forming an irreversible covalent bond (Wu et al., 2016). The nucleophilic addition to an α,β-unsaturated carbonyl compound, known as a Michael addition, results in the formation of an irreversible enzyme-inhibitor complex that inactivates the kinase. Covalent inhibitors are highly selective as they target a specific cysteine residue in the active site (Bhullar et al., 2018). There are several FDA approved covalent inhibitors, for example, afatinib (Gilotrif) is a dual HER2/EGFR inhibitor indicated for the treatment of patients with metastatic non-small cell lung cancer (Keating, 2016).

One of the major flaws of conventional treatment is the development of drug resistance due to the heterogeneous expression of drug targets within a tumour

(McGranahan & Swanton, 2015, Ramon, Castellvi et al., 2018). For example, a $HER2^+$ breast cancer classification requires only 30% of the cells to stain positive for HER2 by immunocytochemistry (Dai et al., 2014). Targeted treatment eliminates sensitive subclones but allows the growth of resistant subclones and the progression of emergent subclones (Figure 1-21) (Ramon et al., 2018). Conventional monotherapies increase the likelihood of drug resistance and are often less effective at killing cancer cells than the combination therapy approach (Blagosklonny, 2004). Combination therapy utilises two or more treatments to target different cellular pathways, working in a synergistic manner to destroy cancer cells (Yap et al., 2013). Therefore combinations of drugs are currently being investigated in numerous clinical trials to increase the response to treatments in tumour cells (Bayat Mokhtari et al., 2017, Lee & Nan, 2012).

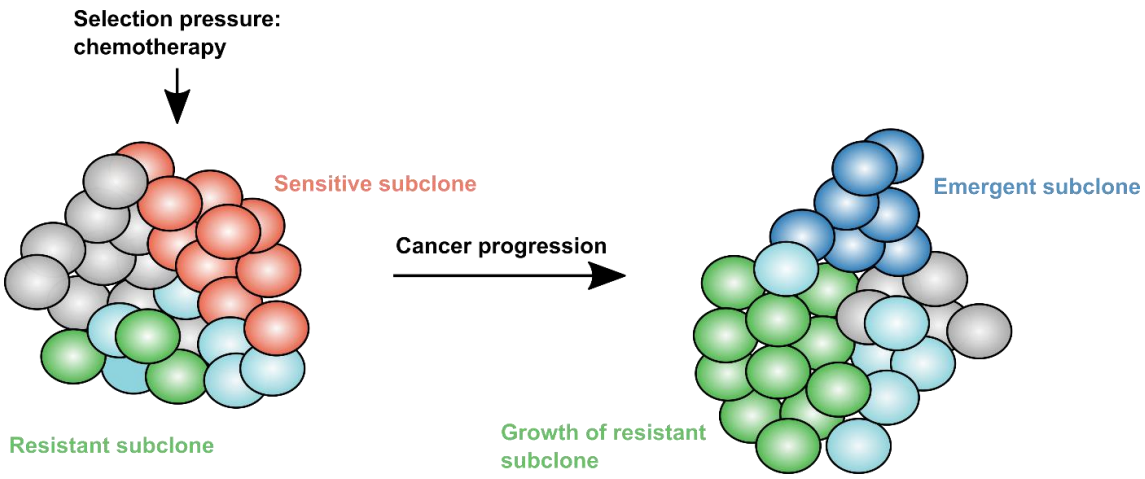

Figure 1-21. Schematic of drug resistance in a solid tumour. In this model, chemotherapy kills sensitive subclones but resistant subclones survive. As the cancer progresses, growth of resistant subclones occurs as well as the development of emergent subclones.

1.4 Project Aims

Current understanding discussed above demonstrates the challenges currently faced with cancer treatment. The heterogeneous nature of cancer and the complexity of cellular signalling means that a single treatment approach is often ineffective and eventually leads to drug resistance. MNK1/2 present an attractive therapeutic target as they are dispensable for normal development and act at the convergence point of p38MAPK and ERK pathways, commonly upregulated in cancer cells. However, evidence for a compensatory feedback mechanism linking the PI3K/AKT/mTOR pathway and the MNK/eIF4E pathway has been reported both experimentally and clinically, where downregulation of one pathway correlated with the activation of the other, supporting cancer survival. The work described in the following chapters aims to investigate the pharmacological inhibition of MNK1/2 and other translational targets, with the objective of preventing feedback initiation and therefore reducing the likelihood of drug resistance in cancer therapy.

2 Materials and Methods

2.1 Cell Culture

MRC5 human male foetal lung fibroblasts, SV40 transformed were sourced from the European Collection of Cell Cultures (ECACC). Breast cancer cell lines BT-549, MDA-MB-231, and SK-BR-3 were sourced from the American Type Culture Collection (ATCC, Manassas, VA, USA), US. The human AML cell lines MOLM-13 and MV4-11 were purchased from the German Collection of Microorganisms and Cell Cultures (DSMZ, Braunschweig, Germany). The human prostate cancer cell lines PC-3 and LNCaP were kindly donated by the Genome Damage and Stability Centre (GDSC) at the University of Sussex. Cell lines were maintained in Minimal Essential Medium with Glutamax and Earl's salts (MEM, Gibco), supplemented with 10% (v/v) foetal bovine serum (FBS, Pan Biotech) at 37°C in a humidified atmosphere with 5% CO_2.

2.1.1 Cell Passage

Cell passage was performed when cells were 70-80% confluent. Adherent cells were first washed with Dubecco's Phosphate Buffered Saline without calcium chloride or magnesium chloride (DPBS, Sigma Aldrich) prior to the addition of cell dissociation agent, TripLE Select using 1 $mLcm^{-2}$ (ThermoFisherScientific).

2.1.2 Storage of Cells

Cells were frozen in a freezing medium containing 90% FBS and 10% DMSO. 1ml cryo-vials of cells were stored in a Mr. Frosty™ overnight at -80^{o}C before being transferred to a liquid nitrogen cryostore.

2.2 Cell Viability

To assess cell viability *in vitro*, all cell lines were seeded into 96-well plates at various cell densities per 100 µL media, then treated with 0.2% (v/v) DMSO or varying concentrations of compounds for 72 hr. Cell viability was measured

using the CellTiter-Blue reagent (Promega, Madison, WI, USA) with fluorescence recorded at 560Ex/590Em using a Synergy HT Multi-Detection Reader (BioTek, Winooski, VT, USA). Relative cell viability at a given inhibitor concentration was determined by comparing the fluorescence to that of DMSO treated cells.

2.3 Migration Assays

2.3.1 Scratch Assay

A 5 cm diameter culture dish containing a confluent monolayer of cells were starved in serum free growth medium for 16 hours. A “wound” was scratched into the monolayer of cells using a P-20 pipette tip. The serum-free medium was aspirated and replaced with 2 mL of serum-containing medium. Inhibitors were added at this point and images were taken at various indicated time points using a Nikon Eclipse TS100 light microscope, (10x objective lens).

2.3.2 Wound Healing Assay

The Oris Universal Cell Migration Assembly kit was purchased from AMS Biotechnology (Europe) Ltd and the assay was performed according to the manufacturer’s instructions. Briefly, a single cell suspension (5×10^4 cells/well/100 µL for MDA-MB-231 cells) was loaded into stopper-loaded wells in a 96-well plate. Cells were incubated in a humidified chamber (37°C, 5% CO_2) for 4 hours to permit cell attachment. To start cell migration, the stoppers were removed, cells were washed with sterile PBS and fresh complete medium was added. Images were taken at various indicated time points using an Optika XDS-2 light microscope, (4x objective lens). Data were analysed with ImageJ software (National Institute of Health, Bethesda, MA, USA).

2.3.3 Trans-well Cell Migration Assay

Using the xCELLigence DP device from Roche Diagnostics real-time measurements of cell migration on MRC5 cells were performed. Cells were seeded at 30,000 per well in CIM-Plates 16 (Roche Diagnostics) in serum-free

medium in the presence or absence of inhibitors. Full growth medium was used as a chemo-attractant in the lower chamber. As cells pass through the 8 μm pores towards the chemo-attractant they adhere to the underside of the filter, embedded with a gold micro-electrode. This produces an electrical impedance signal, which correlates with the number of migrating cells. Cell index is an arbitrary unit based upon the measured cell-electrode impedance derived by the software using the calculation as described in Sun et al (2012).

2.4 Immunoblotting

Cellular lysates were prepared using lysis buffer (20 mM MOPS pH 7.4, 100 mM KCl, 1 mM DTT, 1 mM EDTA, 2 mM benzamidine, 25 mM NaF, 5 μg/mL leupeptin, 10 mM chymostatin, 1 μM microcystin LR, 1 X EDTA-free protease inhibitor cocktail (Roche)). The concentration of lysate protein was determined by Bradford assay (Bio-Rad). Immunoblotting was performed using the Mini-PROTEAN Tetra Cell System (Bio-Rad) with 20 μg of lysate protein. The primary antibodies used were β-actin (Abcam), cleaved PARP (Cell Signalling Technologies), AMPK (phospho-Thr172; Cell Signalling Technologies), eIF4E-(phospho-Ser209; Abcam), p70S6K(phospho-Thr389; Cell Signalling Technologies), p44/42 MAPK (ERK1/2) (phospho-Thr202/Tyr204; Cell Signalling Technologies), 4E-BP1 (Cell Signalling Technologies), p38MAPK (phospho-Thr180/Tyr182; Cell Signalling Technologies), MNK1 (phospho-Thr197/202; Cell Signalling Technologies), ribosomal protein S6 (phospho-Ser240/244; Cell Signalling Technologies), eIF4E (Cell Signalling Technologies), AKT (phospho-Thr308; Abcam), ULK1 (phospho-Ser555; Cell Signalling Technologies) and Anti-LC3B (Sigma).

2.5 *In Vitro* Kinase Assays

Compounds were tested as single-dose duplicates at 1 μM by Reaction Biology Kinase HotSpot screening. The enzyme activity (%) of the compound relative to the DMSO control was evaluated in a panel of five kinases.

2.6 Flow Cytometry

Cells were seeded at 1 × 10^5 in 12-well plates and allowed to adhere overnight. The cells were treated with the indicated concentrations of inhibitors for 24 hours. Samples were collected and fixed in 70%(v/v) ethanol for 1 hour. For cell cycle analysis, fixed cells were treated with 10 µg/mL RNAse A for 45 min before the addition of 50 µg/mL propidium iodide for 15 min and then analysed by FACs using the Accuri C6 Flow Cytometer.

2.7 3D Cell Culture

A centrifugal forced-aggregation method was used to generate MDA-MB-231 spheroids. Briefly, cells were detached from the flasks by trypsin, washed twice with PBS, resuspended, and counted. MDA-MB-231 cells were seeded in Costar Low Attachment U-bottom 96-well plates at 2000 cells/well/100 µL of normal growth media. A 6% (w/v) Matrigel Matrix (Corning, Corning, NY, USA) media mix was prepared on ice and 100 µL added to each well, to give a final 3% Matrigel Matrix solution. Plates were then centrifuged for 2 min at 1200 g at 4°C, and incubated for three days at 37°C, 5% CO_2. Established spheroids were treated with test compounds at various concentrations and analysed using the Celigo High Throughput Micro-Well Image Cytometer after 4, 6, and 8 days of incubation.

2.8 Chemical Synthesis

2.8.1 General Procedures

Chemical synthesis was performed by myself unless otherwise stated. All reactions were carried out in air using commercial-grade starting materials, solvents, and reagents. The progress of all reactions was monitored by thin layer chromatography (TLC, Silver Spring, MD, USA) using commercially available glass silica gel plates (60 Å, F254). The mobile phase was generally a solvent mixture, and the visualization was undertaken using UV light. All NMR spectra were measured on a Varian NMR 500 spectrometer (Palo Alto, CA,

USA) at 500 MHz 1H). Chemical shifts are quoted in parts per million (ppm; % relative to a residual solvent peak for 1H). Chromatographic purifications were undertaken using an ISCO purification unit, Combi Flash RF 75 PSI, using Biotage silica gel columns. LC-MS (Shimadzu Mass Directed Liquid Chromatography mass spectrometry, Kyoto, Japan) purity analyses were undertaken using a 5 µm C18 110 Å column.

2.8.2 Experimental

2.8.2.1 Synthesis of Compound 1: 4-((4-fluoro-2-isopropoxyphenyl)amino)-5-methylthieno[2,3-d]pyrimidine-6-carboxylic acid

Methyl 4-((4-fluoro-2-isopropoxyphenyl)amino)-5-methylthieno[2,3-d] pyrimidine-6-carboxylate.

To a solution of 4-fluoro-2-isopropoxyaniline (185 mg, 0.904 mmol) in 1,4-dioxane (5 mL) were added methyl 4-chloro-5-methylthieno[2,3-d]-pyrimidine-6-carboxylate (219 mg, 0.902 mmol) and p-toluene sulfonic acid monohydrate (45 mg, 0.24 mmol). The reaction mixture was heated at 150°C under microwave irradiation for 15 minutes (30 minutes in Teo et al., 2015) and concentrated using the rotary evaporator. The residue was dissolved in DCM (dichloromethane) 25 mL and washed with brine twice. The organic layer was dried over magnesium sulphate and concentrated under reduced pressure. The residue was purified by chromatography (silica gel, DCM ramping to DCM: EtOAc 5% after 10 minutes) to give a white solid (170 mg).

4-((4-Fluoro-2-isopropoxyphenyl)amino)-5-methyl thieno[2,3-d] pyrimidine-6-carboylic acid.

To a solution of Methyl 4-((4-fluoro-2-isopropoxyphenyl)amino-5-methyl thieno[2,3-d] pyrimidine-6-carboxylate (170 mg, 0.45 mmol) in a mixture of THF/MeOH/H_2O (1:1:1, 60 mL) was added LiOH (366 mg, 15.3 mmol). The reaction mixture was dissolved by sonication and heating prior to adding LiOH. The reaction mixture was stirred at room temperature overnight and washed with DCM (20 mL). The aqueous layer was heated at 50°C for 10 minutes and acidified to pH 3 with 2 M HCl. The precipitate was filtered, washed with H_2O (3

x 25 mL) and dried under reduced pressure to give 4-((4-Fluoro-2-isopropoxyphenyl)amino)-5-methyl thieno[2,3-d] pyrimidine-6-carboylic acid as a white solid. ^{1}H NMR (DMSO-d_6) δ 1.32 (d, 6H, OCH(CH_3)$_2$), 3.07 (s, 3H, thienomethyl), 4.80 (m, 1H, OCH(CH_3)$_2$), 6.82 (dd, 1H, aromatic-H), 7.10 (dd, 1H, aromatic-H), 8.57 (s, 1H, pyrimidal-H), 13.66 (s, 1H, RCO_2H). Elemental analysis of $C_{17}H_{16}FN_3O_3S$: Carbon 56.39%, Hydrogen 4.38%, Nitrogen 11.56% (expected 56.50%, 4.46% and 11.63% respectively). These data were in agreement with those in the literature.

2.8.2.2 Synthesis of Hybrid Compound 6: 3-[4-(morpholin-4-yl)thieno[3,2-d]pyrimidin-2-yl]phenyl-4-{[4-fluoro-2-(propan-2-yloxy)phenyl]amino}-5-methylthieno[2,3-d]pyrimidine-6-carboxylate

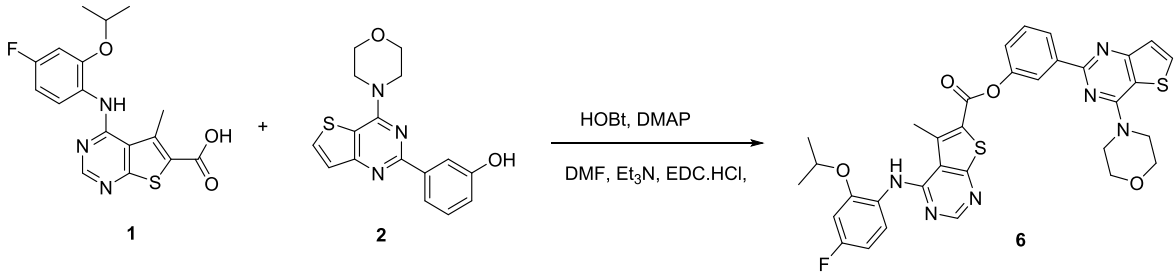

To 4-((4-fluoro-2-isopropoxyphenyl)amino)-5-methylthieno[2,3-d]pyrimidine-6-carboxylic acid, **1**, (40 mg, 0.11 mmol) in DMF (2 mL) was added 1-ethyl-3-(3-dimethylaminopropyl)carbodiimide hydrochloride (EDC.HCl) (20 mg, 0.1 mmol), 1-hydroxybenzotriazole hydrate (HOBT) (16 mg, 0.1 mmol), 3-[4-(4-morpholinyl)thieno[pyrimidin-2-yl]phenol (33 mg, 0.1 mmol), triethylamine (100 µL, 0.67 mmol) and 4-dimethylaminopyridine (catalytic). The reaction mixture was stirred at RT overnight. The reaction mixture was diluted with ethyl acetate (10 mL) and washed twice with brine and once with sodium carbonate (sat). The organic layer was separated, dried ($MgSO_4$), filtered and concentrated *in vacuo*. The residue was purified by ISCO Combiflash as above to afford an off-white solid (16 mg, 24%). Due to the low yielding reaction, no ^{13}C NMR spectrum was recorded. ^{1}H NMR ($CDCl_3$) 1.45 (6H, d, J = 6 Hz), 3.23 (3H, s), 3.90 – 3.93 (4H, m), 4.07- 4.11 (4H, m), 4.66 (1H, sept, J = 6 Hz), 6.71 (2H, dd,

J= 10, 3 Hz), 7.34- 7.36 (1H, m), 7.53 – 7.57 (2H, m), 7.77 (1H, d, J = 5.5 Hz), 8.33 (1H, dd, J= 2.5, 1.5 Hz), 8.44-8.47 (2H, m), 8.68 (1H, s), 8.83 (1H, dd, J =9, 6 Hz). HRMS: $C_{33}H_{29}FN_6O_4S_2$. H+; Calcd 667.1748; Found 667.1728. Elemental anal. Calcd, for $C_{33}H_{29}FN_6O_4S_2$. 0.75 CH_2Cl_2; C, 56.27; H, 4.27; N, 11.67; Fnd, C, 56.79; H, 4.42; N, 11.63.

2.8.2.3 Synthesis of Hybrid Compound 7: 2-[4-amino-1-(propan-2-yl)-1H-pyrazolo[3,4-d]pyrimidin-3-yl]-1H-indol-6-yl 4-{[4-fluoro-2-(propan-2-yloxy)phenyl]amino}-5-methylthieno[2,3-d]pyrimidine-6-carboxylate

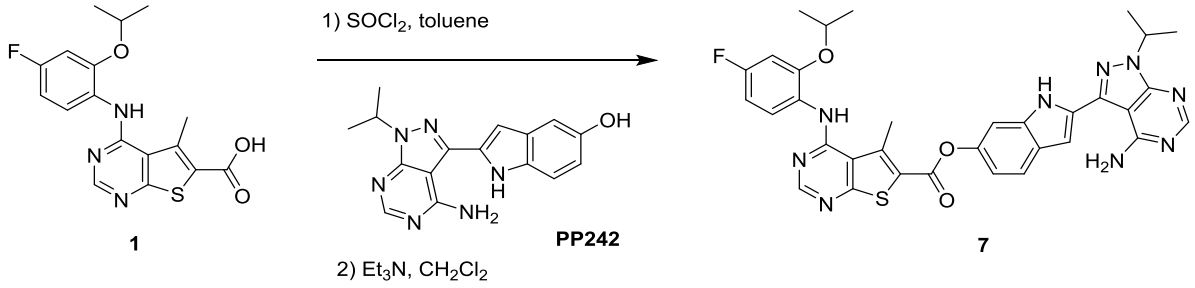

To compound **1**, 4-((4-fluoro-2-isopropoxyphenyl)amino)-5-methylthieno[2,3-d]pyrimidine-6-carboxylic acid, (39 mg, 0.11 mmol) in toluene (8 mL) was added thionyl chloride (15 µL, 0.2 mmol), one drop of dimethylformamide (DMF), and the reaction mixture was refluxed for two hours. After cooling, volatiles were removed in vacuo. The residue was re-dissolved in dichloromethane (2 mL) and reconcentrated then redissolved in dichloromethane (2 mL). To the reaction mixture was added PP242**,** 2-[4-amino-1-(propan-2-yl)-1H-pyrazolo[3,4-d]pyrimidin-3-yl]-1H-indol-5-ol, (35 mg, 0.11 mmol) and excess triethylamine (95 µl) in dichloromethane (2 mL) and the reaction mixture was stirred at RT overnight. The reaction mixture was extracted with dichloromethane (10 mL) and washed (sat. $NaHCO_3$ solution, 10 mL). The organic extracts were separated, dried ($MgSO_4$) then filtered and concentrated *in vacuo*. Pure product was obtained by chromatography on an ISCO Combiflash from dichloromethane (neat) to EtOAc/dichloromethane (9:1) gradient. A red crystalline solid (10 mg, 14% yield) was obtained from a $CDCl_3$ solution, one crystal of which was studied in the solid state. Due to the low yielding reaction, no ^{13}C NMR spectrum was recorded.^1H NMR ($CDCl_3$) 1.27 (6H, d, J = 6 Hz),

1.44 (6H,d, J = 5 Hz), 3.22 (3H, s), 4.68 (1H, sept, J = 6 Hz), 5.21 (1H, sept, J = 6 Hz), 6.04 (2H, br s), 6.73 (2H, dd, J= 10, 3 Hz), 6.90 (1H, s), 7.13 (1H, m), 7.48 (2H, d, J = 2 Hz), 8.42 (2H, d, J = 2 Hz), 8.67 (1H, s), 8.81 (1H, dd, J =9, 6 Hz), 9.30 (1H, s). HPLC purity (>96 %). HRMS: $C_{33}H_{29}FN_6O_4S_2$. H^+ calcd; 652.2249; found 652.2256.

2.9 Commercial inhibitors

Inhibitor	**Target**	**Supplier**
Cercosporamide	MNK1/2, JAK3	Tocris Bioscience
CGP57380	MNK1/2	Tocris Bioscience
PP242	mTORC1/2	Med Chem Express
Staurosporine	Multiple	Sigma Aldrich
RK-33	DDX3	Sellekchem
RO-3306	CDK1	Sigma Aldrich
PI-103	PI3K	Sellekchem

2.10 Statistics

All statistical analyses were performed using GraphPad Prism 7 software (La Jolla, CA, USA). *In vitro* log dose-response curves were calculated using nonlinear regression with variable slope after normalising absorbance to DMSO treated controls, with the concentration required to inhibit the Resorufin response by 50% reported as the IC_{50}.

2.11 Molecular modelling

Molecular modelling was performed using UCSF Chimera (Pettersen, Goddard et al., 2004) following attendance at a ligand-protein docking and computer-aided drug design course at the Swiss Institute of Bioinformatics (SIB).

2.12 RNA extraction and qRT-PCR

RNA extractions were performed using the Qiagen miRNeasy RNA extraction kit, with an on-column DNase digestion. RNA concentrations were measured on a NanoDrop 1000 spectrophotometer. For qRT-PCR, RNA samples were diluted to a consistent concentration then cDNA was prepared in duplicate using a High Capacity cDNA Reverse Transcription Kit from Life Technologies with random primers. A control “no RT” reaction was performed in parallel to confirm that all genomic DNA had been degraded. qRT-PCR was performed on each cDNA in duplicate (i.e. two technical replicates), using TaqMan Universal PCR Master Mix, No AmpErase UNG (Life Technologies)) and TaqMan DDX3X assay (Life Technologies). GAPDH and HPRT1 were used for normalisation.

2.13 CRISPR

A protocol based on the CRISPR-Cas9 endonuclease (Ran et al., 2013) was used to create genetic modification to MRC5 cells.

2.13.1 Design of sgRNA

The genomic DNA sequence from the gene of interest was imported from Ensembl into Benchling, after cross-referencing with Uniprot. The CRISPR sgRNA design tool was used to analyse a 1 kb fragment of the region of interest and locate suitable target sites by identifying 20-bp sequences directly upstream of any 5’NGG (PAM sequence). Both on- and off-target sites were computationally predicted, allowing selection of the three highest ranked sgRNA sequences. Primers were also designed at this stage for future use in the surveyor assay. Using Primer-Blast, oligonucleotides were designed to anneal approximately 500 bp upstream and downstream from the intended target site.

sgRNA	**5’-3’**	**3’-5’**
1	CACCGAACAAACACTCGCTTAGCAG	AAACCTGCTAAGCGAGTGTTTGTTC
2	CACCGGTGGCAGTGGAAAATGCGCT	AAACAGCGCATTTTCCACTGCCACC
3	CACCGCGAGTTCTCGGTACTCTTCA	AAACTGAAGAGTACCGAGAACTCGC

Oligonucleotide	**5’-3’**

pF	AAAGGGGAGCGAATGCGTAA
pR2	TTTCCACTCCGGAAACGCAG

2.13.2 Cloning of sgRNA into the pSpCas9(BB) Vector for Co-expression with Cas9

The top and bottom strands of the oligonucleotides for each sgRNA were resuspended in nuclease-free water to a final concentration of 100 µM. The following mixture was prepared for phosphorylation and annealing the top and bottom strands of the sgRNA oligos:

Component	**Volume (**µL)
sgRNA top (100 µM)	1
sgRNA bottom (100 µM)	1
T4 ligation buffer 10x	1
T4 PNK	1
ddH_20	6
Total	**10**

2.13.3 Functional Validation of sgRNA

MRC5 cells were maintained in MEM with 10% FBS at 37°C and 5% CO_2. Cell maintenance and passage was performed as detailed previously in the tissue culture protocol above.

2.13.4 Transfection of MRC5

Cells were seeded in a 6-well plate at a density of 1 x 10^5 cells/ 500 µL MEM without selection 16 hours prior to transfection. Individual wells were seeded for each sgRNA plasmid and for the YFP-control plasmid. Cells were transfected at 70-90% confluency with Lipofectamine 2000 according to the manufacturer's instructions. For pSpCas9(sgRNA) plasmids, 500 ng of sequence verified plasmid was transfected. In addition, a YFP plasmid was transfected to monitor transfection efficiency. After 24 hours, the cells were checked for transfection efficiency using a standard epi-fluorescent microscope. After 48 hours, G418

was added at 400 µg/ml and cells were incubated at 37°C for five days. Cells that had undergone successful transfection with a pSpCas9(sgRNA) plasmid were resistant to G418, whilst those that had not (including YFP-control) died. The pSpCas9(sgRNA) transfected cells were dissociated from the plate, pelleted and re-suspended in complete media. 100 µL of each sample of pSpCas9(sgRNA) transfected cells (sgRNA1, sgRNA2 and sgRNA3) were utilised for the surveyor assay and the remainder were taken forward for the limiting dilution.

2.13.5 Surveyor Assay for Assessment of CRISPR Cleavage Efficiency

Genomic DNA extraction was performed on each polyclonal pSpCas9(sgRNA) transfected cell line (sgRNA1, sgRNA2 and sgRNA3) and wildtype MRC5. The Sigma Aldrich Genelute mammalian genomic DNA miniprep kit was used for DNA extraction. The extracted DNA was normalised to a final concentration of 100-200 ng/µL with ddH_2O. PCR was performed using oligonucleotides pF and pR2 (see above) on wildtype MRC5 (negative control) and each pSpCas9(sgRNA) transfected cell line (sgRNA1, sgRNA2 and sgRNA3). The PCR product (5 µL) was resolved on a 1% (w/v) agarose gel to check for single band products using a high UV transilluminator.

Component	**Volume (µL)**
5x Phusion HF buffer	4
10 mM dNTPs	0.4
Oligonucleotide pF	0.5
Oligonucleotide pR2	0.5
Template DNA (100 ng)	Variable
Phusion DNA polymerase	0.5
Nuclease-free water	Up to 20
Total	**20**

The following cycling conditions were used:

Cycle number	**Denature**	**Anneal**	**Extend**

1	95°C, 2 min		
2-31	95°C, 20 sec	60°C, 20 sec	72°C, 30 sec
32			72°C, 3 min

The following components were added directly to the remaining 15 µL of PCR product for each sample:

Component	**Volume (**µL)
NEB buffer #2	2
ddH_2O	2.5
T7E1	0.5
Total	**5**

The mixture was incubated at 37°C for 30 mins before adding 1 µL 0.5M EDTA to stop the reaction. The final products were resolved on a 1% (w/v) agarose gel and imaged using a high UV transilluminator. The negative control showed one band corresponding to the size of the PCR product, whereas the pSpCas9(sgRNA) transfected cell lines (sgRNA1, sgRNA2 and sgRNA3) had smaller fragments indicating efficient cleavage (data not shown).

2.13.6 Isolation of clonal cell lines by dilution

Cells were counted and diluted in MEM with 10% FBS to a final concentration of 0.33 cells per 100 µL to reduce the likelihood of having multiple cells per well. Using a multi-channel pipette, 100 µL of diluted cells were added to each well of a 96-well plate, two plates were prepared for each sample of pSpCas9(sgRNA) transfected cells (sgRNA1, sgRNA2 and sgRNA3). The putative monoclonal cell lines were grown in MEM with 10% FBS for a further for 21 days, before each line was transferred to culture flasks for further growth.

2.13.7 Initial Knockout Validation by Western Blotting

Putative monoclonal cell lines were harvested and lysed according to the standard protocol, with their eluate resolved by SDS-PAGE and Western

blotting (Section 2.4). Primary antibodies for monitoring the loading and for the protein of interest were utilised as indicated.

2.13.8 Genotyping by Sanger Sequencing

A genomic DNA extraction was performed on knockout cell lines confirmed by Western blotting. The 1000 bp region surrounding the target sequence for the sgRNA-directed Cas9 was amplified by PCR and subsequently sequenced by GATC Biotech.

3 Dual-inhibition of MNK-eIF4E and PI3K/AKT/mTOR Pathways and the Effect on Cell Migration

3.1 Introduction

During translation initiation, the cap structure on eukaryotic mRNA facilitates the recruitment of initiation factors to allow ribosome binding and initiation at the correct start site (Sonenberg & Hinnebusch, 2009). eIF4E interacts directly with the cap and forms complexes on its convex surface with either inhibitory regulatory proteins (4E binding proteins, 4E-BPs; see Section 1.1.4.1) or with the scaffold proteins, eIF4GI and eIF4GII. *In vivo* eIF4G exists partly in the form of a complex with eIF4E and eIF4A, constituting the initiation factor eIF4F (see Section 1.1.1). Within the sequences of eIF4GI and eIF4GII there are domains that interact with eIF4E, eIF4A, eIF3, PABP and the kinases, MNK1/2, which modulate the phosphorylation of eIF4E on Ser209 (Beggs et al., 2015, Klann & Dever, 2004). MNK1 and MNK2, which act at the convergence point of ERK and p38MAPK, phosphorylate eIF4E at the physiological site *in vitro* and *in vivo* (Bhat et al., 2015). In contrast, the association of 4E-BPs with eIF4E is modulated by phosphorylation events controlled *via* the mTORC1 signalling pathway. (Figure 3-1). Current models suggest that hypophosphorylated 4E-BP1 binds to eIF4E to inhibit cap-dependent translation, a process readily reversed following its phosphorylation. In several model systems, the dissociation of hyperphosphorylated 4E-BP1 from eIF4E leads to the binding of eIF4G to eIF4E, promoting the phosphorylation of eIF4E and the initiation of protein synthesis. This increased level of phosphorylation of eIF4E also correlates with an increase in levels of mesenchymal markers such as N-cadherin, fibronectin and vimentin, along with the acquisition of invasive properties and increased cell migration (Robichaud et al., 2015).

MKNK1 and MKNK2 genes were altered by mutation, deletion and amplification. Bioinformatic analysis using cBioPortal, found that MKNK1 and MKNK2 were amplified by copy number in 18.7% of queried samples in neuroendocrine prostate cancer. Both genes were also amplified in pancreatic (17%), ovarian (13%) and breast (10%) cancers (Figure 3-2A). High levels of

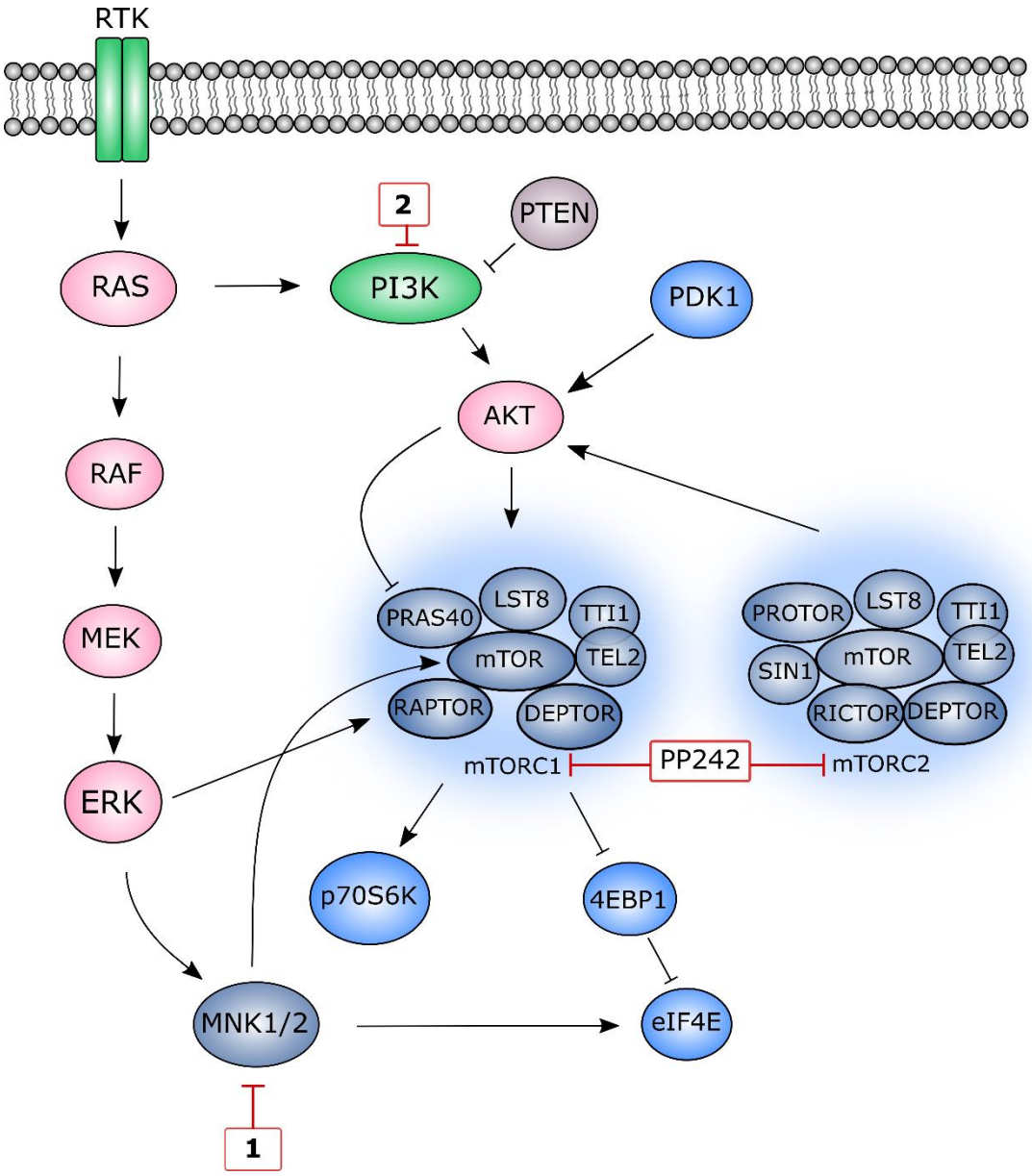

Figure 3-1. A simplified schematic representation of MNK1/ 2 and mTOR pathways. Red boxes depict several inhibitors of specific pathway components used in this study. MNK1/2 lie at the convergence point of both the p38MAPK pathway and ERK pathways and upon activation, phosphorylate eIF4E. Class I PI3 kinases are activated by RTKs resulting in the conversion of PIP2 to PIP3, a secondary messenger that is essential for AKT translocation to the plasma membrane. The level of PIP3 is negatively regulated by the tumour suppressor, PTEN. AKT is partially activated by PDK1 and becomes fully activated upon phosphorylation at Ser473, a process that can be catalysed by multiple proteins. mTOR forms two distinct multiprotein complexes, mTORC1 and mTORC2. mTORC1 is activated indirectly through AKT, which also phosphorylates the negative regulator, PRAS40. Activated mTORC1 stimulates protein translation by phosphorylating 4E-BP1 on several residues, releasing eIF4E allowing it to participate in translation initiation. In addition to phosphorylating other translational targets, mTORC1 also phosphorylates p70S6 kinase (p70S6K), which becomes fully activated following PDK1-mediated phosphorylation.

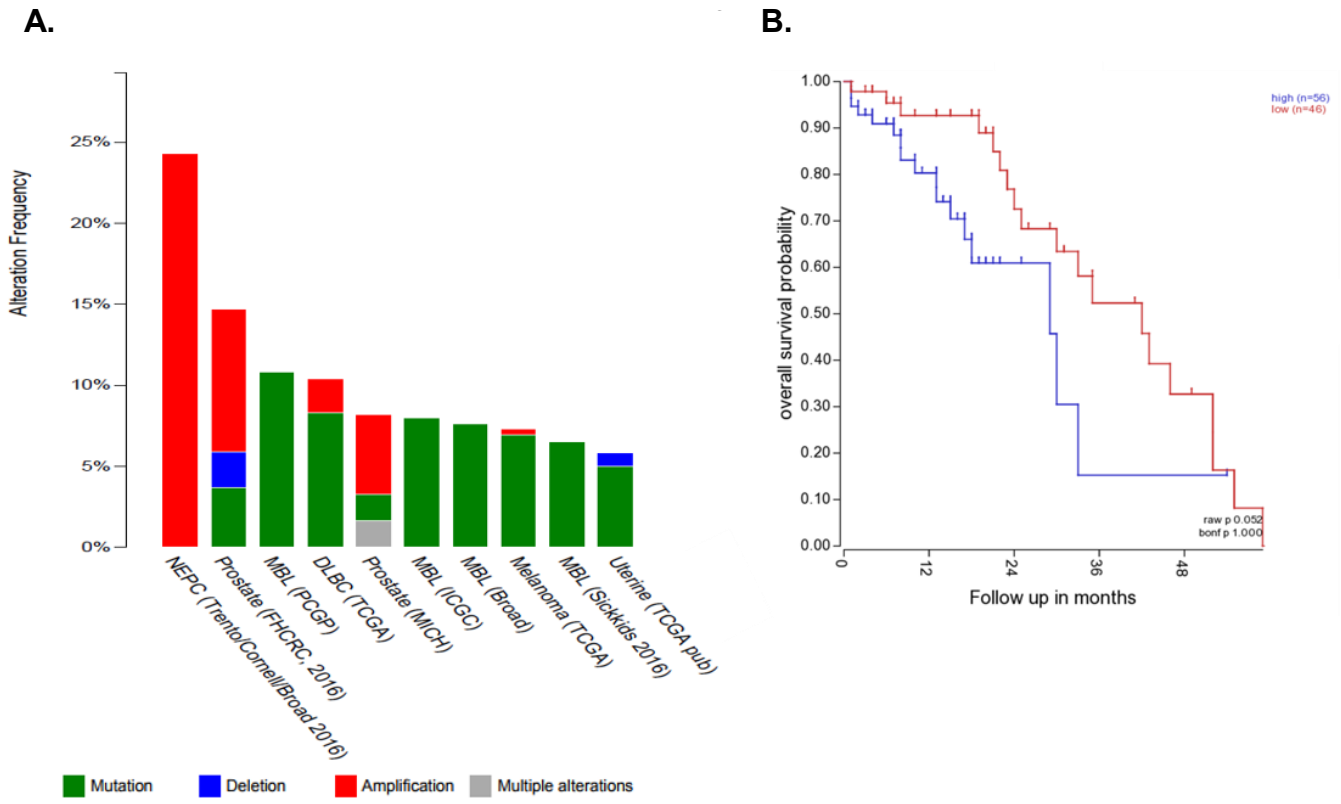

Figure 3-2. Bioinformatic analysis of MKNK1 and MKNK2. A. Cross-cancer alteration summary for MKNK1, MKNK2 using cBioPortal (showing the top ten studies in which most alterations occurred). The histogram is colour-coded to indicate the alteration type. **B.** Kaplan Meier analysis of MKNK1 in pancreatic ductal adenocarcinoma (132 samples) showing that high MKNK1 expression correlates with a lower overall survival probability (Stratford et al., 2010).

MKNK1 reduced survival time in several studies, including in a recent pancreatic ductal adenocarcinoma study, shown in Figure 3-2B (Stratford et al., 2010).

MNK1/2 are key regulators of the translational machinery, and their primary target is eIF4E (Truitt et al., 2015). eIF4E is a general translation factor, which has the potential to selectively enhance a subset of mRNAs involved in oncogenesis upon eIF4E phosphorylation on Ser209 by MNK1/2. The phosphorylated form of eIF4E has strong links to carcinogenesis (Hou et al., 2012). Recent studies have found that high levels of eIF4E-P coincided with poor clinical outcome and chemoresistance in human cancers ((Bhat et al., 2015, Li et al., 2017, Mamane et al., 2007). In addition, MNK1/2 provide an attractive cancer target as MNK1/2 KO mice were found to be completely viable (Ueda et al., 2004).

Cancer cells require elevated protein synthesis and exhibit augmented activity of the translation machinery. Exploiting this “addiction” to protein synthesis has emerged as a promising therapeutic option for cancer treatment (Teo et al., 2015b). As outlined above, eIF4E is necessary for mRNA translation and its availability and phosphorylation are regulated by the PI3K/AKT/mTOR and MNK1/2 pathways, respectively. There is now evidence for a direct functional interaction between the AKT/mTOR pathway and the MNK/eIF4E pathway. Recent work has shown evidence for a MNK-associated mTORC1 complex (Figure 3-3). In T cell activation, active MNK facilitates mTORC1 association with its downstream substrates and stabilises the interaction of mTORC1 with TEL2 (Phosphatidyl Inositol 3' Kinase-related Kinase (PIKK) stabiliser) (Brown & Gromeier, 2017) and prevents DEPTOR binding to the complex. This interaction between MNK and mTORC1/TEL2 is believed to support mTORC1/substrate proximity in a MNK-responsive manner and is required for efficient T cell activation and for mitogenic signalling (Brown & Gromeier, 2017). However, the AKT/mTOR pathway and the MNK/eIF4E pathway are not always linked in this way. This was reported recently, where the downregulation of one pathway correlated with the activation of the other, which subsequently supported cell proliferation and cell survival in prostate and lung cancer

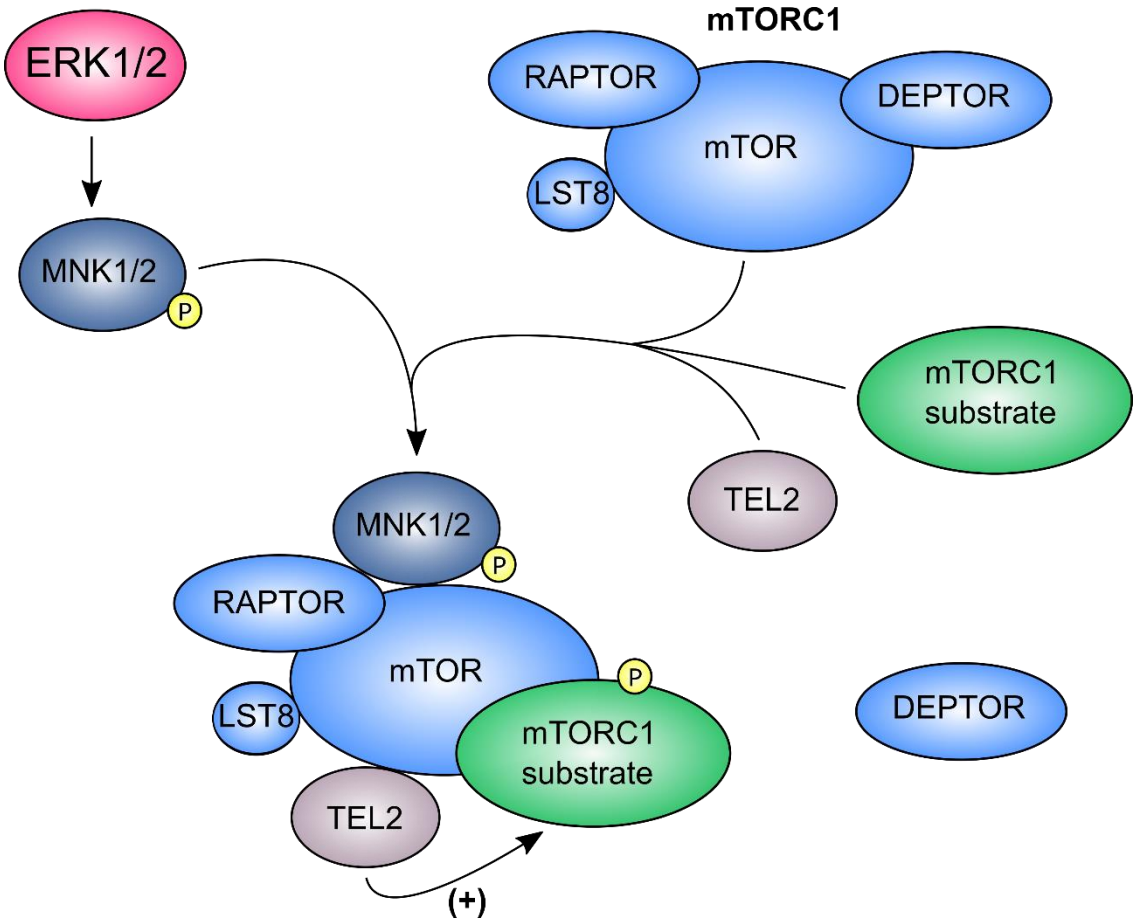

Figure 3-3. MNK1/2 controls mTORC1: substrate association. MNK1/2 regulates mTORC1 signalling and associates with mTORC1 directly. This interaction results in the displacement of DEPTOR, while enhancing TEL2:mTORC1 binding. The latter stabilises mTORC1/substrate interactions whilst DEPTOR prevents TEL2 binding and reduces mTORC1/substrate binding (Adapted from (Brown & Gromeier, 2017)).

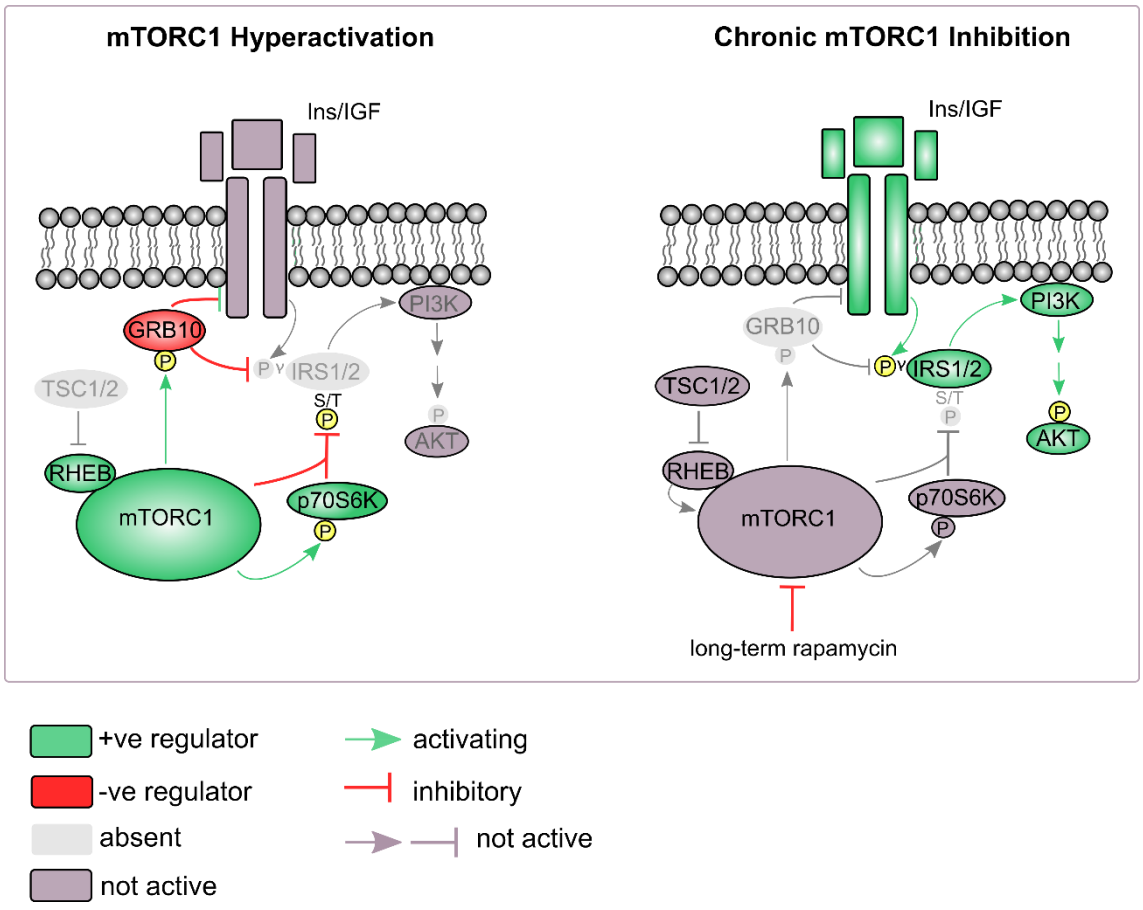

Figure 3-4. The role of mTORC1 in regulating growth factor signalling. mTORC1 orchestrates feedback inhibition of PI3K-AKT signalling by activating GRB10 while inhibiting IRS proteins. Acute mTORC1 inhibition leads to dephosphorylation of GRB10 and IRS1, whilst chronic mTORC1 inhibition leads to changes in the levels of IRS and GRB10 proteins. (Adapted from (Hsu et al., 2011)).

(Folkes et al., 2008, Hemmings & Restuccia, 2015). The apparent interplay between the MNK and mTOR signalling pathways provides a novel therapeutic opportunity to target aggressive migratory cancers (O'Connor et al., 1997, Teo et al., 2015a).

Increases in the eIF4E/4E-BP1 ratio, limits the effect of mTOR inhibitors in regulating levels of eIF4E available to participate in translation initiation (Apsel et al., 2008, Grzmil et al., 2011). Inhibiting MNK kinases may prevent such feedback initiation by targeting eIF4E signalling downstream of mTOR (Zheng & Jiang, 2015). This was observed in both prostate cancer and glioblastoma cell lines, when simultaneous inhibition of MNK1/2 kinases and mTORC1 suppressed cell cycle progression and blocked proliferation. This effect was increasingly pronounced when dual inhibition was employed as opposed to the treatment of single-agents (Folkes et al., 2008, Hemmings & Restuccia, 2015).

Many small molecule inhibitors have been developed to target constitutively active protein kinases and have made a considerable impact in cancer therapy (Bianchini et al., 2008). However, inhibitor-resistant kinases can evolve rapidly in the presence of the drug and the development of drug resistance points towards the need for a multi-targeted approach (Coles, 2012, Vassilev, 2006). Therefore, combinations of drugs are often used to increase the response to treatment in tumour cells. The complex nature of cancer and intra-tumour heterogeneity has led to the concept of hybrid drugs, which act on multiple targets with the need to deliver more than one drug concurrently. This approach involves the linking of two selected pharmacophores that act against different therapeutic intracellular targets simultaneously (Coles, 2012).

It is pertinent at this stage to present an overview of physiochemical parameters relevant to drug discovery including Lipinski's rules. Lipinski’s rule of five predicts that poor absorption or permeation is more likely when a drug candidate has more than five hydrogen bond donors, more than ten hydrogen bond acceptors, a molecular weight greater than 500 and a log P value greater than 5 (Lipinski et al., 2001). The Veber rules propose that in addition to the Lipinski rules, other parameters exist for the description of drug likeness. One of

these parameters being the number of rotatable bonds, an indication of molecular flexibility. Furthermore Veber et al (2002) found that the polar surface area can be used as a reliable indicator of permeation. A total polar surface area (TPSA) of 140 $Å^2$ or above leads to reduced uptake over the lipid bilayer (Veber et al., 2002).

The work described here provides the proof of principle for the development of dual MNK1/2 and PI3K/mTOR inhibiting hybrid molecules and describes their subsequent synthesis. These agents may be an effective option in the treatment of highly migratory cancers through the inhibition of eIF4E.

3.2 Results

3.2.1 Homology Modelling of MNK1 and Predicted Binding Mode of Compound 1

The catalytic domains of MNK1 and MNK2 share 78% sequence identity and are highly conserved ((Oyarzabal et al., 2010). MNK1/2 also possess an unusual (Asp-Phe-Asp) DFD motif in place of the Asp-Phe-Gly (DFG) motif found in all other protein kinases. The DFD motif has less affinity for ATP than the equivalent DFG motif present in other kinases. This is due to a 180° rotation relative to the DFG motif, which locks the kinase in the DFD-out conformation. The Phe in the activation segment flips into the ATP binding site, which obstructs the ATP binding pocket and prevents binding (Jauch et al., 2005).

The design of novel MNK inhibitors has been slow due to the lack of structural information available. MNK1 and MNK2 crystal structures only exist in their DFD/out, inactive conformation (PDB: 2HW6 and 2AC3, respectively). There is one crystal structure available for the active conformation of MNK2 bound to staurosporine (PDB: 2HW7). This has been accomplished by mutating the DFD motif to the generic DFG motif found in other kinases (Jauch et al., 2006, Jauch et al., 2005).

There are three main classes of kinase inhibitors (discussed in detail in Section 1.3.5.1.1). Type I inhibitors, for example, CGP57380 and cercosporamide work by targeting the ATP-binding site in MNK1/2. The ATP-binding site is well-conserved between kinases and so type I inhibitors often have many off-target effects. Cercosporamide was also found to inhibit kinases such as Jak3, GSK3, ALK4 and PIM1 in addition to the MNKs (Basnet et al., 2015). Type II kinase inhibitors exploit both the ATP-binding site and the less conserved adjacent hydrophobic pocket (allosteric site) created by the kinase activation loop (Teo et al., 2015a, Zhao et al., 2014). Following an extensive literature search, type II inhibitor, MNKI-19, was found to be a potent MNK1/2 inhibitor in the nanomolar range in cell-free kinase assays ((Teo et al., 2015a). Subsequent work refers to MNKI-19 as compound **1**.

Based upon the available crystal structures, a homology model of active MNK1 bound to compound **1** was created. Chimera and Modeller were used to build a homology model of MNK1 in the active form (DFD-in) using PDB: 2HW7 as a template. The consensus amino acid sequence of MNK1 was imported into Chimera from Uniprot (Q9BUB5). A BLAST was run on the query sequence and the highest scoring hits displayed (Figure 3-5). A multiple sequence alignment (MSA) was performed on the query sequence and the template PDB: 2HW7 from the BLAST search. The consensus sequence produced from the MSA was used to generate a series of models using Modeller.

A number of models were produced and ranked according to the percentage probability of having the correct fold:

- GA341 - model score derived from statistical potentials; a value > 0.7 generally indicates a reliable model, >95% probability of having the correct fold;
- zDOPE - normalized Discrete Optimized Protein Energy (DOPE), an atomic distance-dependent statistical score; negative values indicate better models.

The initial models showed poor zDOPE scores due to the termini of the query extending beyond the template (PDB: 2HW7) structure, leading to unreliable modelling. The termini were removed and the models rescored. The top-scoring model was selected and used to predict the binding mode of compound **1** (Figure 3-6).The MNK1 homology model was prepared for docking using AutoDock Vina. A number of predictions for the binding mode of compound **1** were proposed. The top scoring (most likely) binding mode was chosen (Figure 3-7). The pyrimidine moiety occupies the ATP-binding pocket, while the fluoroaniline projects into the large hydrophobic pocket.

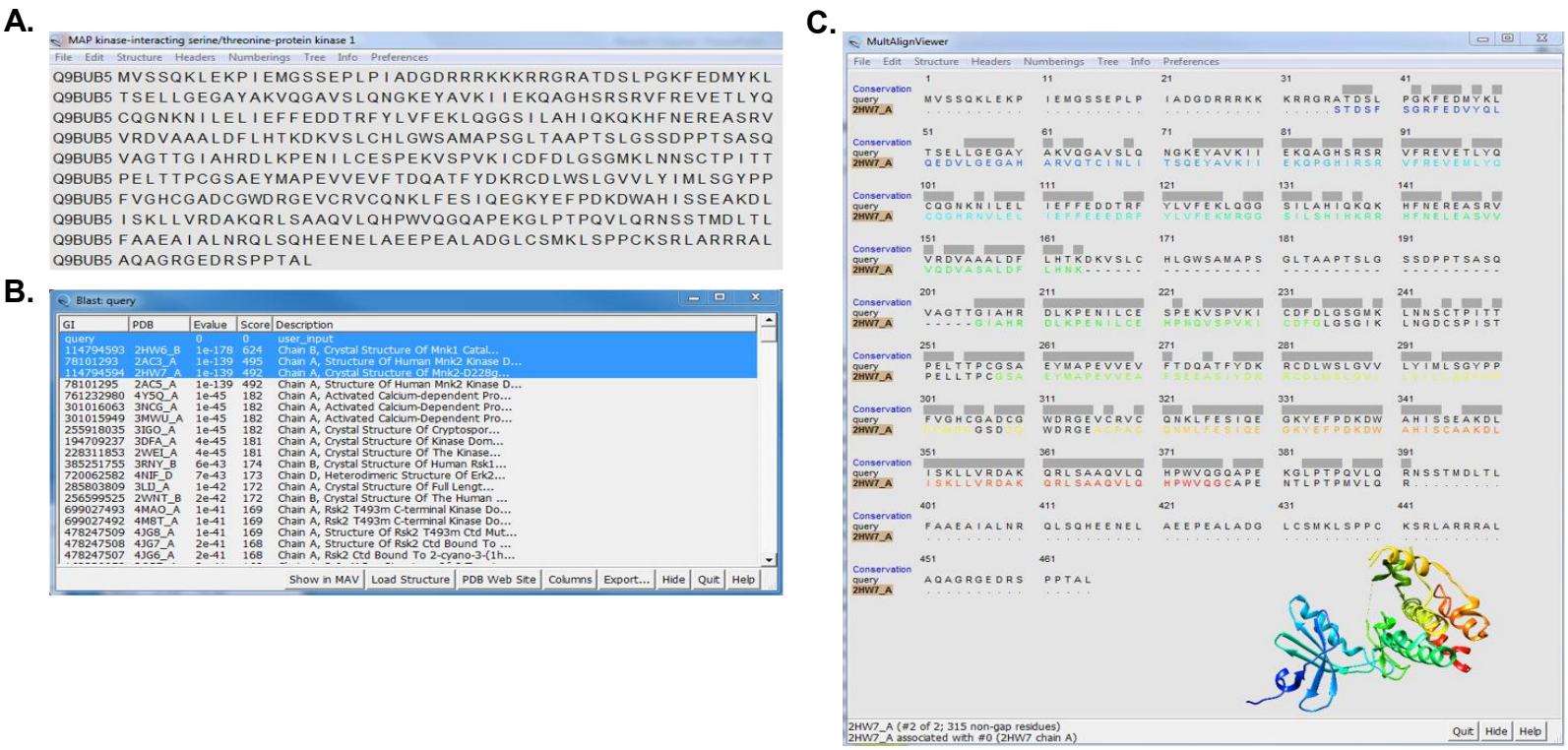

Figure 3-5. BLAST search and multiple sequence alignment (MSA) of MNK1 protein. A. Consensus amino acid sequence of MNK1 imported from Uniprot (Q9BUB5). **B.** BLAST of consensus amino acid sequence of MNK1 showing the highest scoring matches in blue. **C.** Multiple sequence alignment (MSA) of the query sequence, MNK1, and the template (PDB: 2HW7). Completely conserved residues are capitalized and shown in colour from N-terminal blue to C-terminal red. Black capital letters represent highly conserved residues (80% or greater) and black dots represent gaps in the sequence. Molecular graphics and analyses were performed with the UCSF Chimera package (Pettersen et al., 2004).

A.

Modeller Results

Columns Fetch Scores

▶ Treatment of Chosen Models

Model	GA341	zDOPE	Estimated RMSD	Estimated Overlap (3.5 Å)
#1.1	1.00	0.18	6.515	0.600
#1.2	1.00	0.30	6.882	0.556
#1.3	1.00	0.15	6.561	0.585
#1.4	1.00	0.09	6.371	0.613
#1.5	1.00	0.15	6.668	0.592

Hide Quit Help

C.

File Compounds Column Selection

S	Score	RMSD l.b.	RMSD u.b.
V	-7.8	0.0	0.0
V	-7.6	3.122	6.511
V	-7.6	3.102	4.742
V	-7.4	3.496	6.366
V	-7.3	2.263	3.089
V	-7.3	5.9	8.835
V	-7.3	4.38	7.203
V	-7.2	2.371	3.727
V	-7.1	3.811	6.814

B.

Figure 3-6. Homology modelling of MNK1. A. Modeller was used to generate a series of models of MNK1 in the active form**.** Models were produced and ranked according to the percentage probability of having the correct fold. **B.** Illustration of Model 1.4, the best overall fitting model. Coloured from N-terminal (blue) to C-terminal (red). **C.** Docking of compound **1** in model #1.4. Each line of the table represents each docking solution. The RMSD lb (lower bound) and RMSD ub (upper bound) of a docked ligand are calculated by AutoDock Vina. This indicates how similar each position is to the best-scoring position found. Molecular graphics and analyses were performed with the UCSF Chimera package (Pettersen et al., 2004).

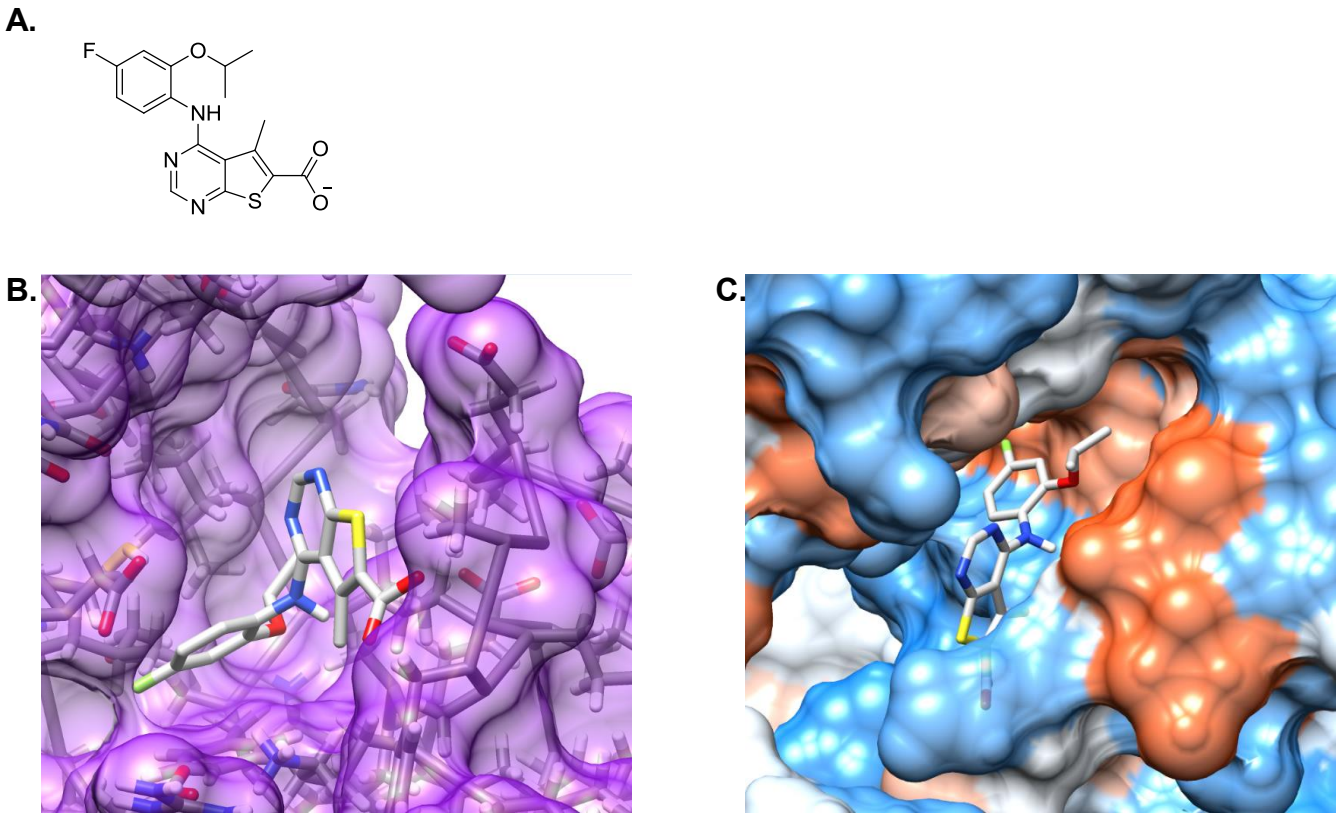

Figure 3-7. Predicted binding mode of compound 1. A. Structure of compound **1**. **B.** MNK1 homology model shown in purple with the highest scoring predicted binding mode of compound **1** (grey). **C.** MNK1 homology model coloured by hydrophobicity surface: from blue for the most hydrophilic, to white, to red for the most hydrophobic. Molecular graphics and analyses were performed with the UCSF Chimera package (Pettersen et al., 2004).

3.2.2 Synthesis of MNK1/2 Inhibitor, Compound 1

Compound **1** was not available commercially and was synthesised in two steps (Figures 3-8 to 3-11). The first step was a nucleophilic aromatic substitution reaction and can be explained by the addition-elimination mechanism. This involves the addition of a nucleophile, an electron-rich group or atom, followed by the elimination of the leaving group. In a carbon-chlorine bond, the chlorine is more electronegative than the carbon. The carbon in the carbon-chlorine bond is electrophilic i.e. has a partial positive charge. The amino group on the fluoroaniline acts as a nucleophile. The second step involves the base-catalysed hydrolysis of the ester formed in the first step. A strong base, LiOH, hydrolyses the ester to a carboxylate salt and produces methanol as a byproduct. The carboxylate salt is then protonated to form the carboxylic acid, the final product (Figures 3-10 and 3-11). This thienopyrimidinyl compound provides a scaffold for the development of future novel compounds and hybrid drugs.

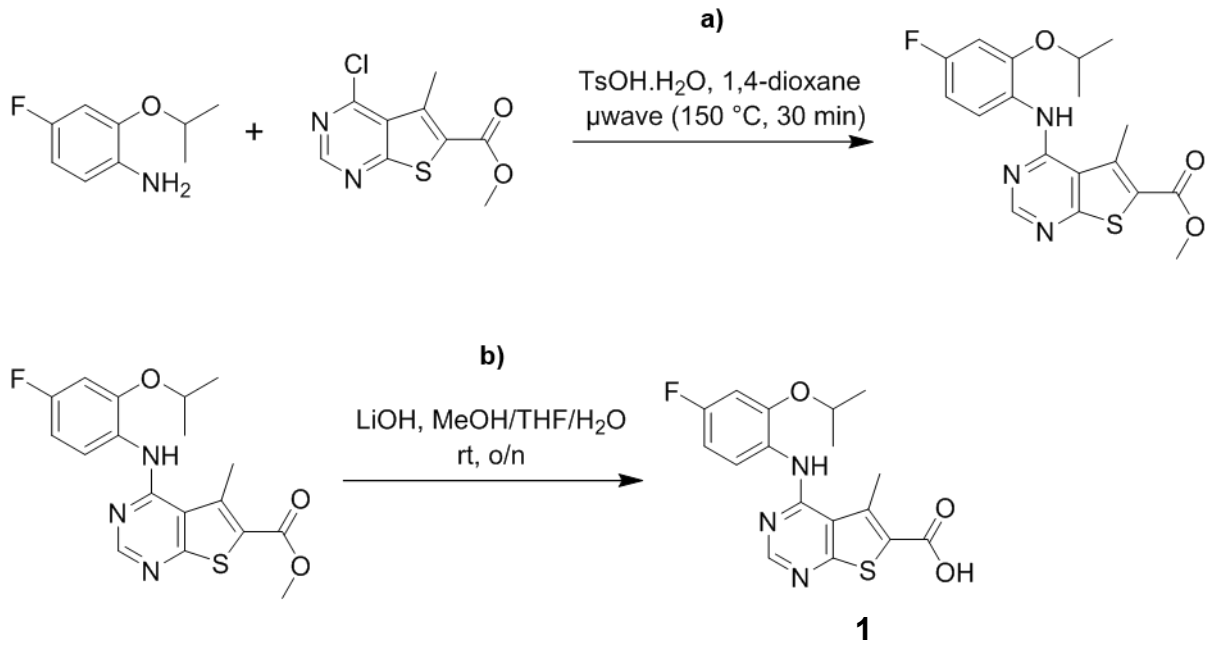

Figure 3-8. Synthesis of thienopyrimidinyl derivative, 1. a) Aromatic substitution under microwave conditions. **b)** Hydrolysis of the ester to produce the final compound.

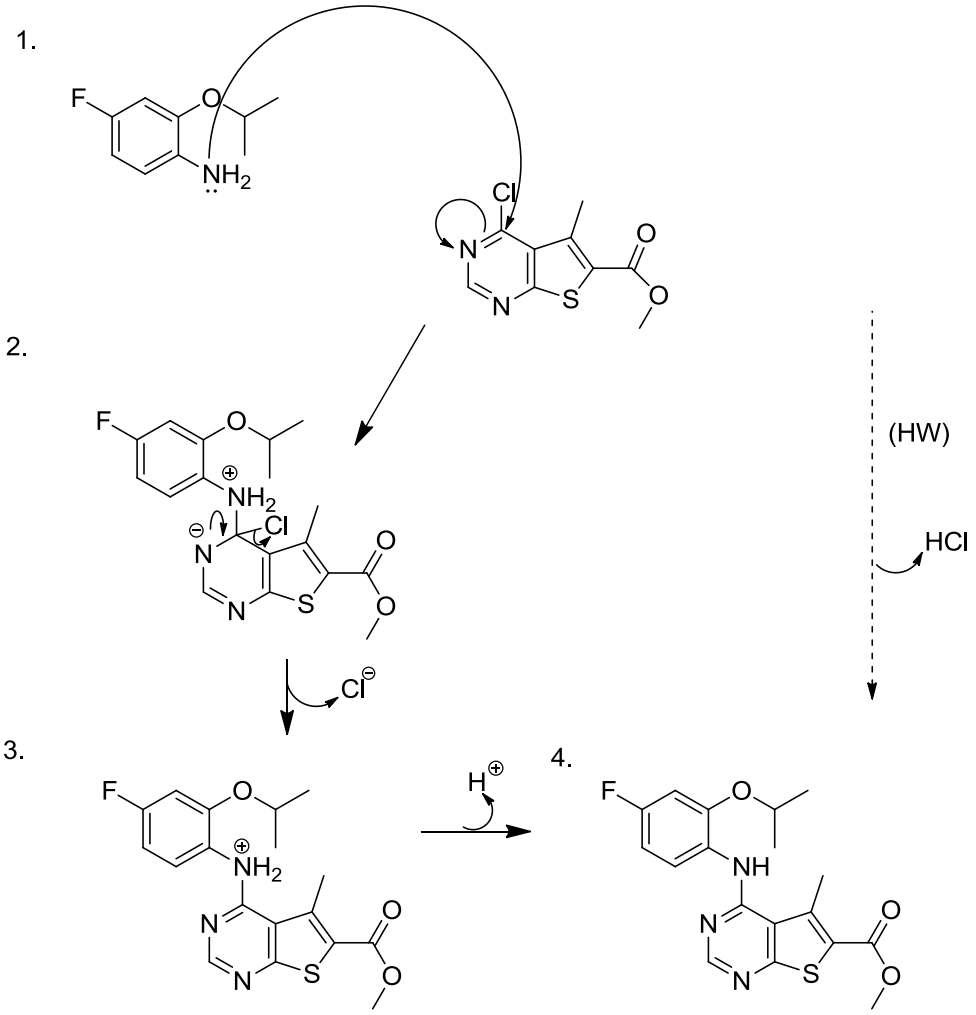

Figure 3-9. Proposed mechanism of aromatic substitution.

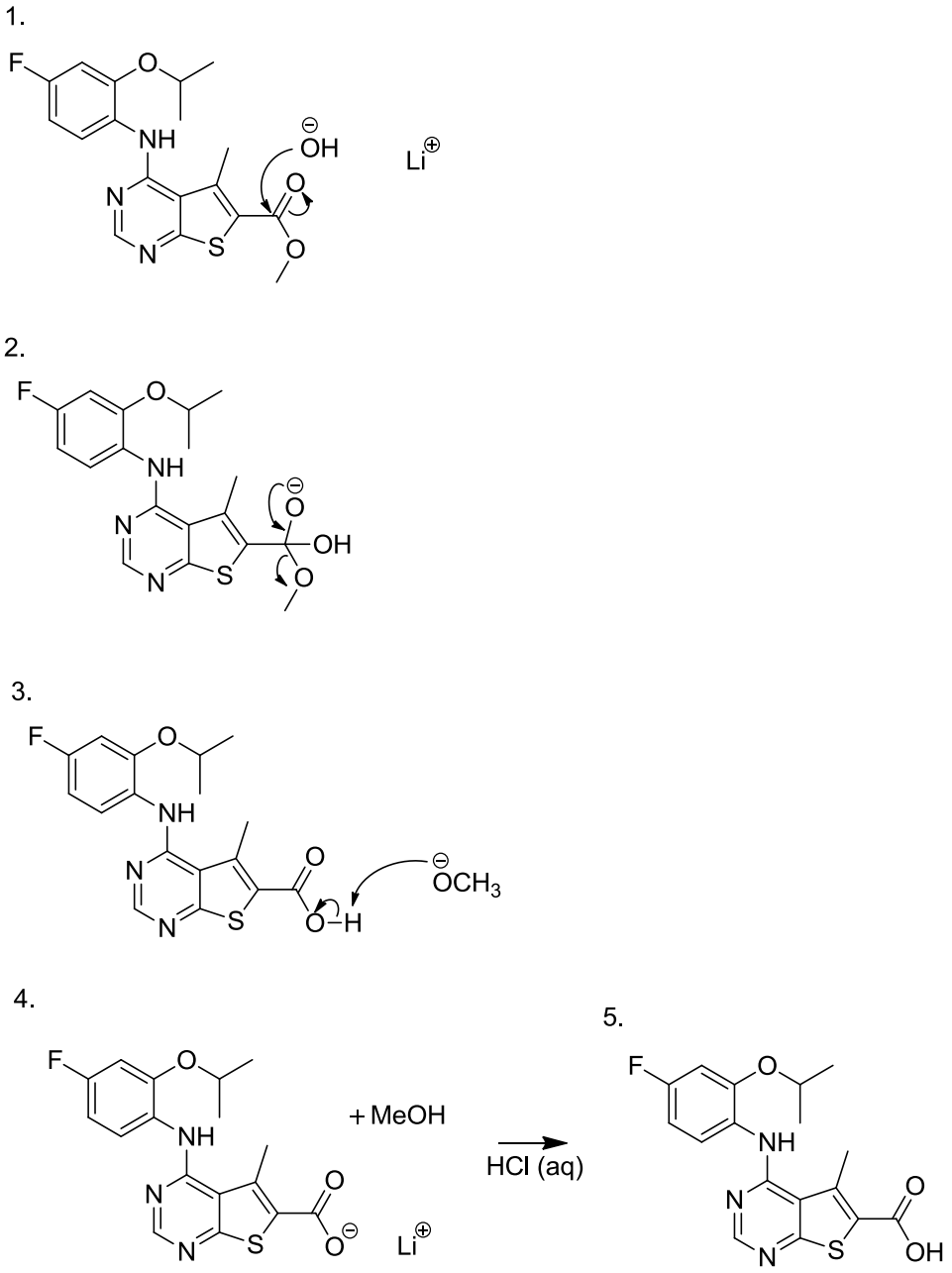

Figure 3-10. Proposed mechanism of ester hydrolysis.

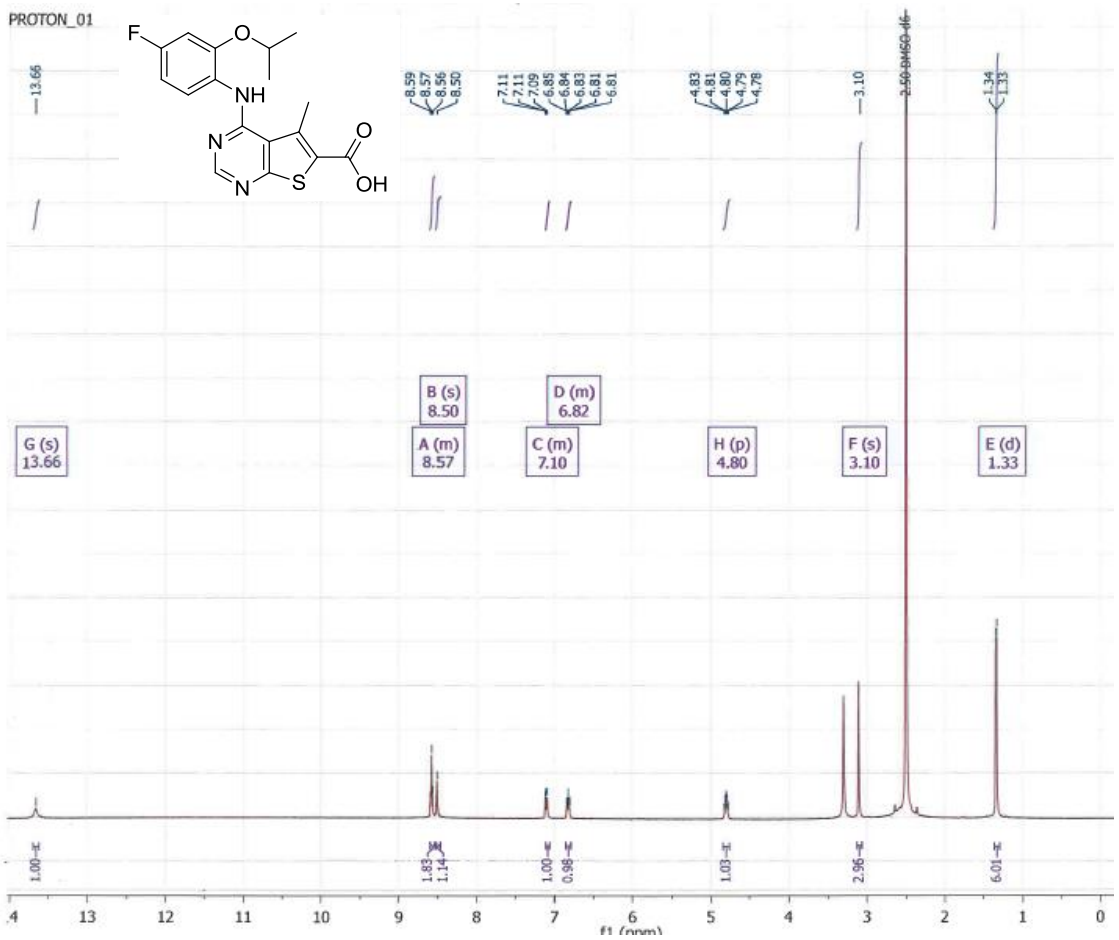

Figure 3-11. ^{1}H NMR (DMSO-d_6) spectrum of compound 1.

3.2.3 Compound 1 Inhibits eIF4E Phosphorylation

MNK1 and MNK2 lie downstream of both p38MAPK and ERK pathways and phosphorylate Ser209 of eIF4E, enhancing translation of specific mRNAs involved in cell survival (Hou et al., 2012). Western blot analysis was carried out to determine if compound **1** was an effective MNK1/2 inhibitor in cells. MRC5 cells were chosen on the basis that they exhibited a relatively high basal level of eIF4E-P and could be used in future work to study cell migration. As shown in Figure 3-12A and quantified in Figure 3-12B, compound **1** reduced the level of eIF4E phosphorylation in concentration-dependent manner, being effective at concentrations above 2.5 µM. As expected, the known MNK1/2 inhibitors CGP57380 and cercosporamide, also caused a reduction in eIF4E phosphorylation. The inactive form of CGP57380 (neg CGP) had no effect on eIF4E phosphorylation compared to the DMSO control.

Compound **1** was profiled against a panel of kinases to assess its activity against several targets including upstream MNK1/2 proteins, AKT and p38MAPK, to be confident that the reduction in phosphorylation of eIF4E was due to the effect of compound **1** on its intended target, MNK1/2. Compound **1** was found to be a very potent inhibitor of MNK1/2 (Figure 3-12C) and showed greater inhibitory activity towards eIF4E phosphorylation compared to cercosporamide, reported previously in the literature (Beggs et al., 2015). Compound **1** had no effect on AKT or p38MAPK activity *in vitro*, however, compound **1** did have a significant off-target effect on the kinase, PIM1. PIM1 is a serine/ threonine kinase, which has been shown to have roles in cell survival, proliferation and differentiation (Shah et al., 2008). It is also implicated in translational control, as studies have identified 4E-BP1 as a target. PIM1 phosphorylates 4E-BP1 on Thr37/Thr46, priming the protein for subsequent phosphorylation. Partial PIM1 inhibition by compound **1** may promote the hypophosphorylated form of 4E-BP1, increasing the ratio of 4E- BP1 -bound eIF4E thereby inhibiting translation rates (Chen et al., 2011).

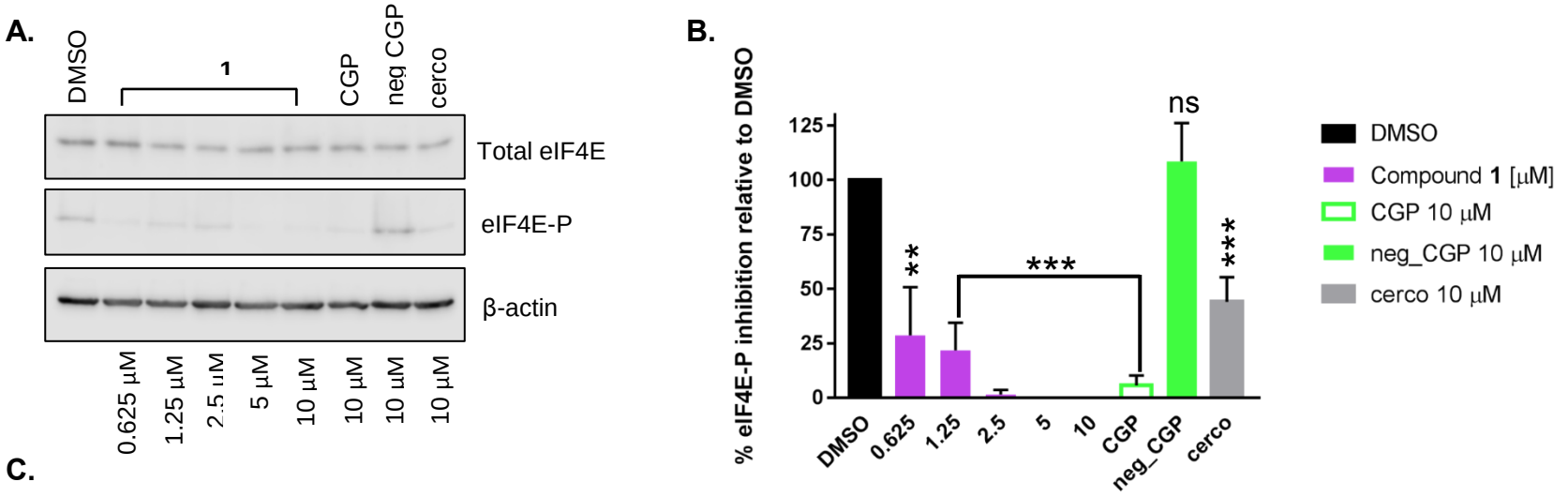

C.

Kinase:	% Enzyme activity (relative to DMSO)	
	Compound 1	
	Data 1	Data 2
AKT1	110.03	105.00
MNK1	3.64	2.53
MNK2	1.87	0.79
P38a/MAPK14	125.49	119.86
PIM1	43.11	42.99

Figure 3-12. Validation of target inhibition by compound 1. A. Western blot analysis showing the effect of **1** at different concentrations on eIF4E phosphorylation at Ser209. MRC5 cells were incubated with DMSO alone or the indicated concentrations of inhibitors for 24 hours. Cellular lysates were prepared and immunoblotting was performed using 20µg of total lysate protein, as described in the Materials and Methods. **B.** Quantification of eIF4E phosphorylation levels relative to DMSO. Data are presented as the means ± SD, n=3 (ns = non-significant; **p ≤ 0.01 and ***p ≤ 0.001). **C.** Selectivity of **1** against a panel of kinases. Compounds were tested under commercial conditions in single dose duplicates at 1 µM and reactions were carried out at 10 µM ATP (Reaction Biology HotSpot Screening).

3.2.4 Compound 1 has no Significant Effect on Cell viability

The equivalent concentrations of compound **1** used in the Western blots (Figure 3-12) were taken forward to assess for effects on cell viability over 72 hours in MRC5 cells (Figure 3-13A). In comparison to the DMSO control, there appeared to be no significant effect of compound **1** on cell viability. Similarly, CGP57380, neg CGP57380 and cercoporamide had no effect on cell viability under these assay conditions. The cell titer blue assay was also used to detect cell viability in various cancer cell lines (Figure 3-13B). Cells were incubated with compound **1** at a set concentration of 5 µM for 72 hours. The data were slightly more variable in the two leukemia cell lines used here (MOLM-13 and MV-4-11); however, no significant effect on cell viability was observed in any of the cell lines tested (MRC5, BT-549, MDA-MB-231 and SK-BR- 3).

In order to test whether compound **1** had an effect on cell proliferation, cells were incubated with DMSO alone or compound **1** at either 1 µM or 10 µM and cell numbers counted over a period of 48 hours. Cell number did not change significantly relative to the DMSO control.

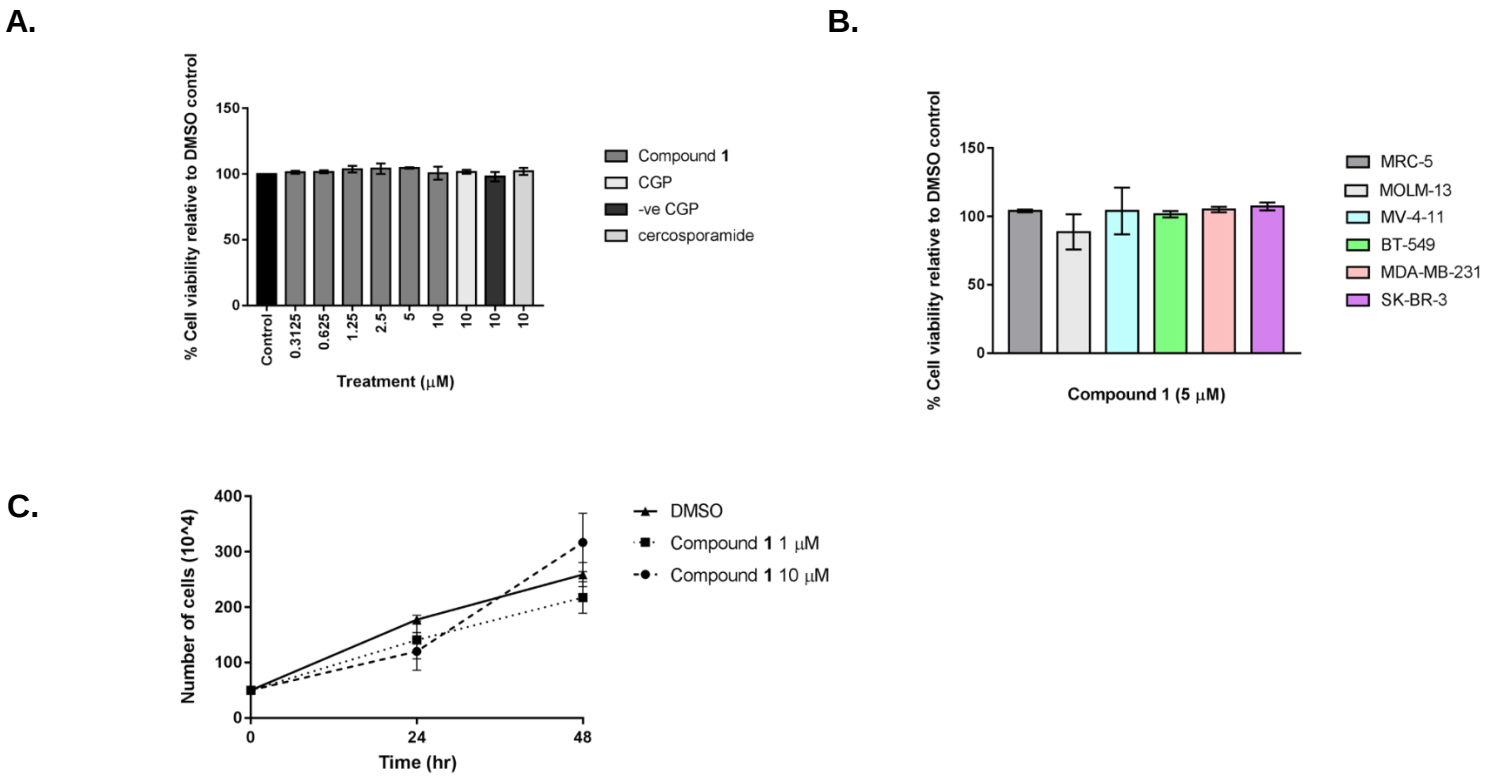

Figure 3-13. Cell viability of compound 1. A. MRC5 cells were treated for 72 hours with compound **1** at the indicated concentrations. **B.** Various cell lines were treated for 72 hours with compound **1** at 5 μM. Viability was assessed by Cell Titer Blue assay (see Materials and Methods for details). Data are presented as the means ± SD, n=3. **C.** Cell proliferation assay of compound **1** on MRC5 cell lines. MRC5 cells were treated for 48 hours with compound **1** as a single-agent. Data are presented as the means ± SD, n=3.

3.2.5 Dual-inhibition of MNK-eIF4E and PI3K-AKT-mTOR in MRC5 Cells

MNK1/2 phosphorylate eIF4E on Ser209, enhancing the translation of specific mRNAs involved in cell survival and metastasis. MNK1/2 kinases are an attractive therapeutic target as they are dispensable during normal development and hence could be used to selectively kill cancer cells (Teo et al., 2015b). In this study, highly migratory MRC5 lung fibroblasts and MDA-MB-231 breast cancer cells were both used to probe the response of dual-inhibition of the eIF4E-MNK pathway and PI3K-AKT-mTOR pathways (Figure 3-1). In MRC5 cells, compound **1** was found to reduce the level of eIF4E phosphorylation in a concentration-and time-dependent manner, being effective at concentrations above 1 μM for 4 hours or longer (Figure 3-15A and 3-15B). In contrast, CGP57380, a known MNK inhibitor (Figure 3-15A, lane 8) and staurosporine, a pan-general kinase inhibitor, (Figure 3-15A, lane 9) had no effect on eIF4E-P under these assay conditions. The inhibition of MNK1/2 did not affect the upstream activation of MNK1/2, or lead to an increase in cell stress, as observed by the constant level of AMPK T172 phosphorylation in relation to the DMSO control. Increased incubation time with compound **1** for 16 hours and above, resulted in partial inhibition of 4E-BP1 phosphorylation, as depicted by an increase in the level of the less-phosphorylated form of 4E-BP1 upon Western blotting (Figure 3-15A and 3-15B). This could reflect the inhibition of MNK resulting in decreased binding of TEL2 to mTORC1, promoting DEPTOR binding, inhibition of substrate binding to RAPTOR and decreased phosphorylation of 4E-BP1 (Figure 3-3).

To assess the significance of simultaneous MNK1/2 and PI3K inhibition, an effective PI3K p110α inhibitor, 3-[4-(4-morpholinyl)thieno[pyrimidin-2-yl]phenol, compound **2**, (Folkes et al., 2008), was used to observe the effect on various signalling molecules (Figures 3-14 and 3-15C). The efficacy of compound **2** as a PI3K inhibitor was measured by monitoring the inhibition of phosphorylation of AKT-T308. This phosphorylation is PI3K-dependent, resulting from the conversion of PIP2 to PIP3 and the activation of membrane-bound PDK1 (Hemmings & Restuccia, 2015). Compound **2** was found to inhibit AKT-T308

phosphorylation at concentrations greater than 100 nM in MRC5 cells. The observed effect of compound **2** on mTOR signalling was also as predicted, with mTORC1 substrates, 4E-BP1 and p70S6K inhibited in a dose-dependent manner. In addition, ribosomal protein S6 (rpS6) phosphorylation was also inhibited (Figure 3-15C).

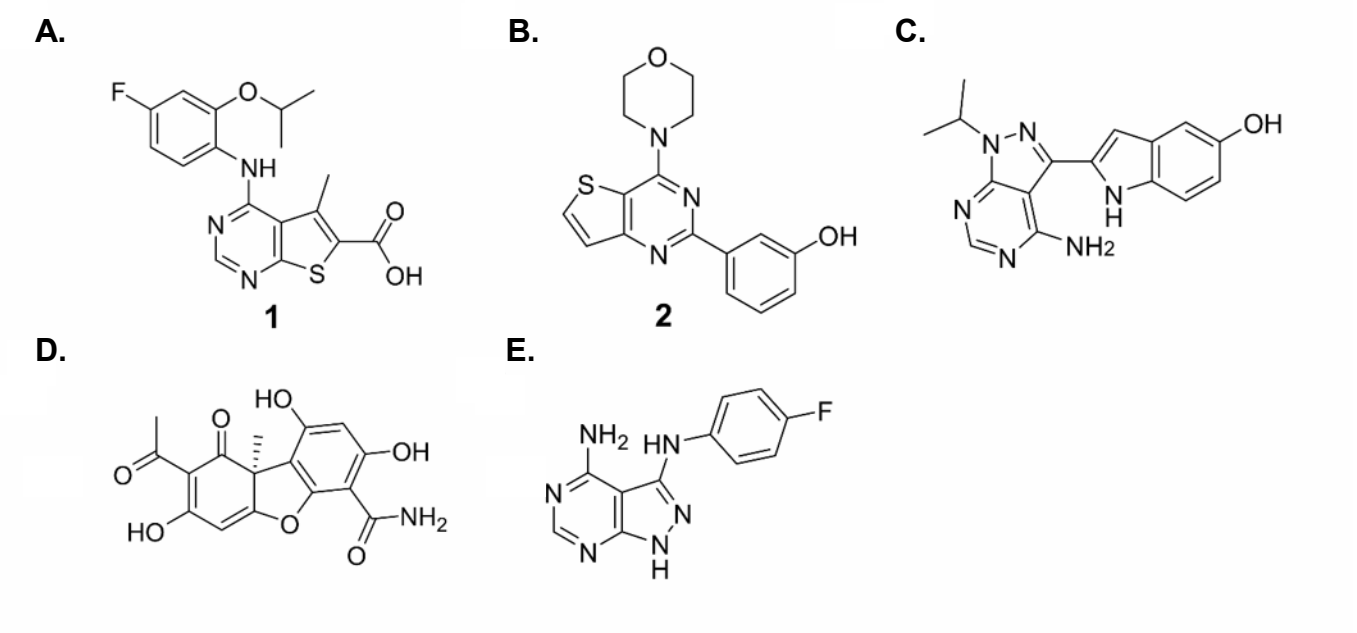

Figure 3-14. Inhibitors used for combination studies. A. Structure of **1**, a MNK1/2 inhibitor. **B.** Structure of **2**, a PI3K p110α inhibitor. **C.** Structure of PP242, an mTORC1/2 inhibitor. **D.** Structure of cercosporamide, a MNK1/2 inhibitor. **E.** Structure of CGP57380, a MNK1/2 inhibitor.

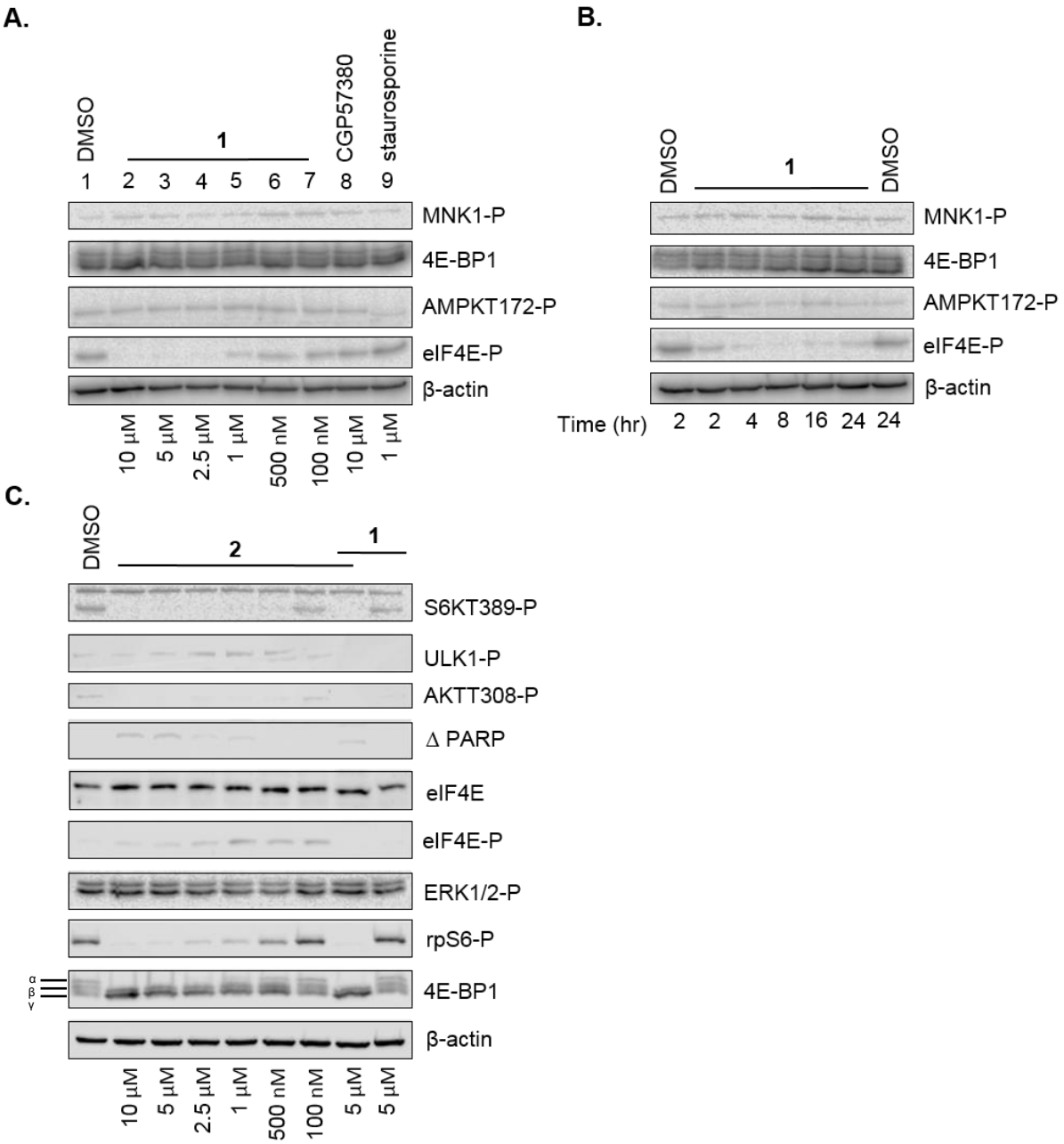

Figure 3-15. Representative Western blot analysis of both the eIF4E-MNK and PI3K-AKT-mTOR pathways in the presence of inhibitors. A. Western blot analysis showing the effect of different concentrations of **1** on eIF4E-P and various signalling molecules. MRC5 fibroblast cells were incubated with DMSO alone (lane 1) or with the indicated concentrations of inhibitors for 24 hours. Cellular lysates were prepared and immunoblotting was performed using 20 µg of total lysate protein, as described in the Materials and Methods. **B.** Western blot analysis showing the effect of **1** incubation time on eIF4E-P and various signalling molecules. MRC5 fibroblast cells were incubated with DMSO alone (lane 1) or with **1** (5 µM) for the indicated times. **C.** Western blot analysis showing the effect of different concentrations of **2** on AKT308 and various signalling molecules and the effect of **2** in combination with **1**. MRC5 fibroblast cells were incubated with DMSO alone (lane 1) or with the indicated concentrations of inhibitors for 24 hours.

This is explained by the shared sequence similarity in the C-terminal kinase domain of both mTOR and PI3K (Zheng & Jiang, 2015). Interestingly, compound **2** also appeared to reduce the level of eIF4E-P at high concentrations, suggesting an overlapping function in the eIF4E-MNK pathway. The phosphorylation of eIF4E was abolished when compound **2** was used in combination with compound **1**. When monitored by Western blotting, the level of eIF4E protein remained constant throughout the drug treated cells. A low level of cleaved PARP was observed when compound **2** was used at high concentrations alone or in combination with **1** (Figure 3-15C), indicating apoptosis was occurring at elevated final drug concentrations.

In addition to targeting the mTORC1 signalling pathway at the level of PI3K, this study used the well-studied pyrimidine derivative, PP242 (torkinib). PP242 (Figure 3-14) has an IC_{50} of 8 nM in cell-free assays and selectively targets both mTORC1 and mTORC2 complexes over PI3K isoforms (Apsel et al., 2008) (Figure 3-1). Consistent with published data (Apsel et al., 2008), PP242 at a 1 μM final concentration inhibited the hyperphosphorylation of 4E-BP1 (Figures 3-16A and B, lanes 1 vs lanes 2). In addition, PP242 treatment of cells also inhibited other targets downstream of mTORC1, including p70S6K (Thr389 phosphorylation) and rpS6 phosphorylation (Figure 3-16B). There was a low level of cell death in cells exposed to the compound **1**/PP242 combination, with more cleaved PARP observed at the highest concentration of compound **1** (10 μM; lane 2). Incubation of cells with PP242 at 1 μM final concentration in combination with various concentrations of compound **1** did not affect the efficacy of the latter on eIF4E-P. In a similar manner, the level of ERK-P appeared to be unaffected under all of the conditions tested.

mTORC1 is an important regulator of autophagy. Autophagy involves the proteolytic degradation of cytosolic components in the lysosome. Its role is essential for balancing the cell's energy resources, removing misfolded or aggregated proteins and eliminating intracellular pathogens (Glick et al., 2010). mTORC1 induces autophagy in response to stress and starvation conditions. However, under normal physiological conditions, mTORC1 directly phosphorylates the ULK1 kinase complex (ULK1-ATG13-FIP200-ATG101),

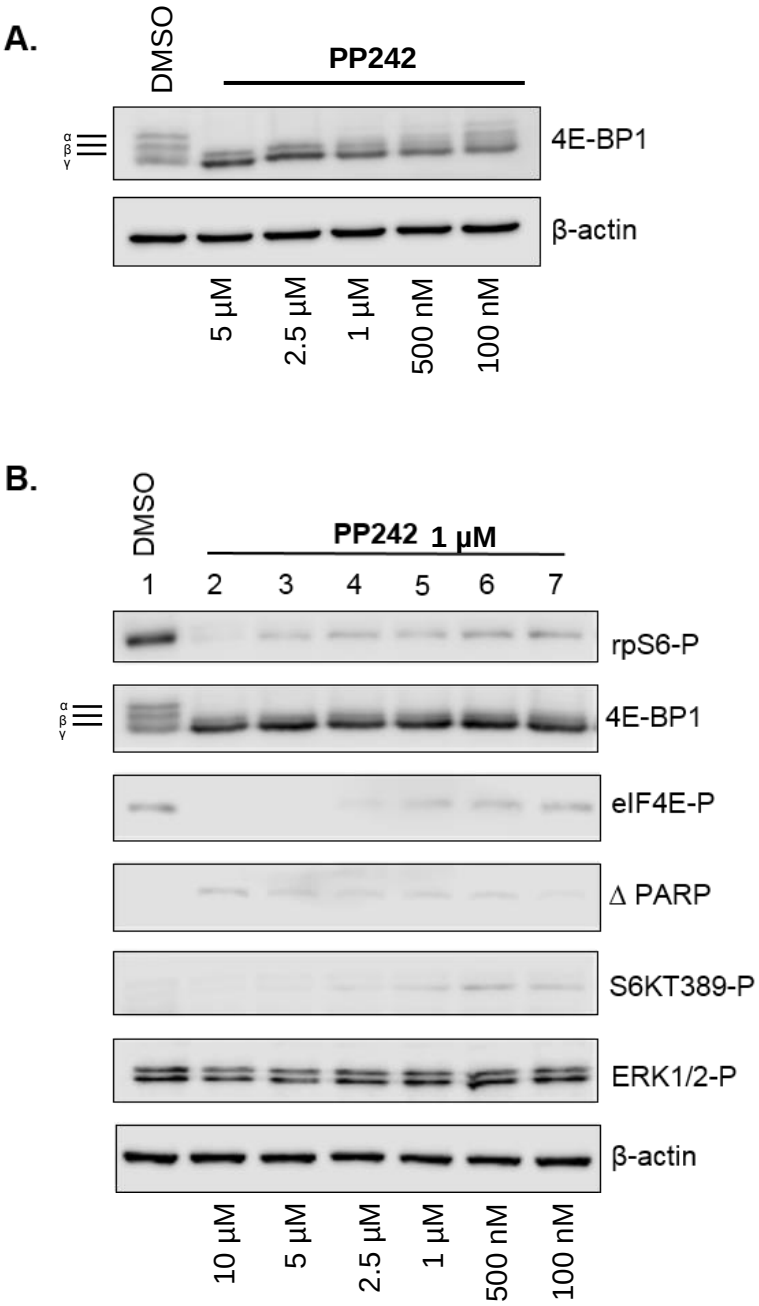

Figure 3-16. Representative Western blot analysis of both the eIF4E-MNK and PI3K-AKT-mTOR pathways in the presence of inhibitors. A. Western blot analysis showing the effect of different concentrations of PP242 on 4E-BP1 phosphorylation. MRC5 cells were incubated with DMSO alone (lane 1) or the following final concentrations of PP242: lane 2: 5 µM, lane 3: 2.5 µM, lane 4: 1 µM, lane 5: 500 nM, lane 6: 100 nM. **B.** Western blot showing the effect of different concentrations of **1** in combination with PP242 1 µM. Cells were incubated with DMSO alone (lane 1) or the following final concentrations of inhibitors: lane 2: **1** 10 µM, PP242 1 µM, lane 3: **1** 5 µM, PP242 1µM, lane 4: **1** 2.5 µM, PP242 1 µM lane 5: **1** 1 µM, PP242 1 µM, lane 6: **1** 500 nM, PP242 1 µM lane 7: **1** 100 nM, PP242 1 µM Cellular lysates were prepared and immunoblotting was performed using 20µg of total lysate protein, as described in the Materials and Methods.

inhibiting autophagosome formation and hence autophagy (Chiarini et al., 2015, Cope et al., 2014, Laplante & Sabatini, 2012) (Fig 3-17). Figure 3-18C shows that low concentrations of compound **2** (<2.5 μM) stimulated the phosphorylation of ULK1, an event which prevents autophagosome formation (Cope et al., 2014). This is indicative of active mTORC1 signalling in the treated cells and further supports the evidence of dose-dependent inhibition of mTORC1 activity by compound **2**. Microtubule-associated protein 1 light chain 3 beta (LC3B-I) can also be used to monitor autophagy in treated cells. To enable its recruitment to autophagosomal membranes, LC3B-I is conjugated to phosphatidylethanolamine to form LC3-phosphatidylethanolamine conjugate (LC3-II). The addition of phosphatidylethanolamine can be detected by Western blotting, resulting in increased migration upon SDS-PAGE (Tanida et al., 2008). In Figure 3-18A, the shift in intensity from LC3B-I to LC3B-II is clearly visible when MRC5 cells are treated with 5 μM compound **2** for 24 hours. These data suggest that when used independently, high doses of compound **2** (>2.5 μM) stimulate autophagy. Relative to the DMSO control, compound **1** used either alone or in combination with compound **2** had no effect on autophagy, as monitored by conversion of LC3B-I to LC3B-II. In contrast, a shift in intensity from LC3B-I to LC3B-II was observed when MRC5 cells were treated with 5 μM PP242 for 24 hours. Relative to the DMSO control, PP242 used either alone or in combination with compound **1** stimulated autophagy, and promoted the cleavage of PARP, indicative of apoptosis (Figure 3-18B).

3.2.6 Inhibition of the MNK1/2 and PI3K-AKTmTOR Pathways Slows the Rate of Migration in MDA-MB-231 Cells

The phosphorylation of eIF4E has been shown to correlate with an increase in levels of migration and enhanced expression of mesenchymal markers such as N-cadherin, fibronectin and vimentin (Robichaud et al., 2015). Disrupting cellular migration is a promising therapeutic option for the treatment of cancer (Levin, 2005). Here, the rate of migration of a breast cancer cell line has been assessed using real-time monitoring of cell migration.

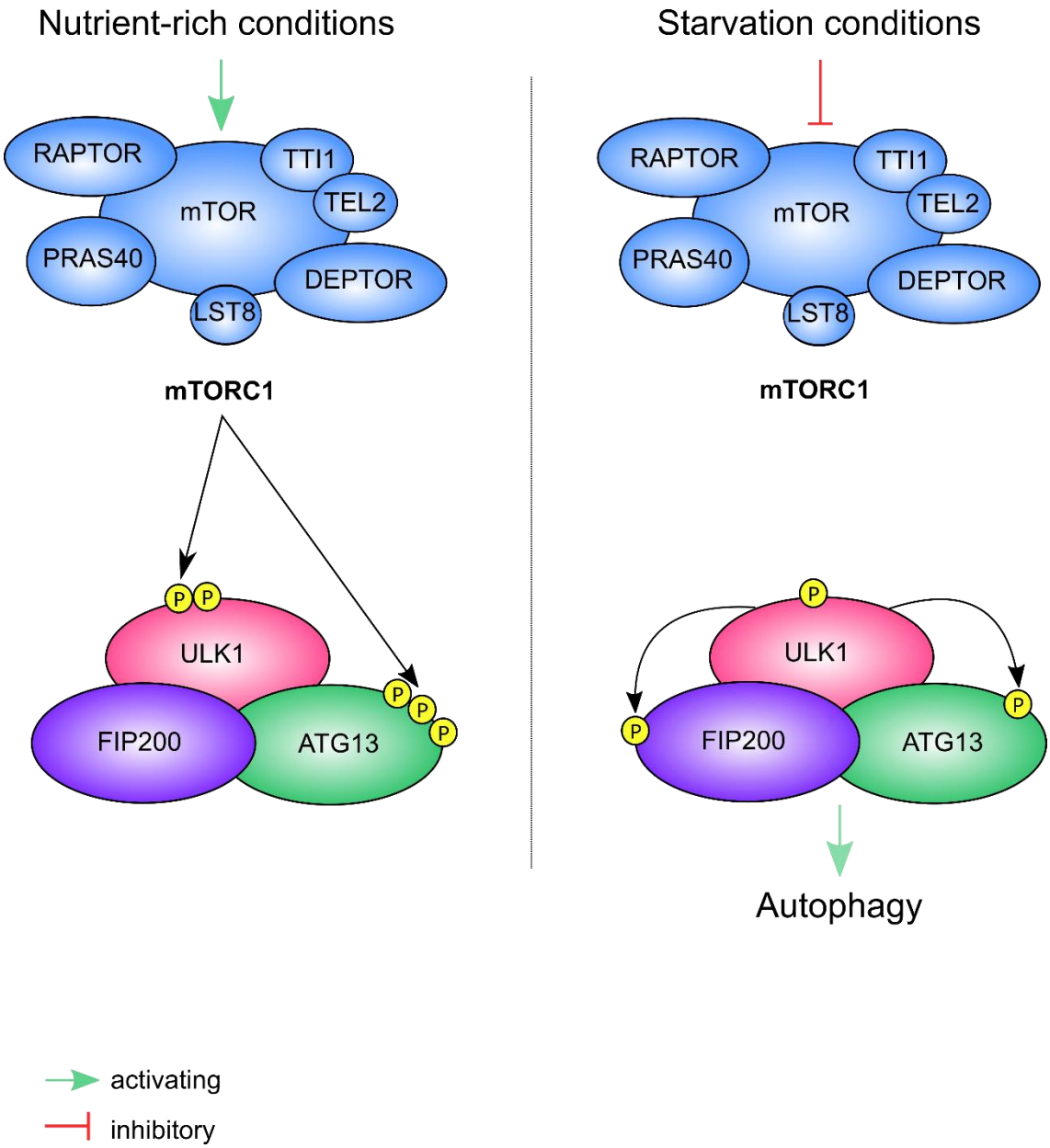

Figure 3-17. Regulation of autophagy by mTORC1. In nutrient rich conditions mTORC1 represses autophagy by phosphorylating ULK1 and ATG13, preventing autophagosome formation. Glucose or amino acid starvation results in the repression of mTOR activity. Subsequently, ULK1 phosphorylates both FIP200 and ATG13, activating downstream effector proteins leading to autophagy (Adapted from (Randall-Demllo, Chieppa et al., 2013).

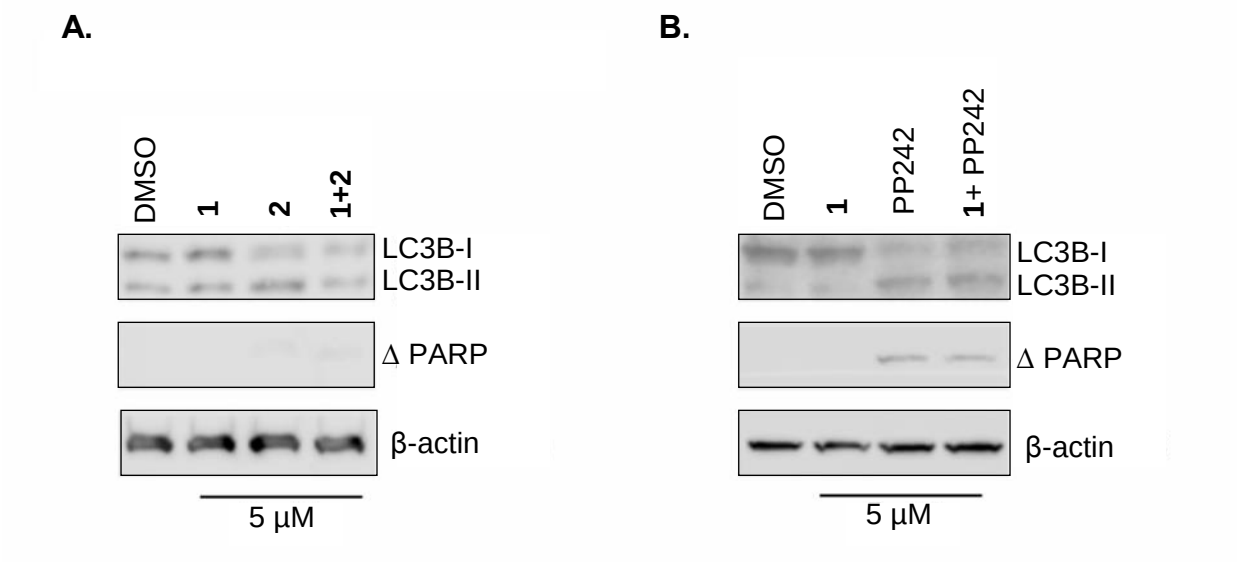

Figure 3-18. The effects of MNK1/ 2, mTOR and PI3K inhibition on cell death and autophagy. a) Representative Western blot analysis for the expression of LC3B and cleaved PARP in MRC5 cells treated with DMSO, compound **1**, compound **2** and a combination compounds **1** and **2** for 24 hr, n=3. **b)** Representative Western blot analysis for the expression of LC3B and cleaved PARP in MRC5 cells treated with DMSO, compound **1**, PP242 and a combination of compound **1**/ PP242 for 24 hr. Cellular lysates were prepared and immunoblotting was performed using 20 µg of total lysate protein, as described in the Materials and Methods

MDA-MB-231 cells were incubated in the absence or presence of various inhibitors alone or in combination as they moved towards a chemo-attractant. Cell migration kinetics were recorded on a RTCA DP instrument for 12 hours. As shown in Figure 3-19A (and quantified in Figure 3-19B), when cells were treated with a combination of compounds **1** and **2** (both at 1 μM final concentration), a substantial reduction in cell migration was observed relative to the DMSO control or when compounds **1** or **2** were used as single agents.

Cell viability data demonstrated that the MNK1/2 inhibitor, compound **1**, exhibited minimal cytotoxicity at 1 μM in MDA-MB-231 cells (Figures 3-19E and F). In contrast, the PI3K inhibitor, compound **2**, reduced cell viability to 75%, when used either as a single agent or in combination with compound **1**. The synergistic effect of MNK1/2 and PI3K inhibition on cell migration led to the investigation of inhibition of both MNK1/2 and mTORC1/2, but using PP242. The latter, impaired cell migration to the greatest extent (Figure 3-19C), although this could in part be explained by a reduction in cell viability to 60% seen with this compound (Figure 3-19F). A combination of compound **1** with PP242 appeared to rescue the effect of PP242 used alone, with the cell index returning to the level of the DMSO control (Figure 3-19C). One possible explanation for this reflects a recent publication demonstrating that MNK forms a complex with mTORC1, promoting mTORC1 association with TEL2, which facilitates efficient mTORC1/substrate binding (Brown & Gromeier, 2017). The dual inhibition of MNK1/2 and mTORC1/2 significantly reduced cell viability to 35% on control levels (Figure 3-19F), an observation that has been reproduced in several cancer cell lines (Bianchini et al., 2008, Grzmil et al., 2011). The rescue effect seen when a combination of MNK1/2 and mTORC1/2 inhibition was used in the cell migration assay suggests only a selected pool of surviving cells were scored in this assay.

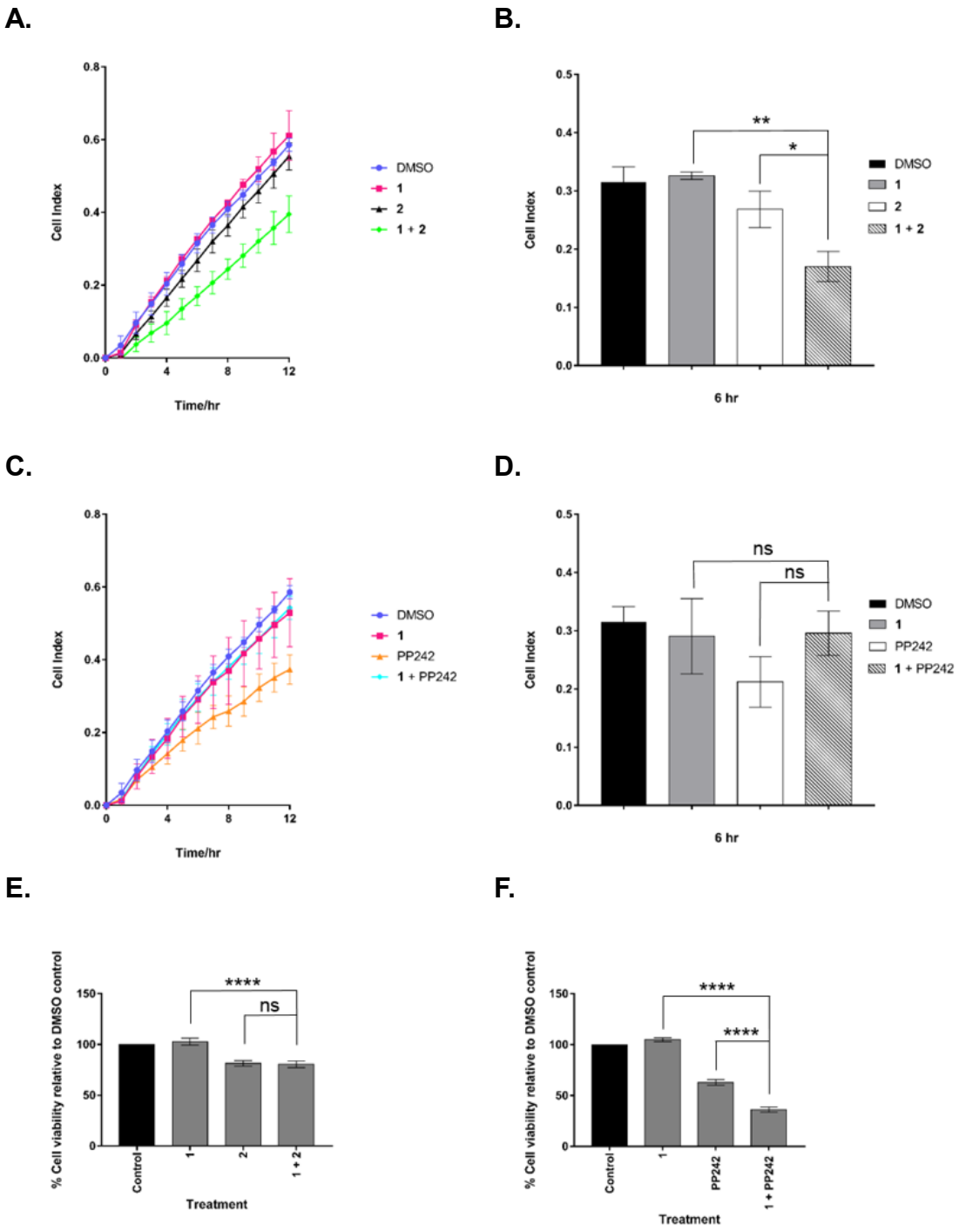

Figure 3-19. Cell viability and kinetics of migration in drug-treated MDA-MB-231 cells. Cell migration in real time was analysed by the xCELLigence RTCA. A. and **C.** show the cell indexes over 12 hours for each drug treatment at 1 µM. **B.** and **D.**, cell migration analysis at 6 hr. **E.** and **F.** Viability was assessed by Cell Titer Blue assay. MDA-MB-231 cells were treated for 72 hours with indicated drugs at 1 µM. Data are mean ± S.D, n = 3 (ns = non-significant; *p ≤ 0.05; **p ≤ 0.01 and ****p ≤ 0.0001).

3.2.7 The Combination of MNK1/2 and mTORC1/2 Inhibition Induces G1 Cell Cycle Arrest in MDA-MB-231 Cells

FACs analysis was employed to determine whether a combination of MNK1/2 and PI3K or mTORC1/2 inhibition was associated with arresting the cell cycle at a specific stage in proliferating MDA-MB-231 cells over a period of 24 hours. The CDK1 inhibitor, R0-3306, was used as a control for the arrest of cells at the G2/M phase border (Vassilev, 2006). Following incubation, cells were isolated, fixed and stained as described the Materials and Methods. As demonstrated in Figure 3-20A, each phase of the cell cycle was observed in unsynchronised cells incubated with DMSO. The MNK1/2 inhibitor, compound **1**, had no effect on cell cycle distribution, whereas both mTORC1/2 and PI3K inhibition, (PP242 and compound **2**, respectively) increased the number of cells in the G1 phase of the cell cycle (quantified in Figure 4-20B). However, following exposure to a combination of compound **1** and PP242 at 5 μM, the number of cells corresponding to the G1 phase was increased, while the numbers of cells in the S and G2/M phases were decreased, suggesting a weak block in the G1 phase of the cell cycle.

A.

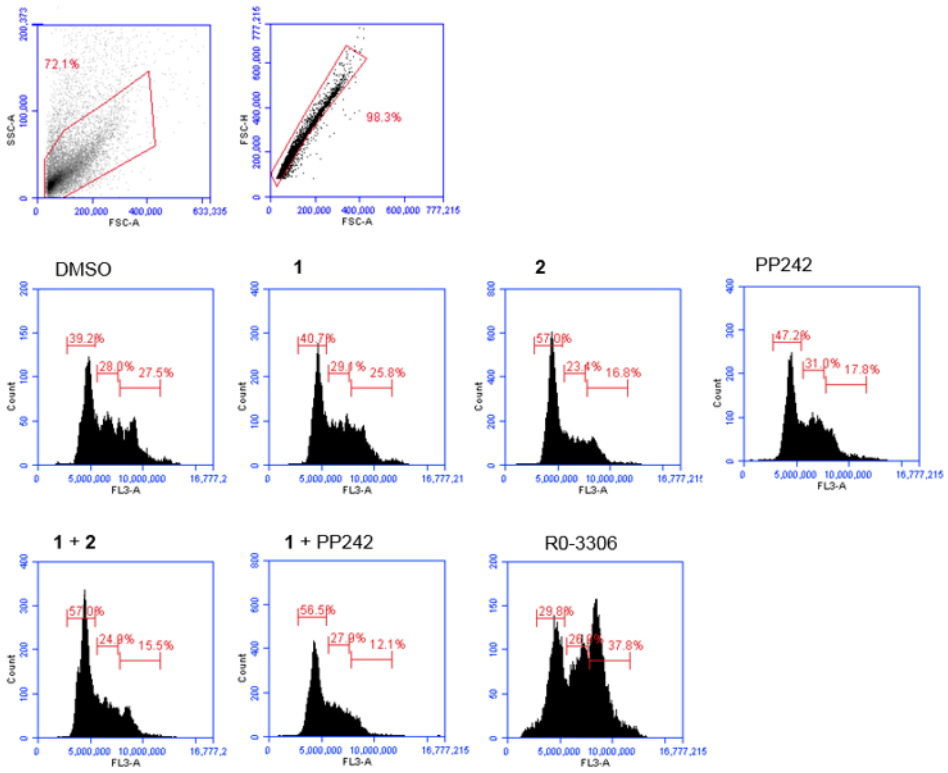

B.

	% G0/ G1	% S	% G2/ M
DMSO	42.0 ± 3.9	28.8 ± 1.1	24.7 ± 3.9
1	42.4 ± 2.4	29.3 ± 0.2	24.2 ± 2.3
2	57.4 ± 0.6	23.8 ± 0.6	15.9 ± 1.3
PP242	48.6 ± 2.0	30.0 ± 1.4	17.7 ± 0.2
1 + 2	58.6 ± 2.3	24.4 ± 0.8	14.5 ± 1.5
1 + PP242	54.5 ± 2.8	28.9 ± 1.3	13.3 ± 1.6
R0-3306 10μM	33.7 ± 5.4	28.8 ± 2.6	32.6 ± 7.4

Figure 3-20. Flow cytometry analysis of the effect of compound 1, compound 2 and PP241 both as single agents and in combination (5 μM) on cell cycle progression. The cells were treated with the indicated concentrations of inhibitors for 24 hours. Samples were fixed and treated with propidium iodide and then analysed by FACs using the Accuri C6 Flow Cytometer (see Materials and Methods). Gating was performed sequentially to eliminate cellular debris. **A.** Representative plots for MDA-MB-231 cells treated for 24 hr with indicated inhibitors at 5 μM unless otherwise stated in the data table. **B.** Data are mean ± S.D, n = 2.

3.2.8 Synthesis of Hybrid Agents

Based upon the observations above and literature precedence, it was postulated that a compound containing both MNK1/2 and PI3K/mTOR inhibitory activities might be very effective against cellular migration. A further aim of this work was to synthesise novel hybrid molecules based upon compound **1** and either PP242 or compound **2** used in this study. The desired outcome was the development of a novel, single molecular framework incorporating both moieties. The hybrid concept covers either permanent or prodrug, cleavable dual-action molecules, i) or ii) (Figure 3-21). The “type ii)” hybrid compounds (**6** and **7**) were prepared as outlined in Figure 3-22. Compound **6** was prepared *via* a simple one-pot synthesis as detailed in the Materials and Methods. Compound **7** was prepared by initially converting the carboxylic acid functionality of the starting material, compound **1** (Teo et al., 2015a) into an acid chloride. This intermediate then underwent an esterification reaction with PP242, leading to the formation of compound 7 in the presence of base. The final products were fully characterised by HRMS and ^{1}H NMR (Figures 3-23 and 3-24). Single crystals of both compounds **6** and **7** were isolated from a chloroform solution and the resulting X-ray analysis is depicted in Figure 3-25 which showed the expected connectivity i.e. the ester bonds in the products (Coles, 2012).

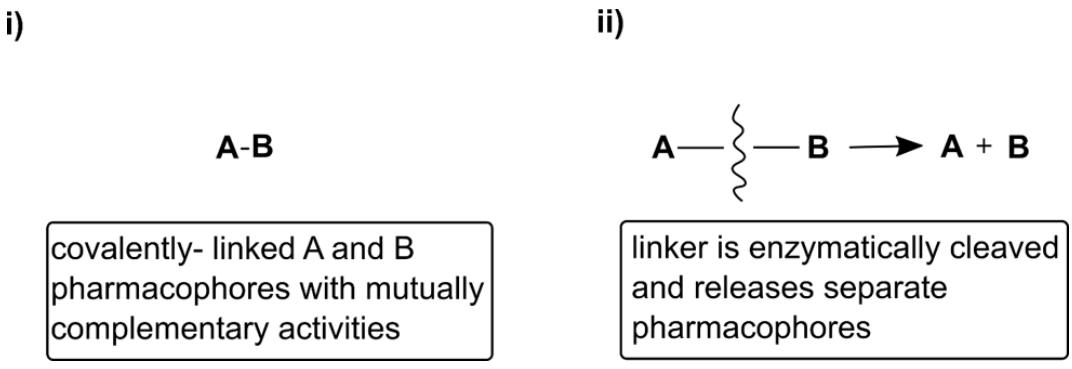

Figure 3-21. “Permanent” vs. cleavable hybrid approach.

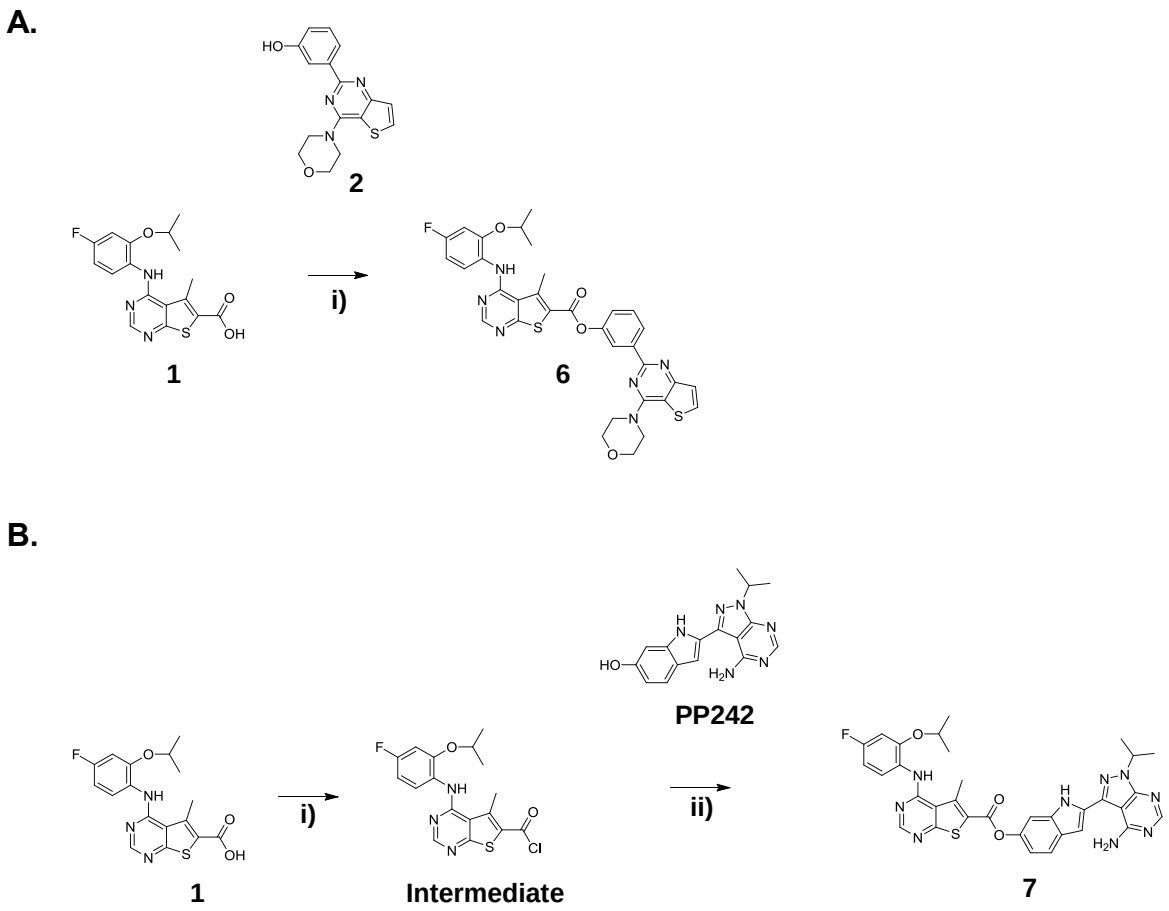

Figure 3-22. Synthesis of ester-linked, cleavable hybrid molecules. Reagents and conditions: **A.** i) DMF, Et_3N, EDC hydrochloride, HOBt, DMAP, RT overnight **B.** i) $SOCl_2$, toluene, reflux 2 h ii) Et_3N, CH_2Cl_2, RT overnight**.**

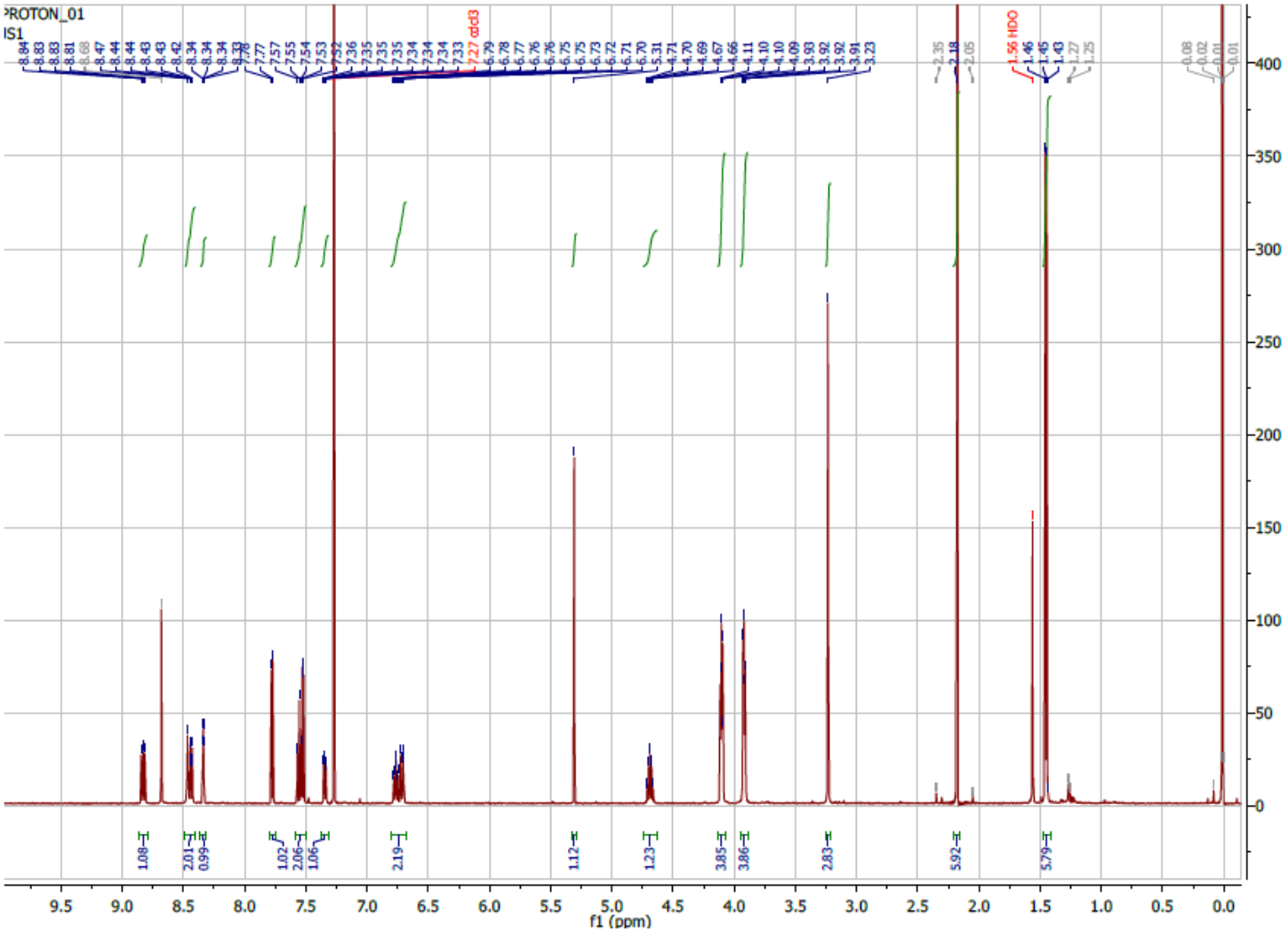

Figure 3-23. ^{1}H NMR ($CDCl_3$) spectrum of compound 6 (acetone signal at 2.19).

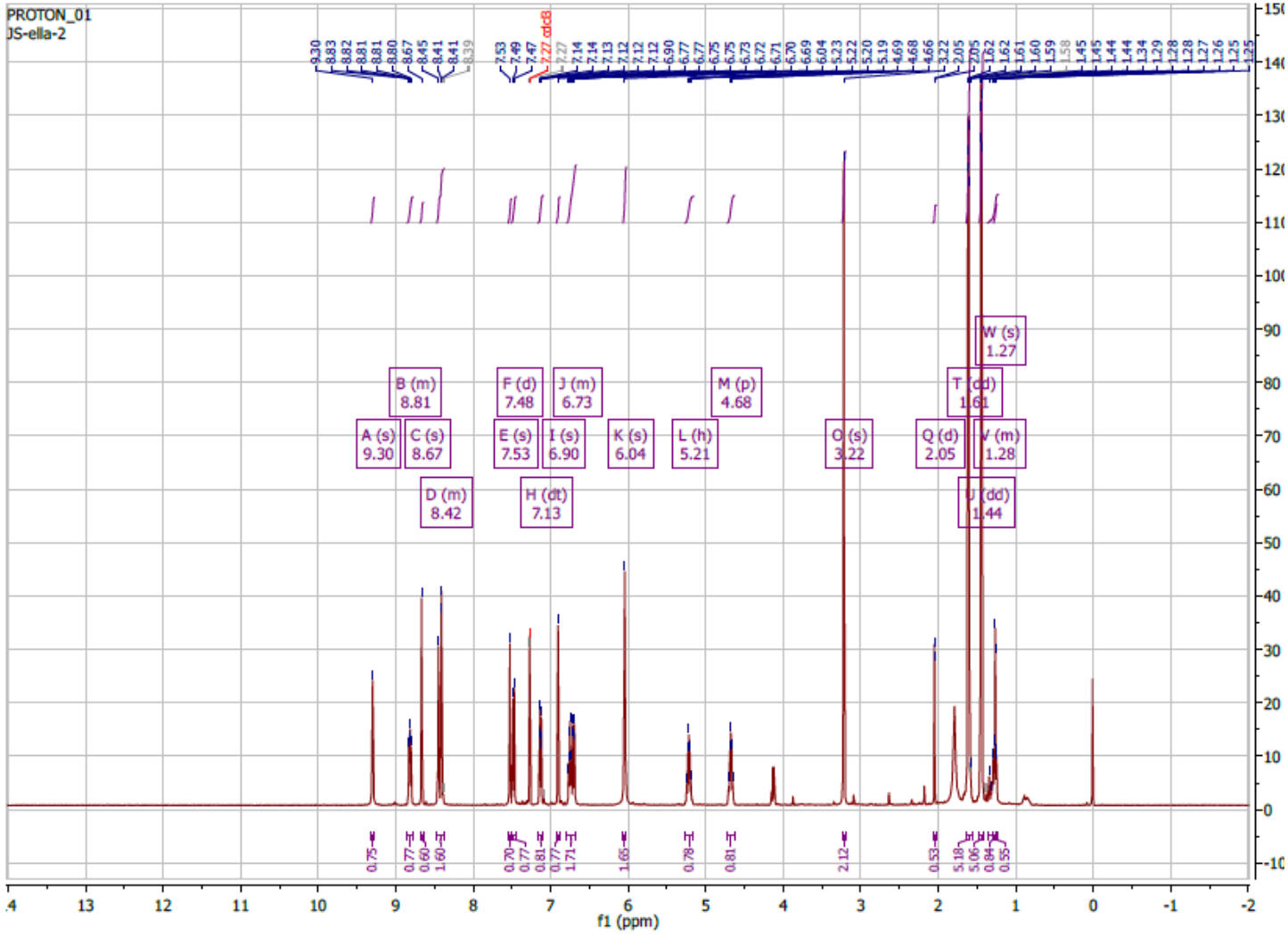

Figure 3-24. ^{1}H NMR ($CDCl_3$) spectrum of compound 7.

A.

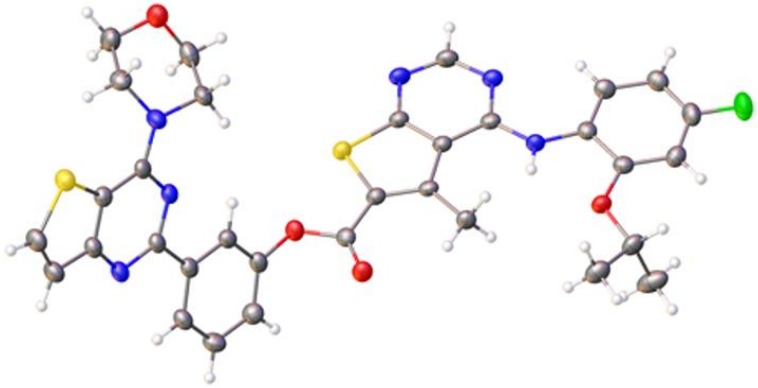

B.

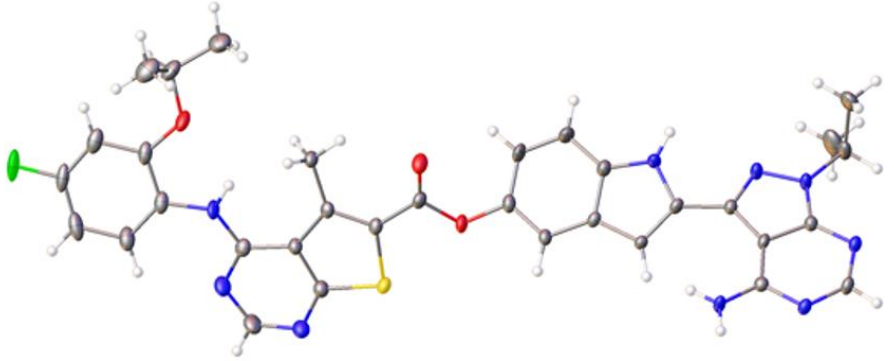

Figure 3-25. Crystal structures of hybrid agents. A. Compound **6** (CCDC 1813013), **B.** Compound **7** (CCDC 1813012).

3.2.9 *In Vitro* Analysis of Hybrid Agents in MRC5 Cells

Compounds **6** and **7** were screened for activity in MRC5 cells by Western blotting (Figures 3-26A and B) and compared with known kinase inhibitors, PI-103 and staurosporine. Cells were incubated in the absence or presence of inhibitors for 24 hours and extracts were prepared as described in the Materials and Methods. During this work it was found that both compounds **6** and **7** were difficult to solubilise in DMSO and delivery onto cells at a known final concentration was problematic. Following Western blot analysis of extracts, in contrast to compounds **1** and **2** together, compound **6** failed to show any noticeable effect on either PI3K or MNK1/2 signalling output relative to the DMSO control. This was reflected by the finding that compound **6** had little effect on phosphorylation of AKT-T308 or on the levels of eIF4E phosphorylation, respectively. mTORC1 read-outs, 4E-BP1, p70S6K Thr389-P and phospho-ribosomal S6 protein also indicated a lack of inhibition of mTORC1 signalling with effective inhibition seen with compounds **1** and **2** together. In addition, ULK1-P and AMPKT172-P were unaffected by the inhibitors used, indicating that cells had not activated a general stress response. When compared to the DMSO control, compound **7** slightly reduced the level of eIF4E-P when tested at the highest concentration (10 μM). Similarly, mTORC1 inhibition was observed at this highest concentration, reflected by the collapse of the broad 4E-BP1 signal into a condensed band and a reduction in rpS6 phosphorylation (Figure 3-26B). There was a low level of cleaved PARP in cells treated with the 1:1 mixture of compound **1**/PP242 and in cells treated with compound **7**, suggesting that this combination in both forms contributed to cell death.

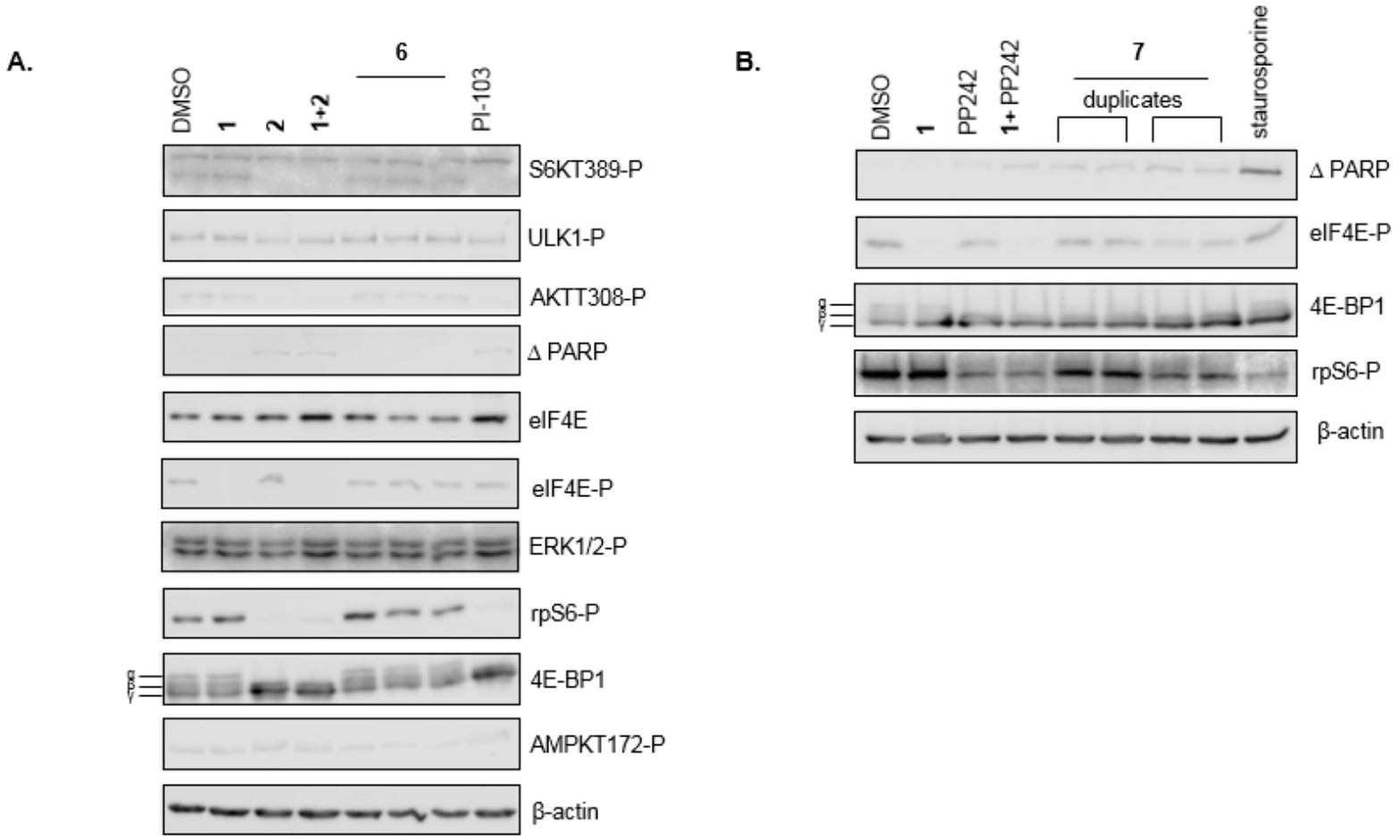

Figure 3-26. Characterisation of hybrid agents. A. and **B.** Western blot analysis showing the effect of different concentrations of compounds **6** and **7** respectively on various signalling molecules. MRC5 fibroblast cells were incubated with DMSO alone or with the indicated concentrations of inhibitors for 24 hours. Cellular lysates were prepared and immunoblotting was performed using 20 µg of total lysate protein, as described in the Materials and Methods.

3.3 Discussion

The results presented in this chapter document the synthesis and initial characterisation of compound **1**, a potent MNK1/2 inhibitor. This inhibitor was previously shown to be more selective than commercially available MNK inhibitors, cercosporamide and CGP57380, and also predicted to have fewer off-target effects. However, selectivity profiling revealed that compound **1** also showed some activity against PIM1, a serine/ threonine protein kinase involved in cell survival and proliferation. PIM1 is implicated in numerous signal transduction pathways and is highly expressed in lymphoid and haemopoietic tissues (Eichmann et al., 2000). PIM1 sits downstream in the JAK/STAT pathway and phosphorylates a large subset of cellular substrates (Tursynbay et al., 2016). It is involved in regulating myc transcriptional activity, cell cycle progression and inhibits pro-apoptotic proteins, such as BAD, MAP3K5 and FOXO3 (Gu et al., 2009, Morishita et al., 2008). PIM1 negatively regulates cyclin-dependent kinase inhibitor, p27Kip1, at both the transcriptional and post-translational level (Morishita et al., 2008). As mentioned in Section 3.2.3, PIM1 has a role in translational control through its interaction with 4E-BP1 and the subsequent release of eIF4E. Interestingly, a feedback loop between eIF4E and c-myc has been observed; eIF4E promotes the expression of c-myc, which can in turn drive eIF4E expression (Clemens & Bommer, 1999, Lin et al., 2008, Rosenwald et al., 1993). PIM1 is also associated with MCL-1, a protein with an oncogenic, pro-survival role. A previous study has shown that PIM1 inhibitor, SGI-1776, reduced MCL-1 transcript and protein levels, inducing apoptosis in FLT3-ITD AML cells (Chen et al., 2011). Further studies investigating this off-target effect may be beneficial in characterising compound **1**. Modelling of PIM1 and MNK1 proteins revealed that although the proteins had relatively low % sequence identity between them (~26%), the proteins are structurally very similar (Figure 3-27). This may account for the off-target effect of compound 1 on PIM1 kinase.

MNK1/2 are serine/threonine protein kinases that phosphorylate eIF4E on Ser209, leading to the preferential translation of oncogenic proteins (reviewed in Section 1.2). To determine whether the compound **1** inhibitor was functional in

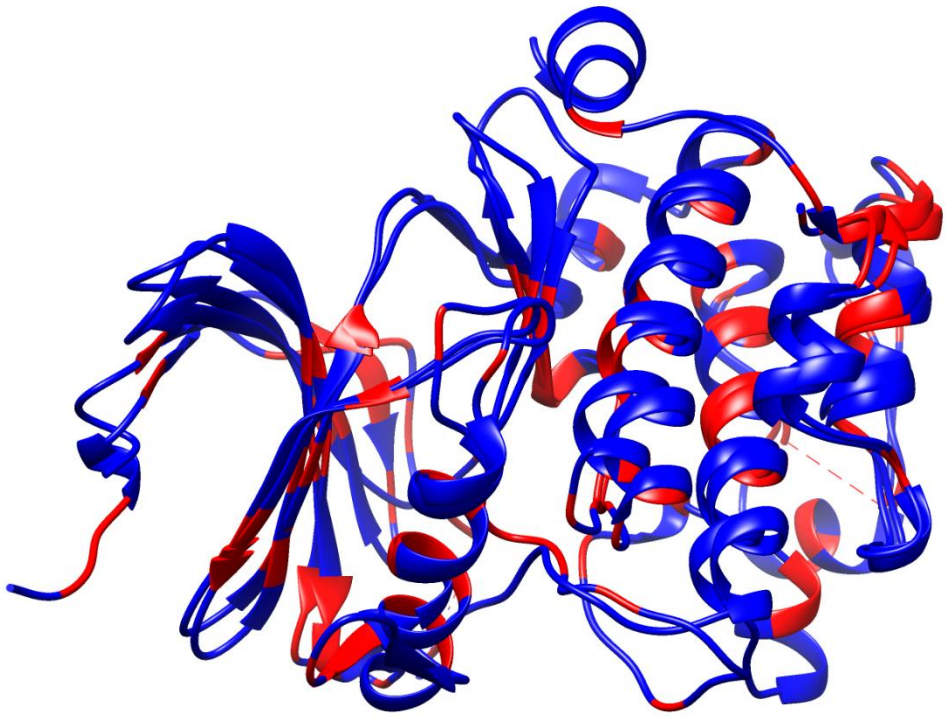

Figure 3-27. Structural alignment of PIM1 kinase and MNK1. The two proteins are superimposed and coloured according to conservation. Highly conserved regions are coloured in red and less conserved regions are coloured in blue. Molecular graphics and analyses were performed with the UCSF Chimera package (Pettersen et al., 2004).

MRC-5 cells, its ability to inhibit eIF4E phosphorylation was tested. Compound **1** reduced the level of eIF4E phosphorylation in a concentration-dependent manner, being effective at concentrations above 2.5 µM. The phosphorylated form of eIF4E is correlated with an increase in mesenchymal markers and poor clinical outcome in human cancers. Therefore, targeting the translational machinery through the inhibition of eIF4E is a promising therapeutic option for the treatment of aggressive metastatic cancers. The only available crystal structure of MNK1 is in the DFD-out (inactive) conformation, which has hindered the docking attempts of small-molecule inhibitors. In contrast, a crystal structure of MNK2 exists in the DFD-in (active) conformation. The MNK2D228G-staurosporine complex (PDB: 2HW7), provides a valuable source of structural information. The homology model of active MNK1 using PDB: 2HW7 as a template may aid the design of selective MNK inhibitors. The predicted binding mode of compound **1** in the MNK1 homology model indicated the fluoroaniline projected into the hydrophobic pocket adjacent to the DFD-motif. This information provides a starting point for further structural modification of compound **1**. Using MDA-MB-231 cells, this work has determined that a synergistic combination of MNK1/2 and PI3K inhibitors slowed the rate of cell migration. Additionally, a combination of MNK1/2 and mTORC1/2 inhibitors resulted in cell cycle arrest and a decrease in cell viability to a greater extent than when the inhibitors were used as single agents. This led to the attempted development of novel hybrid entities, encapsulating MNK1/2 and PI3K/mTOR inhibitory activities. However, in part due to solubility issues, the novel hybrid compounds did not prove to be effective *in vivo*. The poor solubility of compounds **6** and **7** can be explained in part by their physiochemical properties, including their high molecular weight (>500), TPSA (>140 $Å^2$), clog P (>5) (Table 3-1). Both compounds **6** and **7**, violate two of Lipinski's rules, by exceeding a molecular weight of 500 and a log P value of 5. Compounds **6** and **7** also violate one of Veber's rules, by surpassing a TPSA of 140 $Å^2$ (Veber et al., 2002). The relatively high log P values of compounds **6** and **7** may imply reduced membrane permeability. Highly lipophilic compounds with high log P values permeate poorly through membranes as they aggregate in the hydrophobic interior of the membrane bilayer (Leeson & Springthorpe, 2007).

Although molecular hybridisation approaches hold significant promise, they currently face considerable challenges as therapeutic modalities (Berube, 2016, Cai et al., 2010, de Lera & Ganesan, 2016, Fortin & Berube, 2013, Gediya et al., 2008, Nepali et al., 2014, Patel et al., 2014, Rodrik-Outmezguine et al., 2016, Woo et al., 2011). However, simultaneous MNK1/2 and PI3K/mTOR inhibition warrants further investigation as a therapeutic option for treating aggressive migratory cancers (Lineham et al., 2017). Subsequent work will look at the development of novel analogues of the MNK1/2 inhibitor, compound **1,** with a view to enhance the potency and specificity against the target protein.

	1	2	PP242	6	7
Physiochemical Properties					
Molecular weight	361.39 g/ mol	313.37 g/ mol	308.34 g/ mol	656.75 g/ mol	651.71 g/ mol
Rotatable bonds	5	2	2	9	9
H-bond acceptors	6	4	4	9	9
H-bond donors	2	1	3	1	3
TPSA (Topological Polar Surface Area)	112.58 $Å^2$	86.72 $Å^2$	105.64 $Å^2$	168.07 $Å^2$	186.99 $Å^2$
Lipophilicity					
Log $P_{o/w}$	3.67	2.61	1.98	6.35	5.72
Druglikeness					
Lipinski	Yes	Yes	Yes	2 violations: MW >500 Log P >5	2 violations: MW >500 Log P > 5
Veber	Yes	Yes	Yes	1 violation: TPSA >140	1 violation: TPSA >140

Table 3-1. Physiochemical properties and lipophilicity prediction of inhibitors used in this study, calculated using SwissADME software (Daina, Michielin et al., 2017).

4 Probing the Anticancer Action of Novel Ferrocene Analogues of MNK Inhibitors

4.1 Introduction

The incorporation of ferrocene into drugs has attracted significant attention in the field of medicinal chemistry, and several ferrocene derivatives have been investigated (Figure 4-1), including ferroquine and ferrocifen (Figure 4-1B), which act as antimalarial and anticancer compounds, respectively (Patra & Gasser, 2017). Ferrocene is a nontoxic, air- and water-stable complex, comprised of an iron atom sandwiched between two cyclopentadienyl rings (Jaouen et al., 2015). The reversible redox properties of ferrocene have enabled ferrocene derivatives to be used as prodrugs in certain biological environments where ferrocene (Fc) is oxidised to form a cytotoxic ferrocenium cation (Fc^+) (Patra & Gasser, 2017).

Tamoxifen (TAM) is a prodrug that is currently used to treat ER^+ breast cancer (Figure 4-1A). The hydroxylated metabolite, hydroxytamoxifen (OH–TAM), competes with estradiol for binding to ERα and ERβ (Gottardis & Jordan, 1987, Jordan et al., 1980). However, many patients that respond initially to TAM develop resistance to the drug (Ring & Dowsett, 2004). Ferrocenyl analogues of TAM have been investigated as anticancer agents and have been found to have superior activity against both ER^+ and ER^- breast cancer cell lines, in contrast to OH–TAM, which is only active against ER^+ cells (Nguyen et al., 2007). The replacement of the phenyl group in TAM with a ferrocenyl group led to the formation of the prodrug ferrocifen (Fc–TAM) and the hydroxylated metabolite, hydroxyferrocifen (Fc–OH–TAM), which has an IC_{50} of 0.5 μM in TNBC MDA-MB-231 cells (Gormen et al., 2010). The dual action of Fc–OH–TAM is responsible for its increased anticancer activity. In addition to the competitive binding of ER, Fc–OH–TAM loses two electrons and two protons to form a quinone methide intermediate, a Michael acceptor, capable of instigating a cytotoxic response (Bolton, 2014). Fc–OH–TAM was also found to induce cellular senescence, apoptosis, and the formation of reactive oxygen species

(ROS) in a concentration and cell-line dependent manner (de Oliveira et al., 2011, Vessieres et al., 2010, Wlassoff et al., 2007).

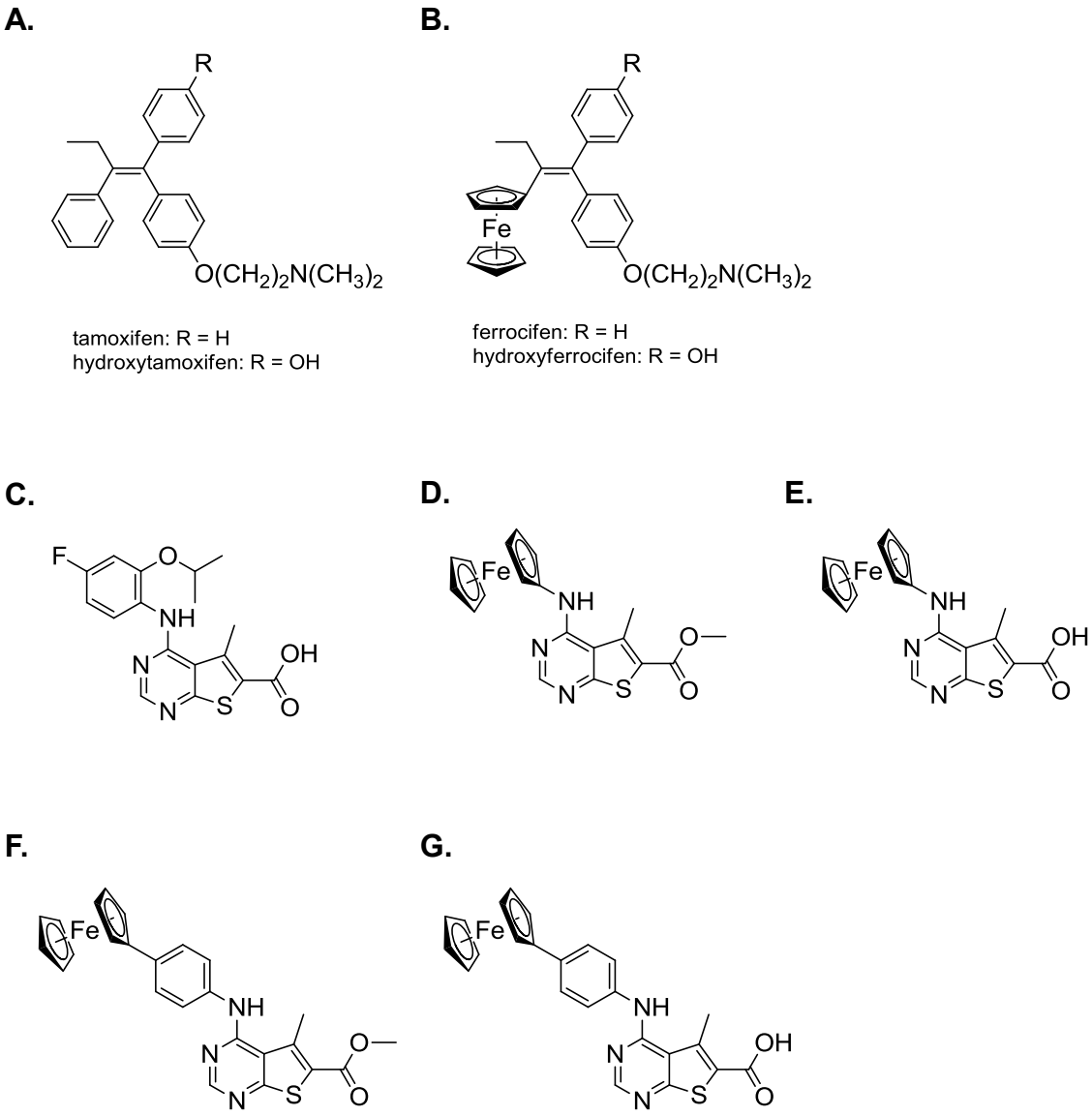

Figure 4-1. Chemical structures of inhibitors and ferrocene derivatives. A. and **B.** Structures of prodrugs and hydroxylated drugs; tamoxifen and ferrocifen, **C.** structure of compound **1,** a MNK1/2 inhibitor, **D.** structure of methyl ester ferrocene derivative, **2**, **E.** structure of ferrocene derivative, **3**, **F.** structure of methyl ester ferrocene derivative, **4**, **G.** structure of ferrocene derivative, **5**.

The Spencer lab (Sussex) have previously reported the incorporation of ferrocene, as a phenyl bioisostere, into a variety of different molecules for biological evaluation (Amin et al., 2013, Librizzi et al., 2012, Ocasio et al., 2017, Spencer et al., 2009). Using a known MNK1/2 inhibitor, compound **1** (Figure 4-1C) as a starting point, the following work describes the initial characterisation of novel ferrocene containing compounds in tissue culture cells (Figures 4-1D and E). From our previous research, we envisaged that the introduction of a ferrocene group would both enhance the binding potency and potentially confer other desirable biological properties to the molecules.

4.2 Results

4.2.1 Molecular Modelling of Compound 1 Reveals a Large Hydrophobic Cavity in MNK2

The crystal structures of MNK1 and MNK2 are available in the DFD-out (inactive) conformation, which blocks ATP-binding (Hou et al., 2013, Kannan et al., 2015). A crystal structure of MNK2-D228G in complex with staurosporine (PDB: 2HW7) was used to model the MNK1/2 inhibitor, **1** (Figures 4-2A and B). This mutation from wildtype DFD to the canonical DFG motif creates a structure that has both DFG-in and DFG-out conformations that ease crystallisation of the protein (Jauch et al., 2005). The predicted binding mode of compound **1** in MNK2-D228G indicates that the pyrimidine moiety occupies the ATP-binding pocket, the carboxyl group is solvent exposed, and the fluoroaniline projects into the large hydrophobic pocket. There are a few important interactions to note (Figure 4-2B). Firstly, the aromatic side chain of gatekeeper residue, Phe159, provides an electron rich surface that allows the formation of cation-π interactions between the active site and compound **1**. The cations present on the edge of the fluoroaniline ring interact with the face of the benzene ring present in Phe159.

A.

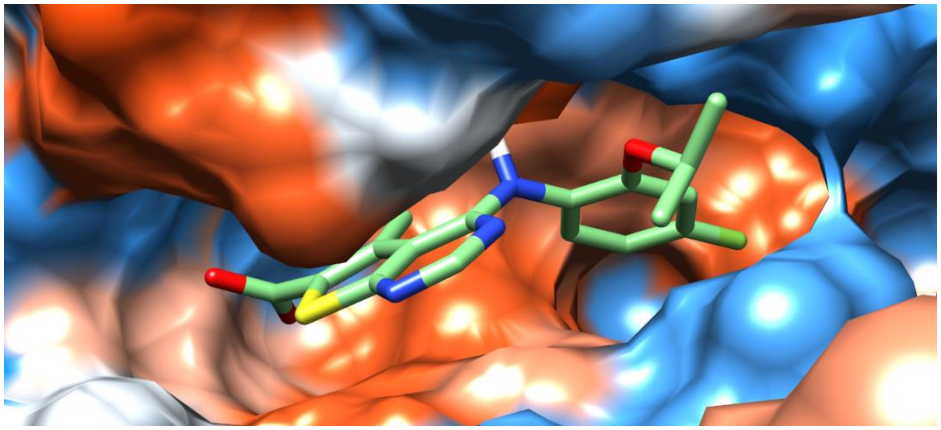

B.

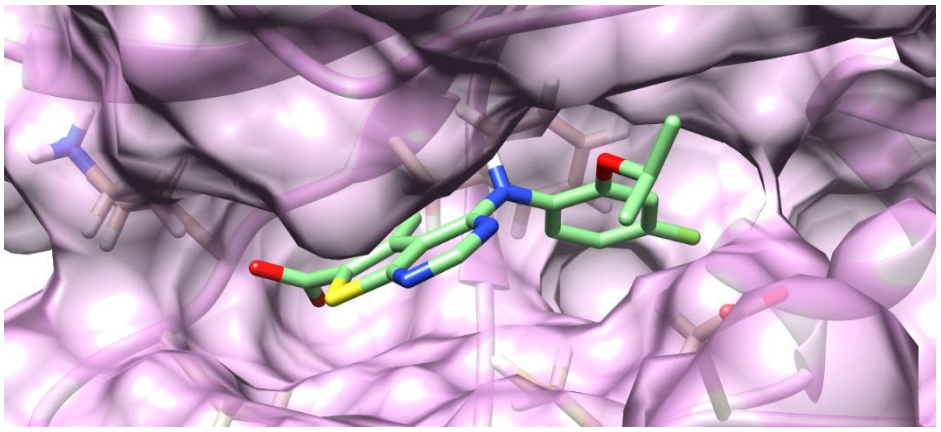

C.

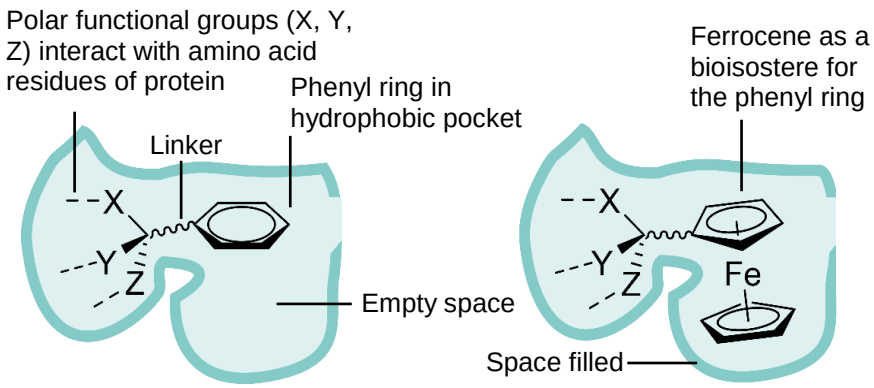

Figure 4-2. Docking of compound 1 in MNK2 crystal structure. A. Predicted binding mode of compound **1** in MNK2-D228G (PDB code: 2HW7) coloured by hydrophobicity surface: from blue for the most hydrophilic, to white, to red for the most hydrophobic. **B**. Important regions within the MNK2 active site and proposed interactions with compound **1**. Molecular graphics and analyses were performed with the UCSF Chimera package (Pettersen et al., 2004). **C.** Ferrocene as a bioisostere (adapted from Patra & Gasser, 2017).

There is also a strong sulphur-aromatic interaction between the pre-DFG Cys225 residue and the pyrimidine in compound **1,** with the sigma hole of the S atom accepting pi electrons. Modelling of compound **1** revealed a large hydrophobic pocket, a region that could be exploited by substituting the aniline ring with a bulkier group such as ferrocene (Figure 4-2C). In order to predict the binding mode of the ferrocene derivatives, compounds **3** and **5**, the structures were manually altered. The sandwich-structure of ferrocene prevents the modelling software from recognising the structural features of the compound. The ferrocene groups were therefore substituted for an adamantyl group, a ferrocene bioisostere, to produce similar compounds for modelling (Figures 4-3A and B). The most likely binding modes of each compound are depicted in Figures 4-3C and D.

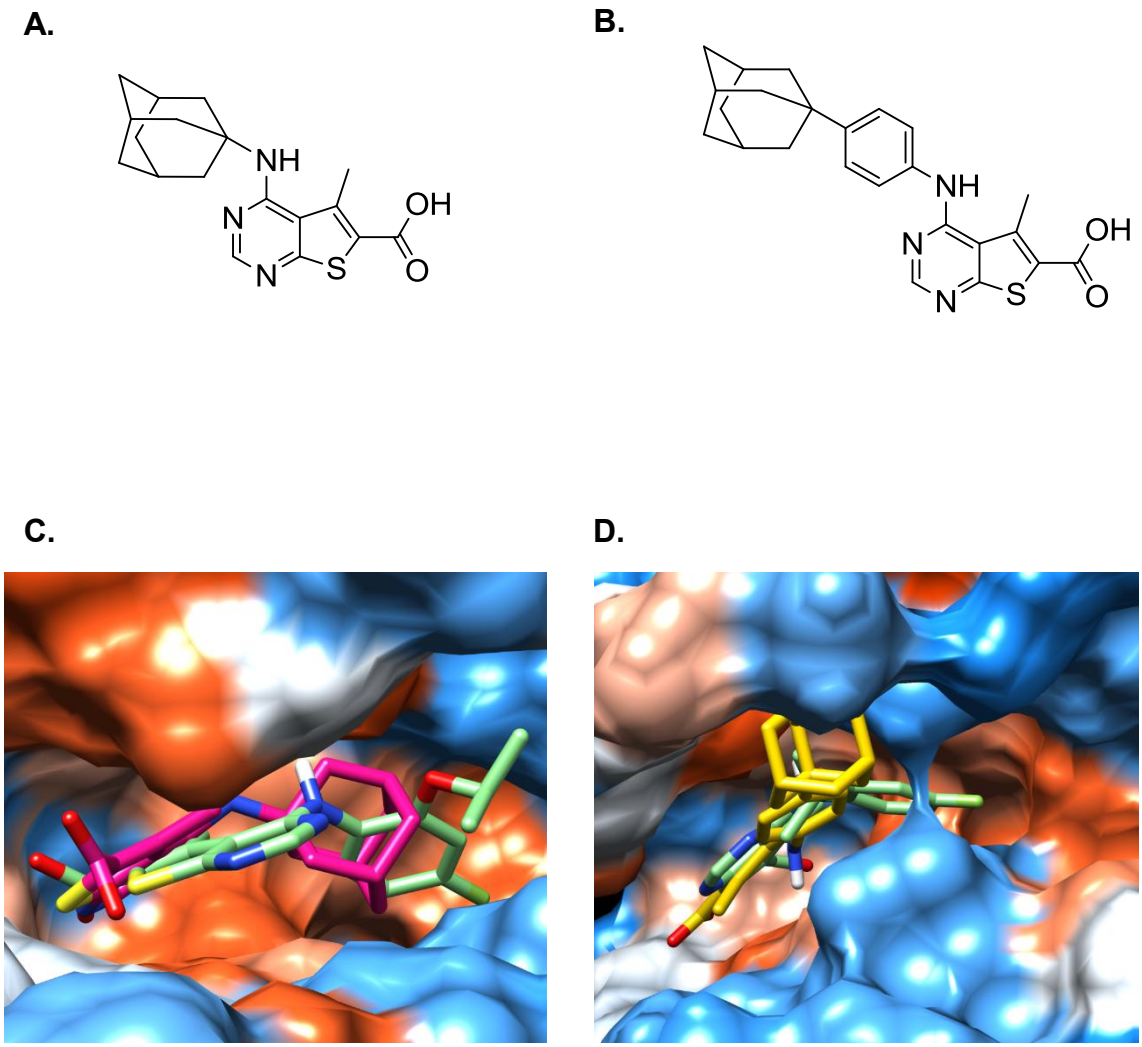

Figure 4-3. Docking of ferrocene-like compounds in MNK2 crystal structure. A. Structure of the "ferrocene-like" compound **3** used for molecular modelling, with the ferrocene moiety substituted for an adamantyl group. **B.** Structure of the "ferrocene-like" compound **5** used for molecular modelling, with the ferrocene moiety substituted for an adamantyl group. **C.** Predicted binding mode of "ferrocene-like" compound **3** in MNK2-D228G (PDB code: 2HW7) coloured by hydrophobicity surface: from blue for the most hydrophilic, to white, to red for the most hydrophobic. **D.** Predicted binding mode of "ferrocene-like" compound **5** in MNK2-D228G. Molecular graphics and analyses were performed with the UCSF Chimera package (Pettersen et al., 2004).

4.2.2 Ferrocene Analogues of Compound 1

The preparation of the ferrocene analogues (compounds **3** and **5;** Figure 4-1) was conducted in collaboration with Dr. Storm Hassell-Hart using an analogous strategy to the synthesis of **1** (Figure 4-1C) (Teo et al., 2015b). In both instances, microwave-mediated acid-catalysed S_NAr (nucleophilic aromatic substitution) followed by basic hydrolysis to remove the ester group enabled us to synthesise the desired inhibitors in good to excellent yields (Figure 4-4). A solid-state determination confirmed the crystal structure of **3** (Figure 4-5).

4.2.3 *In Vitro* Analysis of Compounds 1, 3, and 5 in Cancer Cell Lines

To test whether the compounds **1**, **3** and **5** had any effect on cell viability, a number of mammalian cancer cell lines were incubated with DMSO alone or with different final concentrations of compounds for 72 hours. Cell viability was determined using the Cell Titer Blue assay (as described in Section 2.2). These data are summarised in Table 4-1 and show that compound **1** had no significant effect on cell viability in any of the three breast cancer cell lines tested, including TNBC cell lines (BT-549 and MDA-MB-231) and the $HER2^+$ breast cancer cell line, SK-BR-3. However, **1** did decrease cell viability in MOLM-13 cells and MV-4-11 acute myeloid leukaemia (AML) cell lines, with IC_{50} values of 5.39 µM and 9.72 µM, respectively. The cell viability of compound **3** treated cancer cell lines varied according to cell type. Compound **3** appears to have greater potency against BT-549 and MDA-MB-231 cells and is less effective against the $HER2^+$ breast cancer cell line, SK-BR-3. The effect of **3** on cell viability in AML cell lines was cell-line-specific, with no significant effect on MOLM-13 and a moderate decrease in cell viability observed in MV-4-11. Compound **5** showed the highest potency, with an IC_{50} < 2 µM in four of the cell lines tested. Compounds **3** and **5** both showed greater potency towards the TNBC cell line, MDA-MB-231, with IC_{50} values of 2.83 µM and 0.55 µM, respectively (Table 5-1 and Figure 5-6). The sensitivity of MDA-MB-231 towards **5** prompted further evaluation and **5** was taken forward for additional studies.

A.

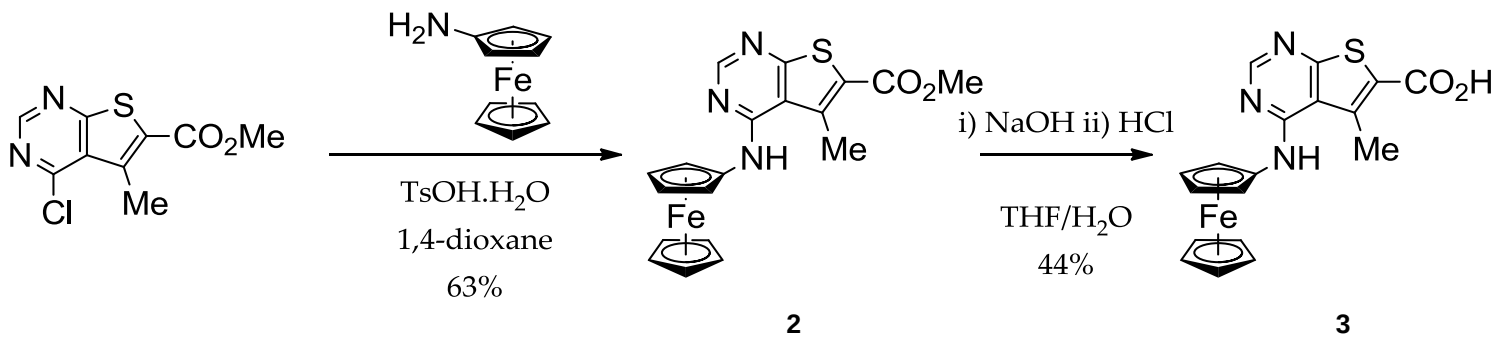

B.

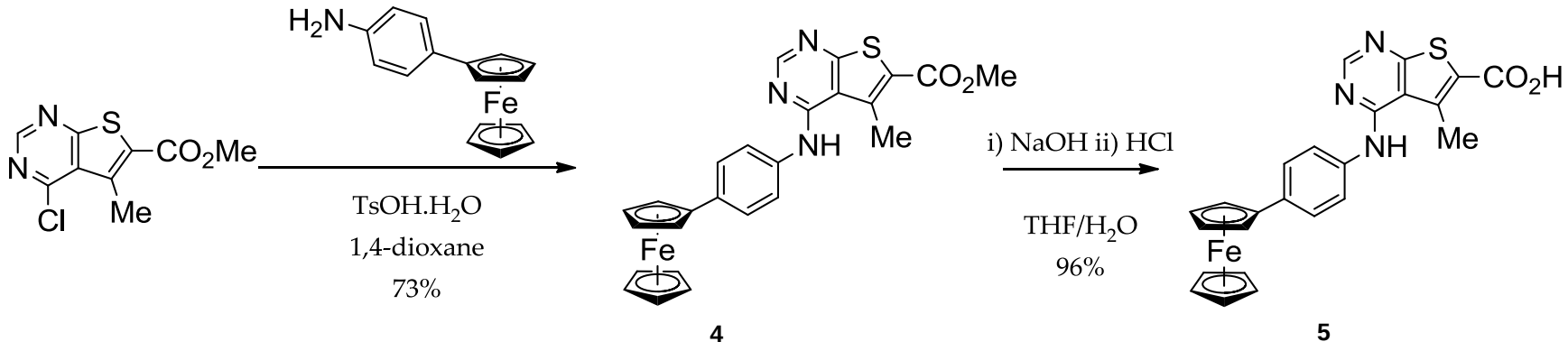

Figure 4-4. Schematic of ferrocene analogue synthesis. A. Synthesis of ferrocene analogue, **3**, **B.** synthesis of ferrocene analogue, **5**.

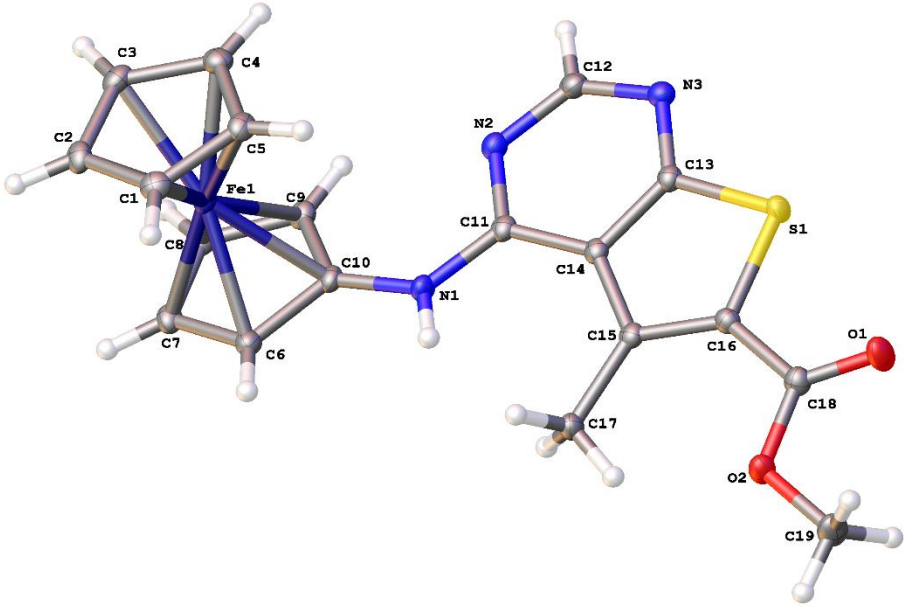

Figure 4-5. **Crystal structure of compound 3** (CCDC 1862154).

Cell Line	Compound IC_{50} (μM)		
	1	3	5
BT-549	n.s	6.67	1.73
MDA-MB-231	n.s	2.83	0.55
SK-BR-3	n.s	114.30	10.63
MOLM-13	5.39	n.s	1.82
MV-4-11	9.72	8.37	1.98

Table 4-1. IC_{50} values of compound 1 vs ferrocene analogues 3 and 5 *in vitro* (μM). Cells were treated for 72 hr and assessed by Cell Titer Blue assay. IC_{50} values are given as mean of three independent experiments (n=3), n.s, non-significant.

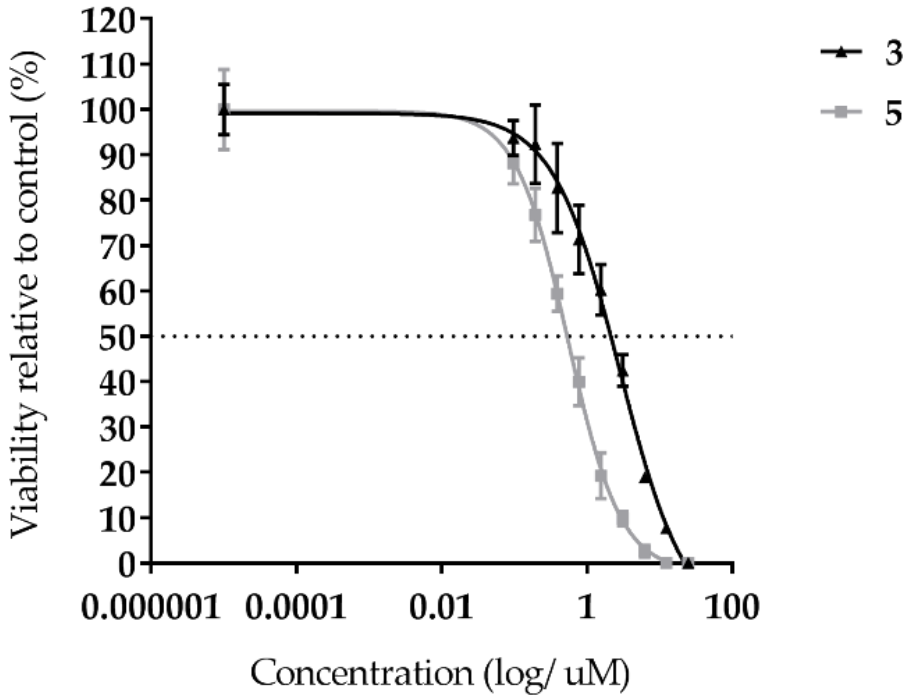

Figure 4-6. Dose-response curves for ferrocene analogues, 3 and 5 in MDA-MB-231 cells. Cells were treated for 72 hr and assessed by Cell Titer Blue assay. Data shown as mean ± SD of triplicate wells and are representative of three independent experiments (n=3).

To investigate the effect of compounds **3** and **5** on cell signalling processes, MDA-MB-231 cells were incubated with 5 μM of **3** and **5** for either 6 hr or 24 hr, extracts prepared and equal amount of protein analysed by SDS-PAGE and Western blotting (Figure 4-7). Surprisingly, although **1** has been shown to prevent phosphorylation of eIF4E on Ser209 (Chapter 3), Figure 4-7 shows that incubation of cells with 5 μM of compound **3** or **5** for 6 hr had no effect on the level of eIF4E phosphorylation. An increase in incubation time to 24 hr did not result in an inhibition of eIF4E phosphorylation (Figure 4-7, lanes 5 and 6 vs lane 4); the slight increase in eIF4E phosphorylation observed in all the latter cells probably reflects an overall increase in cellular growth over the 24 hr incubation. In addition, the treatment of MDA-MB-231 cells with **3** and **5** as single agents did not appear to effect PI3-K signalling, indicated by little change in the level of phosphorylation of AKT(T308-P) in comparison to the DMSO vehicle. Phosphorylation of p70S6K (T389) and ERK1/2 (T202/Y204) were not inhibited upon incubation of cells with the ferrocene analogues, **3** and **5**, either at 6 hr or 24 hr. However, there was a slight increase in the level of rpS6 and ERK1/2 phosphorylation when cells were incubated with **5** at 5 μM, eluding to a possible role of **5** in modulating ERK1/2 and rpS6 phosphorylation at early times.

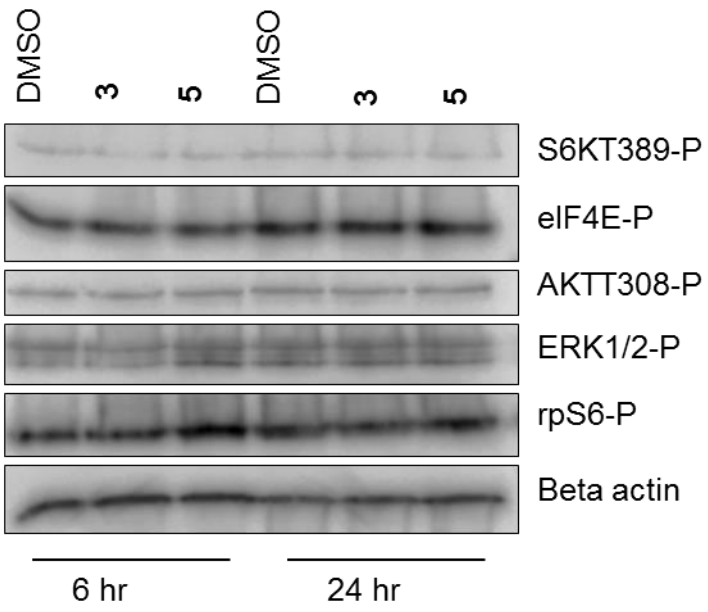

Figure 4-7. Representative Western blot analysis of both 3- and 5-treated MDA-MB-231 cells. Western blot analysis showing the effect of 5 µM of **3** and **5** on the phosphorylation status of S6K, eIF4E, AKT, ERK and spS6 after 6 hr and 24 hr incubation. MDA-MB-231 cells were incubated with DMSO alone (lanes 1 and 4), **3** (lanes 2 and 5) or with **5** (lanes 3 and 6). Cellular lysates were prepared and immunoblotting was performed using the indicated antibodies using 20 µg of total lysate protein, as described in the Materials and Methods.

4.2.4 Treatment of MDA-MB-231 Cells with Compound 5 Increases the Rate of Cell Migration

TNBC is an aggressive form of breast cancer typified by highly migratory and invasive cells (Podo et al., 2010). To investigate the effect of **1** and **5** on cell migration, the rate of migration of the TNBC cell line, MDA-MB-231, was assessed in the absence or presence of compounds, using real-time monitoring of cell migration (Figure 4-8). MDA-MB-231 cells were analysed in the presence of DMSO alone, compound **1**, or compound **5** as they moved towards a chemo-attractant. Cell migration kinetics were recorded on an RTCA DP (Real-Time Cell Analyser Dual-Plate) instrument for 12 hr. As shown in Figure 4-8A, when cells were treated with **1** at 1 μM final concentration, a slight, reproducible increase in cell migration was observed. The effect of **5** at 1 μM concentration on cell migration was more substantial, with a significant increase in cell migration at 6 hr relative to the DMSO control (Figure 4-8B). This might reflect the possible role of **5** in modulating ERK1/2 and rpS6 phosphorylation at early times (Figure 4-7), events commonly associated with cell growth. It may also be a result of oncogene activation, driven by cellular stress and subsequent eIF2α phosphorylation (Garcia-Jimenez & Goding, 2019) (discussed in Section 1.1.4.3).

4.2.5 Analysis of Compounds 1 and 5 on MDA-MB-231 Spheroid Growth

Three dimensional (3D) cell culture is an artificially created environment in which cultured cells are permitted to grow and interact with their surroundings in all three dimensions. Unlike classical 2D environments, a 3D culture allows cells *in vitro* to grow in all directions, similar to how they might function *in vivo*. As MDA-MB-231 cells grow in 3D culture, the sensitivity of these cells to compound **1** and **5** was monitored under these conditions. Having established the optimal conditions for spheroid assembly (detailed in Materials and Methods), the effect of increasing concentrations of compounds **1** and **5** on spheroid growth was examined as described in Figure 4-9. Three-day-old spheroids were treated with DMSO alone, compound **1**, or **5** and their growth monitored using the Celigo Image Cytometer. Whole-well bright-field images were acquired multiple

days after adding the test compounds and the tumour spheroid diameter was measured to provide a quantitative analysis of spheroid growth (Figures 4-9A and B).

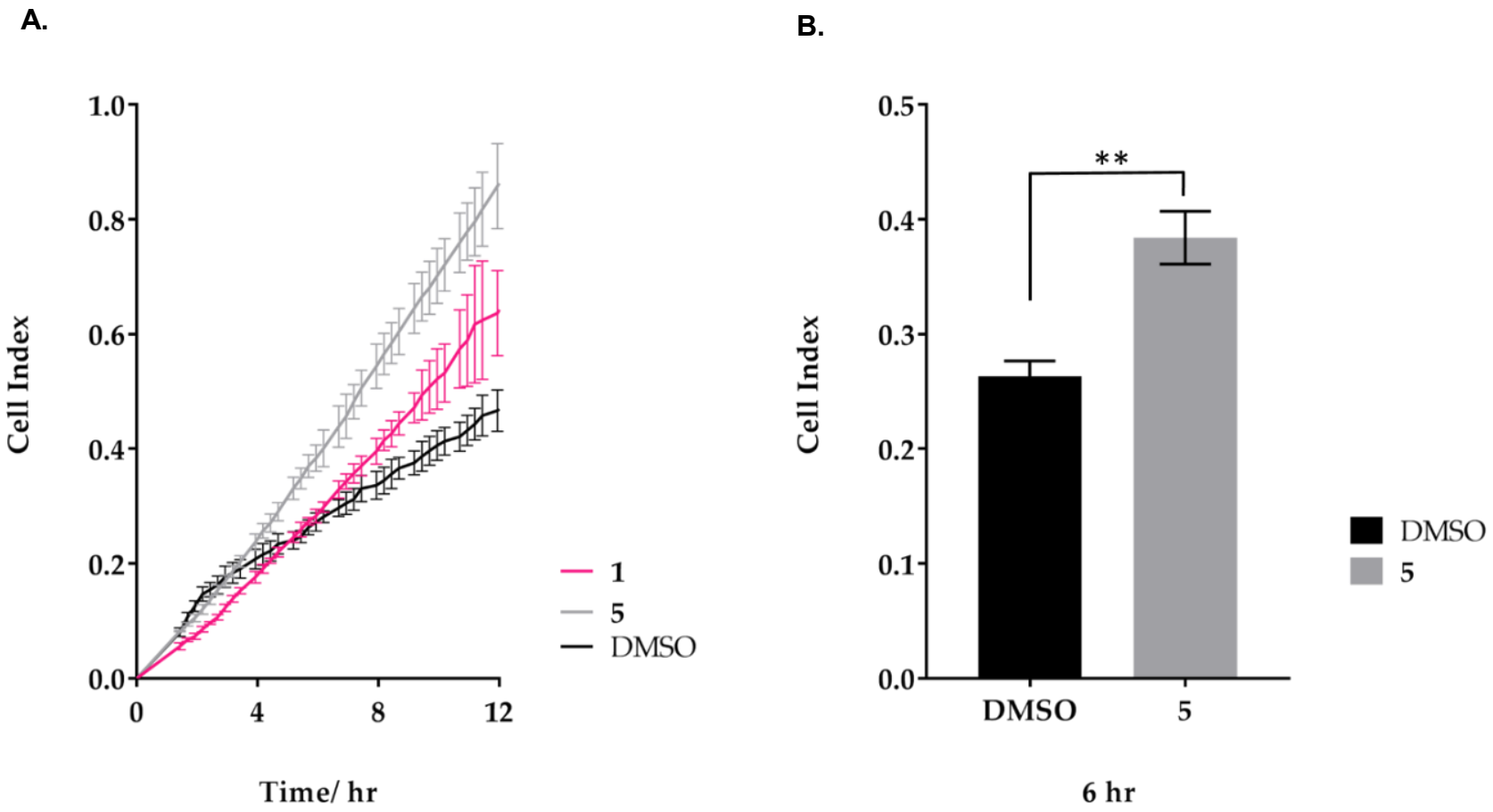

Figure 4-8. Kinetics of migration in MDA-MB-231 cells incubated with ferrocene compounds. Cell migration in real time was analysed by the xCELLigence RTCA. **A.** shows the average cell indexes over 12 hr for each drug treatment (1 μM), **B.** cell migration analysis at 6 hr, data shown as mean ± S.D, n=3 (**p ≤0.01).

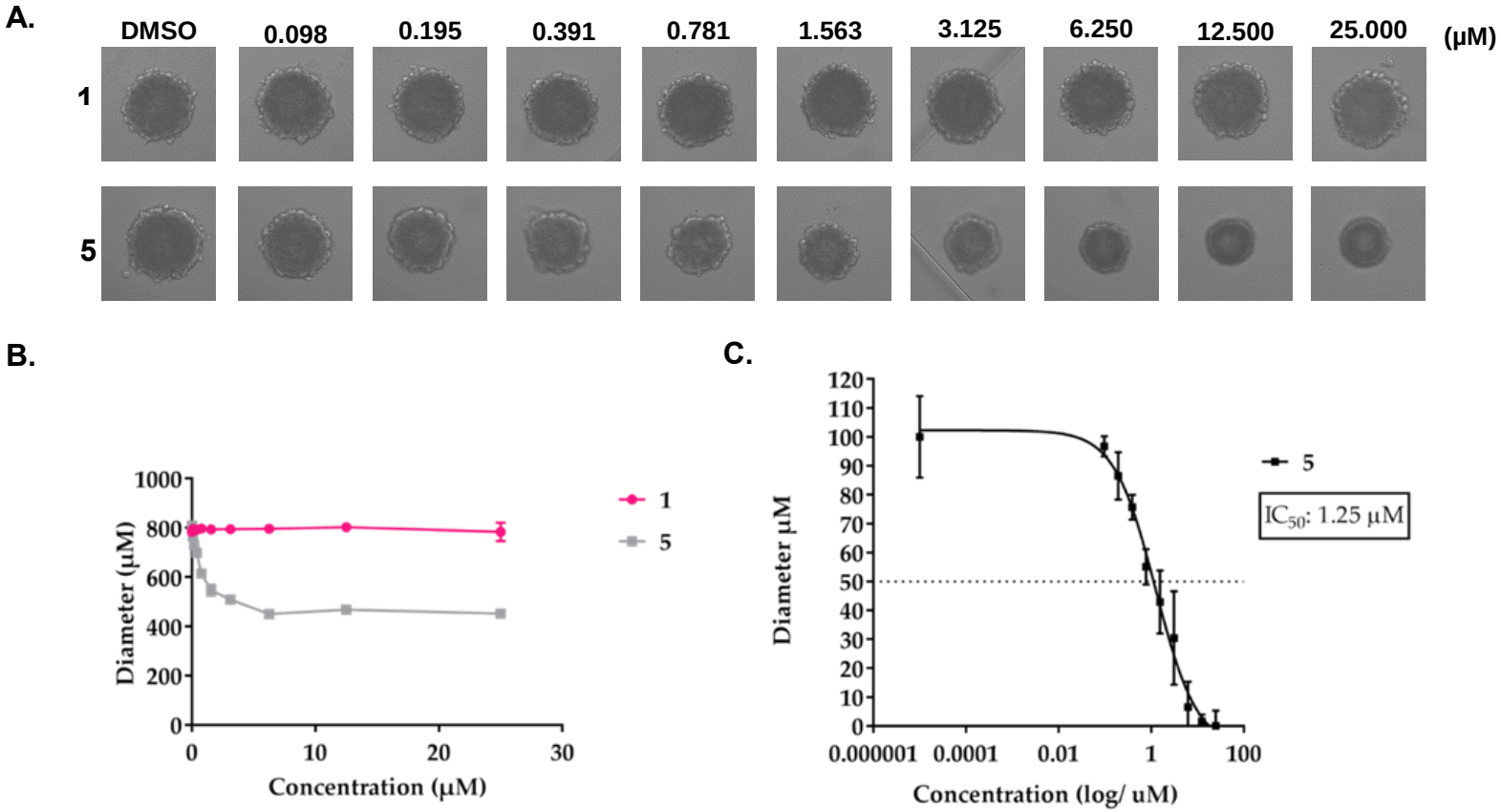

Figure 4-9. Assessment of growth in MDA-MB-231 spheroids incubated with ferrocene compounds. MDA-MB-231 cells were treated for 4 days with **1** and **5** as single-agents. Spheroids were imaged and analysed using the Celigo High Throughput Micro-Well Image Cytometer. **A.** Representative bright-field images of MDA-MB-231 spheroids after 4 days. **B.** The diameter of MDA-MB-231 spheroids after 4 days incubation in the absence of presence of ferrocene compounds was measured using ImageJ software. **C.** Spheroid diameter dose-response curve for compound-**5**-treated spheroids. Data shown as mean ± S.D of triplicate wells (n=3).

Results show that compound **1** had no effect on spheroid diameter, even at the highest concentration of 25 µM. In contrast, **5** showed a concentration-dependent growth inhibition of MDA-MB-231 spheroids. A dose-response curve was plotted for **5** and was used to calculate an IC_{50} value of 1.25 µM (Figure 5-9C), approximately twice the IC_{50} value reported in the 2D cell viability assay (IC_{50}: 0.55 µM). As with cell growth characteristics, these results indicate that drug susceptibility can vary between 2D and 3D assays and a combination of assays are required to ascertain drug effectiveness.

4.2.6 *In Vitro* Kinase Assays Report that Compound 5 has no Effect on MNK1/2 Kinase Activity

Incubation of cells with compound **5** had no effect on the level of eIF4E phosphorylation and caused a small increase in p70S6K and ERK1/2 phosphorylation at early times (Figure 4-7). To gain further insights into what kinase(s) **5** might be targeting in the cell, *in vitro* target validation of **1** and **5** was carried out using a commercial kinase screening assay (provided by Reaction Biology; Table 4-2); for costs reasons and due to its weaker affinity, **3** was not included in this screen. As expected, compound **1** dramatically reduced MNK1 and MNK2 enzyme activity to ~3% and ~1.5%, respectively, relative to the DMSO vehicle. Compound **1** had a significant off-target effect on PIM1, in which enzyme activity was reduced to <50%. This may be explained by the structural similarity between MNK1/2 and PIM1 (discussed in Section 3.3). The inhibition of MNK1/2 by compound **1** did not affect upstream protein kinases, AKT or p38MAPK (Lineham et al., 2018). In contrast, **5** had no effect on percentage (%) enzyme activity in any of the protein kinases screened. These data are in agreement with findings presented in Figure 4-7; an extensive screening panel would be required for a more in-depth understanding of the targets on compound **5**.

Kinase:	% Enzyme Activity (relative to DMSO controls)			
	1		5	
	Data 1	Data 2	Data 1	Data 2
AKT1	110.03	105.00	106.92	105.28
MNK1	3.64	2.53	115.13	111.38
MNK2	1.87	0.79	97.56	96.04
P38a/MAPK14	125.49	119.86	126.41	125.76
PIM1	43.11	42.99	118.37	117.29

Table 4-2. Selectivity of compound 1 and 5 against a panel of kinases (% enzyme activity relative to DMSO vehicle). Compounds were tested under standard commercial conditions (in single dose duplicates at 1 µM) and reactions were carried out at 10 µM ATP by Reaction Biology Kinase HotSpot Screening. Enzyme activity >100% may be due to a real stimulatory effect or an artefact due to interference of the compound with the measurement.

4.3 Discussion

Structural modelling of compound **1** (Figure 4-1) in the active site of MNK kinase revealed a large hydrophobic pocket that could be exploited with a bulkier group such as a ferrocene (Figures 4-2 and 4-3). Although the ferrocene derivatives, **3** and **5** (Figures 4-1D and E; Figure 4-4), showed no activity against MNK1/2 (Figure 4-7), their potency in cancer cell lines is promising. It is unsurprising that compound **1** has no significant effect on cell viability, as the MNK kinases are not required for normal development (Teo et al., 2015b). MNK1/2 inhibitors exert their effect by preventing the drive of oncogenic signalling through the inhibition of eIF4E phosphorylation. The IC_{50} values for the two ferrocene compounds follow a similar pattern across the range of cell lines tested (Table 4-1), with both compounds more effective against TNBC lines and less effective in the $HER2^+$ cell line, SK-BR-3. This could reflect a variation in the levels of cellular target proteins, or a difference in the rate of metabolism. It is possible that the ferrocene itself is responsible for the anticancer activity. The production of reactive oxygen species (ROS) in the Fenton reaction has been proposed as a mechanism of cytotoxicity in other ferrocene derivatives (Tabbi, Cassino et al., 2002). Indeed, the anticancer compound, Fc–OH–TAM, elicits an oestrogen receptor-independent mechanism of action in addition to its competitive binding of ER. Additionally, ROS production was associated with cell cycle arrest and cellular senescence in Fc–OH–TAM-treated breast cancer cells (Vessieres et al., 2010). The IC_{50} values for compound **5** and Fc–OH–TAM in MDA-MB-231 were both ~0.5 µM (Table 4-1), which suggests ROS production may be involved in the mode of action for **5**.

The synthesised compounds were submitted to a commercial small kinase-screening panel aimed at assessing their ability to inhibit the activity of selected kinases. These data summarised in Table 4-2, suggest that the ferrocene derivative **5** targets alternative cellular pathways than those investigated. These findings are in agreement with a lack of effect on MNK1/2 and AKT signalling, as determined by Western blotting (Figure 4-7). Interestingly, **5**, and to a lesser extent **3**, increased the rate of migration in MDA-MB-231 cells. The reasons for this unexpected result are unclear. Compound **5** may target a negative regulator

of cell migration; alternatively, the increase in migration rate may be a result of cellular stress. Western blotting also suggested that the level of rpS6 and ERK1/2 phosphorylation increased upon incubation with **5**, indicating a possible role of **5** in the inhibition of protein phosphatases. Further analysis would require an extensive kinase screen to validate the targets of these compounds. Additional eIF2α assays would also elucidate the role of cellular stress induced by the ferrocene compounds used in this study. These data, in agreement with the literature, highlight the potential of ferrocene-based compounds such as ferrocifen as anticancer agents.

5 Genetic knockdown and Pharmacological Inhibition of DDX3X and its Effect on Cell Migration

7.1 Introduction

The exact role of DDX3X in translation has yet to be elucidated. The most studied function is its role in promoting the translation of specific mRNAs containing a high degree of secondary structure in their 5'UTR through its interaction with eIF4F. However, contradicting evidence suggests that DDX3X represses cap-dependent translation by binding to and inhibiting eIF4E (Shih et al., 2008), as well as promoting stress granule formation. Furthermore, DDX3X can have both oncogenic and tumour suppressor properties depending on the cancer type and the expression level of interacting partners. To help unravel this, as described, the CRISPR-Cas9 system was used to induce a site-directed non-homologous end joining (NHEJ) event in the first exon of DDX3X. Following repair the aim was to create a frameshift mutation and subsequently, a premature stop codon to decrease expression of DDX3X protein in MRC5 fibroblasts (summarised in Figure 5-1). Following on from the characterisation of the cell lines developed, subsequent analysis focussed on the pharmacological inhibition of the ATP-dependent helicase function of DDX3X in prostate cancer cell lines bearing both high and low DDX3X protein expression levels.

5.1 Results

5.1.1 The Generation of a DDX3X Knockdown Cell Line

The CRISPR-Cas9 system is comprised of two parts, the Cas9 endonuclease and the targeting RNA. The targeting RNA, also known as a small guide RNA (sgRNA), is a duplex RNA consisting of a CRISPR RNA, transacting RNA (tracrRNA) and a spacer located at the 5'end of the CRISPR RNA. The spacer finds an identical sequence on the target DNA named the protospacer. Another sequence directly downstream of the protospacer, known as the protospacer adjacent motif (PAM) must also be recognised by the CRISPR-Cas9 complex

before cleavage occurs. The Cas9 endonuclease then creates a double stranded break three nucleotides upstream of the PAM site.

A protocol based on the CRISPR-Cas 9 endonuclease (Ran et al., 2013) was used to create a genetic modification to DDX3X in MRC5 cells. The experimental workflow is summarised in Figure 5-2 and begins with the *in silico* design of sgRNAs. The genomic DNA sequence from DDX3X was imported from Ensembl® into Benchling®, after cross-referencing with Uniprot®.

Next, the CRISPR sgRNA design tool was used to analyse a 1 kb fragment of the region of interest and locate suitable target sites by identifying 20-bp sequences directly upstream of any 5'NGG (PAM sequence). Both on- and off-target sites were computationally predicted, allowing selection of the three highest ranked sgRNA sequences, i.e. highest on-target with lowest off-target scores (Figure 5-3). Following the construction of sequence-verified pSpCas9 (sgRNA) plasmids, subsequent transfection into MRC5 cells using Lipofectamine® and clonal expansion, extracts were prepared from the cell lines derived here and aliquots containing equal amounts of protein resolved by SDS-PAGE. Western blotting was used to screen the putative monoclonal DDX3X knockout cells generated by this method. As shown in Figure 5-4A, the decreased expression of DDX3X protein in clones 2A, 2C and 1F cell lines initially indicated that the DDX3X gene had been successfully deleted. However, following several cell passages, further Western blotting analysis of the cell lines suggested only a partial knockout of DDX3X had occurred (Figures 5-4B and C). A commercial company was also used to generate DDX3X knockout in HAP1 cells (derived from a chronic myelogenous leukaemia (CML); a similar result of a partial knockout was also obtained with the cells (data not shown), suggesting that total loss of DDX3X protein was likely lethal to cells.

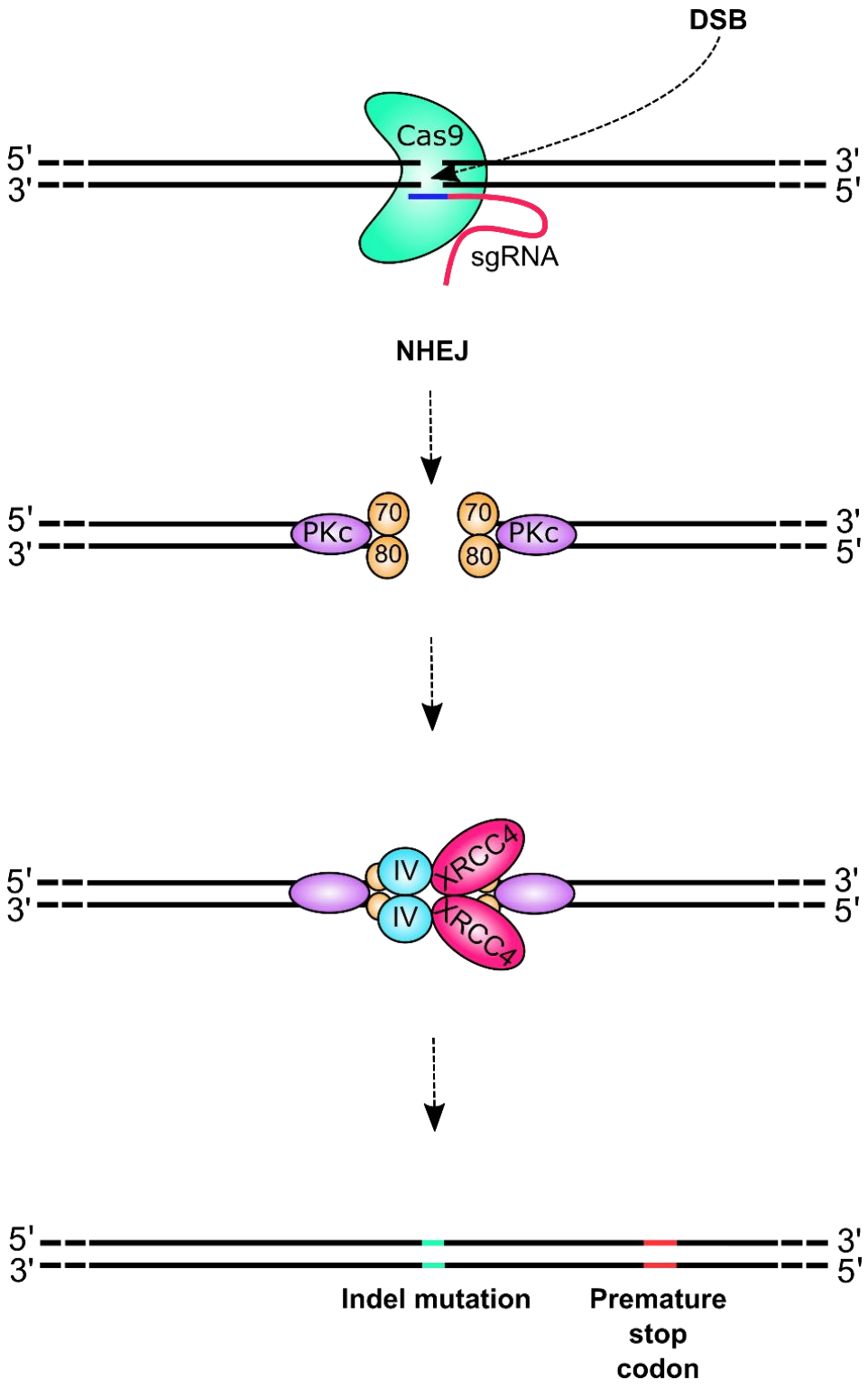

Figure 5-1. Simplified model of double strand break (DSB) repair by the non-homologous end joining pathway (NHEJ). RNA-guided Cas9 nuclease (green) induces a DSB that can be repaired by the error-prone NHEJ pathway. The ends of the DSB are processed by the Ku heterodimer (Ku70 and Ku80), which forms a complex with DNA-PKc. The DNA ends are processed by additional enzymes and re-joined by the DNA ligase IV/XRCC4. NHEJ directed DSB repair may result in random indel mutations at the site of the Cas9 induced "nick". Indel mutations within a coding region create a frameshift mutation, which may lead to the generation of a premature stop codon, and ultimately a gene knockout.

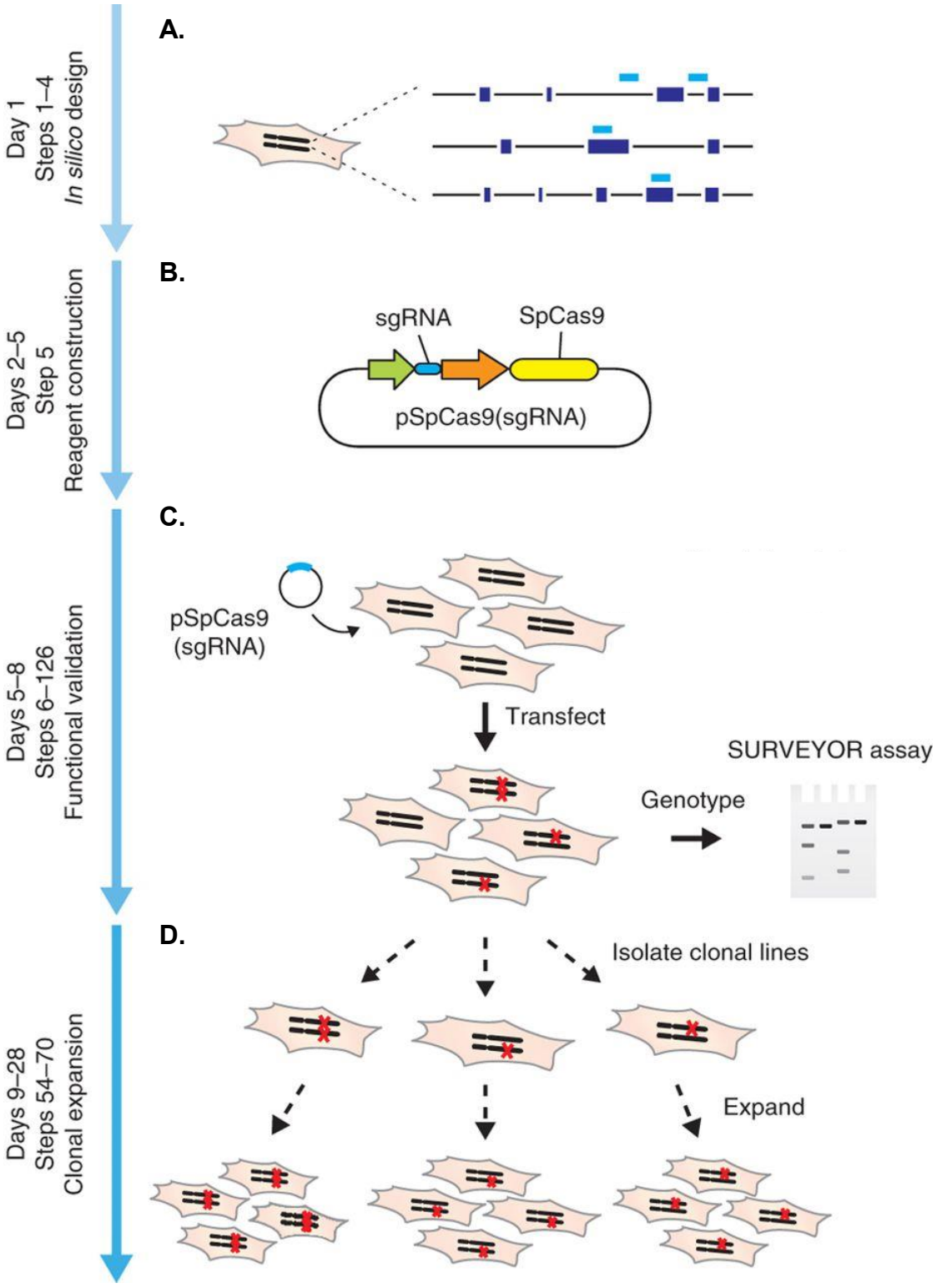

Figure 5-2. Experimental workflow of CRISPR-Cas9 gene knockout in mammalian cells using a protocol from Ran et al., 2013. A. Guide RNAs (sgRNAs) were designed using a CRISPR design tool built into Benchling® (light blue bars). **B.** sgRNAs were then cloned into a pSpCas9(BB) plasmid, containing both sgRNA scaffold backbone (BB) and Cas9. **C.** The resulting sequence-verified pSpCas9(sgRNA) plasmids were transfected into MRC5 cells and the surveyor assay was used to assess cleavage ability. **D.** Limiting dilution was used to isolate clones. These cell lines were expanded to derive isogenic cell lines with specific mutations. (Figure taken and adapted from Ran et al., 2013).

To verify that the level of DDX3X mRNA was significantly reduced in CRISPR generated DDX3X clonal cell lines 2C and 2A, comparative qRT-PCR (described in the Materials and Methods) was used to measure the level of DDX3X mRNA in knockout cell lines. In comparison to wildtype levels, there was a reduction in DDX3X mRNA in both cell lines, with the greatest reduction seen in clone 2A (Figure 5-5). These data clearly show that the selected MRC5 clones 2A and 2C exhibit CRISPR-Cas9-mediated, but partial reduction of DDX3X mRNA and protein expression. To determine whether loss of DDX3X protein caused any changes in level of other initiation factors, cell extracts were further characterised by Western blotting and the level of expression of various translation factors and signalling molecules were analysed. Figure 5-6 shows that, relative to wildtype cells, there was no change in the total levels of translation factors analysed in this study when DDX3X protein levels were reduced.

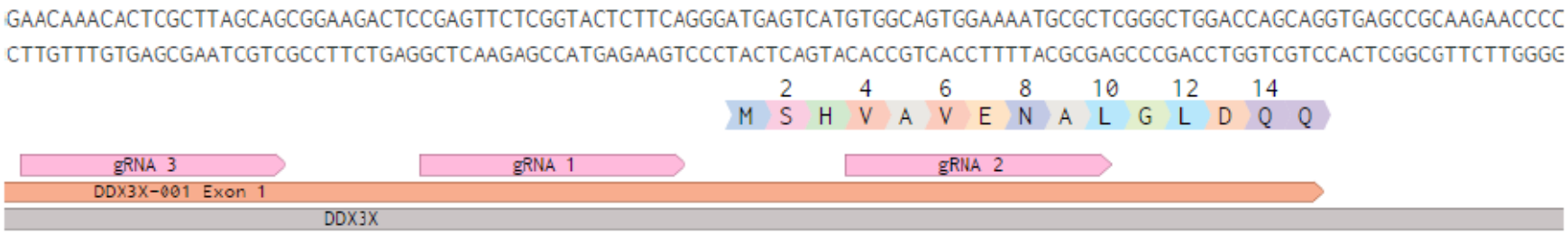

Figure 5-3. Schematic of the 20-nt guide sequences used to target the Cas9 nuclease to the genomic DNA sequence of DDX3X. sgRNA sequences 1,2 and 3 are highlighted in pink. The sgRNAs were designed to cleave the DNA slightly upstream or in the protein coding region of Exon 1 of DDX3X.

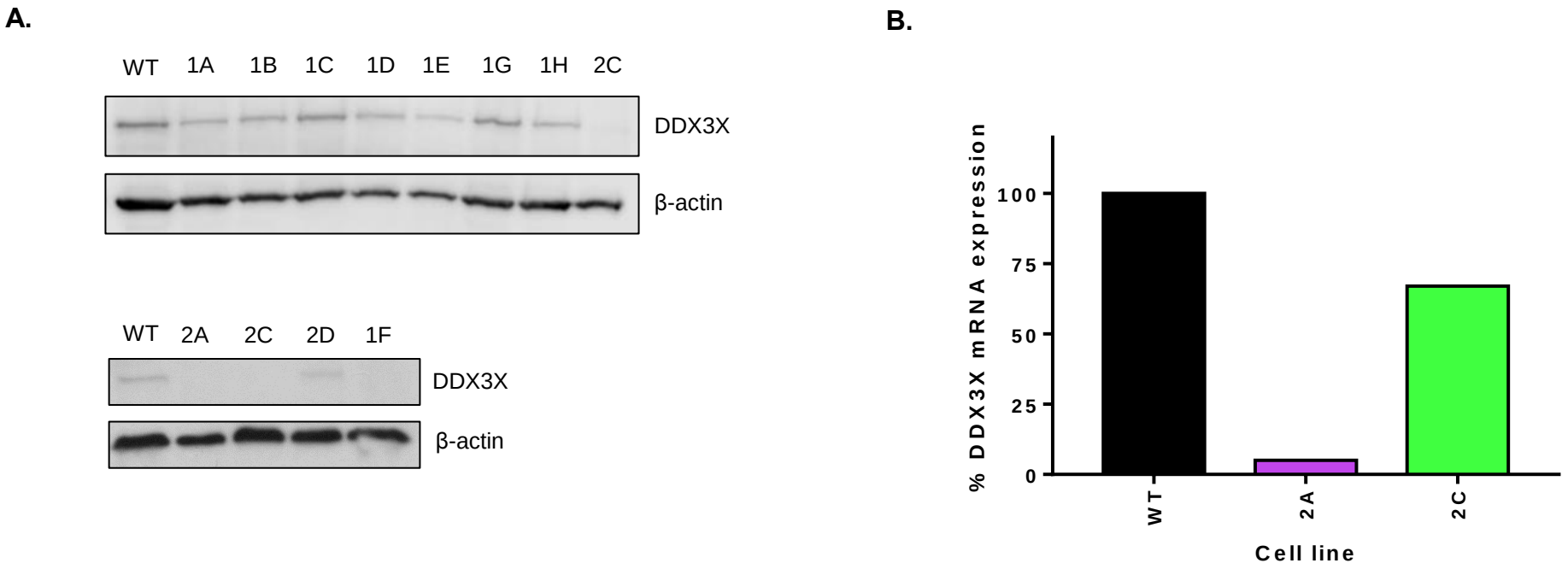

Figure 5-4. CRISPR-Cas9-mediated reduction of DDX3X protein expression and mRNA expression in MRC5 cells. A. Cells were cultured as described in the Materials and Methods and the CRISPR-Cas 9 system was used to produce clonal cells lines as indicated. Extracts were prepared from these cells as described in Materials and Methods and aliquots containing 20 µg protein were resolved by SDS-PAGE and visualised using Western blotting with the antibodies indicated. WT shows parental cells and the others were derived clones. **B.** CRISPR-Cas9-mediated reduction of DDX3X mRNA expression in MRC5 cells as determined by qRT-PCR. mRNA was extracted and processed as described in the Materials and Methods. qRT-PCR was used to show the effect of CRISPR-generated DDX3X knock-outs on the level of DDX3X mRNA in comparison to parental (WT) MRC5. GAPDH and HPRT1 mRNA levels were used to normalise the levels of mRNAs across different samples.

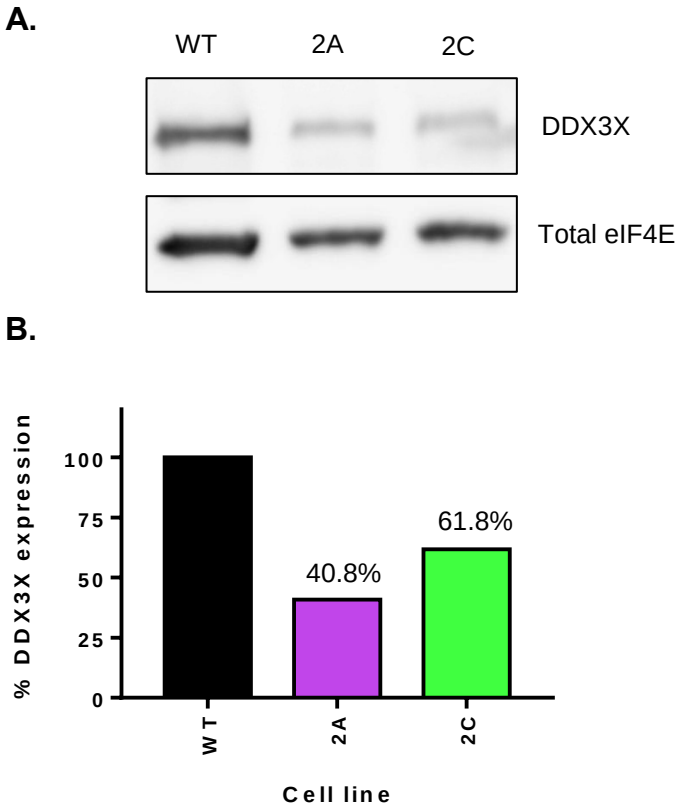

Figure 5-5. CRISPR-Cas9-mediated reduction of DDX3X protein expression in MRC5 cells. **A**. Representative Western blot of WT MRC5 cells and clonal lines 2A and 2C after several passages (performed in conjunction with V. William 2017). **B.** Quantification of DDX3X expression levels in WT, 2A and 2C cell lines. Levels of DDX3X expression were quantified relative to total eIF4E (set at 100%).

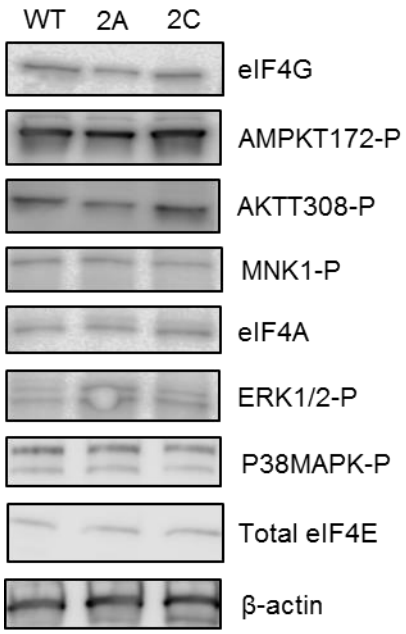

Figure 5-6. Reduction of DDX3X protein levels does not change the level of signalling molecules in derived cell clones, 2A and 2C. Cells were cultured described in the Materials and Methods and the CRISPR-Cas9 system was used to produce clonal cell lines as described in Figure 7.5. Extracts were prepared cells as described and aliquots containing 20 µg protein were resolved by SDS-PAGE and proteins visualised using Western blotting with the antibodies indicated.

5.1.2 A Reduction in DDX3X Protein Level Impedes Cell Migration in MRC5 Cells

To investigate the effect of decreased levels of DDX3X expression on cell migration, an initial phenotypic characterisation of DDX3X knockdown cell lines was carried out using the scratch assay described in the Materials and Methods. This measures both the proliferation and migration of cells as they attempt to fill a gap in the confluent culture induced by scratching cells off the surface of the plate. Figure 5-7 shows that DDX3X knockdown clones, 2C and 2A were reduced in their ability to migrate and fill in the gap in the culture in comparison to wildtype cells. These data suggest that DDX3X protein is required for efficient cell migration under these assay conditions. The rate of migration was further assessed using a variation of the classical scratch assay, known as the Oris cell migration assay®. To examine the effect of partial depletion of DDX3X on cell migration, wound closure was monitored in serum-starved cells (to reduce cell proliferation). Wildtype MRC5 cells and DDX3X knockdown clone 2A cells were seeded into stopper-loaded wells in a 96-well plate for 4 hours to permit cell attachment. To start cell migration, the stoppers were removed, cells were washed with PBS and fresh serum-free medium was added. Images were taken every 4 hours and analysed using Image J software (Figure 5-8A). As shown in Figure 5-8B, these data show that a partial depletion of DDX3X resulted in a decreased rate of wound closure.

5.1.3 Molecular Modelling of DDX3X Inhibitor, RK-33, in DDX3X Crystal Structure

Following several unsuccessful attempts to knockout DDX3X expression using a CRISPR-Cas9 system in MRC5 fibroblasts, efforts were then focussed on investigating the pharmacological inhibition of DDX3X. The X-ray crystal structure of the conserved DEAD domain and helicase domain of human DDX3X in complex with AMP (PDB: 2I4I) was used to analyse the most likely binding mode of RK-33, a known DDX3X helicase inhibitor (Figures 5-9A-D). The predicted docking pose revealed that RK-33 binds the ATP-binding cleft, with the imadazolone ring stacked above Tyr200 (Figure 5-9D).

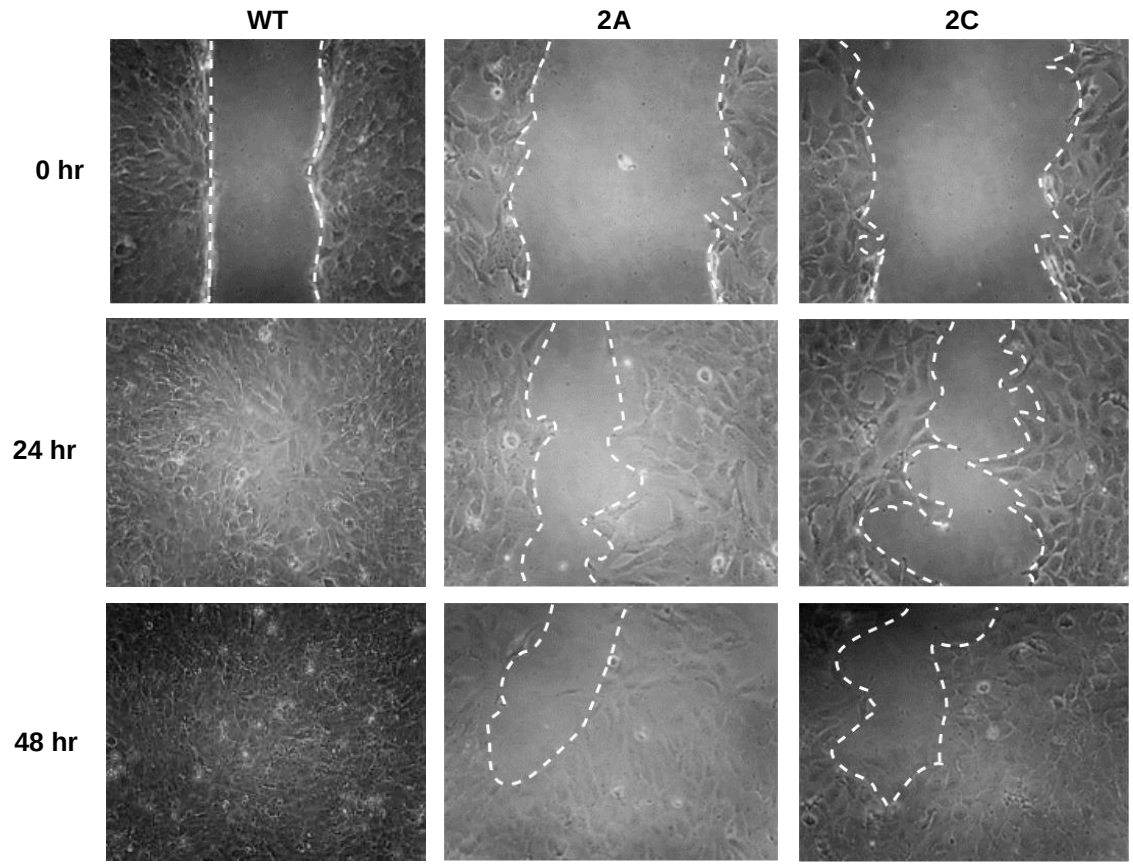

Figure 5-7. Scratch-wound healing assay showing the effect of DDX3X knockdown on wound healing over a period of 48 hours. Scratch assays were carried out as described in the Materials and Methods. Briefly, confluent cells were grown in serum-free media for 12 hours prior to incubation in complete DMEM; a P-20 pipette tip was used to make a “wound” in the confluent monolayer of cells and images were then taken at 24 hr and 48 hr time periods of wound healing. Representative images are shown here with white dashed lines drawn around the wound (n=3).

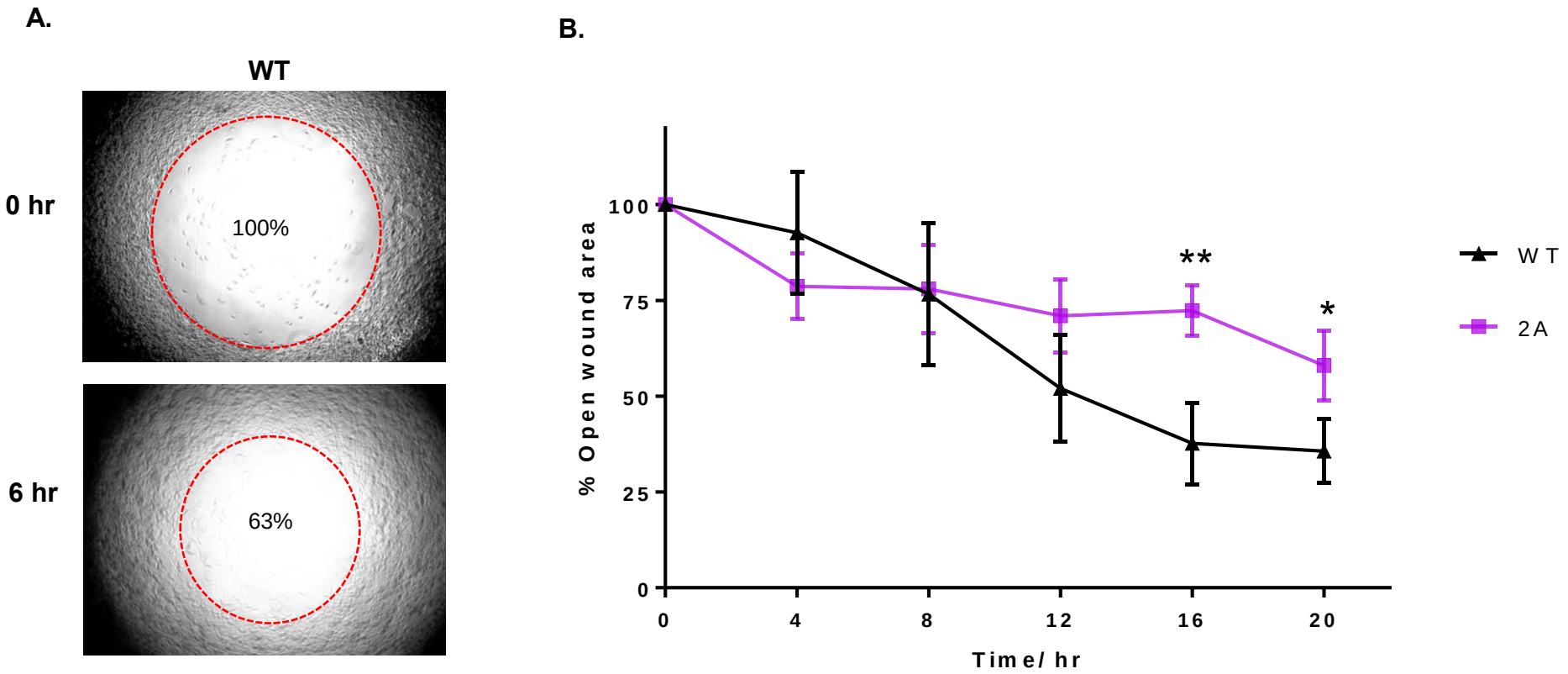

Figure 5-8. Reduction in DDX3X protein levels impedes cell migration in MRC5 cells. A. An example of the wound healing assay in WT MRC5 cells. Bright-field images were taken at indicated time points following bung removal at 0 hr. Wound closure was measured using Image J software (illustrated by the red dashed circles) and expressed as % of open wound area relative 0 hr. **B.** Wound-healing assays were carried out as described using parental (WT) and DDX3X-depleted clonal cell line, 2A, over a period of 20 hours. Data are presented as the means ± S.D, n=3 (*$p \leq 0.05$; **$p \leq 0.01$).

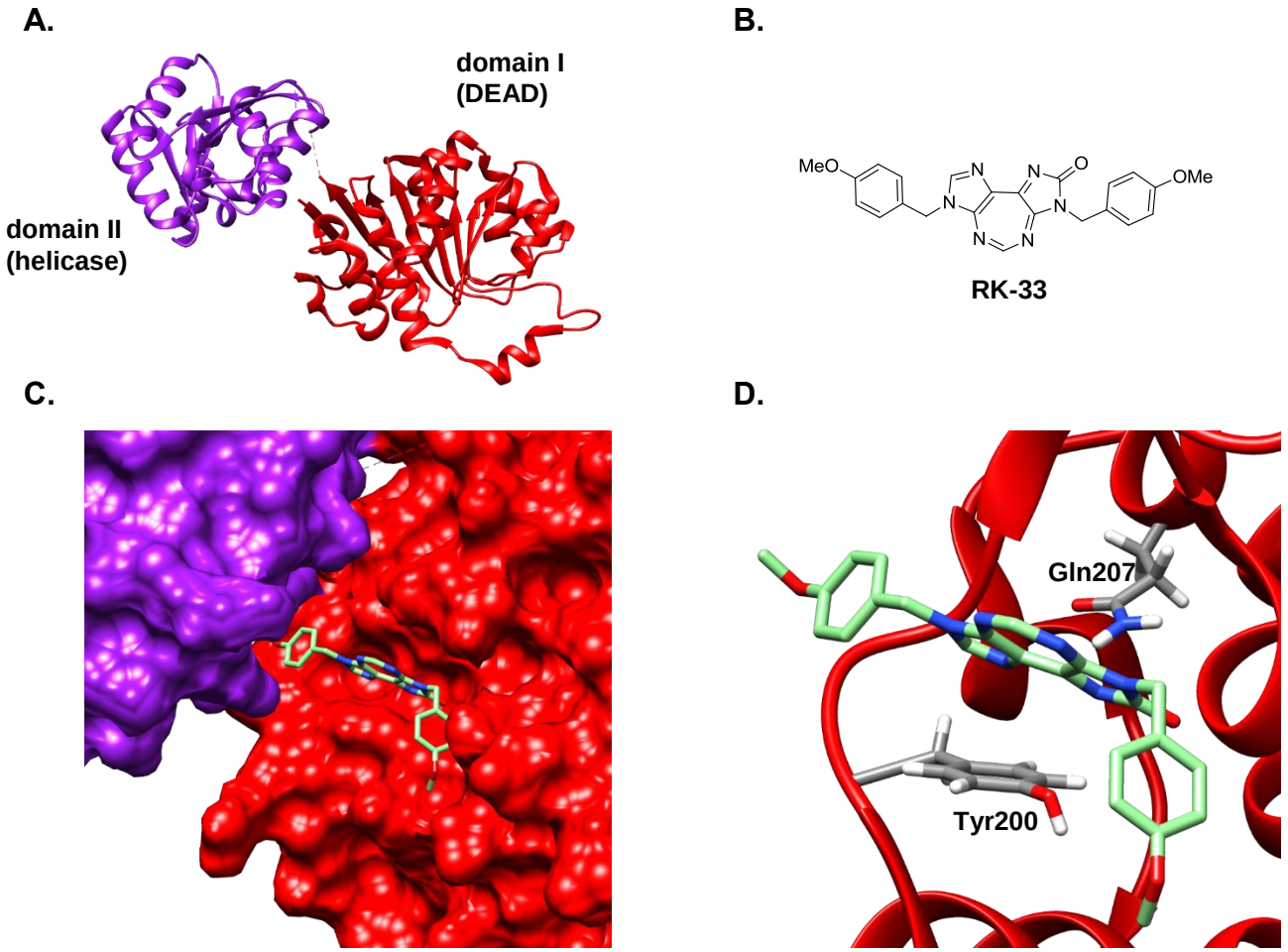

Figure 5-9. Docking of RK-33 in DDX3X crystal structure. A. Secondary structure of DDX3X, DEAD domain shown in red and Helicase domain shown in purple (PDB: 2I4I). **B.** Chemical structure of DDX3X inhibitor, RK-33**. C.** Predicted binding mode of RK-33 in DDX3X (PDB: 2I4I). **D.** Close up of proposed interactions between RK-33 and the ATP-binding site of DDX3X. Molecular graphics and analyses were performed with the UCSF Chimera package (Pettersen et al., 2004).

RK-33 forms hydrogen bond interactions with Gln207 and Tyr200 residues as also depicted by Bol et al., (2015). The predicted binding mode supports the hypothesis that RK-33 inhibits the ATP-dependent helicase activity of DDX3X by blocking the binding of ATP.

5.1.4 *In Vitro* Analysis of RK-33 in Prostate Cancer Cell Lines

Recent work by Xie et al., (2017) reported that DDX3X expression correlated with an increased aggressive phenotype in prostate cancer cell lines and in patient samples (Xie et al., 2016). Their prior studies identified the expression of levels of DDX3X across a panel of prostate cancer cell lines (Xie et al., 2016). To test whether DDX3X expression levels had an effect on the cell viability of cells treated with RK-33, the compound was tested in two prostate cancer cell lines, one with high DDX3X expression levels (LNCaP) and one with low expression levels (PC-3). Cell viability was assessed in both LNCaP cells and PC-3 cells treated with RK-33 over a period of 72 hours and determined by the Cell Titer Blue assay (Figures 5-10A and 5-10B). These data show that RK-33 decreased cell viability in both LNCaP and PC-3 cell lines, with IC_{50} values of 7.2 μM and 10 μM, respectively. The LNCaP cells were slightly more sensitive to RK-33 inhibition, relative to PC-3 cells with low DDX3X expression levels.

5.1.5 *In Vitro* Analysis of RK-33 in Combination with MNK1/2 Inhibitor, Compound 1 in Prostate Cancer Cell Lines

Owing to the prominent roles that both DDX3X and MNK1/2 play in translation, it was hypothesised that the inhibition of both proteins simultaneously may lead to a significant reduction in cell viability. As shown in Figures 5-10, compound **1** had no significant effect on cell viability when tested as a single agent in either LNCaP (Figure 5-10C) or PC-3 cells (Figure 5-10D). Cell viability was then analysed in LNCaP and PC-3 cell lines with RK-33 and compound **1** added in combination (Figure 5-11). No apparent difference was observed in the LNCaP cells when treated with RK-33 as a single agent or in combination with compound **1**, with both IC_{50} values of approximately 7 μM in each case. However, a reduction of cell viability was observed in PC-3 cells treated with a

combination of RK-33 and compound **1**, demonstrated by a drop in IC_{50} value from 10 µM to 5.9 µM (Figure 5-11B).

In order to explain the apparent increase in cell death in PC-3 cells treated with a combination of RK-33 and compound **1**, the level of eIF4E phosphorylation in these cells was measured by Western blotting (Figure 5-12A). Quantification of these data from three independent experiments showed that basal level of eIF4E-P was approximately three-fold greater in LNCaP cells in comparison to PC-3 cells (Figure 5-12B). The level of eIF4E phosphorylation was similar in PC-3, MRC5 cells and another prostate cancer cell line, DU145 cells (Figure 5-12B). The relatively low levels of eIF4E phosphorylation in PC-3 cells may explain their sensitivity toward the combination of RK-33/compound **1**. In contrast, the relatively high level of eIF4E-P in LNCaP cells suggests resistance to the RK-33/compound **1** treatment, a phenomenon that has been observed in other cancers (Li et al., 2017).

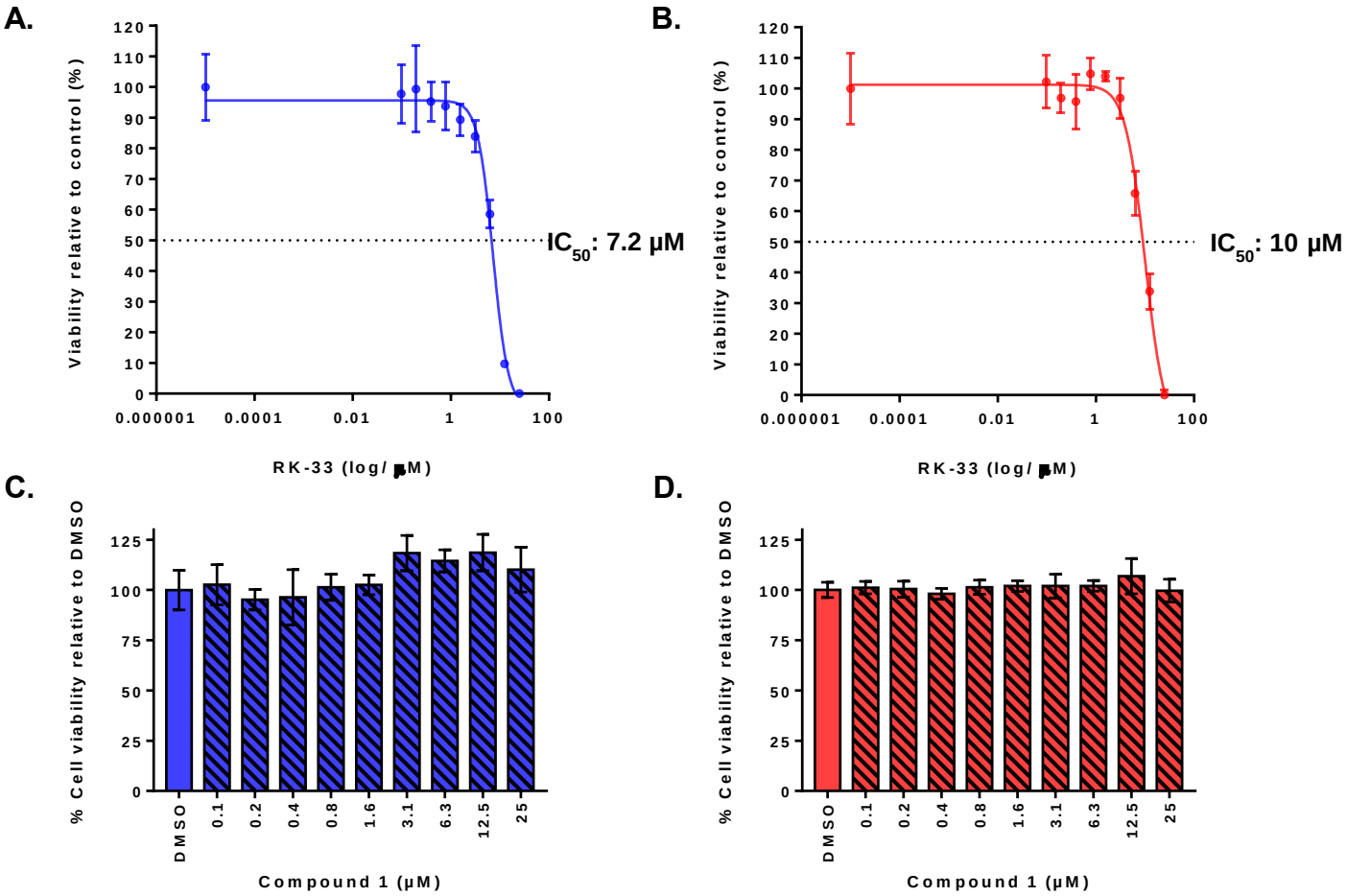

Figure 5-10. Cell viability of RK-33 and MNK1/2 inhibitor, compound 1, in prostate cancer cell lines. A. Dose-response curve for RK-33 treated LNCaP cells. **B.** Dose-response curve for RK-33 treated PC-3 cells. Cells were treated for 72 hr and assessed by Cell Titer Blue assay. Data shown as mean ± SD of triplicate wells. **C.** Cell viability of compound **1**. LNCaP cells were treated for 72 hours with compound **1** at the indicated concentrations. **D.** Cell viability of compound **1**. PC-3 cells were treated for 72 hours with compound **1** at the indicated concentrations and assessed by Cell Titer Blue assay.

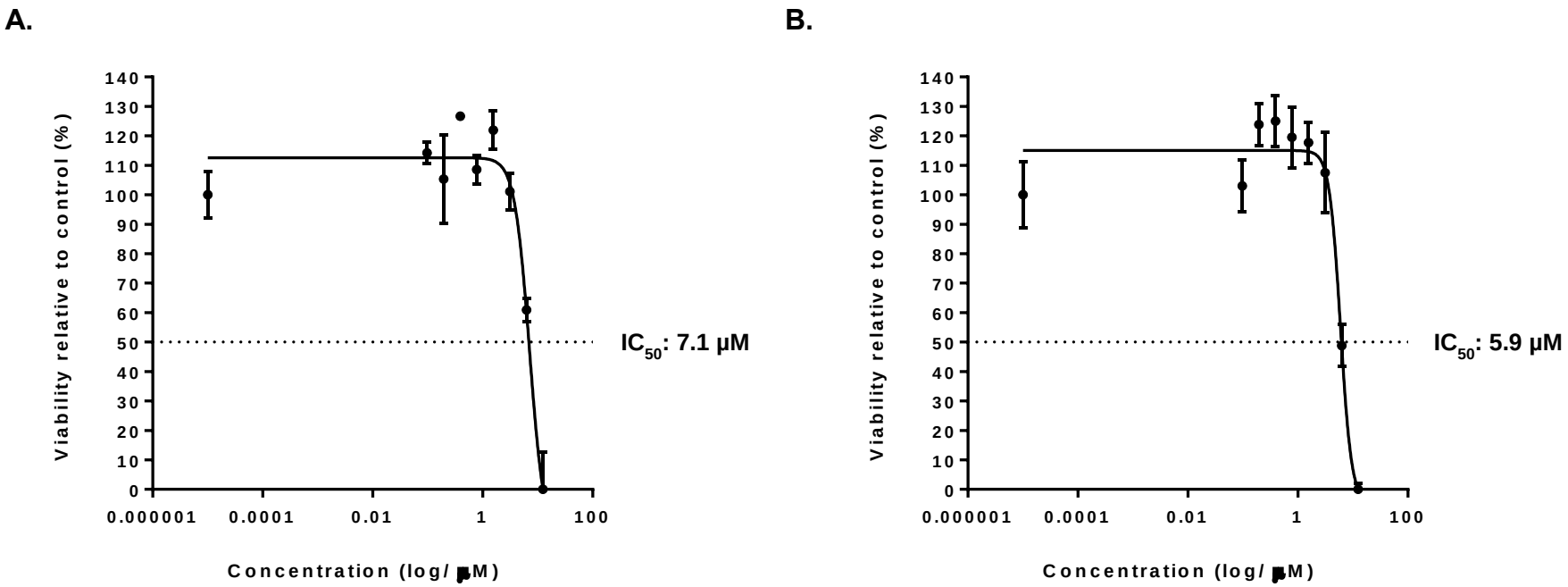

Figure 5-11. Cell viability of RK-33 in combination with MNK1/2 inhibitor, compound 1, in prostate cancer cell lines. A. Dose-response curve for RK-33 and compound **1** treated LNCaP cells. **B**. Dose-response curve for RK-33 and compound **1** treated PC-3 cells. Cells were treated for 72 hr in a 1:1 ratio of drugs and assessed by Cell Titer Blue assay. Data shown as mean ± S.D of triplicate wells.

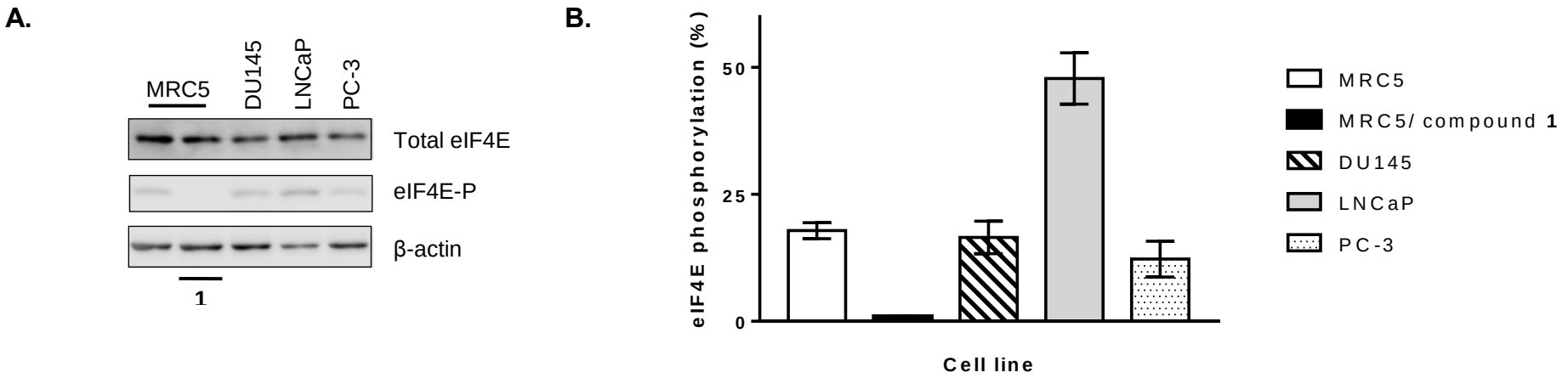

Figure 5-12. Quantification of eIF4E-phosphorylation level in a panel of prostate cancer cell lines. A. Representative Western blot analysis of cell lines: MRC5, MRC5 treated with 5 µM of compound **1**, DU145, LNCaP and PC-3. Cells were incubated for 24 hours and aliquots of extract (20 µg of total protein) were resolved by SDS–PAGE and visualised using immunoblotting. **B.** Levels of eIF4E-P expression were quantified relative to total eIF4E (set at 100%) in the indicated cell lines.

5.1.6 Treatment of PC-3 Cells with RK-33 Increases their Rate of Migration

As RK-33 was found to reduce cell viability in the prostate cancer cell lines tested, the question asked was whether RK-33 treatment of PC-3 cells effected their migration. PC-3 cells were chosen to investigate the rate of cell migration due to the spindle-like morphology of LNCaP cells, making it difficult to analyse the area of the "wound" accurately (Figures 5-13A and B). For this assay, cell migration was measured for 6 hr, both in the presence or absence of serum (Figures 5-14A and 5-14B, respectively). These data show that there was no significant difference in results obtained between serum starved and serum fed cells. This was expected for analysis at the 6 hour time point in the migration protocol. Surprisingly, Figure 5-14 shows that incubation of cells with 5 µM RK-33 increases the rate of migration in comparison to cells incubated with DMSO alone. Compound **1** has no significant effect on cell migration when used as a single agent. Interestingly, when used in combination, compound **1** appeared to decrease the effect of RK-33 on cell migration. This "rescue" effect of compound **1** was also observed in previous experiments (see Section 3.2.6).

In an attempt to explain this, Western blotting was carried out on PC-3 cells to examine the potential effects of RK-33 alone and in combination on the levels of proteins involved in signalling and migration (Figure 5-15). PC-3 cells were incubated with DMSO (lane 1), RK-33 at various concentrations (lanes 2-4) and compound **1** as a single agent (lane 5), or in combination with RK-33 (lane 6) for 6 hours. Analysis of cell extracts shows that there were no gross changes in the expression levels of 4E-BP1, eIF4G, eIF4A, or DDX3X. Similarly, levels of caprin and actin, proteins involved in cell migration, were also unchanged. In contrast, taking into account protein loading, the level of total eIF4E was reduced in PC-3 cells treated with a combination of RK-33 and compound **1** compared to DMSO alone (lane 6 vs lane 1). As expected, compound **1** was found to reduce the level of eIF4E phosphorylation in PC-3 cells when used as a single agent or in combination with RK-33.

A.

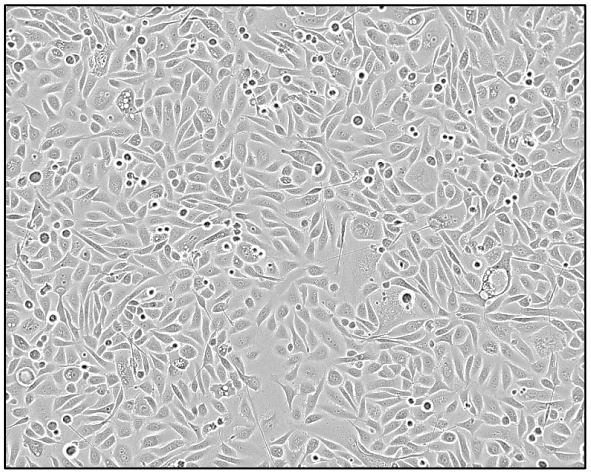

PC-3 cells
(Low DDX3X expression)

B.

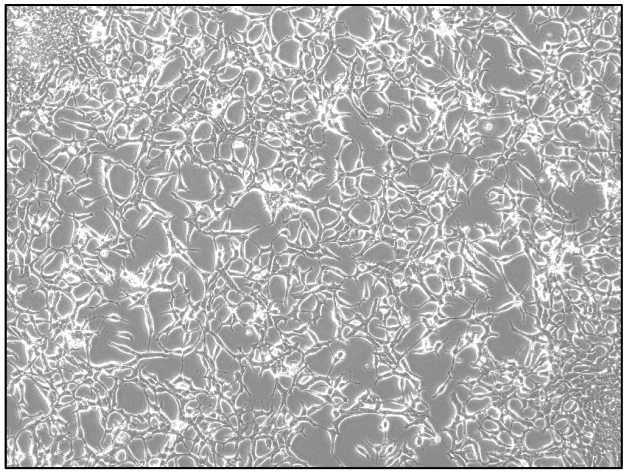

LNCaP cells
(High DDX3X expression)

Figure 5-13. Morphology of prostate cancer cells. A. Bright-field image of PC-3 cells. **B.** Bright-field image of LNCaP cells. (Both images taken from the American Type Culture Collection- ATCC).

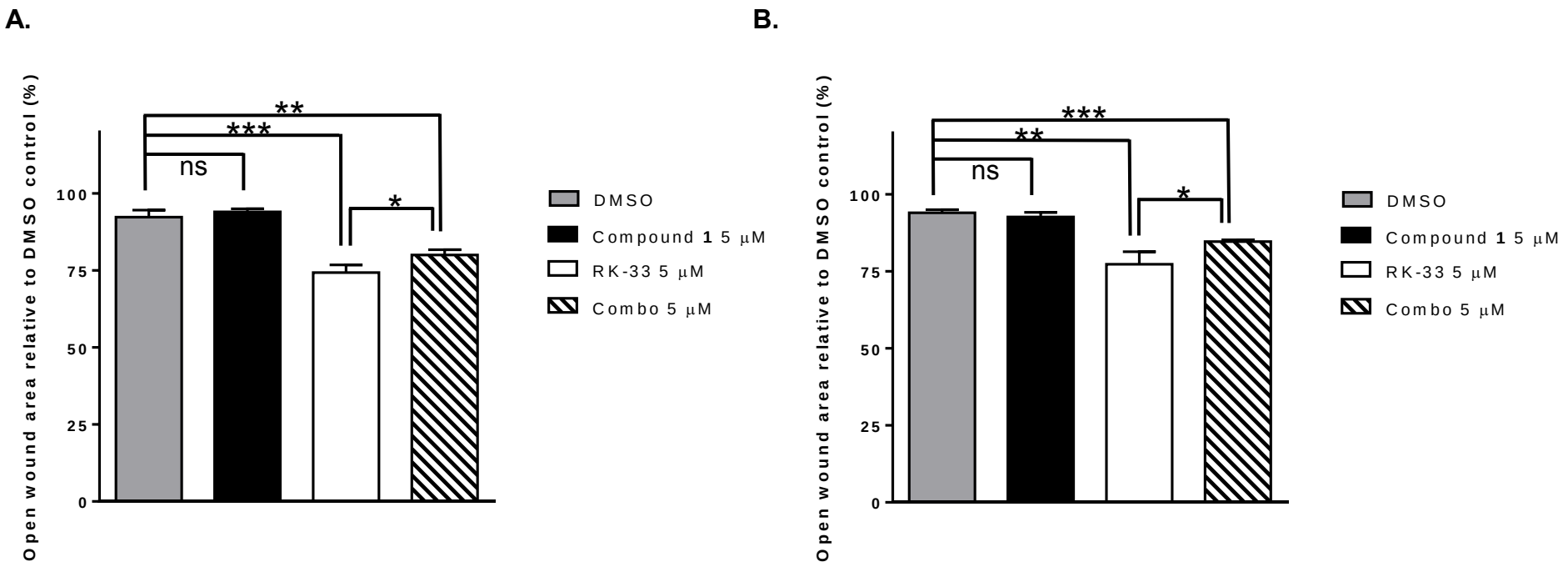

Figure 5-14. Wound-healing assay showing the effect of RK-33 inhibition alone or in combination with MNK1/2 inhibition over a period of 6 hours. **A.** Wound healing was measured PC-3 cells cultured in serum-free media exposed to DMSO, compound **1** at 5 μM and RK-33 at 5 μM alone and in combination with compound **1** at 5 μM each. **B.** Wound healing was measured in PC-3 cells cultured in complete media exposed to DMSO, compound **1** at 5 μM and RK-33 at 5 μM alone and in combination with compound **1** at 5 μM each. Cell migration was measured using Image J software and each well was normalised to the migration of cells at time 0. Data are mean ± S.D, n=3 (ns= non-significant, *p ≤ 0.05; **p ≤ 0.01; and ***p ≤ 0.001).

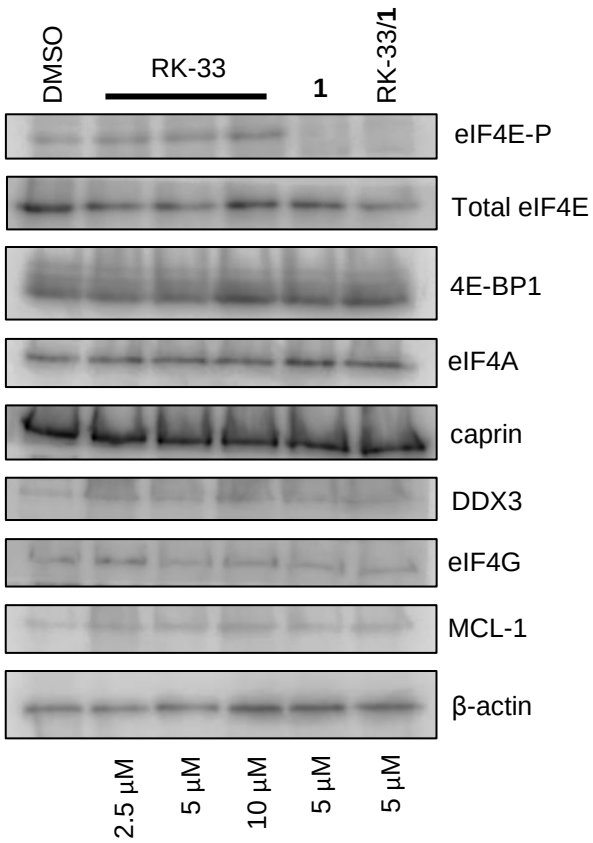

Figure 5-15. Representative Western blot analysis of PC-3 cells in the presence of RK-33 and compound 1, alone or in combination. Western blot analysis showing the effect of different concentrations of RK-33 on various signalling molecules. PC-3 cells were incubated with DMSO alone or with the indicated concentrations of inhibitors for 6 hours.

5.2 Discussion

DDX3X is a DEAD-box helicase that is dysregulated in many cancers. Consequently, there are increasing efforts to investigate the effect of DDX3X inhibition in different types of cancer. In the work described here, the CRISPR Cas9 system was utilised in an attempt to knockout the DDX3X gene in MRC5 cells, derived from a male patient. Attempts to knockout expression were made in-house using MRC5 fibroblasts and by a commercial venture to knockout DDX3X expression in HAP-1 cells Western blotting of a resulting in-house cell clone showed that the surviving cells had only a partial knockdown of DDX3X to approximately 40% of control levels (Figure 5-4), although mRNA levels were severely depleted (Figure 5-5). The failure to generate a full DDX3X knockout may be due to the impairment of NHEJ in these cells. In a study by Bol et al (2015) knockdown of DDX3X resulted in reduced NHEJ activity in lung cancer cells (Bol et al., 2015). The NHEJ pathway is the predominant pathway for the repair of DSB in the G1/S phase of the cell cycle and as DDX3X has been found to facilitate the G1/S transition (Section 1.1.1.2), a DDX3X knockout may arrest cells in G1. Subsequent DNA damage would result in the accumulation of DSB and ultimately lead to cell death. A recent study found that murine DDX3X was essential for both embryo and extraembryonic development. DDX3X ablation led to embryonic lethality (Chen et al., 2016). The resulting DDX3X knockdown clone was taken forward for further analysis and was found to have reduced migration ability (Figure 5-8), which further suggests a role for DDX3X in migration.

RK-33 is a small molecule inhibitor of DDX3X, which binds to and inhibits the ATP-binding site of DDX3X (Figure 5-9), resulting in the abrogation of helicase activity. In the work described here, the biological effects of RK-33 were tested in two prostate cancer cell lines and effects on cell viability was measured by Cell Titer Blue Assay. The data presented in Figure 7-13 shows that LNCaP cells (with high levels of DDX3X expression) showed are greater sensitivity towards RK-33 than PC-3 cells (with lower levels of DDX3X). The combination of RK-33 with MNK1/2 inhibitor, compound **1**, resulted in a small, but significant synergistic effect (Figure 5-11). This combination treatment led to an increase in

cell death and a reduction in IC_{50} value from 10 μM to ~6 μM in PC-3 cell. Although significant, the effect was not dramatic enough to point towards an effective combination treatment with clinical implications.

The effect of inhibition of DDX3X by RK-33 on cell migration was then assessed in PC-3 cells. Wound closure using either serum-starved or serum-fed cells was measured after a period of 6 hours. Interestingly, RK-33 appeared to accelerate the rate of wound closure when tested at 5 μM in both serum-starved and fed conditions (Figure 5-14). These data differ from work carried out by Xie et al (2016) who observed a reduced ability to close “scratches” after 36 hours of RK-33 treatment (Xie et al., 2016). This difference probably reflects inhibition of cell proliferation in cells incubated with RK-33 for longer times (Bol et al., 2015). The data presented here highlights the cancer-dependent effects of DDX3X knockdown or inhibition. This reflects the pleiotropic functions of DDX3X, its potential as an anti-cancer target and further underlines the need for more research in this area.

6 Thesis Summary

6.1 Final Discussion

The overexpression and de-regulation of translation factors, in particular, eIF4E, have been linked to the pathogenesis of many aggressive human cancers. The phosphorylation of eIF4E by MNK1/2 kinase correlates with invasive and metastatic behaviour, through the preferential translation of mRNAs encoding mesenchymal markers such as N-cadherin, fibronectin, MMPs and vimentin (Robichaud et al., 2015). The level of eIF4E expression has also been found to reflect the level of mitogenic proteins such as c-myc, VEGFR and cyclins, alongside anti-apoptotic proteins, such as MCL-1 and BCL-2 (Grzmil et al., 2014; Lu et al., 2016). Experimental evidence has shown that the availability of eIF4E for translation can be repressed through the inhibition of mTORC1 (Figure 3-1; reviewed in Laplante & Sabatini, 2012). Additionally, work has shown that silencing MNK1/2 attenuates eIF4E phosphorylation and reduces the translation of mRNAs involved in metastasis (Astanehe et al., 2012; Diab et al., 2014). However, the independent suppression of either pathway induces complex feedback loops that stimulate activation of alternative signalling pathways (Figures 1-19 and 3-4). As eIF4E lies at the convergence point of both the mTOR and MNK/eIF4E pathways (Figure 1-9), this provides an opportunity for dual targeting of these pathways. Multi-targeted therapy is becoming an increasingly popular approach to combat drug resistance. Hybrid molecules incorporate several moieties that bind to, and inhibit different biological targets, delivering a double-blow to cells. In this regard, the complementary mTOR and MNK pathways are a promising target for such hybrid agents in the treatment of aggressive migratory cancers.

In the work described here, a thorough literature search was first performed to identify a potent MNK1/2 inhibitor with desirable properties that would enable further modifications. In **Chapter three**, compound **1**, a known MNK1/2 inhibitor (not available commercially) was synthesised and characterised in a range of mammalian cell lines. Compound **1** was shown to have no effect on cell viability

in the variety of cell lines tested. This was anticipated as seminal work by Ueda et al (2004) found that mice with a targeted deletion of both MNK1 and MNK2 exhibited a total lack of eIF4E phosphorylation but were completely viable. This led to the development of novel MNK1/2 inhibitor hybrid agents based upon compound **1**. It was determined that a synergistic combination of MNK1/2 and PI3K p110α inhibitors slowed the rate of cell migration in MDA-MB-231 cells (Figure 3-19A and 3-19B). Additionally, this work showed that a combination of MNK1/2 and mTORC1/2 inhibitors resulted in cell cycle arrest (Figure 3-20) and a decrease in cell viability (Figure 3-19F) to a greater extent in comparison to when the inhibitors were used as single agents. These inhibitors are ATP-competitive and work by binding to and inhibiting the ATP-binding site. These findings led to the attempted development of novel hybrid entities, encapsulating MNK1/2 and PI3K/mTOR inhibitory activities. Although molecular hybridisation approaches hold significant promise, they currently face considerable challenges as therapeutic modalities. For example, both hybrid agents are undoubtedly poorly soluble due to their high molecular weight and lipophilicity. Both compounds **6** and **7**, violate two of Lipinski's rules, by exceeding a molecular weight of 500 and a log P value of 5. Both hybrid compounds also violate one of Veber's rules, by surpassing a TPSA of 140 $Å^2$ (Veber et al., 2002). Highly lipophilic compounds permeate poorly through membranes as they aggregate in the hydrophobic interior of the membrane bilayer (Leeson & Springthorpe, 2007). Current work in the Spencer Lab aims to improve the solubility of these novel hybrid molecules by introducing hydrophilic polyethylene glycol (PEG) linkers to conjugate the two chemical entities.

The work described in **Chapter four** describes the characterisation of novel ferrocene containing compounds based upon the MNK1/2 inhibitor, compound **1**. Structural modelling of compound **1** in the active site of MNK kinase revealed a large hydrophobic pocket that could be exploited with a bulkier group such as a ferrocene. Although the ferrocene derivatives showed no activity against MNK1/2, their potency in cancer cell lines was promising. Cell viability was determined using the Cell Titer Blue assay and the ferrocene-containing compounds exhibited low micromolar IC_{50} values in several cancer cell lines (Table 4-1). MDA-MB-231 cells were particularly sensitive to these ferrocene

compounds and were used to assess these compounds when cells were grown in 3D culture (spheroids). It is generally believed that tumour spheroids provide a more biologically relevant environment to screen potential compounds (Lv, Hu et al., 2017). The work described here indicated that the more potent of the two ferrocene derivatives was found to significantly reduce spheroid diameter in conjunction with a decrease in cell viability. It is possible that the ferrocene itself was responsible for these effects and the production of ROS in the Fenton reaction has been proposed as a mechanism of cytotoxicity in other ferrocene derivatives (Tabbiet et al., 2002). Future work would aim to determine if the reduction in cell viability is due to the generation of ROS. This would be investigated by the use of a commercial assay, which utilises fluorogenic probes to measure generalised oxidative stress in cells in a 96-well plate format.

Finally, the work described in **Chapter five** was focussed on an alternative translational target, an RNA helicase, termed DDX3X. Firstly, it was shown that genetic knockdown of DDX3X in MRC5 cells led to a reduction in cell migration. These data concurred with previous work by Chen et al (2015) who found that DDX3X depletion suppressed cell motility in HeLa cells in a scratch assay. In my work described here, prostate cancer cells (PC-3) with an intrinsically low level of DDX3X were treated with RK-33, an inhibitor of the ATP-dependent helicase function of DDX3X. Surprisingly, these data revealed that RK-33 actually increased migration in these cells over a period of 6 hours, when assayed using the wound healing “bung” assay. These conflicting data highlight the limitations of performing cell migration assays over varying time periods. The traditional scratch/wound healing assays require controls to account for cell proliferation and visual analysis of data is often subjective. The trans-well cell migration assay using the xCELLigence DP device tracks cells in real-time as they migrate towards a chemo-attractant. The latter assay is very sensitive and produces quantitative data; however, it measures individual cell migration as opposed to cells migrating on mass to close a wound. Recent advances in technology have revolutionised the wound healing assay. An automated wound healing assay has been developed by Acea Biosciences®, which generates a uniform “scratch” in each well of a 96-well plate. Wound healing can then be measured in real-time, providing a reproducible quantitative measure of cell

migration. It would be pertinent to repeat these assays with the DDX3X knockdown cells and RK-33 treated cells using such a system.

In addition to effects on cell migration, knockdown of DDX3X has been reported to result in reduced a reduced level of NHEJ activity (Bol et al., 2015a). This prompted us to investigate DDX3X inhibitor, RK-33, in combination with olaparib, a PARP inhibitor. Olaparib is approved for the treatment of germline BRCA mutated (gBRCAm) HER2-negative metastatic breast cancer and is currently in phase I clinical trials for the treatment of glioblastoma in combination with radiotherapy +/-temozolomide (Fulton et al., 2018). The combination of both RK-33 and olaparib may induce synthetic lethality by targeting both NHEJ and homologous recombination (HR) pathways. There is also potential for DDX3X inhibitors to be used as a second-line therapy to combat olaparib resistance in treatment of breast cancer.

6.2 Future Perspectives

In summary, targeting the translational machinery remains an exciting option for the treatment of cancers. In the last few years there has been an explosion in the development of MNK1/2 inhibitors, both in academia and in industry (Reich et al., 2018, Yang et al., 2018). This further provides evidence for the role MNK1/2 plays in chemoresistance and the potential of using MNK1/2 inhibitors in combination with other chemotherapeutic agents in the treatment of aggressive cancers. A CRISPR-Cas9 screen run in parallel with a siRNA screen of MNK in combination with other proteins would be useful to identify synergy between targets, and aid the development of novel hybrids.

As discussed in the section above, further work analysing the compounds synthesised in this study would clarify their mode of action in cells. In particular, apoptosis assays and eIF2α assays may provide more information on the data obtained from migration and cell viability experiments. Mass spectrometry could also be performed to analyse the cellular uptake of compounds and indicate hybrid molecule solubility.

Recent work has further elucidated the role of DDX3X in medulloblastoma. To date, all DDX3X mutations reported in medulloblastoma occur in the helicase domain. A study aimed to identify the RNA targets and binding ability of wildtype DDX3X compared to the medulloblastoma-related DDX3R534H variant, with impaired catalytic activity, in HEK293 cells. Data showed that the mutant form bound less avidly to RNA than the wildtype form, although the transcriptome targets were similar. Although a reduction in translation initiation efficiency was observed, mutant DDX3X maintained extensive protein-protein interactions (Oh et al., 2016). A seperate study found that cancer-related DDX3X mutations promoted the assembly of stress granules and impaired mRNA translation. Missense mutations in DDX3X were found to impair global protein synthesis by several mechanisms (Valentin-Vega et al., 2016). These data suggest that drugs that limit the formation of stress granules may reverse the translation impairment caused by cancer-related DDX3X mutations and offer a potential treatment option for tumours containing mutant DDX3X.

6.3 Published Work

1. Copsey AC, Cooper S, Parker R, Lineham E, Lapworth C, Jallad D, et al. The helicase, DDX3X, interacts with poly(A)-binding protein 1 (PABP1) and caprin-1 at the leading edge of migrating fibroblasts and is required for efficient cell spreading. Biochem J. 2017;474(18):3109-20.

2. Lineham E, Spencer J, Morley SJ. Dual abrogation of MNK and mTOR: a novel therapeutic approach for the treatment of aggressive cancers. Future Med Chem. 2017;9(13):1539-55.

3. Lineham E, Tizzard GJ, Coles SJ, Spencer J, Morley SJ. Synergistic effects of inhibiting the MNK-eIF4E and PI3K/AKT/mTOR pathways on cell migration in MDA-MB-231 cells. Oncotarget. 2018;9:14148-59.

4. Sansook S, Lineham E, Hassell-Hart S, Tizzard G, Coles S, Spencer J et al. Probing the Anticancer Action of Novel Ferrocene Analogues of MNK Inhibitors. Molecules. 2018;23(9):2126.

References

Abekhoukh S, Bardoni B (2014) CYFIP family proteins between autism and intellectual disability: links with Fragile X syndrome. Front Cell Neurosci 8: 81

Alain T, Morita M, Fonseca BD, Yanagiya A, Siddiqui N, Bhat M, Zammit D, Marcus V, Metrakos P, Voyer LA, Gandin V, Liu Y, Topisirovic I, Sonenberg N (2012) eIF4E/4E-BP ratio predicts the efficacy of mTOR targeted therapies. Cancer Res 72: 6468-76

Allemand E, Guil S, Myers M, Moscat J, Caceres JF, Krainer AR (2005) Regulation of heterogenous nuclear ribonucleoprotein A1 transport by phosphorylation in cells stressed by osmotic shock. Proceedings of the National Academy of Sciences of the United States of America 102: 3605-10

Altman JK, Szilard A, Konicek BW, Iversen PW, Kroczynska B, Glaser H, Sassano A, Vakana E, Graff JR, Platanias LC (2013) Inhibition of Mnk kinase activity by cercosporamide and suppressive effects on acute myeloid leukemia precursors. Blood 121: 3675-81

Amin J, Chuckowree IS, Wang M, Tizzard G, J., Coles SJ, Spencer J (2013) Synthesis of Oxindole-Based Bioorganometallic Kinase Inhibitors Incorporating One or More Ferrocene Groups. Organometallics 32: 5818-5825

Apsel B, Blair JA, Gonzalez B, Nazif TM, Feldman ME, Aizenstein B, Hoffman R, Williams RL, Shokat KM, Knight ZA (2008) Targeted polypharmacology: discovery of dual inhibitors of tyrosine and phosphoinositide kinases. Nat Chem Biol 4: 691-9

Asimomytis A, Karanikou M, Rodolakis A, Vaiopoulou A, Tsetsa P, Creatsas G, Stefos T, Antsaklis A, Patsouris E, Rassidakis GZ (2016) mTOR downstream effectors, 4EBP1 and eIF4E, are overexpressed and associated with HPV status in precancerous lesions and carcinomas of the uterine cervix. Oncol Lett 12: 3234-3240

Astanehe A, Finkbeiner MR, Krzywinski M, Fotovati A, Dhillon J, Berquin IM, Mills GB, Marra MA, Dunn SE (2012) MKNK1 is a YB-1 target gene responsible for imparting trastuzumab resistance and can be blocked by RSK inhibition. Oncogene 31: 4434-46

Avdulov S, Li S, Michalek V, Burrichter D, Peterson M, Perlman DM, Manivel JC, Sonenberg N, Yee D, Bitterman PB, Polunovsky VA (2004) Activation of translation complex eIF4F is essential for the genesis and maintenance of the malignant phenotype in human mammary epithelial cells. Cancer Cell 5: 553-63

Aylett CH, Sauer E, Imseng S, Boehringer D, Hall MN, Ban N, Maier T (2016) Architecture of human mTOR complex 1. Science 351: 48-52

Bagrodia S, Derijard B, Davis RJ, Cerione RA (1995) Cdc42 and PAK-mediated signaling leads to Jun kinase and p38 mitogen-activated protein kinase activation. The Journal of biological chemistry 270: 27995-8

Basnet SK, Diab S, Schmid R, Yu M, Yang Y, Gillam TA, Teo T, Li P, Peat T, Albrecht H, Wang S (2015) Identification of a Highly Conserved Allosteric Binding Site on Mnk1 and Mnk2. Mol Pharmacol 88: 935-48

Bayat Mokhtari R, Homayouni TS, Baluch N, Morgatskaya E, Kumar S, Das B, Yeger H (2017) Combination therapy in combating cancer. Oncotarget 8: 38022-38043

Beggs JE, Tian S, Jones GG, Xie J, Iadevaia V, Jenei V, Thomas G, Proud CG (2015) The MAP kinase-interacting kinases regulate cell migration, vimentin expression and eIF4E/CYFIP1 binding. Biochem J 467: 63-76

Beltran H, Prandi D, Mosquera JM, Benelli M, Puca L, Cyrta J, Marotz C, Giannopoulou E, Chakravarthi BV, Varambally S, Tomlins SA, Nanus DM, Tagawa ST, Van Allen EM, Elemento O, Sboner A, Garraway LA, Rubin MA, Demichelis F (2016) Divergent clonal evolution of castration-resistant neuroendocrine prostate cancer. Nat Med 22: 298-305

Berti DA, Seger R (2017) The Nuclear Translocation of ERK. Methods Mol Biol 1487: 175-194

Berube G (2016) An overview of molecular hybrids in drug discovery. Expert Opin Drug Discov 11: 281-305

Beugnet A, Wang X, Proud CG (2003) Target of rapamycin (TOR)-signaling and RAIP motifs play distinct roles in the mammalian TOR-dependent phosphorylation of initiation factor 4E-binding protein 1. The Journal of biological chemistry 278: 40717-22

Bhat M, Robichaud N, Hulea L, Sonenberg N, Pelletier J, Topisirovic I (2015) Targeting the translation machinery in cancer. Nat Rev Drug Discov 14: 261-278

Bhullar KS, Lagaron NO, McGowan EM, Parmar I, Jha A, Hubbard BP, Rupasinghe HPV (2018) Kinase-targeted cancer therapies: progress, challenges and future directions. Mol Cancer 17: 48

Bianchini A, Loiarro M, Bielli P, Busa R, Paronetto MP, Loreni F, Geremia R, Sette C (2008) Phosphorylation of eIF4E by MNKs supports protein synthesis, cell cycle progression and proliferation in prostate cancer cells. Carcinogenesis 29: 2279-88

Blagosklonny MV (2004) Analysis of FDA approved anticancer drugs reveals the future of cancer therapy. Cell Cycle 3: 1035-42

Bol GM, Vesuna F, Xie M, Zeng J, Aziz K, Gandhi N, Levine A, Irving A, Korz D, Tantravedi S, Heerma van Voss MR, Gabrielson K, Bordt EA, Polster BM, Cope L, van der Groep P, Kondaskar A, Rudek MA, Hosmane RS, van der Wall E et al. (2015) Targeting DDX3 with a small molecule inhibitor for lung cancer therapy. EMBO Mol Med 7: 648-69

Bolton JL (2014) Quinone Methide Bioactivation Pathway: Contribution to Toxicity and/or Cytoprotection? Curr Org Chem 18: 61-69

Botlagunta M, Vesuna F, Mironchik Y, Raman A, Lisok A, Winnard P, Jr., Mukadam S, Van Diest P, Chen JH, Farabaugh P, Patel AH, Raman V (2008) Oncogenic role of DDX3 in breast cancer biogenesis. Oncogene 27: 3912-22

Brai A, Fazi R, Tintori C, Zamperini C, Bugli F, Sanguinetti M, Stigliano E, Este J, Badia R, Franco S, Martinez MA, Martinez JP, Meyerhans A, Saladini F, Zazzi M, Garbelli A, Maga G, Botta M (2016) Human DDX3 protein is a valuable

target to develop broad spectrum antiviral agents. Proceedings of the National Academy of Sciences of the United States of America 113: 5388-93

Bramham CR, Jensen KB, Proud CG (2016) Tuning Specific Translation in Cancer Metastasis and Synaptic Memory: Control at the MNK-eIF4E Axis. Trends Biochem Sci 41: 847-58

Brown MC, Gromeier M (2017) MNK inversely regulates TELO2 vs. DEPTOR to control mTORC1 signaling. Mol Cell Oncol 4: e1306010

Bushell M, Wood W, Carpenter G, Pain VM, Morley SJ, Clemens MJ (2001) Disruption of the interaction of mammalian protein synthesis eukaryotic initiation factor 4B with the poly(A)-binding protein by caspase- and viral protease-mediated cleavages. The Journal of biological chemistry 276: 23922-8

Buxade M, Morrice N, Krebs DL, Proud CG (2008) The PSF.p54nrb complex is a novel Mnk substrate that binds the mRNA for tumor necrosis factor alpha. The Journal of biological chemistry 283: 57-65

Buxade M, Parra JL, Rousseau S, Shpiro N, Marquez R, Morrice N, Bain J, Espel E, Proud CG (2005) The Mnks are novel components in the control of TNF alpha biosynthesis and phosphorylate and regulate hnRNP A1. Immunity 23: 177-89

Buxade M, Parra-Palau JL, Proud CG (2008) The Mnks: MAP kinase-interacting kinases (MAP kinase signal-integrating kinases). Front Biosci 13: 5359-73

Cai X, Zhai HX, Wang J, Forrester J, Qu H, Yin L, Lai CJ, Bao R, Qian C (2010) Discovery of 7-(4-(3-ethynylphenylamino)-7-methoxyquinazolin-6-yloxy)-N-hydroxyheptanamide (CUDc-101) as a potent multi-acting HDAC, EGFR, and HER2 inhibitor for the treatment of cancer. J Med Chem 53: 2000-9

Cargnello M, Roux PP (2011) Activation and function of the MAPKs and their substrates, the MAPK-activated protein kinases. Microbiology and molecular biology reviews : MMBR 75: 50-83

Carriere A, Cargnello M, Julien LA, Gao H, Bonneil E, Thibault P, Roux PP (2008) Oncogenic MAPK signaling stimulates mTORC1 activity by promoting RSK-mediated raptor phosphorylation. Curr Biol 18: 1269-77

Cate JH (2017) Human eIF3: from 'blobology' to biological insight. Philos Trans R Soc Lond B Biol Sci 372

Chan CC, Dostie J, Diem MD, Feng W, Mann M, Rappsilber J, Dreyfuss G (2004) eIF4A3 is a novel component of the exon junction complex. RNA 10: 200-9

Chang PC, Chi CW, Chau GY, Li FY, Tsai YH, Wu JC, Wu Lee YH (2006) DDX3, a DEAD box RNA helicase, is deregulated in hepatitis virus-associated hepatocellular carcinoma and is involved in cell growth control. Oncogene 25: 1991-2003

Chen CY, Chan CH, Chen CM, Tsai YS, Tsai TY, Wu Lee YH, You LR (2016) Targeted inactivation of murine Ddx3x: essential roles of Ddx3x in placentation and embryogenesis. Hum Mol Genet 25: 2905-2922

Chen HH, Yu HI, Cho WC, Tarn WY (2015) DDX3 modulates cell adhesion and motility and cancer cell metastasis via Rac1-mediated signaling pathway. Oncogene 34: 2790-800

Chen LS, Redkar S, Taverna P, Cortes JE, Gandhi V (2011) Mechanisms of cytotoxicity to Pim kinase inhibitor, SGI-1776, in acute myeloid leukemia. Blood 118: 693-702

Chiarini F, Evangelisti C, McCubrey JA, Martelli AM (2015) Current treatment strategies for inhibiting mTOR in cancer. Trends Pharmacol Sci 36: 124-35

Cho S, Kim JH, Back SH, Jang SK (2005) Polypyrimidine tract-binding protein enhances the internal ribosomal entry site-dependent translation of p27Kip1 mRNA and modulates transition from G1 to S phase. Molecular and cellular biology 25: 1283-97

Chrestensen CA, Shuman JK, Eschenroeder A, Worthington M, Gram H, Sturgill TW (2007) MNK1 and MNK2 regulation in HER2-overexpressing breast cancer lines. The Journal of biological chemistry 282: 4243-52

Clancy S, Brown W (2008) Translation: DNA to mRNA to Protein. 1: 101

Cobbold LC, Spriggs KA, Haines SJ, Dobbyn HC, Hayes C, de Moor CH, Lilley KS, Bushell M, Willis AE (2008) Identification of internal ribosome entry segment (IRES)-trans-acting factors for the Myc family of IRESs. Molecular and cellular biology 28: 40-9

Cobbold LC, Wilson LA, Sawicka K, King HA, Kondrashov AV, Spriggs KA, Bushell M, Willis AE (2010) Upregulated c-myc expression in multiple myeloma by internal ribosome entry results from increased interactions with and expression of PTB-1 and YB-1. Oncogene 29: 2884-91

Coles SJG, P. A (2012) Changing and challenging times for service crystallography. *Chem Sci* 3: 683-689

Cope CL, Gilley R, Balmanno K, Sale MJ, Howarth KD, Hampson M, Smith PD, Guichard SM, Cook SJ (2014) Adaptation to mTOR kinase inhibitors by amplification of eIF4E to maintain cap-dependent translation. J Cell Sci 127: 788-800

Cowan-Jacob SW (2006) Structural biology of protein tyrosine kinases. Cell Mol Life Sci 63: 2608-25

Cox AD, Fesik SW, Kimmelman AC, Luo J, Der CJ (2014) Drugging the undruggable RAS: Mission possible? Nat Rev Drug Discov 13: 828-51

Cuadrado A, Nebreda AR (2010) Mechanisms and functions of p38 MAPK signalling. Biochem J 429: 403-17

Culjkovic B, Topisirovic I, Skrabanek L, Ruiz-Gutierrez M, Borden KL (2006) eIF4E is a central node of an RNA regulon that governs cellular proliferation. J Cell Biol 175: 415-26

Dai X, Chen A, Bai Z (2014) Integrative investigation on breast cancer in ER, PR and HER2-defined subgroups using mRNA and miRNA expression profiling. Sci Rep 4: 6566

Daina A, Michielin O, Zoete V (2017) SwissADME: a free web tool to evaluate pharmacokinetics, drug-likeness and medicinal chemistry friendliness of small molecules. Sci Rep 7: 42717

Das S, Maitra U (2001) Functional significance and mechanism of eIF5-promoted GTP hydrolysis in eukaryotic translation initiation. Progress in nucleic acid research and molecular biology 70: 207-31

DaSilva J, Xu L, Kim HJ, Miller WT, Bar-Sagi D (2006) Regulation of sprouty stability by Mnk1-dependent phosphorylation. Molecular and cellular biology 26: 1898-907

Davis MI, Hunt JP, Herrgard S, Ciceri P, Wodicka LM, Pallares G, Hocker M, Treiber DK, Zarrinkar PP (2011) Comprehensive analysis of kinase inhibitor selectivity. Nature biotechnology 29: 1046-51

de Lera AR, Ganesan A (2016) Epigenetic polypharmacology: from combination therapy to multitargeted drugs. Clin Epigenetics 8: 105

de Oliveira AC, Hillard EA, Pigeon P, Rocha DD, Rodrigues FA, Montenegro RC, Costa-Lotufo LV, Goulart MO, Jaouen G (2011) Biological evaluation of twenty-eight ferrocenyl tetrasubstituted olefins: cancer cell growth inhibition, ROS production and hemolytic activity. Eur J Med Chem 46: 3778-87

Di Tommaso P, Moretti S, Xenarios I, Orobitg M, Montanyola A, Chang JM, Taly JF, Notredame C (2011) T-Coffee: a web server for the multiple sequence alignment of protein and RNA sequences using structural information and homology extension. Nucleic acids research 39: W13-7

Diab S, Kumarasiri M, Yu M, Teo T, Proud C, Milne R, Wang S (2014) MAP kinase-interacting kinases--emerging targets against cancer. Chem Biol 21: 441-52

Diab S, Li P, Basnet SK, Lu J, Yu M, Albrecht H, Milne RW, Wang S (2016) Unveiling new chemical scaffolds as Mnk inhibitors. Future Med Chem 8: 271-85

Diab S, Teo T, Kumarasiri M, Li P, Yu M, Lam F, Basnet SK, Sykes MJ, Albrecht H, Milne R, Wang S (2014) Discovery of 5-(2-(phenylamino)pyrimidin-4-yl)thiazol-2(3H)-one derivatives as potent Mnk2 inhibitors: synthesis, SAR analysis and biological evaluation. ChemMedChem 9: 962-72

Ditton HJ, Zimmer J, Kamp C, Rajpert-De Meyts E, Vogt PH (2004) The AZFa gene DBY (DDX3Y) is widely transcribed but the protein is limited to the male germ cells by translation control. Hum Mol Genet 13: 2333-41

Eddy J, Maizels N (2006) Gene function correlates with potential for G4 DNA formation in the human genome. Nucleic acids research 34: 3887-96

Edwin F, Anderson K, Patel TB (2010) HECT domain-containing E3 ubiquitin ligase Nedd4 interacts with and ubiquitinates Sprouty2. The Journal of biological chemistry 285: 255-64

Efeyan A, Sabatini DM (2010) mTOR and cancer: many loops in one pathway. Current opinion in cell biology 22: 169-76

Eulalio A, Huntzinger E, Izaurralde E (2008) Getting to the root of miRNA-mediated gene silencing. Cell 132: 9-14

Fabbro D, Cowan-Jacob SW, Moebitz H (2015) Ten things you should know about protein kinases: IUPHAR Review 14. Br J Pharmacol 172: 2675-700

Fabian JR, Vojtek AB, Cooper JA, Morrison DK (1994) A single amino acid change in Raf-1 inhibits Ras binding and alters Raf-1 function. Proceedings of the National Academy of Sciences of the United States of America 91: 5982-6

Fairman-Williams ME, Guenther UP, Jankowsky E (2010) SF1 and SF2 helicases: family matters. Curr Opin Struct Biol 20: 313-24

Faller WJ, Jackson TJ, Knight JR, Ridgway RA, Jamieson T, Karim SA, Jones C, Radulescu S, Huels DJ, Myant KB, Dudek KM, Casey HA, Scopelliti A, Cordero JB, Vidal M, Pende M, Ryazanov AG, Sonenberg N, Meyuhas O, Hall MN et al. (2015) mTORC1-mediated translational elongation limits intestinal tumour initiation and growth. Nature 517: 497-500

Fan W, Wang W, Mao X, Chu S, Feng J, Xiao D, Zhou J, Fan S (2016) Elevated levels of p-Mnk1, p-eIF4E and p-p70S6K proteins are associated with tumor recurrence and poor prognosis in astrocytomas. J Neurooncol

Feng Z, Hu W, de Stanchina E, Teresky AK, Jin S, Lowe S, Levine AJ (2007) The regulation of AMPK beta1, TSC2, and PTEN expression by p53: stress, cell and tissue specificity, and the role of these gene products in modulating the IGF-1-AKT-mTOR pathways. Cancer Res 67: 3043-53

Feoktistova K, Tuvshintogs E, Do A, Fraser CS (2013) Human eIF4E promotes mRNA restructuring by stimulating eIF4A helicase activity. Proceedings of the National Academy of Sciences of the United States of America 110: 13339-44

Finn RS, Dering J, Conklin D, Kalous O, Cohen DJ, Desai AJ, Ginther C, Atefi M, Chen I, Fowst C, Los G, Slamon DJ (2009) PD 0332991, a selective cyclin D kinase 4/6 inhibitor, preferentially inhibits proliferation of luminal estrogen receptor-positive human breast cancer cell lines in vitro. Breast Cancer Res 11: R77

Folkes AJ, Ahmadi K, Alderton WK, Alix S, Baker SJ, Box G, Chuckowree IS, Clarke PA, Depledge P, Eccles SA, Friedman LS, Hayes A, Hancox TC, Kugendradas A, Lensun L, Moore P, Olivero AG, Pang J, Patel S, Pergl-Wilson GH et al. (2008) The identification of 2-(1H-indazol-4-yl)-6-(4-methanesulfonyl-piperazin-1-ylmethyl)-4-morpholin-4-yl-t hieno[3,2-d]pyrimidine (GDC-0941) as a potent, selective, orally bioavailable inhibitor of class I PI3 kinase for the treatment of cancer. J Med Chem 51: 5522-32

Fortin S, Berube G (2013) Advances in the development of hybrid anticancer drugs. Expert Opin Drug Discov 8: 1029-47

Friday BB, Adjei AA (2008) Advances in targeting the Ras/Raf/MEK/Erk mitogen-activated protein kinase cascade with MEK inhibitors for cancer therapy. Clin Cancer Res 14: 342-6

Fry DW, Harvey PJ, Keller PR, Elliott WL, Meade M, Trachet E, Albassam M, Zheng X, Leopold WR, Pryer NK, Toogood PL (2004) Specific inhibition of cyclin-dependent kinase 4/6 by PD 0332991 and associated antitumor activity in human tumor xenografts. Mol Cancer Ther 3: 1427-38

Fulton B, Short SC, James A, Nowicki S, McBain C, Jefferies S, Kelly C, Stobo J, Morris A, Williamson A, Chalmers AJ (2018) PARADIGM-2: Two parallel

phase I studies of olaparib and radiotherapy or olaparib and radiotherapy plus temozolomide in patients with newly diagnosed glioblastoma, with treatment stratified by MGMT status. Clin Transl Radiat Oncol 8: 12-16

Furic L, Rong L, Larsson O, Koumakpayi IH, Yoshida K, Brueschke A, Petroulakis E, Robichaud N, Pollak M, Gaboury LA, Pandolfi PP, Saad F, Sonenberg N (2010) eIF4E phosphorylation promotes tumorigenesis and is associated with prostate cancer progression. Proceedings of the National Academy of Sciences of the United States of America 107: 14134-9

Gandin V, Masvidal L, Cargnello M, Gyenis L, McLaughlan S, Cai Y, Tenkerian C, Morita M, Balanathan P, Jean-Jean O, Stambolic V, Trost M, Furic L, Larose L, Koromilas AE, Asano K, Litchfield D, Larsson O, Topisirovic I (2016a) mTORC1 and CK2 coordinate ternary and eIF4F complex assembly. Nat Commun 7: 11127

Gandin V, Masvidal L, Hulea L, Gravel SP, Cargnello M, McLaughlan S, Cai Y, Balanathan P, Morita M, Rajakumar A, Furic L, Pollak M, Porco JA, Jr., St-Pierre J, Pelletier J, Larsson O, Topisirovic I (2016b) nanoCAGE reveals 5' UTR features that define specific modes of translation of functionally related MTOR-sensitive mRNAs. Genome Res 26: 636-48

Gao M, Zhang X, Li D, He P, Tian W, Zeng B (2016) Expression analysis and clinical significance of eIF4E, VEGF-C, E-cadherin and MMP-2 in colorectal adenocarcinoma. Oncotarget

Garbelli A, Beermann S, Di Cicco G, Dietrich U, Maga G (2011) A motif unique to the human DEAD-box protein DDX3 is important for nucleic acid binding, ATP hydrolysis, RNA/DNA unwinding and HIV-1 replication. PLoS One 6: e19810

Garbelli A, Radi M, Falchi F, Beermann S, Zanoli S, Manetti F, Dietrich U, Botta M, Maga G (2011) Targeting the human DEAD-box polypeptide 3 (DDX3) RNA helicase as a novel strategy to inhibit viral replication. Curr Med Chem 18: 3015-27

Garcia-Aranda M, Redondo M (2017) Protein Kinase Targets in Breast Cancer. International journal of molecular sciences 18

Garcia-Jimenez C, Goding CR (2019) Starvation and Pseudo-Starvation as Drivers of Cancer Metastasis through Translation Reprogramming. Cell Metab 29: 254-267

Garcia-Recio EM, Pinto-Diez C, Perez-Morgado MI, Garcia-Hernandez M, Fernandez G, Martin ME, Gonzalez VM (2016) Characterization of MNK1b DNA Aptamers That Inhibit Proliferation in MDA-MB231 Breast Cancer Cells. Mol Ther Nucleic Acids 5: e275

Garuti L, Roberti M, Bottegoni G (2010) Non-ATP competitive protein kinase inhibitors. Curr Med Chem 17: 2804-21

Gavrin LK, Saiah E (2013) Approaches to discover non-ATP site kinase inhibitors. MedChemComm

Gediya LK, Khandelwal A, Patel J, Belosay A, Sabnis G, Mehta J, Purushottamachar P, Njar VC (2008) Design, synthesis, and evaluation of novel mutual prodrugs (hybrid drugs) of all-trans-retinoic acid and histone deacetylase

inhibitors with enhanced anticancer activities in breast and prostate cancer cells in vitro. J Med Chem 51: 3895-904

Genheden M, Kenney JW, Johnston HE, Manousopoulou A, Garbis SD, Proud CG (2015) BDNF stimulation of protein synthesis in cortical neurons requires the MAP kinase-interacting kinase MNK1. J Neurosci 35: 972-84

Gingras AC, Raught B, Gygi SP, Niedzwiecka A, Miron M, Burley SK, Polakiewicz RD, Wyslouch-Cieszynska A, Aebersold R, Sonenberg N (2001) Hierarchical phosphorylation of the translation inhibitor 4E-BP1. Genes & development 15: 2852-64

Glauser DA, Schlegel W (2007) Sequential actions of ERK1/2 on the AP-1 transcription factor allow temporal integration of metabolic signals in pancreatic beta cells. FASEB J 21: 3240-9

Glick D, Barth S, Macleod KF (2010) Autophagy: cellular and molecular mechanisms. J Pathol 221: 3-12

Gormen M, Pigeon P, Top S, Hillard EA, Huche M, Hartinger CG, de Montigny F, Plamont MA, Vessieres A, Jaouen G (2010) Synthesis, cytotoxicity, and COMPARE analysis of ferrocene and [3]ferrocenophane tetrasubstituted olefin derivatives against human cancer cells. ChemMedChem 5: 2039-50

Gottardis MM, Jordan VC (1987) Antitumor actions of keoxifene and tamoxifen in the N-nitrosomethylurea-induced rat mammary carcinoma model. Cancer Res 47: 4020-4

Graff JR, Konicek BW, Carter JH, Marcusson EG (2008) Targeting the eukaryotic translation initiation factor 4E for cancer therapy. Cancer Res 68: 631-4

Graff JR, Konicek BW, Vincent TM, Lynch RL, Monteith D, Weir SN, Schwier P, Capen A, Goode RL, Dowless MS, Chen Y, Zhang H, Sissons S, Cox K, McNulty AM, Parsons SH, Wang T, Sams L, Geeganage S, Douglass LE et al. (2007) Therapeutic suppression of translation initiation factor eIF4E expression reduces tumor growth without toxicity. J Clin Invest 117: 2638-48

Grifo JA, Abramson RD, Satler CA, Merrick WC (1984) RNA-stimulated ATPase activity of eukaryotic initiation factors. The Journal of biological chemistry 259: 8648-54

Gruner S, Peter D, Weber R, Wohlbold L, Chung MY, Weichenrieder O, Valkov E, Igreja C, Izaurralde E (2016) The Structures of eIF4E-eIF4G Complexes Reveal an Extended Interface to Regulate Translation Initiation. Mol Cell 64: 467-479

Grzmil M, Huber RM, Hess D, Frank S, Hynx D, Moncayo G, Klein D, Merlo A, Hemmings BA (2014) MNK1 pathway activity maintains protein synthesis in rapalog-treated gliomas. J Clin Invest 124: 742-54

Grzmil M, Morin P, Jr., Lino MM, Merlo A, Frank S, Wang Y, Moncayo G, Hemmings BA (2011) MAP kinase-interacting kinase 1 regulates SMAD2-dependent TGF-beta signaling pathway in human glioblastoma. Cancer Res 71: 2392-402

Gu J, Ruppen ME, Cai P (2005) lipase-catalyzed regioselective esterification of rapamycin: synthesis of temsirolimus (CCI-779). Org Lett 7: 3945-8

Guertin DA, Sabatini DM (2007) Defining the role of mTOR in cancer. Cancer Cell 12: 9-22

Guertin DA, Stevens DM, Saitoh M, Kinkel S, Crosby K, Sheen JH, Mullholland DJ, Magnuson MA, Wu H, Sabatini DM (2009) mTOR complex 2 is required for the development of prostate cancer induced by Pten loss in mice. Cancer Cell 15: 148-59

Guertin DA, Stevens DM, Thoreen CC, Burds AA, Kalaany NY, Moffat J, Brown M, Fitzgerald KJ, Sabatini DM (2006) Ablation in mice of the mTORC components raptor, rictor, or mLST8 reveals that mTORC2 is required for signaling to Akt-FOXO and PKCalpha, but not S6K1. Dev Cell 11: 859-71

Guil S, Long JC, Caceres JF (2006) hnRNP A1 relocalization to the stress granules reflects a role in the stress response. Molecular and cellular biology 26: 5744-58

Gulhati P, Bowen KA, Liu J, Stevens PD, Rychahou PG, Chen M, Lee EY, Weiss HL, O'Connor KL, Gao T, Evers BM (2011) mTORC1 and mTORC2 regulate EMT, motility, and metastasis of colorectal cancer via RhoA and Rac1 signaling pathways. Cancer Res 71: 3246-56

Gumireddy K, Baker SJ, Cosenza SC, John P, Kang AD, Robell KA, Reddy MV, Reddy EP (2005) A non-ATP-competitive inhibitor of BCR-ABL overrides imatinib resistance. Proceedings of the National Academy of Sciences of the United States of America 102: 1992-7

Gwinn DM, Shackelford DB, Egan DF, Mihaylova MM, Mery A, Vasquez DS, Turk BE, Shaw RJ (2008) AMPK phosphorylation of raptor mediates a metabolic checkpoint. Mol Cell 30: 214-26

Hallberg B, Rayter SI, Downward J (1994) Interaction of Ras and Raf in intact mammalian cells upon extracellular stimulation. The Journal of biological chemistry 269: 3913-6

Harding HP, Novoa I, Zhang Y, Zeng H, Wek R, Schapira M, Ron D (2000) Regulated translation initiation controls stress-induced gene expression in mammalian cells. Mol Cell 6: 1099-108

Hay N (2010) Mnk earmarks eIF4E for cancer therapy. Proceedings of the National Academy of Sciences of the United States of America 107: 13975-6

Hay N, Sonenberg N (2004) Upstream and downstream of mTOR. Genes & development 18: 1926-45

Heerma van Voss MR, van Diest PJ, Raman V (2017) Targeting RNA helicases in cancer: The translation trap. Biochim Biophys Acta 1868: 510-520

Hefner Y, Borsch-Haubold AG, Murakami M, Wilde JI, Pasquet S, Schieltz D, Ghomashchi F, Yates JR, 3rd, Armstrong CG, Paterson A, Cohen P, Fukunaga R, Hunter T, Kudo I, Watson SP, Gelb MH (2000) Serine 727 phosphorylation and activation of cytosolic phospholipase A2 by MNK1-related protein kinases. The Journal of biological chemistry 275: 37542-51

Hemmings BA, Restuccia DF (2015) The PI3K-PKB/Akt pathway. Cold Spring Harb Perspect Biol 7

Hietakangas V, Cohen SM (2008) TOR complex 2 is needed for cell cycle progression and anchorage-independent growth of MCF7 and PC3 tumor cells. BMC Cancer 8: 282

Higa GM, Abraham J (2007) Lapatinib in the treatment of breast cancer. Expert Rev Anticancer Ther 7: 1183-92

Hinnebusch AG (2005) Translational regulation of GCN4 and the general amino acid control of yeast. Annu Rev Microbiol 59: 407-50

Hinnebusch AG, Lorsch JR (2012) The mechanism of eukaryotic translation initiation: new insights and challenges. Cold Spring Harb Perspect Biol 4

Hogbom M, Collins R, van den Berg S, Jenvert RM, Karlberg T, Kotenyova T, Flores A, Karlsson Hedestam GB, Schiavone LH (2007) Crystal structure of conserved domains 1 and 2 of the human DEAD-box helicase DDX3X in complex with the mononucleotide AMP. Journal of molecular biology 372: 150-9

Holz MK, Ballif BA, Gygi SP, Blenis J (2005) mTOR and S6K1 mediate assembly of the translation preinitiation complex through dynamic protein interchange and ordered phosphorylation events. Cell 123: 569-80

Hou J, Lam F, Proud C, Wang S (2012) Targeting Mnks for cancer therapy. Oncotarget 3: 118-31

Hou J, Teo T, Sykes MJ, Wang S (2013) Insights into the Importance of DFD-Motif and Insertion I1 in Stabilizing the DFD-Out Conformation of Mnk2 Kinase. ACS Med Chem Lett 4: 736-41

Hsieh AC, Liu Y, Edlind MP, Ingolia NT, Janes MR, Sher A, Shi EY, Stumpf CR, Christensen C, Bonham MJ, Wang S, Ren P, Martin M, Jessen K, Feldman ME, Weissman JS, Shokat KM, Rommel C, Ruggero D (2012) The translational landscape of mTOR signalling steers cancer initiation and metastasis. Nature 485: 55-61

Hsieh AC, Ruggero D (2010) Targeting eukaryotic translation initiation factor 4E (eIF4E) in cancer. Clin Cancer Res 16: 4914-20

Hsu PP, Kang SA, Rameseder J, Zhang Y, Ottina KA, Lim D, Peterson TR, Choi Y, Gray NS, Yaffe MB, Marto JA, Sabatini DM (2011) The mTOR-regulated phosphoproteome reveals a mechanism of mTORC1-mediated inhibition of growth factor signaling. Science 332: 1317-22

Inoki K, Ouyang H, Zhu T, Lindvall C, Wang Y, Zhang X, Yang Q, Bennett C, Harada Y, Stankunas K, Wang CY, He X, MacDougald OA, You M, Williams BO, Guan KL (2006) TSC2 integrates Wnt and energy signals via a coordinated phosphorylation by AMPK and GSK3 to regulate cell growth. Cell 126: 955-68

Inoki K, Zhu T, Guan KL (2003) TSC2 mediates cellular energy response to control cell growth and survival. Cell 115: 577-90

Iqbal N, Iqbal N (2014) Imatinib: a breakthrough of targeted therapy in cancer. Chemother Res Pract 2014: 357027

Ishida T, Doi M, Ueda H, Inoue M, Scheldrick GM (1988) Specific ring stacking interaction on the tryptophan-7-methylguanine system: Comparative crystallographic studies of indole derivatives-7-methylguanine base, nucleoside,

and nucleotide complexes. . Journal of the American Chemical Society 110: 2286-2294

Ishida T, Iyo H, Ueda H, Doi M, Inoue M, Nishimura S, Kitamura K (1991) Importance of simultaneous co-operation of hydrogen bond pairing and stacking interactions for recognition of guanine base of a peptide: X-ray crystal analysis of 7-methylguanosine-5' -phosphate-tryptophanylglutamic acid complex. Journal of the Chemical Society, Perkin Transactions 1: 1847-1853

Iyer G, Hanrahan AJ, Milowsky MI, Al-Ahmadie H, Scott SN, Janakiraman M, Pirun M, Sander C, Socci ND, Ostrovnaya I, Viale A, Heguy A, Peng L, Chan TA, Bochner B, Bajorin DF, Berger MF, Taylor BS, Solit DB (2012) Genome sequencing identifies a basis for everolimus sensitivity. Science 338: 221

Jacinto E, Loewith R, Schmidt A, Lin S, Ruegg MA, Hall A, Hall MN (2004) Mammalian TOR complex 2 controls the actin cytoskeleton and is rapamycin insensitive. Nat Cell Biol 6: 1122-8

Jackson RJ (2013) The current status of vertebrate cellular mRNA IRESs. Cold Spring Harb Perspect Biol 5

Jackson RJ, Hellen CU, Pestova TV (2010) The mechanism of eukaryotic translation initiation and principles of its regulation. Nature reviews Molecular cell biology 11: 113-27

Jaouen G, Vessieres A, Top S (2015) Ferrocifen type anti cancer drugs. Chem Soc Rev 44: 8802-17

Jauch R, Cho MK, Jakel S, Netter C, Schreiter K, Aicher B, Zweckstetter M, Jackle H, Wahl MC (2006) Mitogen-activated protein kinases interacting kinases are autoinhibited by a reprogrammed activation segment. The EMBO journal 25: 4020-32

Jauch R, Jakel S, Netter C, Schreiter K, Aicher B, Jackle H, Wahl MC (2005) Crystal structures of the Mnk2 kinase domain reveal an inhibitory conformation and a zinc binding site. Structure 13: 1559-68

Jhanwar-Uniyal M, Amin AG, Cooper JB, Das K, Schmidt MH, Murali R (2017) Discrete signaling mechanisms of mTORC1 and mTORC2: Connected yet apart in cellular and molecular aspects. Adv Biol Regul

Jiang L, Gu ZH, Yan ZX, Zhao X, Xie YY, Zhang ZG, Pan CM, Hu Y, Cai CP, Dong Y, Huang JY, Wang L, Shen Y, Meng G, Zhou JF, Hu JD, Wang JF, Liu YH, Yang LH, Zhang F et al. (2015) Exome sequencing identifies somatic mutations of DDX3X in natural killer/T-cell lymphoma. Nat Genet 47: 1061-6

Johnson RW (2002) Sirolimus (Rapamune) in renal transplantation. Curr Opin Nephrol Hypertens 11: 603-7

Johnston S, Pippen J, Jr., Pivot X, Lichinitser M, Sadeghi S, Dieras V, Gomez HL, Romieu G, Manikhas A, Kennedy MJ, Press MF, Maltzman J, Florance A, O'Rourke L, Oliva C, Stein S, Pegram M (2009) Lapatinib combined with letrozole versus letrozole and placebo as first-line therapy for postmenopausal hormone receptor-positive metastatic breast cancer. J Clin Oncol 27: 5538-46

Jordan VC, Allen KE, Dix CJ (1980) Pharmacology of tamoxifen in laboratory animals. Cancer Treat Rep 64: 745-59

Joshi S, Platanias LC (2014) Mnk kinase pathway: Cellular functions and biological outcomes. World J Biol Chem 5: 321-33

Kannan S, Poulsen A, Yang HY, Ho M, Ang SH, Eldwin TS, Jeyaraj DA, Chennamaneni LR, Liu B, Hill J, Verma CS, Nacro K (2015) Probing the binding mechanism of Mnk inhibitors by docking and molecular dynamics simulations. Biochemistry 54: 32-46

Keating GM (2016) Afatinib: A Review in Advanced Non-Small Cell Lung Cancer. Target Oncol 11: 825-835

Kim YK, Hahm B, Jang SK (2000) Polypyrimidine tract-binding protein inhibits translation of bip mRNA. Journal of molecular biology 304: 119-33

Kittler H, Tschandl P (2018) Driver mutations in the mitogen-activated protein kinase pathway: the seeds of good and evil. Br J Dermatol 178: 26-27

Klann E, Dever TE (2004) Biochemical mechanisms for translational regulation in synaptic plasticity. Nat Rev Neurosci 5: 931-42

Knauf U, Tschopp C, Gram H (2001) Negative regulation of protein translation by mitogen-activated protein kinase-interacting kinases 1 and 2. Molecular and cellular biology 21: 5500-11

Komar AA, Hatzoglou M (2011) Cellular IRES-mediated translation: the war of ITAFs in pathophysiological states. Cell Cycle 10: 229-40

Konicek BW, Stephens JR, McNulty AM, Robichaud N, Peery RB, Dumstorf CA, Dowless MS, Iversen PW, Parsons S, Ellis KE, McCann DJ, Pelletier J, Furic L, Yingling JM, Stancato LF, Sonenberg N, Graff JR (2011) Therapeutic inhibition of MAP kinase interacting kinase blocks eukaryotic initiation factor 4E phosphorylation and suppresses outgrowth of experimental lung metastases. Cancer Res 71: 1849-57

Kosciuczuk EM, Saleiro D, Kroczynska B, Beauchamp EM, Eckerdt F, Blyth GT, Abedin SM, Giles FJ, Altman JK, Platanias LC (2016) Merestinib blocks Mnk kinase activity in acute myeloid leukemia progenitors and exhibits antileukemic effects in vitro and in vivo. Blood 128: 410-4

Kozak M (1987) At least six nucleotides preceding the AUG initiator codon enhance translation in mammalian cells. Journal of molecular biology 196: 947-50

Kozak M (1989) The scanning model for translation: an update. J Cell Biol 108: 229-41

Kozak M (1995) Adherence to the first-AUG rule when a second AUG codon follows closely upon the first. Proceedings of the National Academy of Sciences of the United States of America 92: 2662-6

Kufareva I, Abagyan R (2008) Type-II kinase inhibitor docking, screening, and profiling using modified structures of active kinase states. J Med Chem 51: 7921-32

Lai FP, Szczodrak M, Block J, Faix J, Breitsprecher D, Mannherz HG, Stradal TE, Dunn GA, Small JV, Rottner K (2008) Arp2/3 complex interactions and actin network turnover in lamellipodia. The EMBO journal 27: 982-92

Lai MC, Chang WC, Shieh SY, Tarn WY (2010) DDX3 regulates cell growth through translational control of cyclin E1. Molecular and cellular biology 30: 5444-53

Lama D, Pradhan MR, Brown CJ, Eapen RS, Joseph TL, Kwoh CK, Lane DP, Verma CS (2017) Water-Bridge Mediates Recognition of mRNA Cap in eIF4E. Structure 25: 188-194

Laplante M, Sabatini DM (2012) mTOR signaling in growth control and disease. Cell 149: 274-93

Lazaris-Karatzas A, Montine KS, Sonenberg N (1990) Malignant transformation by a eukaryotic initiation factor subunit that binds to mRNA 5' cap. Nature 345: 544-7

Lee AS, Kranzusch PJ, Cate JH (2015) eIF3 targets cell-proliferation messenger RNAs for translational activation or repression. Nature 522: 111-4

Lee AS, Kranzusch PJ, Doudna JA, Cate JH (2016) eIF3d is an mRNA cap-binding protein that is required for specialized translation initiation. Nature 536: 96-9

Lee DF, Kuo HP, Chen CT, Hsu JM, Chou CK, Wei Y, Sun HL, Li LY, Ping B, Huang WC, He X, Hung JY, Lai CC, Ding Q, Su JL, Yang JY, Sahin AA, Hortobagyi GN, Tsai FJ, Tsai CH et al. (2007) IKK beta suppression of TSC1 links inflammation and tumor angiogenesis via the mTOR pathway. Cell 130: 440-55

Lee JH, Nan A (2012) Combination drug delivery approaches in metastatic breast cancer. J Drug Deliv 2012: 915375

Leeson PD, Springthorpe B (2007) The influence of drug-like concepts on decision-making in medicinal chemistry. Nat Rev Drug Discov 6: 881-90

Levin EG (2005) Cancer therapy through control of cell migration. Curr Cancer Drug Targets 5: 505-18

Li Y, Wang H, Wang Z, Makhija S, Buchsbaum D, LoBuglio A, Kimberly R, Zhou T (2006) Inducible resistance of tumor cells to tumor necrosis factor-related apoptosis-inducing ligand receptor 2-mediated apoptosis by generation of a blockade at the death domain function. Cancer Res 66: 8520-8

Li Z, Sun Y, Qu M, Wan H, Cai F, Zhang P (2017) Inhibiting the MNK-eIF4E-beta-catenin axis increases the responsiveness of aggressive breast cancer cells to chemotherapy. Oncotarget 8: 2906-2915

Librizzi M, Longo A, Chiarelli R, Amin J, Spencer J, Luparello C (2012) Cytotoxic effects of Jay Amin hydroxamic acid (JAHA), a ferrocene-based class I histone deacetylase inhibitor, on triple-negative MDA-MB231 breast cancer cells. Chem Res Toxicol 25: 2608-16

Linder P, Jankowsky E (2011) From unwinding to clamping - the DEAD box RNA helicase family. Nature reviews Molecular cell biology 12: 505-16

Lineham E, Spencer J, Morley SJ (2017) Dual abrogation of MNK and mTOR: a novel therapeutic approach for the treatment of aggressive cancers. Future Med Chem 9: 1539-1555

Lineham E, Tizzard GJ, Coles SJ, Spencer J, Morley S (2018) Synergistic effects of inhibiting the MNK-eIF4E and PI3K/AKT/mTOR pathways on cell migration in MDA-MB-231 cells. Oncotarget

Liu B, Liu F (2014) Feedback regulation of mTORC1 by Grb10 in metabolism and beyond. Cell Cycle 13: 2643-4

Liu P, Gan W, Chin YR, Ogura K, Guo J, Zhang J, Wang B, Blenis J, Cantley LC, Toker A, Su B, Wei W (2015) PtdIns(3,4,5)P3-Dependent Activation of the mTORC2 Kinase Complex. Cancer Discov 5: 1194-209

Liu P, Gan W, Inuzuka H, Lazorchak AS, Gao D, Arojo O, Liu D, Wan L, Zhai B, Yu Y, Yuan M, Kim BM, Shaik S, Menon S, Gygi SP, Lee TH, Asara JM, Manning BD, Blenis J, Su B et al. (2013) Sin1 phosphorylation impairs mTORC2 complex integrity and inhibits downstream Akt signalling to suppress tumorigenesis. Nat Cell Biol 15: 1340-50

Liu Q, Kirubakaran S, Hur W, Niepel M, Westover K, Thoreen CC, Wang J, Ni J, Patricelli MP, Vogel K, Riddle S, Waller DL, Traynor R, Sanda T, Zhao Z, Kang SA, Zhao J, Look AT, Sorger PK, Sabatini DM et al. (2012) Kinome-wide selectivity profiling of ATP-competitive mammalian target of rapamycin (mTOR) inhibitors and characterization of their binding kinetics. The Journal of biological chemistry 287: 9742-52

Liu Q, Wang J, Kang SA, Thoreen CC, Hur W, Ahmed T, Sabatini DM, Gray NS (2011) Discovery of 9-(6-aminopyridin-3-yl)-1-(3-(trifluoromethyl)phenyl)benzo[h][1,6]naphthyridin-2(1H)-one (Torin2) as a potent, selective, and orally available mammalian target of rapamycin (mTOR) inhibitor for treatment of cancer. J Med Chem 54: 1473-80

Liu T, Li R, Zhao H, Deng J, Long Y, Shuai MT, Li Q, Gu H, Chen YQ, Leng AM (2016) eIF4E promotes tumorigenesis and modulates chemosensitivity to cisplatin in esophageal squamous cell carcinoma. Oncotarget

Liu Y, Sun L, Su X, Guo S (2016) Inhibition of eukaryotic initiation factor 4E phosphorylation by cercosporamide selectively suppresses angiogenesis, growth and survival of human hepatocellular carcinoma. Biomed Pharmacother 84: 237-243

Lu C, Makala L, Wu D, Cai Y (2016) Targeting translation: eIF4E as an emerging anticancer drug target. Expert Rev Mol Med 18: e2

Lugowska I, Kosela-Paterczyk H, Kozak K, Rutkowski P (2015) Trametinib: a MEK inhibitor for management of metastatic melanoma. Onco Targets Ther 8: 2251-9

Lv D, Hu Z, Lu L, Lu H, Xu X (2017) Three-dimensional cell culture: A powerful tool in tumor research and drug discovery. Oncol Lett 14: 6999-7010

Ma L, Chen Z, Erdjument-Bromage H, Tempst P, Pandolfi PP (2005) Phosphorylation and functional inactivation of TSC2 by Erk implications for tuberous sclerosis and cancer pathogenesis. Cell 121: 179-93

Maag D, Fekete CA, Gryczynski Z, Lorsch JR (2005) A conformational change in the eukaryotic translation preinitiation complex and release of eIF1 signal recognition of the start codon. Mol Cell 17: 265-75

Maekawa T, Ashihara E, Kimura S (2007) The Bcr-Abl tyrosine kinase inhibitor imatinib and promising new agents against Philadelphia chromosome-positive leukemias. Int J Clin Oncol 12: 327-40

Maira SM, Stauffer F, Brueggen J, Furet P, Schnell C, Fritsch C, Brachmann S, Chene P, De Pover A, Schoemaker K, Fabbro D, Gabriel D, Simonen M, Murphy L, Finan P, Sellers W, Garcia-Echeverria C (2008) Identification and characterization of NVP-BEZ235, a new orally available dual phosphatidylinositol 3-kinase/mammalian target of rapamycin inhibitor with potent in vivo antitumor activity. Mol Cancer Ther 7: 1851-63

Mamane Y, Petroulakis E, LeBacquer O, Sonenberg N (2006) mTOR, translation initiation and cancer. Oncogene 25: 6416-22

Mamane Y, Petroulakis E, Martineau Y, Sato TA, Larsson O, Rajasekhar VK, Sonenberg N (2007) Epigenetic activation of a subset of mRNAs by eIF4E explains its effects on cell proliferation. PLoS One 2: e242

Manning BD, Tee AR, Logsdon MN, Blenis J, Cantley LC (2002) Identification of the tuberous sclerosis complex-2 tumor suppressor gene product tuberin as a target of the phosphoinositide 3-kinase/akt pathway. Mol Cell 10: 151-62

Marsden S, Nardelli M, Linder P, McCarthy JE (2006) Unwinding single RNA molecules using helicases involved in eukaryotic translation initiation. Journal of molecular biology 361: 327-35

Masuda N, Nishimura R, Takahashi M, Inoue K, Ohno S, Iwata H, Mori Y, Hashigaki S, Muramatsu Y, Nagasawa T, Umeyama Y, Toi M (2018) Palbociclib in combination with letrozole as first-line treatment for advanced breast cancer: A Japanese phase II study. Cancer Sci 109: 803-813

Maurer G, Tarkowski B, Baccarini M (2011) Raf kinases in cancer-roles and therapeutic opportunities. Oncogene 30: 3477-88

McGranahan N, Swanton C (2015) Biological and therapeutic impact of intratumor heterogeneity in cancer evolution. Cancer Cell 27: 15-26

Menon S, Dibble CC, Talbott G, Hoxhaj G, Valvezan AJ, Takahashi H, Cantley LC, Manning BD (2014) Spatial control of the TSC complex integrates insulin and nutrient regulation of mTORC1 at the lysosome. Cell 156: 771-85

Merrick WC (2015) eIF4F: a retrospective. The Journal of biological chemistry 290: 24091-9

Meyer KD, Patil DP, Zhou J, Zinoviev A, Skabkin MA, Elemento O, Pestova TV, Qian SB, Jaffrey SR (2015) 5' UTR m(6)A Promotes Cap-Independent Translation. Cell 163: 999-1010

Morita M, Gravel SP, Hulea L, Larsson O, Pollak M, St-Pierre J, Topisirovic I (2015) mTOR coordinates protein synthesis, mitochondrial activity and proliferation. Cell Cycle 14: 473-80

Morley SJ, Coldwell MJ, Clemens MJ (2005) Initiation factor modifications in the preapoptotic phase. Cell Death Differ 12: 571-84

Nanda JS, Cheung YN, Takacs JE, Martin-Marcos P, Saini AK, Hinnebusch AG, Lorsch JR (2009) eIF1 controls multiple steps in start codon recognition during eukaryotic translation initiation. Journal of molecular biology 394: 268-85

Napoli I, Mercaldo V, Boyl PP, Eleuteri B, Zalfa F, De Rubeis S, Di Marino D, Mohr E, Massimi M, Falconi M, Witke W, Costa-Mattioli M, Sonenberg N, Achsel T, Bagni C (2008) The fragile X syndrome protein represses activity-dependent translation through CYFIP1, a new 4E-BP. Cell 134: 1042-54

Nepali K, Sharma S, Kumar D, Budhiraja A, Dhar KL (2014) Anticancer hybrids--a patent survey. Recent Pat Anticancer Drug Discov 9: 303-39

Nguyen A, Vessières A, Hillard E, Top S, Pigeon P, Jaouen G (2007) Ferrocifens and ferrocifenols as new potential weapons against breast cancer. CHIMIA International Journal for Chemistry 61: 716-724

Niedzwiecka A, Marcotrigiano J, Stepinski J, Jankowska-Anyszka M, Wyslouch-Cieszynska A, Dadlez M, Gingras AC, Mak P, Darzynkiewicz E, Sonenberg N, Burley SK, Stolarski R (2002) Biophysical studies of eIF4E cap-binding protein: recognition of mRNA 5' cap structure and synthetic fragments of eIF4G and 4E-BP1 proteins. Journal of molecular biology 319: 615-35

Niepmann M (2009) Internal translation initiation of picornaviruses and hepatitis C virus. Biochim Biophys Acta 1789: 529-41

O'Loghlen A, Gonzalez VM, Pineiro D, Perez-Morgado MI, Salinas M, Martin ME (2004) Identification and molecular characterization of Mnk1b, a splice variant of human MAP kinase-interacting kinase Mnk1. Exp Cell Res 299: 343-55

Ocasio CJ, Sansook S, Jones R, Roberts JM, Scott TG, Tsoureas N, Coxhead P, Guille M, Tizzard GJ, Coles SJ, Hochegger H, Bradner JE, Spencer J (2017) Pojamide: An HDAC3-Selective Ferrocene Analogue with Remarkably Enhanced Redox-Triggered Ferrocenium Activity in Cells. Organometallics 36: 3276-3283

Oh S, Flynn RA, Floor SN, Purzner J, Martin L, Do BT, Schubert S, Vaka D, Morrissy S, Li Y, Kool M, Hovestadt V, Jones DT, Northcott PA, Risch T, Warnatz HJ, Yaspo ML, Adams CM, Leib RD, Breese M et al. (2016) Medulloblastoma-associated DDX3 variant selectively alters the translational response to stress. Oncotarget 7: 28169-82

Ojha J, Secreto CR, Rabe KG, Van Dyke DL, Kortum KM, Slager SL, Shanafelt TD, Fonseca R, Kay NE, Braggio E (2015) Identification of recurrent truncated DDX3X mutations in chronic lymphocytic leukaemia. Br J Haematol 169: 445-8

Orton KC, Ling J, Waskiewicz AJ, Cooper JA, Merrick WC, Korneeva NL, Rhoads RE, Sonenberg N, Traugh JA (2004) Phosphorylation of Mnk1 by caspase-activated Pak2/gamma-PAK inhibits phosphorylation and interaction of eIF4G with Mnk. The Journal of biological chemistry 279: 38649-57

Oyarzabal J, Zarich N, Albarran MI, Palacios I, Urbano-Cuadrado M, Mateos G, Reymundo I, Rabal O, Salgado A, Corrionero A, Fominaya J, Pastor J, Bischoff JR (2010) Discovery of mitogen-activated protein kinase-interacting kinase 1 inhibitors by a comprehensive fragment-oriented virtual screening approach. J Med Chem 53: 6618-28

Palm W, Park Y, Wright K, Pavlova NN, Tuveson DA, Thompson CB (2015) The Utilization of Extracellular Proteins as Nutrients Is Suppressed by mTORC1. Cell 162: 259-270

Panja D, Kenney JW, D'Andrea L, Zalfa F, Vedeler A, Wibrand K, Fukunaga R, Bagni C, Proud CG, Bramham CR (2014) Two-stage translational control of dentate gyrus LTP consolidation is mediated by sustained BDNF-TrkB signaling to MNK. Cell Rep 9: 1430-45

Parra-Palau JL, Scheper GC, Wilson ML, Proud CG (2003) Features in the N and C termini of the MAPK-interacting kinase Mnk1 mediate its nucleocytoplasmic shuttling. The Journal of biological chemistry 278: 44197-204

Parsyan A, Svitkin Y, Shahbazian D, Gkogkas C, Lasko P, Merrick WC, Sonenberg N (2011) mRNA helicases: the tacticians of translational control. Nature reviews Molecular cell biology 12: 235-45

Passmore LA, Schmeing TM, Maag D, Applefield DJ, Acker MG, Algire MA, Lorsch JR, Ramakrishnan V (2007) The eukaryotic translation initiation factors eIF1 and eIF1A induce an open conformation of the 40S ribosome. Mol Cell 26: 41-50

Patel H, Chuckowree I, Coxhead P, Guille M, Wang M, Zuckermann A, Williams RS, Librizzi M, Paranal RM, Bradner JE (2014) Synthesis of hybrid anticancer agents based on kinase and histone deacetylase inhibitors. MedChemComm 5: 1829-1833

Patra M, Gasser G (2017) The medicinal chemistry of ferrocene and its derivatives. Nature Reviews Chemistry 1: 0066

Paul MK, Mukhopadhyay AK (2004) Tyrosine kinase - Role and significance in Cancer. Int J Med Sci 1: 101-115

Pavitt GD, Ron D (2012) New insights into translational regulation in the endoplasmic reticulum unfolded protein response. Cold Spring Harb Perspect Biol 4

Peabody DS, Berg P (1986) Termination-reinitiation occurs in the translation of mammalian cell mRNAs. Molecular and cellular biology 6: 2695-703

Pestova TV, Kolupaeva VG, Lomakin IB, Pilipenko EV, Shatsky IN, Agol VI, Hellen CU (2001) Molecular mechanisms of translation initiation in eukaryotes. Proceedings of the National Academy of Sciences of the United States of America 98: 7029-36

Pestova TV, Lomakin IB, Lee JH, Choi SK, Dever TE, Hellen CU (2000) The joining of ribosomal subunits in eukaryotes requires eIF5B. Nature 403: 332-5

Peter D, Igreja C, Weber R, Wohlbold L, Weiler C, Ebertsch L, Weichenrieder O, Izaurralde E (2015) Molecular architecture of 4E-BP translational inhibitors bound to eIF4E. Mol Cell 57: 1074-1087

Pettersen EF, Goddard TD, Huang CC, Couch GS, Greenblatt DM, Meng EC, Ferrin TE (2004) UCSF Chimera--a visualization system for exploratory research and analysis. J Comput Chem 25: 1605-12

Phillips A, Blaydes JP (2008) MNK1 and EIF4E are downstream effectors of MEKs in the regulation of the nuclear export of HDM2 mRNA. Oncogene 27: 1645-9

Pickering BM, Willis AE (2005) The implications of structured 5' untranslated regions on translation and disease. Semin Cell Dev Biol 16: 39-47

Podo F, Buydens LM, Degani H, Hilhorst R, Klipp E, Gribbestad IS, Van Huffel S, van Laarhoven HW, Luts J, Monleon D, Postma GJ, Schneiderhan-Marra N, Santoro F, Wouters H, Russnes HG, Sorlie T, Tagliabue E, Borresen-Dale AL, Consortium F (2010) Triple-negative breast cancer: present challenges and new perspectives. Mol Oncol 4: 209-29

Pooggin MM, Ryabova LA (2018) Ribosome Shunting, Polycistronic Translation, and Evasion of Antiviral Defenses in Plant Pararetroviruses and Beyond. Front Microbiol 9: 644

Powles T, Wheater M, Din O, Geldart T, Boleti E, Stockdale A, Sundar S, Robinson A, Ahmed I, Wimalasingham A, Burke W, Sarker SJ, Hussain S, Ralph C (2016) A Randomised Phase 2 Study of AZD2014 Versus Everolimus in Patients with VEGF-Refractory Metastatic Clear Cell Renal Cancer. Eur Urol 69: 450-6

Pyronnet S, Imataka H, Gingras AC, Fukunaga R, Hunter T, Sonenberg N (1999) Human eukaryotic translation initiation factor 4G (eIF4G) recruits mnk1 to phosphorylate eIF4E. The EMBO journal 18: 270-9

Qin X, Jiang B, Zhang Y (2016) 4E-BP1, a multifactor regulated multifunctional protein. Cell Cycle 15: 781-6

Querol-Audi J, Sun C, Vogan JM, Smith MD, Gu Y, Cate JH, Nogales E (2013) Architecture of human translation initiation factor 3. Structure 21: 920-8

Ramon YCS, Castellvi J, Hummer S, Peg V, Pelletier J, Sonenberg N (2018) Beyond molecular tumor heterogeneity: protein synthesis takes control. Oncogene 37: 2490-2501

Randall-Demllo S, Chieppa M, Eri R (2013) Intestinal epithelium and autophagy: partners in gut homeostasis. Front Immunol 4: 301

Ray BK, Lawson TG, Kramer JC, Cladaras MH, Grifo JA, Abramson RD, Merrick WC, Thach RE (1985) ATP-dependent unwinding of messenger RNA structure by eukaryotic initiation factors. The Journal of biological chemistry 260: 7651-8

Reich SH, Sprengeler PA, Chiang GG, Appleman JR, Chen J, Clarine J, Eam B, Ernst JT, Han Q, Goel VK, Han EZR, Huang V, Hung INJ, Jemison A, Jessen KA, Molter J, Murphy D, Neal M, Parker GS, Shaghafi M et al. (2018) Structure-based Design of Pyridone-Aminal eFT508 Targeting Dysregulated Translation by Selective Mitogen-activated Protein Kinase Interacting Kinases 1 and 2 (MNK1/2) Inhibition. J Med Chem 61: 3516-3540

Renna M (2016) Commentary: Overcoming mTOR resistance mutations with a new-generation mTOR inhibitor. Front Pharmacol 7: 431

Richter-Cook NJ, Dever TE, Hensold JO, Merrick WC (1998) Purification and characterization of a new eukaryotic protein translation factor. Eukaryotic initiation factor 4H. The Journal of biological chemistry 273: 7579-87

Ring A, Dowsett M (2004) Mechanisms of tamoxifen resistance. Endocr Relat Cancer 11: 643-58

Robichaud N, del Rincon SV, Huor B, Alain T, Petruccelli LA, Hearnden J, Goncalves C, Grotegut S, Spruck CH, Furic L, Larsson O, Muller WJ, Miller WH, Sonenberg N (2015) Phosphorylation of eIF4E promotes EMT and

metastasis via translational control of SNAIL and MMP-3. Oncogene 34: 2032-42

Rodrik-Outmezguine VS, Chandarlapaty S, Pagano NC, Poulikakos PI, Scaltriti M, Moskatel E, Baselga J, Guichard S, Rosen N (2011) mTOR kinase inhibition causes feedback-dependent biphasic regulation of AKT signaling. Cancer Discov 1: 248-59

Rodrik-Outmezguine VS, Okaniwa M, Yao Z, Novotny CJ, McWhirter C, Banaji A, Won H, Wong W, Berger M, de Stanchina E, Barratt DG, Cosulich S, Klinowska T, Rosen N, Shokat KM (2016) Overcoming mTOR resistance mutations with a new-generation mTOR inhibitor. Nature 534: 272-6

Rogers GW, Jr., Lima WF, Merrick WC (2001) Further characterization of the helicase activity of eIF4A. Substrate specificity. The Journal of biological chemistry 276: 12598-608

Rosenwald IB, Lazaris-Karatzas A, Sonenberg N, Schmidt EV (1993) Elevated levels of cyclin D1 protein in response to increased expression of eukaryotic initiation factor 4E. Molecular and cellular biology 13: 7358-63

Roskoski R, Jr. (2016) Classification of small molecule protein kinase inhibitors based upon the structures of their drug-enzyme complexes. Pharmacol Res 103: 26-48

Roux PP, Ballif BA, Anjum R, Gygi SP, Blenis J (2004) Tumor-promoting phorbol esters and activated Ras inactivate the tuberous sclerosis tumor suppressor complex via p90 ribosomal S6 kinase. Proceedings of the National Academy of Sciences of the United States of America 101: 13489-94

Roux PP, Shahbazian D, Vu H, Holz MK, Cohen MS, Taunton J, Sonenberg N, Blenis J (2007) RAS/ERK signaling promotes site-specific ribosomal protein S6 phosphorylation via RSK and stimulates cap-dependent translation. The Journal of biological chemistry 282: 14056-64

Rozen F, Edery I, Meerovitch K, Dever TE, Merrick WC, Sonenberg N (1990) Bidirectional RNA helicase activity of eucaryotic translation initiation factors 4A and 4F. Molecular and cellular biology 10: 1134-44

Rozengurt E, Soares HP, Sinnet-Smith J (2014) Suppression of feedback loops mediated by PI3K/mTOR induces multiple overactivation of compensatory pathways: an unintended consequence leading to drug resistance. Mol Cancer Ther 13: 2477-88

Ruggero D (2013) Translational control in cancer etiology. Cold Spring Harb Perspect Biol 5

Ruggero D, Montanaro L, Ma L, Xu W, Londei P, Cordon-Cardo C, Pandolfi PP (2004) The translation factor eIF-4E promotes tumor formation and cooperates with c-Myc in lymphomagenesis. Nat Med 10: 484-6

Ryabova LA, Pooggin MM, Hohn T (2002) Viral strategies of translation initiation: ribosomal shunt and reinitiation. Progress in nucleic acid research and molecular biology 72: 1-39

Sabatini DM (2017) Twenty-five years of mTOR: Uncovering the link from nutrients to growth. Proceedings of the National Academy of Sciences of the United States of America 114: 11818-11825

Sabatini DM, Erdjument-Bromage H, Lui M, Tempst P, Snyder SH (1994) RAFT1: a mammalian protein that binds to FKBP12 in a rapamycin-dependent fashion and is homologous to yeast TORs. Cell 78: 35-43

Sancak Y, Peterson TR, Shaul YD, Lindquist RA, Thoreen CC, Bar-Peled L, Sabatini DM (2008) The Rag GTPases bind raptor and mediate amino acid signaling to mTORC1. Science 320: 1496-501

Santag S, Siegel F, Wengner AM, Lange C, Bomer U, Eis K, Puhler F, Lienau P, Bergemann L, Michels M, von Nussbaum F, Mumberg D, Petersen K (2017) BAY 1143269, a novel MNK1 inhibitor, targets oncogenic protein expression and shows potent anti-tumor activity. Cancer Lett 390: 21-29

Sarbassov DD, Ali SM, Sengupta S, Sheen JH, Hsu PP, Bagley AF, Markhard AL, Sabatini DM (2006) Prolonged rapamycin treatment inhibits mTORC2 assembly and Akt/PKB. Mol Cell 22: 159-68

Sarbassov DD, Guertin DA, Ali SM, Sabatini DM (2005) Phosphorylation and regulation of Akt/PKB by the rictor-mTOR complex. Science 307: 1098-101

Saxton RA, Sabatini DM (2017) mTOR Signaling in Growth, Metabolism, and Disease. Cell 169: 361-371

Scheper GC, Morrice NA, Kleijn M, Proud CG (2001) The mitogen-activated protein kinase signal-integrating kinase Mnk2 is a eukaryotic initiation factor 4E kinase with high levels of basal activity in mammalian cells. Molecular and cellular biology 21: 743-54

Scheper GC, Parra JL, Wilson M, Van Kollenburg B, Vertegaal AC, Han ZG, Proud CG (2003) The N and C termini of the splice variants of the human mitogen-activated protein kinase-interacting kinase Mnk2 determine activity and localization. Molecular and cellular biology 23: 5692-705

Sebolt-Leopold JS, English JM (2006) Mechanisms of drug inhibition of signalling molecules. Nature 441: 457-62

Sedrani R, Cottens S, Kallen J, Schuler W (1998) Chemical modification of rapamycin: the discovery of SDZ RAD. Transplant Proc 30: 2192-4

Segovia-Mendoza M, Gonzalez-Gonzalez ME, Barrera D, Diaz L, Garcia-Becerra R (2015) Efficacy and mechanism of action of the tyrosine kinase inhibitors gefitinib, lapatinib and neratinib in the treatment of HER2-positive breast cancer: preclinical and clinical evidence. Am J Cancer Res 5: 2531-61

Sehgal SN, Baker H, Vezina C (1975) Rapamycin (AY-22,989), a new antifungal antibiotic. II. Fermentation, isolation and characterization. J Antibiot (Tokyo) 28: 727-32

Serra V, Markman B, Scaltriti M, Eichhorn PJ, Valero V, Guzman M, Botero ML, Llonch E, Atzori F, Di Cosimo S, Maira M, Garcia-Echeverria C, Parra JL, Arribas J, Baselga J (2008) NVP-BEZ235, a dual PI3K/mTOR inhibitor, prevents PI3K signaling and inhibits the growth of cancer cells with activating PI3K mutations. Cancer Res 68: 8022-30

Shah OJ, Wang Z, Hunter T (2004) Inappropriate activation of the TSC/Rheb/mTOR/S6K cassette induces IRS1/2 depletion, insulin resistance, and cell survival deficiencies. Curr Biol 14: 1650-6

Shahbazian D, Roux PP, Mieulet V, Cohen MS, Raught B, Taunton J, Hershey JW, Blenis J, Pende M, Sonenberg N (2006) The mTOR/PI3K and MAPK pathways converge on eIF4B to control its phosphorylation and activity. The EMBO journal 25: 2781-91

Sharma D, Jankowsky E (2014) The Ded1/DDX3 subfamily of DEAD-box RNA helicases. Critical reviews in biochemistry and molecular biology 49: 343-60

Shih JW, Tsai TY, Chao CH, Wu Lee YH (2008) Candidate tumor suppressor DDX3 RNA helicase specifically represses cap-dependent translation by acting as an eIF4E inhibitory protein. Oncogene 27: 700-14

Showkat M, Beigh MA, Andrabi KI (2014) mTOR Signaling in Protein Translation Regulation: Implications in Cancer Genesis and Therapeutic Interventions. Mol Biol Int 2014: 686984

Shveygert M, Kaiser C, Bradrick SS, Gromeier M (2010) Regulation of eukaryotic initiation factor 4E (eIF4E) phosphorylation by mitogen-activated protein kinase occurs through modulation of Mnk1-eIF4G interaction. Molecular and cellular biology 30: 5160-7

Siridechadilok B, Fraser CS, Hall RJ, Doudna JA, Nogales E (2005) Structural roles for human translation factor eIF3 in initiation of protein synthesis. Science 310: 1513-5

Six DA, Dennis EA (2000) The expanding superfamily of phospholipase A(2) enzymes: classification and characterization. Biochim Biophys Acta 1488: 1-19

Slentz-Kesler K, Moore JT, Lombard M, Zhang J, Hollingsworth R, Weiner MP (2000) Identification of the human Mnk2 gene (MKNK2) through protein interaction with estrogen receptor beta. Genomics 69: 63-71

Slotkin EK, Patwardhan PP, Vasudeva SD, de Stanchina E, Tap WD, Schwartz GK (2015) MLN0128, an ATP-competitive mTOR kinase inhibitor with potent in vitro and in vivo antitumor activity, as potential therapy for bone and soft-tissue sarcoma. Mol Cancer Ther 14: 395-406

Sonenberg N, Dever TE (2003) Eukaryotic translation initiation factors and regulators. Curr Opin Struct Biol 13: 56-63

Sonenberg N, Hinnebusch AG (2009) Regulation of translation initiation in eukaryotes: mechanisms and biological targets. Cell 136: 731-45

Song J, Takeda M, Morimoto RI (2001) Bag1-Hsp70 mediates a physiological stress signalling pathway that regulates Raf-1/ERK and cell growth. Nat Cell Biol 3: 276-82

Soto-Rifo R, Ohlmann T (2013) The role of the DEAD-box RNA helicase DDX3 in mRNA metabolism. Wiley Interdiscip Rev RNA 4: 369-85

Soto-Rifo R, Rubilar PS, Limousin T, de Breyne S, Decimo D, Ohlmann T (2012) DEAD-box protein DDX3 associates with eIF4F to promote translation of selected mRNAs. The EMBO journal 31: 3745-56

Soto-Rifo R, Rubilar PS, Ohlmann T (2013) The DEAD-box helicase DDX3 substitutes for the cap-binding protein eIF4E to promote compartmentalized translation initiation of the HIV-1 genomic RNA. Nucleic acids research 41: 6286-99

Spencer J, Mendham AP, Kotha AK, Richardson SC, Hillard EA, Jaouen G, Male L, Hursthouse MB (2009) Structural and biological investigation of ferrocene-substituted 3-methylidene-1,3-dihydro-2H-indol-2-ones. Dalton Trans: 918-21

Spriggs KA, Stoneley M, Bushell M, Willis AE (2008) Re-programming of translation following cell stress allows IRES-mediated translation to predominate. Biol Cell 100: 27-38

Stead RL, Proud CG (2013) Rapamycin enhances eIF4E phosphorylation by activating MAP kinase-interacting kinase 2a (Mnk2a). FEBS Lett 587: 2623-8

Stoneley M, Subkhankulova T, Le Quesne JP, Coldwell MJ, Jopling CL, Belsham GJ, Willis AE (2000) Analysis of the c-myc IRES; a potential role for cell-type specific trans-acting factors and the nuclear compartment. Nucleic acids research 28: 687-94

Stoneley M, Willis AE (2004) Cellular internal ribosome entry segments: structures, trans-acting factors and regulation of gene expression. Oncogene 23: 3200-7

Stransky N, Egloff AM, Tward AD, Kostic AD, Cibulskis K, Sivachenko A, Kryukov GV, Lawrence MS, Sougnez C, McKenna A, Shefler E, Ramos AH, Stojanov P, Carter SL, Voet D, Cortes ML, Auclair D, Berger MF, Saksena G, Guiducci C et al. (2011) The mutational landscape of head and neck squamous cell carcinoma. Science 333: 1157-60

Stratford JK, Bentrem DJ, Anderson JM, Fan C, Volmar KA, Marron JS, Routh ED, Caskey LS, Samuel JC, Der CJ, Thorne LB, Calvo BF, Kim HJ, Talamonti MS, Iacobuzio-Donahue CA, Hollingsworth MA, Perou CM, Yeh JJ (2010) A six-gene signature predicts survival of patients with localized pancreatic ductal adenocarcinoma. PLoS Med 7: e1000307

Stuttfeld E, Aylett CH, Imseng S, Boehringer D, Scaiola A, Sauer E, Hall MN, Maier T, Ban N (2018) Architecture of the human mTORC2 core complex. Elife 7

Sun M, Song L, Li Y, Zhou T, Jope RS (2008) Identification of an antiapoptotic protein complex at death receptors. Cell Death Differ 15: 1887-900

Tabbi G, Cassino C, Cavigiolio G, Colangelo D, Ghiglia A, Viano I, Osella D (2002) Water stability and cytotoxic activity relationship of a series of ferrocenium derivatives. ESR insights on the radical production during the degradation process. J Med Chem 45: 5786-96

Tanaka K, Babic I, Nathanson D, Akhavan D, Guo D, Gini B, Dang J, Zhu S, Yang H, De Jesus J, Amzajerdi AN, Zhang Y, Dibble CC, Dan H, Rinkenbaugh A, Yong WH, Vinters HV, Gera JF, Cavenee WK, Cloughesy TF et al. (2011) Oncogenic EGFR signaling activates an mTORC2-NF-kappaB pathway that promotes chemotherapy resistance. Cancer Discov 1: 524-38

Tanida I, Ueno T, Kominami E (2008) LC3 and Autophagy. Methods Mol Biol 445: 77-88

Teo T, Yang Y, Yu M, Basnet SK, Gillam T, Hou J, Schmid RM, Kumarasiri M, Diab S, Albrecht H, Sykes MJ, Wang S (2015a) An integrated approach for

discovery of highly potent and selective Mnk inhibitors: Screening, synthesis and SAR analysis. Eur J Med Chem 103: 539-50

Teo T, Yu M, Yang Y, Gillam T, Lam F, Sykes MJ, Wang S (2015b) Pharmacologic co-inhibition of Mnks and mTORC1 synergistically suppresses proliferation and perturbs cell cycle progression in blast crisis-chronic myeloid leukemia cells. Cancer Lett 357: 612-23

Thoreen CC, Kang SA, Chang JW, Liu Q, Zhang J, Gao Y, Reichling LJ, Sim T, Sabatini DM, Gray NS (2009) An ATP-competitive mammalian target of rapamycin inhibitor reveals rapamycin-resistant functions of mTORC1. The Journal of biological chemistry 284: 8023-32

Thumma SC, Jacobson BA, Patel MR, Konicek BW, Franklin MJ, Jay-Dixon J, Sadiq A, De A, Graff JR, Kratzke RA (2015) Antisense oligonucleotide targeting eukaryotic translation initiation factor 4E reduces growth and enhances chemosensitivity of non-small-cell lung cancer cells. Cancer Gene Ther 22: 396-401

Tiwari N, Gheldof A, Tatari M, Christofori G (2012) EMT as the ultimate survival mechanism of cancer cells. Semin Cancer Biol 22: 194-207

Tomoo K, Shen X, Okabe K, Nozoe Y, Fukuhara S, Morino S, Ishida T, Taniguchi T, Hasegawa H, Terashima A, Sasaki M, Katsuya Y, Kitamura K, Miyoshi H, Ishikawa M, Miura K (2002) Crystal structures of 7-methylguanosine 5'-triphosphate (m(7)GTP)- and P(1)-7-methylguanosine-P(3)-adenosine-5',5'-triphosphate (m(7)GpppA)-bound human full-length eukaryotic initiation factor 4E: biological importance of the C-terminal flexible region. Biochem J 362: 539-44

Topisirovic I, Ruiz-Gutierrez M, Borden KL (2004) Phosphorylation of the eukaryotic translation initiation factor eIF4E contributes to its transformation and mRNA transport activities. Cancer Res 64: 8639-42

Tothova Z, Kollipara R, Huntly BJ, Lee BH, Castrillon DH, Cullen DE, McDowell EP, Lazo-Kallanian S, Williams IR, Sears C, Armstrong SA, Passegue E, DePinho RA, Gilliland DG (2007) FoxOs are critical mediators of hematopoietic stem cell resistance to physiologic oxidative stress. Cell 128: 325-39

Truitt ML, Conn CS, Shi Z, Pang X, Tokuyasu T, Coady AM, Seo Y, Barna M, Ruggero D (2015) Differential Requirements for eIF4E Dose in Normal Development and Cancer. Cell 162: 59-71

Truitt ML, Ruggero D (2017) New frontiers in translational control of the cancer genome. Nat Rev Cancer 17: 332

Tzivion G, Shen YH, Zhu J (2001) 14-3-3 proteins; bringing new definitions to scaffolding. Oncogene 20: 6331-8

Ueda T, Sasaki M, Elia AJ, Chio, II, Hamada K, Fukunaga R, Mak TW (2010) Combined deficiency for MAP kinase-interacting kinase 1 and 2 (Mnk1 and Mnk2) delays tumor development. Proceedings of the National Academy of Sciences of the United States of America 107: 13984-90

Ueda T, Watanabe-Fukunaga R, Fukuyama H, Nagata S, Fukunaga R (2004) Mnk2 and Mnk1 are essential for constitutive and inducible phosphorylation of

eukaryotic initiation factor 4E but not for cell growth or development. Molecular and cellular biology 24: 6539-49

Valentin-Vega YA, Wang YD, Parker M, Patmore DM, Kanagaraj A, Moore J, Rusch M, Finkelstein D, Ellison DW, Gilbertson RJ, Zhang J, Kim HJ, Taylor JP (2016) Cancer-associated DDX3X mutations drive stress granule assembly and impair global translation. Sci Rep 6: 25996

Van Der Kelen K, Beyaert R, Inze D, De Veylder L (2009) Translational control of eukaryotic gene expression. Critical reviews in biochemistry and molecular biology 44: 143-68

Vartanian R, Masri J, Martin J, Cloninger C, Holmes B, Artinian N, Funk A, Ruegg T, Gera J (2011) AP-1 regulates cyclin D1 and c-MYC transcription in an AKT-dependent manner in response to mTOR inhibition: role of AIP4/Itch-mediated JUNB degradation. Mol Cancer Res 9: 115-30

Vassilev LT (2006) Cell cycle synchronization at the G2/M phase border by reversible inhibition of CDK1. Cell Cycle 5: 2555-6

Veber DF, Johnson SR, Cheng HY, Smith BR, Ward KW, Kopple KD (2002) Molecular properties that influence the oral bioavailability of drug candidates. J Med Chem 45: 2615-23

Vessieres A, Corbet C, Heldt JM, Lories N, Jouy N, Laios I, Leclercq G, Jaouen G, Toillon RA (2010) A ferrocenyl derivative of hydroxytamoxifen elicits an estrogen receptor-independent mechanism of action in breast cancer cell lines. J Inorg Biochem 104: 503-11

Vezina C, Kudelski A, Sehgal SN (1975) Rapamycin (AY-22,989), a new antifungal antibiotic. I. Taxonomy of the producing streptomycete and isolation of the active principle. J Antibiot (Tokyo) 28: 721-6

Villa N, Do A, Hershey JW, Fraser CS (2013) Human eukaryotic initiation factor 4G (eIF4G) protein binds to eIF3c, -d, and -e to promote mRNA recruitment to the ribosome. The Journal of biological chemistry 288: 32932-40

Wagle N, Grabiner BC, Van Allen EM, Hodis E, Jacobus S, Supko JG, Stewart M, Choueiri TK, Gandhi L, Cleary JM, Elfiky AA, Taplin ME, Stack EC, Signoretti S, Loda M, Shapiro GI, Sabatini DM, Lander ES, Gabriel SB, Kantoff PW et al. (2014) Activating mTOR mutations in a patient with an extraordinary response on a phase I trial of everolimus and pazopanib. Cancer Discov 4: 546-53

Walker AJ, Wedam S, Amiri-Kordestani L, Bloomquist E, Tang S, Sridhara R, Chen W, Palmby TR, Fourie Zirkelbach J, Fu W, Liu Q, Tilley A, Kim G, Kluetz PG, McKee AE, Pazdur R (2016) FDA Approval of Palbociclib in Combination with Fulvestrant for the Treatment of Hormone Receptor-Positive, HER2-Negative Metastatic Breast Cancer. Clin Cancer Res 22: 4968-4972

Wang Q, Wei F, Li C, Lv G, Wang G, Liu T, Bellail AC, Hao C (2013) Combination of mTOR and EGFR kinase inhibitors blocks mTORC1 and mTORC2 kinase activity and suppresses the progression of colorectal carcinoma. PLoS One 8: e73175

Wang T, Bray SM, Warren ST (2012) New perspectives on the biology of fragile X syndrome. Curr Opin Genet Dev 22: 256-63

Wang X, Li W, Williams M, Terada N, Alessi DR, Proud CG (2001) Regulation of elongation factor 2 kinase by p90(RSK1) and p70 S6 kinase. The EMBO journal 20: 4370-9

Waskiewicz AJ, Flynn A, Proud CG, Cooper JA (1997) Mitogen-activated protein kinases activate the serine/threonine kinases Mnk1 and Mnk2. The EMBO journal 16: 1909-20

Webb BL, Proud CG (1997) Eukaryotic initiation factor 2B (eIF2B). Int J Biochem Cell Biol 29: 1127-31

Wek RC (2018) Role of eIF2alpha Kinases in Translational Control and Adaptation to Cellular Stress. Cold Spring Harb Perspect Biol

Wells SE, Hillner PE, Vale RD, Sachs AB (1998) Circularization of mRNA by eukaryotic translation initiation factors. Mol Cell 2: 135-40

Wendel HG, De Stanchina E, Fridman JS, Malina A, Ray S, Kogan S, Cordon-Cardo C, Pelletier J, Lowe SW (2004) Survival signalling by Akt and eIF4E in oncogenesis and cancer therapy. Nature 428: 332-7

Wendel HG, Silva RL, Malina A, Mills JR, Zhu H, Ueda T, Watanabe-Fukunaga R, Fukunaga R, Teruya-Feldstein J, Pelletier J, Lowe SW (2007) Dissecting eIF4E action in tumorigenesis. Genes & development 21: 3232-7

Wlassoff WA, Albright CD, Sivashinski MS, Ivanova A, Appelbaum JG, Salganik RI (2007) Hydrogen peroxide overproduced in breast cancer cells can serve as an anticancer prodrug generating apoptosis-stimulating hydroxyl radicals under the effect of tamoxifen-ferrocene conjugate. J Pharm Pharmacol 59: 1549-53

Woo LW, Bubert C, Purohit A, Potter BV (2011) Hybrid dual aromatase-steroid sulfatase inhibitors with exquisite picomolar inhibitory activity. ACS Med Chem Lett 2: 243-7

Wu P, Nielsen TE, Clausen MH (2016) Small-molecule kinase inhibitors: an analysis of FDA-approved drugs. Drug Discov Today 21: 5-10

Xie M, Vesuna F, Botlagunta M, Bol GM, Irving A, Bergman Y, Hosmane RS, Kato Y, Winnard PT, Jr., Raman V (2015) NZ51, a ring-expanded nucleoside analog, inhibits motility and viability of breast cancer cells by targeting the RNA helicase DDX3. Oncotarget

Xie M, Vesuna F, Tantravedi S, Bol GM, Heerma van Voss MR, Nugent K, Malek R, Gabrielson K, van Diest PJ, Tran PT, Raman V (2016) RK-33 Radiosensitizes Prostate Cancer Cells by Blocking the RNA Helicase DDX3. Cancer Res 76: 6340-6350

Yamazaki T, Zaal K, Hailey D, Presley J, Lippincott-Schwartz J, Samelson LE (2002) Role of Grb2 in EGF-stimulated EGFR internalization. J Cell Sci 115: 1791-802

Yanagiya A, Suyama E, Adachi H, Svitkin YV, Aza-Blanc P, Imataka H, Mikami S, Martineau Y, Ronai ZA, Sonenberg N (2012) Translational homeostasis via the mRNA cap-binding protein, eIF4E. Mol Cell 46: 847-58

Yang H, Chennamaneni LR, Ho MWT, Ang SH, Tan ESW, Jeyaraj DA, Yeap YS, Liu B, Ong EH, Joy JK, Wee JLK, Kwek P, Retna P, Dinie N, Nguyen TTH, Tai SJ, Manoharan V, Pendharkar V, Low CB, Chew YS et al. (2018)

Optimization of Selective Mitogen-Activated Protein Kinase Interacting Kinases 1 and 2 Inhibitors for the Treatment of Blast Crisis Leukemia. J Med Chem 61: 4348-4369

Yang H, Rudge DG, Koos JD, Vaidialingam B, Yang HJ, Pavletich NP (2013) mTOR kinase structure, mechanism and regulation. Nature 497: 217-23

Yang HS, Jansen AP, Komar AA, Zheng X, Merrick WC, Costes S, Lockett SJ, Sonenberg N, Colburn NH (2003) The transformation suppressor Pdcd4 is a novel eukaryotic translation initiation factor 4A binding protein that inhibits translation. Molecular and cellular biology 23: 26-37

Yap TA, Omlin A, de Bono JS (2013) Development of therapeutic combinations targeting major cancer signaling pathways. J Clin Oncol 31: 1592-605

Yarden Y, Sliwkowski MX (2001) Untangling the ErbB signalling network. Nature reviews Molecular cell biology 2: 127-37

Zaytseva YY, Valentino JD, Gulhati P, Evers BM (2012) mTOR inhibitors in cancer therapy. Cancer Lett 319: 1-7

Zhang H, Dou J, Yu Y, Zhao Y, Fan Y, Cheng J, Xu X, Liu W, Guan S, Chen Z, shi Y, Patel R, Vasudevan SA, Zage PE, Zhang H, Nuchtern JG, Kim ES, Fu S, Yang J (2015) mTOR ATP-competitive inhibitor INK128 inhibits neuroblastoma growth via blocking mTORC signaling. Apoptosis 20: 50-62

Zhang X, Gureasko J, Shen K, Cole PA, Kuriyan J (2006) An allosteric mechanism for activation of the kinase domain of epidermal growth factor receptor. Cell 125: 1137-49

Zhao J, Zhai B, Gygi SP, Goldberg AL (2015) mTOR inhibition activates overall protein degradation by the ubiquitin proteasome system as well as by autophagy. Proceedings of the National Academy of Sciences of the United States of America 112: 15790-7

Zhao L, Mao Y, Zhou J, Zhao Y, Cao Y, Chen X (2016) Multifunctional DDX3: dual roles in various cancer development and its related signaling pathways. Am J Cancer Res 6: 387-402

Zhao Z, Wu H, Wang L, Liu Y, Knapp S, Liu Q, Gray NS (2014) Exploration of type II binding mode: A privileged approach for kinase inhibitor focused drug discovery? ACS Chem Biol 9: 1230-41

Zheng Y, Jiang Y (2015) mTOR Inhibitors at a Glance. Mol Cell Pharmacol 7: 15-20